# Building Bone

human mesenchymal stromal cells and the identification of genes and processes in osteoblast differentiation

**Andrea M. Brum**

ISBN: 978-94-6380-735-7


Layout and design by Andrea Brum
Cover art by Andrea Brum
Cover art is an artistic representation of cultured human mesenchymal stromal cells with immunofluorescent staining of their nuclei, actin cytoskelon and focal adhesion complexes.

Printed by Uitgeverij BOXPress || proefschriftmaken.nl

Publication of this thesis was supported by:
Erasmus University Rotterdam

# Building Bone

human mesenchymal stromal cells and the identification of genes and processes in osteoblast differentiation

Bot opbouwen

menselijke mesenchymale stromale cellen en de identificatie van genen en processen in osteoblast differentiatie

**Thesis**

to obtain the degree of Doctor from the
Erasmus University Rotterdam
by command of the
rector magnificus

Prof.dr. R.C.M.E. Engels

and in accordance with the decision of the Doctorate Board.

The public defence shall be held on
Friday, 20 March 2020 at 9:30 hours

by

**Andrea Michelle Brum**
born in Castro Valley, USA

Erasmus University Rotterdam

**Doctoral Committee:**

| | |
|---|---|
| **Promotor:** | Prof.dr. J.P.T.M. van Leeuwen |
| **Other members:** | Prof.dr. G.J.V.M. van Osch,<br>Prof.dr. M.J.T. Reinders<br>Prof.dr. J. de Boer |
| **Copromotor:** | Dr. B.C.J. van der Eerden |

# Table of Contents

# Chapter 1

# General Introduction

Andrea M. Brum

## 1.1. Bone

Bone is the calcified tissue that provides support to the soft tissues that make up a body. It allows for movement, such as walking and chewing, and provides every vertebrate creature with their unique shape. The skeleton provides strength, it protects the vital organs, and is a storage site for minerals (e.g. calcium, phosphate). But if we look closer, it is much more than just a hard, inert structure; it is an interactive and vital organ system, sending and receiving molecular signals between its self-contained cells and to and from other tissues and organ systems. While bone and bone cells change and react in response to molecular signals, they are also sensitive to mechanical forces. Mechanical stimulation is sensed by cells deep within the bone, triggering the secretion of hormones and growth factors, and ultimately enhancing bone production[1]. Bone hosts, supports, and stimulates the hematopoietic stem cells and their differentiation into all of the blood cell lineages. Bone is highly-vascularized, allowing for efficient transmission of its embedded minerals, such as calcium, hormones and other molecules to the rest of the body, as well as maintaining calcium homeostasis in the blood. Furthermore, recent research has also demonstrated the endocrine functions of the bone, exemplified by osteocalcin, which is produced by osteoblasts and affects multiple organ systems, playing a role in insulin regulation, testosterone synthesis, and production of monoamine neurotransmitters[2–5].

## 1.2. Bone tissue and cell types

Bone tissue is composed of an extracellular matrix and bone cells. The extracellular matrix primarily consists of type I collagen (90%), with the remaining 10% being a mix of a large number of non-collagenous proteins (e.g. osteocalcin, osteonectin, bone sialoproteins, osteopontin, fibronectin, and various proteoglycans)[6–9]. Non-collagenous proteins participate in the process of matrix maturation, mineralization[9]. The bone matrix not only provides support for bone cells, but also regulates the activity of bone cells through several adhesion molecules, including integrins[8,10,11].

While a great number of cell types are contained within the bone, there are three that are most remarkable for their role in bone metabolism: osteoblasts (bone-forming cells), osteocytes, and osteoclasts (bone resorbing cells) (Fig. **1**).

Osteoblasts are located along the bone surface and comprise 4–6% of the total resident bone cells (Fig. **1**). Mature osteoblasts are cuboidal cells, containing abundant rough endoplasmic reticulum, prominent Golgi apparatus, and various

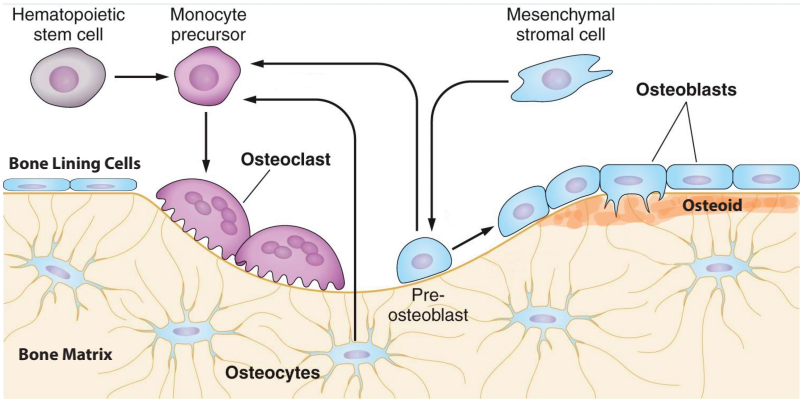


**Figure 1. Bone cells.** Three main cells types are involved in bone formation and remodeling. The osteoblast is the bone building cell, and is derived from the mesenchymal stromal cells. Osteoclasts can further differentiate into osteocytes, bone lining cells, or undergo apoptosis. Osteocytes have an important role as mechanical sensors and signal to the other bone types. Osteoclasts break down bone and derived from the hematopoietic lineage. Image adapted from Riddle et al.[12]

secretory vesicles[13,14]. Osteoblasts come from mesenchymal stromal cells present in bone marrow[15]. The primary function of osteoblasts is synthesis of bone, which includes producing the protein matrix and its subsequent mineralization. Through their function in building bone they accomplish a crucial role in the achievement and maintenance of a correct bone mass, which is accomplished through a close cross-talk with the other bone cells: osteoclasts and osteocytes.

Osteoblasts play a significant role in regulating osteoclastogensis and bone resorption through this cross-talk between the two cells types. Osteoblasts produce both macrophage-Colony Stimulating Factor (M-CSF), which promotes osteoclast proliferation and differentiation[16], and Receptor Activator of Nuclear kappa B Ligand (RANKL), that activates the fusion and differentiation of pre-osteoclasts into mature osteoclasts[17]. Osteoblasts also make osteoprotegerin (OPG), which inhibits osteoclastogenesis and the subsequent bone resorption by functioning as a decoy receptor for RANKL. A correct RANKL/OPG ratio is required to balance bone production and breakdown[18]. Recently a role for the osteoblast in endocrine function has also been discovered through their role in producing osteocalcin. Osteocalcin acts in the pancreas and adipose tissue to regulate insulin regulation, on the testis for testosterone synthesis, and in the brain stimulates the synthesis of monoamine neurotransmitters, inhibits gamma-aminobutyric acid (GABA) synthesis, aids in learning and memory and decreasing anxiety[2–5,19,20]. Osteoblasts have also been shown to regulate hematopoietic stem cells (HSCs) and HSC progenitors: miRNAs carried by osteoblast released extracellular vesicles enhance proliferation of CD34+ hematopoietic stem and progenitor cells, constitutive activity of beta catenin in osteoblasts induces acute myeloid leukaemia, along with genome instability and

chromosome mutations in HSCs, and osteoblasts promote maintenance of the HSC niche and/or hematopoietic progenitor populations[13,21–23].

Osteocytes are easily identifiable by their location, being completely embedded within the calcified bone matrix (Fig. **1**). Osteocytes are derived from terminally differentiated osteoblasts. They are the most numerous cell type in the bone, as well as the most long-lived, having a lifespan up to 25 years. Each osteocyte can have up to 50 long, branched processes that extend through the bone. The processes run inside interconnected canals in the bone, called canaliculi. This allows the processes of the osteocytes to contact neighboring osteocytes through tight and gap-junctions. Their unique shape, distribution and spatial organization optimize them for their job in signal transport and sensing of mechanical forces, making osteocytes one of the master regulators of bone[13,24].

Bone lining cells, as their name suggests, cover the surface of inactive bone and are quiescent, flat-shaped, and also arising from osteoblasts (Fig. **1**). Bone lining cells functions are not completely understood, but it has been shown that in areas not actively undergoing remodeling these cells prevent the direct interaction between osteoclasts and the bone matrix, and also participate in osteoclast differentiation, producing OPG and the RANKL[25,26]. These cells have been seen to have processes extending into bone canaliculi suggesting they are in communication with osteocytes[27,28]. Recent evidence also suggests that in adult bone, bone lining cells can be reactivated to act as mature osteoblasts and osteoblast precursors, ultimately capable of producing a mineralized bone matrix[29–31].

Osteoclasts are a member of the monocyte/macrophage family originating from haematopoietic stem cells (Fig. **1**). Mature, bone resorbing osteoclasts are large multinucleated cells formed by cell–cell fusion of mononuclear preosteoclasts[9]. Osteoclasts are highly polar cells, displaying a ruffled border, where there is folding of the plasma membrane in the area facing bone matrix. This ruffled border is required for their ability to degrade bone[32,33]. In order to resorb mineralized bone tissue, osteoclasts attach to the bone surface and form a seal around the area to be resorbed by binding their integrins with the bone protein, vitronectin. The ruffled border of the osteoclast incorporates a vacuolar-type H+ pump that acidifies the bone matrix beneath the osteoclast. Lysosomal proteases and acid phosphatases are released by the osteoclast to break down the calcified tissue[34,35]. Just as osteoblasts are key regulators of osteoclasts, osteoclasts also influence osteoblasts. Through osteoclast-mediated bone resorption, factors that are known to be strong osteoblast anabolic agents (including transforming growth factor-ß (TGFß), Bone Morphogenetic Proteins (BMPs), Fibroblast Growth Factors (FGFs) and Insulin-like Growth Factor I (IGF-I) are released, leading to recruitment of osteoblast precursors to the site, and activating

matrix deposition and mineralization. Osteoclasts also directly release molecules, termed clastokines, that influence osteoblasts. Interestingly, the clastokines released by osteoclasts both positively (Tartrate-resistant acid phosphatase (TRAcP), Sphingosine-1-Phospahte (S1P), BMP6, Wingless-type 10b (Wnt10b), Hepatocyte Growth Factor (HGF), Collagen Triple Helix Repeat-Containing Protein 1 (CTHRC1)) and negatively (Platelet Derived Growth Factor BB (PDGF BB)) regulate osteoblast recruitment, differentiation, matrix deposition and mineralization. This likely aids in maintaining a balanced ratio between activation and inhibition of bone formation[32,36].

Mesenchymal stromal cells (MSCs), also known as mesenchymal stem cells, marrow stromal cells, and skeletal stem cells, are a multipotent cell with fibroblast spindle-like appearance. They are defined through their ability to differentiate into mesenchymal lineages, including osteoblasts, chondrocytes, and adipocytes (Fig. **2**), *in vitro* and *in vivo*, and for their colony forming capacity, adherence to plastic, and ability of self-renewal[37,38]. It is generally agreed that human MSCs can be identified through expression of specific surface markers being STRO-1, CD44, CD73, CD90, CD105, and CD106 positive and negative for haematopoietic surface markers (CD34, CD45, CD14)[9,39,40]; however, conclusive cell surface markers specific for MSCs are not yet determined and agreed upon and identification of these markers is needed, as has been done for hematopoietic stem cells. Apart from their role in maintaining the populations of mesenchymal lineage cells, MSCs also modulate immune response through secretion of pro- and anti-inflammatory chemokines, organize vascular networks via their interaction with endothelial cells, and support hematopoietic stem cells[37]. MSCs are traditionally found in the bone marrow; however, studies have shown these cells can also be found in other tissues including peripheral blood, umbilical cord blood, synovial membrane, deciduous teeth, amniotic fluid, and adipose tissues. While these varying MSC populations share common properties and the ability to differentiate into osteoblasts, chondrocytes, and adipocytes, some differ in their gene expression profile in ways that reflect their tissue of origin[9,39].

## 1.3. Osteoblast differentiation

### 1.3.1 Mesenchymal stromal cell (MSC)-derived lineages

Osteoblasts are derived from the bone marrow MSCs and, following their activity as osteoblasts, undergo differentiation to form osteocytes, bone line cells or undergo apoptosis[41]. Besides osteoblasts, MSCs give rise to other cell types, including adipocytes and chondrocytes[42] (Fig. **2**). Significant strides have been made in identifying the molecular mechanisms underlying lineage commitment within the

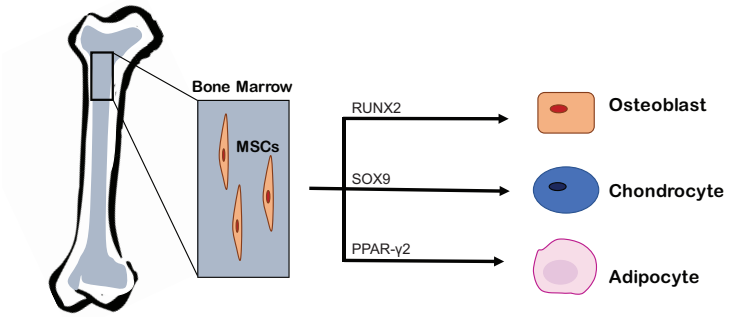


**Figure 2. Mesenchymal stromal cell differentiation.** MSCs reside within the bone marrow and have the capacity to differentiate into a variety of cell types including osteoblasts, chondrocytes, and adipocytes. Lineage commitment requires expression of a master transcription factor.

mesenchymal lineages. Control over the differentiation of MSCs towards the different lineages consists of a cascade of transcription events driven by specific transcription factors that control each other's phenotype-specific gene expression. It has been found that a master gene, one transcription factor, that can induce and start a cascade that leads to the sequential expression of other transcription factors and of phenotype-specific genes, is required for MSC commitment to each of the lineages (Fig. **2**). Runt-related transcription factor 2 (RUNX2), also known as core-binding factor subunit alpha-1 (CBFA1), is considered the master regulator of osteoblast differentiation. The significance was Runx2 demonstrated by the fact that *Runx2*-null mice are devoid of all osteoblasts, born with only a cartilaginous template and no bone[43,44]. In the adipocyte lineage Peroxisome proliferator-activated receptor-gamma 2 (PPAR-γ2) is the master regulator of differentiation, together with other transcription factors, including the CCAAT/enhancer binding (C/EBP) protein family, plays a key role in adipocyte differentiation[45]. The transcription factor Sex determining region Y-box 9 (SOX9) is essential for chondrocyte differentiation, and regulates downstream expression of various chondrocyte genes, and cartilage formation[46]. Interestingly, SOX9 is also crucial in embryonic endochondral bone development. SOX9 mediates the condensation of mesenchymal cells into chondrogenic progenitors, which is a necessary step in commitment of the osteoblast precursors. Ablation of *Sox9* in mice leads to a lack expression of *Runx2* in the axial skeleton, producing mice born with heads, but without limbs; however, if *Sox9* is selectively ablated in precursors after mesenchymal condensation, *Runx2* expression and osteoblastogenesis take place[47]. It should be noted that these differentiation process are highly complex and each of these master regulators may play more subtle roles within the converse lineages[48–51].

1.3.2 Signaling pathways in osteoblast differentiation

Maintaining a proper bone mass requires an intricate network of signaling pathways and molecular cascades. Each pathway feeds back to others and creates a web of positive and negative controls. Over the past several decades a great deal of insight has been gained into the genes and signaling pathways controlling osteoblast differentiation and controlling bone formation. Some examples of the complex signaling networks involved in osteoblast differentiation are described herewith. Members of the TGFß family stimulate RUNX2 expression and matrix protein production and deposition. BMPs can enhance, and in some cases induce, osteoblast differentiation through expression of RUNX2 and Osterix (OSX, encoded by *SP7*)[52]. Wnt family members are essential in regulating commitment of MSCs towards the osteoblast lineage and further osteoblast differentiation. Canonical Wnt signaling regulates osteoblast differentiation and bone formation through beta-catenin stabilization, allowing translocation into the nucleus where it regulates the transcription of Wnt target genes[13,53]. And notably, Wnt co-receptor, Low-Density Lipoprotein (LDL) receptor related protein 5 (Lrp5), regulates bone mass through changes in osteoblast activity[38]. Notch signaling is important in regulating osteoblast differentiation via its role as a negative regulator of osteoblast formation, targeting the stage of MSC differentiation via RUNX2 transcriptional activity[53]. Liver-secreted insulin-like growth factors (IGFs) can enhance OSX expression, trigger osteoblast proliferation, and increase collagen synthesis[52]. Hedgehog (Hh) family members encourage osteoblast differentiation at the progenitor stage via Gli transcription factors that stimulate expression of Runx2[54]. Vascular endothelial growth factors (VEGF) promote differentiation of osteoblasts, increase bone mineralization, regulate osteoclast differentiation and activity, and induce vascularization of developing bones, which is essential for bone growth[55,56].

1.3.3 Stages of osteoblast differentiation

Osteogenic differentiation of MSCs into osteoblasts is a tightly regulated process that progresses through several phases, portrayed in Fig. **3**. In the first phase of differentiation MSCs are driven to the osteogenic lineage by expression of the osteoblast-specific transcription factors, with RUNX2 and OSX being the most critical[43,44,57]. As described in the previous section, RUNX2 is integral to osteoblast differentiation and bone development. Mutations in *RUNX2* in humans leads to a variety of defects resulting in cleidocranial dysplasia[58,59]. In addition to being required for osteoblast differentiation, RUNX2 is also necessary for the proper function of mature osteoblasts, including the synthesis of extracellular matrix (ECM), through its ability to regulate a number of osteoblast-related genes, including osteopontin (*SPP1*),

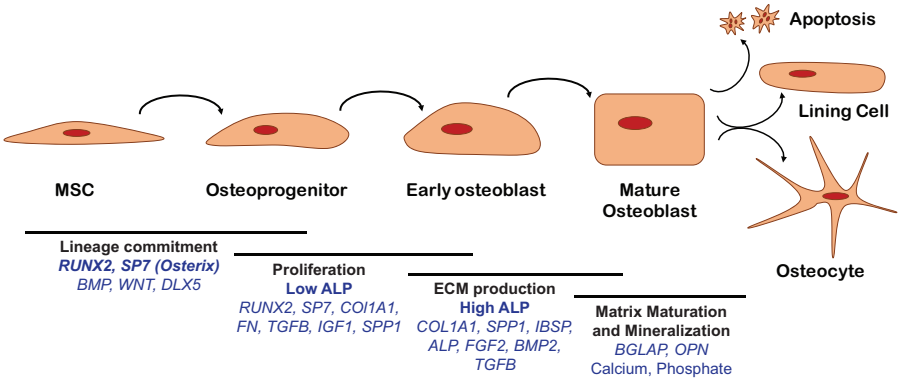


**Figure 3. Stages of osteoblast differentiation.** Osteoblast differentiation is tightly regulated process that involves several stages, each controlled by a number of genes, cytokines, growth factors, and ECM proteins.

bone sialoprotein (*IBSP*), osteocalcin (*BGLAP*), *OPG*, *RANKL*, collagen type I alpha 1 chain (*COL1A1*), and alkaline phosphatase (*ALPL*)[8,53,54]. A high degree of cross talk exists between the varying signaling pathways affecting osteoblast differentiation and bone formation. RUNX2 is at the center of this, acting as the master controller of osteoblast differentiation, and a large number of positive and negative checks are centered around it. Many transcription factors (**Table 1**) have been shown to synergize with RUNX2 to promote osteoblast differentiation by either stimulating RUNX2 expression, enhancing RUNX2 activity or acting as co-activators. On the other hand, a number of other factors (**Table 1**) suppress RUNX2 levels or by blocking RUNX2 DNA binding, nuclear translocation, or protein expression.

Osterix (Osx/SP7), a zinc-finger transcription factor downstream of RUNX2, is necessary for both commitment of MSCs to the osteoblast lineage and further osteoblast differentiation. *Osx* was discovered as a Bmp-inducible gene in murine C2C12 cells, whose deletion in mice resulted in complete absence of osteoblasts in embryos, despite relatively normal expression of *Runx2*[60]. In addition, these mice displayed very little Col1a1, and no expression of *IBSP*, osteonectin (*SPARC*), or *SPP1*. *OSX* expression is stimulated by BMPs and IGF1, and although it is downstream of RUNX2, its activation via BMPs follows both RUNX2-dependent and -independent pathways. Osterix also serves as a negative regulator of Wnt signaling[13,54] and it controls transcriptional expression of the transcription factor Special AT-rich Binding 2 (SATB2)[61], which is important in craniofacial development and osteoblast differentiation[62]. SATB2 interacts with both RUNX2 and Activating Transcription Factor 4 (ATF4) to positively regulate osteoblast markers COL1A1, IBSP, and OCN, at the later stage of osteoblast differentiation[63].

**Table 1: Transcription factors acting on or with RUNX2 to affect osteoblast differentiation**

| Transcription factor name | Gene symbol | Effect on RUNX2 | Ref |
|---|---|---|---|
| v-maf avian musculoaponeurotic fibrosarcoma oncogene homolog | MAF | Enhances | 64 |
| tafazzin | TAZ | Co-activator | 65,66 |
| special AT-rich sequence-binding protein 2 | SATB2 | Stimulates | 62 |
| retinoblastoma protein | RB | Enhances | 67,68 |
| GLI family zinc finger 2 | GLI2 | Stimulates, Enhances | 69 |
| distal-less homeobox 5 | DLX5 | Stimulates | 70,71 |
| Msh homeobox 2 | MSX2 | Stimulates | 72 |
| bagpipe homeobox homolog 1 | NKX3-2 | Stimulates | 73 |
| Twist-related protein 1 | TWIST1 | Inhibits | 74 |
| Heart- and neural crest derivatives-expressed protein 2 | HAND2 | Inhibits binding | 75 |
| Human Immunodeficiency Virus Type I Enhancer Binding Protein 3 | HIVEP3 (Schnurri-3) | Facilitates degradation | 76 |
| GLI Family Zinc Finger 3 | GLI3 | Inhibits binding | 77 |
| Homeobox A2 | HOXA2 | Downregulates | 78 |
| Hes Family BHLH Transcription Factor 1 / Hes Related Family BHLH Transcription Factor With YRPW Motif 1 | HES1/ HEY1 | Inhibits activity | 79,80 |

Following activation of RUNX2 and OSX, osteoprogenitors undergo a proliferation phase and begin to show alkaline phosphatase (ALP) activity. Through this proliferation phase the cells upregulate expression of genes encoding matrix protein and stimulating osteoblast differentiation, including fibronectin (FN), collagen I, TGFβ, TGFβ receptor, VEGF, PDGF, IGF-1, and SPP1[8,13,54,81].

In the next stage of differentiation early osteoblasts (or pre-osteoblasts) are actively engaged in energy demanding process of ECM production and maturation. Osteoblasts secrete collagen proteins (mainly type I), non-collagenous proteins (OCN, osteonectin, bone sialoproteins, osteopontin), and proteoglycans (including decorin and biglycan), forming the bone matrix (osteoid) onto which the mineral will later be deposited[82]. This stage of differentiation is characterized by peak transcription and protein expression of ALP[83]. These matrix producing osteoblasts are characterized by expression of *COL1A1*, *SPP1*, *IBSP*, *ALP*, *FGF2*, *BMP2, TGF*ß, and *PDGF*[13,81,83]. The morphology of the osteoblast is also changing at this time and by the beginning of the mineralization phase (next) osteoblasts have adopted their characteristic large, cuboidal shape[53].

In the final stage of osteoblast differentiation, matrix mineralization occurs, which is characterized by high expression of osteocalcin (BGLAP) and osteopontin (OPN), followed by calcium and phosphate deposition[81,84]. Production of osteocalcin is so high at this point that it is in fact the most abundant non-collagenous protein in bone, after collagen[85]. Mineralization of bone matrix takes place beginning with the osteoblasts releasing matrix vesicles from their apical membrane domain into the newly formed matrix, where the vesicles bind to proteoglycans and other organic

components in the matrix. Calcium phosphate crystals begin forming inside the matrix vesicles and grow through the influx of $Ca^{2+}$ and $PO4^{3-}$, by means of the membrane transporters and enzymes (including ecto-nucleotide pyrophosphatase/phosphodiesterase 1 (ENPP1), ankylosis (ANK), and ALP. The calcium phosphate crystals (hydroxyapatite) elongate and penetrate the matrix vesicle's membrane, finally growing out of the vesicles to form calcifying nodules. The calcifying nodules continue growing, finally leading to collagen mineralization in the surrounding matrix[8,86].

After osteoblasts fulfill their primary role in bone production three possible fates exist for these cells. The osteoblasts either (1) undergo apoptosis, (2) transform into osteocytes embedded within the bone matrix, or (3) become quiescent bone lining cells covering the bone surface. The mechanisms that control final osteoblast fate are still largely yet unknown.

### 1.4. Bone formation, modeling, and remodeling

Throughout life bone is constantly changing, and undergoing continuous turnover to maintain its strength and mass. Bone structure and mass are created or altered in one of three ways: osteogenesis (embryonic bone formation), bone modeling and bone remodeling.

During embryogenesis, osteogenesis occurs either by intramembranous or endochondral ossification. Intramembranous ossification occurs in parts of the skull or craniofacial skeleton, clavicles and scapulae where mesenchymal cells condense, differentiate, and directly produce membranous bone. In endochondral, or indirect, ossification first a cartilaginous template is produced, which slowly is replaced by mineralized bone, and occurs in the long bones and the rest of the skeleton[9].

Once bone is formed, substantial changes in structure and geometry of the bones occur through bone modeling. Throughout development, childhood and even into adulthood adaptation to strain leads to modeling of bone. Examples of this include tibial modeling after removal of fibula for reconstructive surgery[87]. In bone modeling the activities of the osteoblasts and osteoclasts may occur independently[88].

Bone remodeling is the process of removing mature bone tissue followed by subsequent formation of new bone tissue. In healthy adults, bone undergoes constant remodeling, balancing bone formation and bone resorption, with the actions of osteoblasts and osteoclasts being linked, a process known as coupling. This allows bone resorption and then formation to occur at the same location on the bone surface consecutively and maintenance of a healthy bone mass. It has been estimated that the human adult skeleton is renewed by remodeling every 10 years and that 1 million

bone remodeling units (BRUs) are actively engaged in bone turnover at any time[89]. BRUs are made up of osteoblasts and osteoclasts, together with their precursor cells and associated cells (e.g. endothelial cells, nerve cells), with coordinated actions between the cells required for proper bone remodeling to take place[9]. Remodeling is essential for removal of microcracks, that can endanger the integrity of the bone, as well as for maintaining mineral homeostasis in the skeleton and throughout the body. Bone remodeling also plays a role in the maintenance of acid/base balance, and the release of growth factors embedded in bone that are required for the bone remodeling process and attract osteoblast precursors and enhance osteoblast proliferation and differentiation[34,88,91,92]. Remodeling is a process characterized by four phases: (1) the activation phase when the osteoclasts are recruited; (2) the resorption phase, when the osteoclasts digest the underlying bone mineral matrix; (3) the reversal phase, where the osteoclasts undergo apoptosis, the eroded bone surfaces are colonized by reversal cells, and osteoblasts are recruited; and (4) the formation phase, where the osteoblasts lay down new organic bone matrix that subsequently mineralizes (Fig. **4**). This process is driven by complex actions of the various cell types and biochemical factors, and it is sensitive to the loads applied onto the skeleton[92]. Interestingly, a great deal of research recently has focused on the reversal phase, in particular the reversal cells (recently described as identical to osteoprogenitors) that are thought to be key in linking bone formation to resorption[93,94].

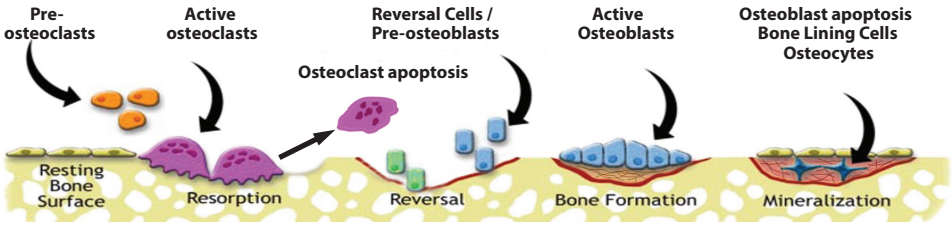


**Figure 4. Bone remodeling.** Bone remodeling is carried out through a series of steps: (1) osteoclast precursors are recruited to the bone surface. (2) mature osteoclasts resorb the bone mineral matrix. (3) a reversal phase where osteoclasts undergo apoptosis and reversal cells and osteoblast precursors are recruited. (4) mature osteoblasts create a new matrix that is mineralized. Adapted from Tou.[90]

### 1.5. Osteoporosis

Osteoporosis, the word itself meaning porous bones, is a common and devastating bone disease that is characterized by low bone mass and deterioration of bone microstructure, which leads to increased bone fragility and susceptibility to fractures (Fig. **5**). Osteoporosis has become a major-medical problem and is now

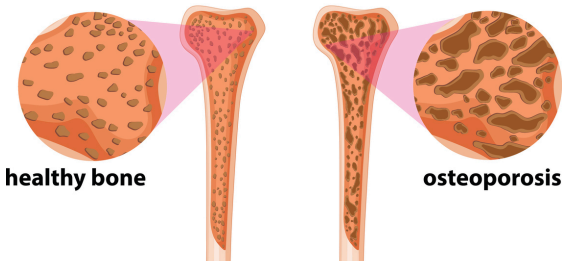


**Figure 5. Depiction of healthy versus osteoporotic bone structure.** Trabecular bone from healthy individuals (left) has a higher mineral density than bone of individuals with osteoporosis (right). Adapter from Ringer[98].

estimated to affect approximately 50 percent of women and 20 percent of men over 50 years of age[95]. The acute clinical concern of osteoporosis is fractures and their subsequent consequences for health; osteoporosis-related fractures, vertebral and hip, are associated with morbidity and increased mortality[96,97]. It is estimated that an osteoporotic fracture occurs once every 8 seconds worldwide[99] and direct healthcare costs in Europe alone are at least €31.7 billion annually[100].

During osteoporosis the coupling process is disturbed, leading to a disruption in bone remodeling where resorption overtakes bone formation[101]. The exact cause of this dysregulation in osteoblast and osteoclast balance and development of osteoporosis is still being unraveled. Diagnosis of osteoporosis itself is usually based upon measuring bone mineral density (BMD) through use of a bone densitometer (most common is a Dual energy X-ray absorptiometry (DXA)). Bone density test results are reported as a number called a T-score that indicates the number of units (standard deviations) that a patient's bone density is above or below the average. Patients with T-scores of -2.5 and below are characterized as having osteoporosis. The cause of osteoporosis is due to a combination of factors, which include genetics, nutrition, lifestyle, estrogen deficiency, calcium and vitamin D deficiency, secondary hyperparathyroidism, impaired stem cell renewal, decreased growth factors, cytokines and inflammation, neural and muscular impairment, drugs affecting balance and coordination, and environmental hazards[102]. Great effort has been put into discovering genetic polymorphisms that can affect bone mass and bone fragility. Most notably a number of polymorphisms have been found that affect the collagen1α1 gene, leading to poor bone quality[102]. Estrogen deficiency is one of the most well-known contributors to osteoporosis, although the precise mechanisms are still being studied. Estrogens act on osteoblasts, osteocytes, and osteoclasts to regulate bone remodeling and maintain bone formation[9,103]. Estrogen deficiency is associated with increases in bone resorption due to increased osteoclast numbers and increased osteoclast activity[89]. The increase in bone resorption following estrogen deficiency is associated with an increase in bone formation (coupling), but the rate of formation is

not able to keep up with the rate of resorption, resulting in a net loss of bone[103]. Other age-related changes, such as reduced levels of growth factors and increases in inflammation are likely affecting the homeostatic bone balance. Increases in the cytokine Tumor Necrosis Factor alpha (TNFα) can inhibit bone formation while stimulating bone resorption[102]. Another cause for the occurrence of osteoporosis is the reduced osteoblastic differentiation capacity of MSCs. It has been seen that with aging there is a decrease in bone mass and increased bone fragility, while at the same time there is an increase in total and bone marrow adiposity[104–106]. There is also evidence of a high correlation between osteoporosis and bone marrow fat. These indicate that there is a shift in the lineage decision-making process of MSCs with increasing age contributing to the development of osteoporosis by increased preference of adipocyte differentiation as opposed to that of osteoblasts. However, despite considerable research for many years, our current understanding of the mechanisms that disrupt osteoblast/osteoclast coupling during bone homeostasis and remodeling, and the associated changes in properties of bone during osteoporosis is still fragmented due to complex interrelationships between bone cells and structural features of bone.

### 1.6. Current treatments for osteoporosis

At present, most osteoporosis treatments thus far aim at inhibiting bone degradation by way of decreasing osteoclast function or production. The treatments are termed anti-resorptive and decrease the rate of remodeling and the amount of resorption cavities. Essentially, anti-resorptive therapy preserve the existing bone mass and structure[107]. Bisphosphonates are the most common anti-resorptives and include alendronate, ibandronate, risedronate, and zoledronic acid. The 50$^{th}$ anniversary of the bisphosphonate discovery was celebrated in 2019. Bisphosphonates bind with high affinity to the mineral matrix of the bone and inhibit osteoclast resorption of the bone, which leads to a decrease in bone turnover[107,108]. An overall increase in BMD is seen with bisphosphonate treatment, likely due to decreased formation of new remodeling units by osteoclasts along with relative maintenance, at least initially, of osteoblast activity[109]. All bisphosphonates are reported to be associated with a rare complication called osteonecrosis of the jaw[108] and, more recently, atypical femur fractures[110].

Denosumab is a newer non-bisphosphonate anti-resorptive drug, which has also shown to reduce the risk of osteoporotic fracture in women and men. It is a human monoclonal antibody against RANKL, the transmembrane protein required for the formation, function, and survival of osteoclasts, leading to decreased bone

resorption[108]. In cortical bone, denosumab can improve cortical bone structure, increasing cortical thickness and decreasing porosity, and it has been reported that this increase in BMD is somewhat greater than with bisphosphonates and lasts longer. A possible reason for the gain in bone is that denosumab maintains physiological bone modelling[88,107,111]. Osteonecrosis of the jaw and atypical femur fractures have also been reported with denosumab use[110,112].

Selective estrogen receptor modulators Raloxifene and Bazedoxifene are both estrogen agonists and antagonists, and act as a weak antiresorptive agent known to reduce the risk of vertebral but not non-vertebral or hip fracture in women with postmenopausal osteoporosis[107]. They also have estrogen antagonistic activity on breast and uterine tissue.

Most anti-resorptive treatments can result in modest increases in BMD; however, these treatments do not result in a true bone anabolic effect, so patients do not regain bone that has been lost at time of diagnosis. Some drugs, especially bisphosphonates due to their prolonged activity in bone, even inhibit osteoblast activity through the coupling of osteoblast and osteoclast activity, which can result in a "frozen bone" state where bone may actually become more brittle as it fails to respond to bone remodeling cues, such as microcracks and systemic mineral requirements.

While there is a need and interest in treatments that act by stimulating bone formation, so called anabolic drugs, the only currently available treatment to increase bone formation is parathyroid hormone. Parathyroid hormone (PTH) is produced naturally in the body and regulates the amount of calcium in bone. PTH treatments (teriparatide, a truncated version of recombinant human PTH(1-34); and abaloparatide, a synthetic analogue of PTH related peptide (PTHrP)) are used to stimulate osteoblasts. The majority of the anabolic effect in trabecular bone is achieved through enhanced osteoclast activity at remodeling sites, with overfilling of remodeling units. By increasing bone production there is also an increased osteoclast activity, as the two are linked, but despite this, studies have shown an overall increase in BMD. On the downside, PTH treatments must be administered daily by subcutaneous injection, are expensive compared to anti-resorptive treatments, appear to primarily increase bone forming activity at sites that are still undergoing bone remodeling rather than at areas of quiescence, and during the early stages of treatment the formation of under-mineralized new bone can occur, which results in little change, or a decrease in BMD at sites such as the hip and radius[107,113]. In addition PTH treatment are limited to 2 years of use due to the potential occurrence of osteosarcomas (seen in rat studies) and are reserved for patients with severe osteoporosis[107,114].

The search for better treatments continues. In order to bring fragile osteoporotic bone back into a healthy state and reduce the risk of new fractures in osteoporosis patients there is a need for new treatments that can replace bone that has already been lost. The future of osteoporosis treatments may include identification of new bone anabolic treatments, but there is also a need to better understand the mechanisms of action by existing drugs and the intricacies of the networks involved in bone production and remodeling as this could lead to improved use of existing treatments.

### 1.7. Aim of this thesis

Understanding the mechanisms that control the differentiation of osteoblasts cells from MSCs is one of the fundamental areas of research of bone biology, and the focus of this thesis. While huge leaps have been made in bone research, primarily through mouse models and cell lines, there is still a great deal unknown about what specific factors stimulate osteoblast differentiation and lead to mineralization of new bone, particularly in human cells and during adult bone formation, remodeling and repair. A better understanding of the predominant signaling networks, their intricate interactions, and what other genes and pathways are involved in human MSC lineage decision making, as well as osteoblast differentiation and function, is required to develop approaches to enhance bone formation and promote fracture healing for patients with disorders such as osteoporosis.

The overall aim of this thesis, through the combined use of bioinformatic, genomic, molecular, and proteomic approaches, is to identify novel compounds affecting, and genes and processes involved in human osteoblast differentiation and bone formation, thus expanding the knowledge of approaches to enhance human osteogenesis. The basis for all of the results presented in this thesis come from microarray gene expression profiling with high temporal resolution of hMSCs undergoing osteoblast differentiation, which identified genes significantly regulated during the differentiation process.

In **Chapter 2** we combine genomic (gene expression microarray of osteogenic differentiating human MSCs) and bioinformatics (the Connectivity Map or CMap) tools to identify a novel bone anabolic compound, Parbendazole, that induces osteoblast differentiation in a subset of the hMSC population through cytoskeletal changes and increased bone morphogenetic protein 2 activity *in vitro*.

Using the same approach as in the previous chapter, in **Chapter 3** we use the CMap to identify additional compounds that both positively and negatively affect *in vitro* human osteoblast differentiation and delve into the important genes mitigating their effects.

**Chapter 4** identifies Chloride Intracellular Channel 3 (*CLIC3)* as new gene regulated specifically during osteoblast differentiation based on differential transcriptional programming of hMSC differentiated towards osteogenic versus adipogenic cell lineages, and examines its crucial function in promoting mineralization.

Mucin1 (*MUC1*) was also identified as a novel, lineage specific gene based on microarray expression profiling of hMSCs undergoing osteogenic and adipogenic differentiation. **Chapter 5** details the *in vivo* role of *Muc1* in bone through a *Muc1* deficient mouse model. Longitudinal studies of these mice allowed us to identify mild temporal changes in the femurs of female mice during aging.

Finally, in **Chapter 6**, the conclusions of the work presented in this thesis are defined. I describe the key findings, discuss their significance in the field of bone biology, and give recommendations for future work.

## References


1. Papachroni, K. K., Karatzas, D. N., Papavassiliou, K. a, Basdra, E. K. & Papavassiliou, A. G. Mechanotransduction in osteoblast regulation and bone disease. *Trends Mol. Med.* **15**, 208–16 (2009).
2. Ferron, M., Hinoi, E., Karsenty, G. & Ducy, P. Osteocalcin differentially regulates beta cell and adipocyte gene expression and affects the development of metabolic diseases in wild-type mice. *Proc. Natl. Acad. Sci. U. S. A.* **105**, 5266–70 (2008).
3. Guntur, A. R. & Rosen, C. J. Bone as an endocrine organ. *Endocr. Pract.* **18**, 758–62 (2012).
4. Oury, F. *et al.* Maternal and offspring pools of osteocalcin influence brain development and functions. *Cell* **155**, 228–41 (2013).
5. Oury, F. *et al.* Endocrine regulation of male fertility by the skeleton. *Cell* **144**, 796–809 (2011).
6. Damsky, C. H. Extracellular matrix-integrin interactions in osteoblast function and tissue remodeling. *Bone* **25**, 95–6 (1999).
7. Marie, P. J. Role of N-cadherin in bone formation. *J. Cell. Physiol.* **190**, 297–305 (2002).
8. Florencio-Silva, R., Sasso, G. R. da S., Sasso-Cerri, E., Simões, M. J. & Cerri, P. S. Biology of Bone Tissue: Structure, Function, and Factors That Influence Bone Cells. *Biomed Res. Int.* **2015**, 421746 (2015).
9. Arvidson, K. *et al.* Bone regeneration and stem cells. *J. Cell. Mol. Med.* **15**, 718–746 (2011).
10. Green, J., Schotland, S., Stauber, D. J., Kleeman, C. R. & Clemens, T. L. Cell-matrix interaction in bone: type I collagen modulates signal transduction in osteoblast-like cells. *Am. J. Physiol. Physiol.* **268**, C1090–C1103 (1995).
11. Saltel, F., Destaing, O., Bard, F., Eichert, D. & Jurdic, P. Apatite-mediated actin dynamics in resorbing osteoclasts. *Mol. Biol. Cell* **15**, 5231–41 (2004).
12. Riddle, R. C. & Clemens, T. L. Bone Cell Bioenergetics and Skeletal Energy Homeostasis. *Physiol. Rev.* **97**, 667–698 (2017).
13. Capulli, M., Paone, R. & Rucci, N. Osteoblast and osteocyte: Games without frontiers. *Arch. Biochem. Biophys.* **561**, 3–12 (2014).
14. Marks, S. C. & Popoff, S. N. Bone cell biology: The regulation of development, structure, and function in the skeleton. *Am. J. Anat.* **183**, 1–44 (1988).
15. Harada, S. & Rodan, G. A. Control of osteoblast function and regulation of bone mass. *Nature* **423**, 349–355 (2003).
16. Felix, R. *et al.* Impairment of macrophage colony-stimulating factor production and lack of resident bone marrow macrophages in the osteopetrotic op/op mouse. *J. Bone Miner. Res.* **5**, 781–9 (1990).
17. Lacey, D. L. *et al.* Osteoprotegerin ligand is a cytokine that regulates osteoclast differentiation and activation. *Cell* **93**, 165–76 (1998).
18. Simonet, W. S. *et al.* Osteoprotegerin: a novel secreted protein involved in the regulation of bone density. *Cell* **89**, 309–19 (1997).
19. Khrimian, L., Obri, A. & Karsenty, G. Modulation of cognition and anxiety-like behavior by bone remodeling. *Mol. Metab.* **6**, 1610–1615 (2017).
20. Otani, T. *et al.* Signaling pathway for adiponectin expression in adipocytes by osteocalcin. *Cell. Signal.* **27**, 532–544 (2015).
21. Kode, A. *et al.* Leukaemogenesis induced by an activating β-catenin mutation in osteoblasts. *Nature* **506**, 240–244 (2014).
22. Morhayim, J. *et al.* Osteoblasts secrete miRNA-containing extracellular vesicles that enhance expansion of human umbilical cord blood cells. *Sci. Rep.* **6**, 32034 (2016).
23. Morrison, S. J. & Scadden, D. T. The bone marrow niche for haematopoietic stem cells. *Nature* **505**, 327–34 (2014).
24. Bonewald, L. F. Chapter 4. Osteocytes. in *Primer on the Metabolic Bone Diseases and Disorders of Mineral Metabolism* (ed. Rosen, C. J.) 22–27 (American Society for Bone and Mineral Research, 2008). doi:10.1002/9780470623992.ch4
25. Andersen, T. L. *et al.* A physical mechanism for coupling bone resorption and formation in adult human bone. *Am. J. Pathol.* **174**, 239–47 (2009).
26. Mosley, J. R. Osteoporosis and bone functional adaptation: mechanobiological regulation of bone architecture in growing and adult bone, a review. *J. Rehabil. Res. Dev.* **37**, 189–99
27. Miller, S. C., de Saint-Georges, L., Bowman, B. M. & Jee, W. S. Bone lining cells: structure and function. *Scanning Microsc.* **3**, 953–60; discussion 960-1 (1989).
28. Aarden, E. M., Nijweide, P. J. & Burger, E. H. Function of osteocytes in bone. *J. Cell. Biochem.* **55**, 287–299 (1994).
29. Matic, I. *et al.* Quiescent Bone Lining Cells Are a Major Source of Osteoblasts During Adulthood. *Stem Cells* **34**, 2930–2942 (2016).
30. Dobnig, H. & Turner, R. T. Evidence that intermittent treatment with parathyroid hormone increases bone formation in adult rats by activation of bone lining cells. *Endocrinology* **136**, 3632–3638 (1995).
31. Kim, S. W. *et al.* Intermittent parathyroid hormone administration converts quiescent lining cells to active

osteoblasts. *J. Bone Miner. Res.* **27**, 2075–2084 (2012).
32. Cappariello, A., Maurizi, A., Veeriah, V. & Teti, A. The Great Beauty of the osteoclast. *Arch. Biochem. Biophys.* **558**, 70–78 (2014).
33. Feher, J. Calcium and Phosphorus Homeostasis II: Target Tissues and Integrated Control. in *Quantitative Human Physiology* (ed. Feher, J.) 836–845 (Academic Press, 2012). doi:10.1016/B978-0-12-382163-8.00091-8
34. Martin, R. B., Burr, D. B., Sharkey, N. A. & Fyhrie, D. P. Growth, Modeling and Remodeling of Bone. in *Skeletal Tissue Mechanics* 95–173 (Springer New York, 2015). doi:10.1007/978-1-4939-3002-9_3
35. Wright, H. L., McCarthy, H. S., Middleton, J. & Marshall, M. J. RANK, RANKL and osteoprotegerin in bone biology and disease. *Curr. Rev. Musculoskelet. Med.* **2**, 56–64 (2009).
36. Teti, A. Mechanisms of osteoclast-dependent bone formation. *Bonekey Rep.* **2**, 449 (2013).
37. Sobacchi, C., Palagano, E., Villa, A. & Menale, C. Soluble Factors on Stage to Direct Mesenchymal Stem Cells Fate. *Front. Bioeng. Biotechnol.* **5**, 32 (2017).
38. Krause, C. *et al.* Chapter 2. Signal Transduction Cascades Controlling Osteoblast Differentiation. in *Primer on the Metabolic Bone Diseases and Disorders of Mineral Metabolism* (ed. Rosen, C. J.) 10–16 (American Society for Bone and Mineral Research, 2008). doi:10.1002/9780470623992.ch2
39. Ullah, I., Subbarao, R. B. & Rho, G. J. Human mesenchymal stem cells - current trends and future prospective. *Biosci. Rep.* **35**, (2015).
40. Chen, Q. *et al.* Fate decision of mesenchymal stem cells: adipocytes or osteoblasts? *Cell Death Differ.* **23**, 1128–1139 (2016).
41. Matsuo, K. & Irie, N. Osteoclast-osteoblast communication. *Arch. Biochem. Biophys.* **473**, 201–9 (2008).
42. Chamberlain, G., Fox, J., Ashton, B. & Middleton, J. Concise review: mesenchymal stem cells: their phenotype, differentiation capacity, immunological features, and potential for homing. *Stem Cells* **25**, 2739–49 (2007).
43. Ducy, P., Zhang, R., Geoffroy, V., Ridall, A. L. & Karsenty, G. Osf2/Cbfa1: a transcriptional activator of osteoblast differentiation. *Cell* **89**, 747–54 (1997).
44. Komori, T. *et al.* Targeted disruption of Cbfa1 results in a complete lack of bone formation owing to maturational arrest of osteoblasts. *Cell* **89**, 755–64 (1997).
45. Rosen, E. D. & Spiegelman, B. M. Molecular Regulation of Adipogenesis. *Annu. Rev. Cell Dev. Biol.* **16**, 145–171 (2000).
46. de Crombrugghe, B. *et al.* Transcriptional mechanisms of chondrocyte differentiation. *Matrix Biol.* **19**, 389–94 (2000).
47. Akiyama, H., Chaboissier, M.-C., Martin, J. F., Schedl, A. & de Crombrugghe, B. The transcription factor Sox9 has essential roles in successive steps of the chondrocyte differentiation pathway and is required for expression of Sox5 and Sox6. *Genes Dev.* **16**, 2813–28 (2002).
48. Bruedigam, C., Koedam, M., Chiba, H., Eijken, M. & van Leeuwen, J. P. T. M. Evidence for multiple peroxisome proliferator-activated receptor gamma transcripts in bone: fine-tuning by hormonal regulation and mRNA stability. *FEBS Lett.* **582**, 1618–24 (2008).
49. Stockl, S. *et al.* Sox9 modulates cell survival and adipogenic differentiation of multipotent adult rat mesenchymal stem cells. *J. Cell Sci.* **126**, 2890–2902 (2013).
50. Stanton, L.-A., Li, J. R. & Beier, F. PPARγ2 expression in growth plate chondrocytes is regulated by p38 and GSK-3. *J. Cell. Mol. Med.* **14**, 242–256 (2010).
51. Stricker, S., Fundele, R., Vortkamp, A. & Mundlos, S. Role of Runx Genes in Chondrocyte Differentiation. *Dev. Biol.* **245**, 95–108 (2002).
52. Celil, A. B. & Campbell, P. G. BMP-2 and insulin-like growth factor-I mediate Osterix (Osx) expression in human mesenchymal stem cells via the MAPK and protein kinase D signaling pathways. *J. Biol. Chem.* **280**, 31353–9 (2005).
53. Long, F. Building strong bones: molecular regulation of the osteoblast lineage. *Nat. Rev. Mol. Cell Biol.* **13**, 27–38 (2012).
54. Rutkovskiy, A., Stensløkken, K.-O. & Vaage, I. J. Osteoblast Differentiation at a Glance. *Med. Sci. Monit. Basic Res.* **22**, 95–106 (2016).
55. Liu, Y. & Olsen, B. R. Distinct VEGF Functions During Bone Development and Homeostasis. *Arch. Immunol. Ther. Exp. (Warsz).* **62**, 363–368 (2014).
56. Zelzer, E. & Olsen, B. R. Multiple Roles of Vascular Endothelial Growth Factor (VEGF) in Skeletal Development, Growth, and Repair. in *Current topics in developmental biology* **65**, 169–187 (2004).
57. Otto, F. *et al.* Cbfa1, a candidate gene for cleidocranial dysplasia syndrome, is essential for osteoblast differentiation and bone development. *Cell* **89**, 765–71 (1997).
58. Mundlos, S. *et al.* Mutations involving the transcription factor CBFA1 cause cleidocranial dysplasia. *Cell* **89**, 773–9 (1997).
59. Lee, B. *et al.* Missense mutations abolishing DNA binding of the osteoblast-specific transcription factor OSF2/CBFA1 in cleidocranial dysplasia. *Nat. Genet.* **16**, 307–10 (1997).
60. Nakashima, K. *et al.* The novel zinc finger-containing transcription factor osterix is required for osteoblast differentiation and bone formation. *Cell* **108**, 17–29 (2002).

61. Tang, W., Li, Y., Osimiri, L. & Zhang, C. Osteoblast-specific Transcription Factor Osterix (Osx) Is an Upstream Regulator of Satb2 during Bone Formation. *J. Biol. Chem.* **286**, 32995–33002 (2011).
62. Dobreva, G. *et al.* SATB2 Is a Multifunctional Determinant of Craniofacial Patterning and Osteoblast Differentiation. *Cell* **125**, 971–986 (2006).
63. Yang, X. *et al.* ATF4 is a substrate of RSK2 and an essential regulator of osteoblast biology; implication for Coffin-Lowry Syndrome. *Cell* **117**, 387–98 (2004).
64. Nishikawa, K. *et al.* Maf promotes osteoblast differentiation in mice by mediating the age-related switch in mesenchymal cell differentiation. *J. Clin. Invest.* **120**, 3455–65 (2010).
65. Hong, J.-H. *et al.* TAZ, a Transcriptional Modulator of Mesenchymal Stem Cell Differentiation. *Science (80-. ).* **309**, 1074–1078 (2005).
66. Cui, C. B., Cooper, L. F., Yang, X., Karsenty, G. & Aukhil, I. Transcriptional Coactivation of Bone-Specific Transcription Factor Cbfa1 by TAZ. *Mol. Cell. Biol.* **23**, 1004–1013 (2003).
67. Thomas, D. M. *et al.* The retinoblastoma protein acts as a transcriptional coactivator required for osteogenic differentiation. *Mol. Cell* **8**, 303–16 (2001).
68. Calo, E. *et al.* Rb regulates fate choice and lineage commitment in vivo. *Nature* **466**, 1110–4 (2010).
69. Shimoyama, A. *et al.* Ihh/Gli2 signaling promotes osteoblast differentiation by regulating Runx2 expression and function. *Mol. Biol. Cell* **18**, 2411–8 (2007).
70. Lee, M.-H. *et al.* Dlx5 specifically regulates Runx2 type II expression by binding to homeodomain-response elements in the Runx2 distal promoter. *J. Biol. Chem.* **280**, 35579–87 (2005).
71. Robledo, R. F., Rajan, L., Li, X. & Lufkin, T. The Dlx5 and Dlx6 homeobox genes are essential for craniofacial, axial, and appendicular skeletal development. *Genes Dev.* **16**, 1089–101 (2002).
72. Satokata, I. *et al.* Msx2 deficiency in mice causes pleiotropic defects in bone growth and ectodermal organ formation. *Nat. Genet.* **24**, 391–5 (2000).
73. Tribioli, C. & Lufkin, T. The murine Bapx1 homeobox gene plays a critical role in embryonic development of the axial skeleton and spleen. *Development* **126**, 5699–711 (1999).
74. Bialek, P. *et al.* A twist code determines the onset of osteoblast differentiation. *Dev. Cell* **6**, 423–35 (2004).
75. Funato, N. *et al.* Hand2 controls osteoblast differentiation in the branchial arch by inhibiting DNA binding of Runx2. *Development* **136**, 615–25 (2009).
76. Jones, D. C. *et al.* Regulation of adult bone mass by the zinc finger adapter protein Schnurri-3. *Science* **312**, 1223–7 (2006).
77. Ohba, S. *et al.* Patched1 haploinsufficiency increases adult bone mass and modulates Gli3 repressor activity. *Dev. Cell* **14**, 689–99 (2008).
78. Kanzler, B., Kuschert, S. J., Liu, Y. H. & Mallo, M. Hoxa-2 restricts the chondrogenic domain and inhibits bone formation during development of the branchial area. *Development* **125**, 2587–97 (1998).
79. Garg, V. *et al.* Mutations in NOTCH1 cause aortic valve disease. *Nature* **437**, 270–274 (2005).
80. Hilton, M. J. *et al.* Notch signaling maintains bone marrow mesenchymal progenitors by suppressing osteoblast differentiation. *Nat. Med.* **14**, 306–314 (2008).
81. Huang, Z., Nelson, E. R., Smith, R. L. & Goodman, S. B. The Sequential Expression Profiles of Growth Factors from Osteroprogenitors to Osteoblasts In Vitro. *Tissue Eng.* **13**, 2311–2320 (2007).
82. Quarles, L. D., Yohay, D. A., Lever, L. W., Caton, R. & Wenstrup, R. J. Distinct proliferative and differentiated stages of murine MC3T3-E1 cells in culture: an in vitro model of osteoblast development. *J. Bone Miner. Res.* **7**, 683–692 (1992).
83. Aubin, J. E. Regulation of osteoblast formation and function. *Rev. Endocr. Metab. Disord.* **2**, 81–94 (2001).
84. Hoemann, C. D., El-Gabalawy, H. & McKee, M. D. In vitro osteogenesis assays: influence of the primary cell source on alkaline phosphatase activity and mineralization. *Pathol. Biol. (Paris).* **57**, 318–23 (2009).
85. Hall, B. K. & Hall, B. K. Osteoblast and Osteocyte Diversity and Osteogenesis In Vitro. *Bones Cartil.* 401–413 (2015). doi:10.1016/B978-0-12-416678-3.00024-0
86. Hasegawa, T. Ultrastructure and biological function of matrix vesicles in bone mineralization. *Histochem. Cell Biol.* **149**, 289–304 (2018).
87. Taddei, F., Balestri, M., Rimondi, E., Viceconti, M. & Manfrini, M. Tibia adaptation after fibula harvesting: an in vivo quantitative study. *Clin. Orthop. Relat. Res.* **467**, 2149–58 (2009).
88. Langdahl, B., Ferrari, S. & Dempster, D. W. Bone modeling and remodeling: potential as therapeutic targets for the treatment of osteoporosis. *Ther. Adv. Musculoskelet. Dis.* **8**, 225–235 (2016).
89. Manolagas, S. C. Birth and Death of Bone Cells: Basic Regulatory Mechanisms and Implications for the Pathogenesis and Treatment of Osteoporosis. *Endocr. Rev.* **21**, 115–137 (2000).
90. Tou, J. C. Resveratrol supplementation affects bone acquisition and osteoporosis: Pre-clinical evidence toward translational diet therapy. *Biochimica et Biophysica Acta - Molecular Basis of Disease* **1852**, 1186–1194 (2014).
91. Aubin, J. E. & Triffitt, J. T. Mesenchymal Stem Cells and Osteoblast Differentiation. *Princ. Bone Biol.* 59–81 (2002). doi:10.1016/B978-012098652-1.50106-2
92. Scheiner, S., Pivonka, P. & Hellmich, C. Coupling systems biology with multiscale mechanics, for computer simulations of bone remodeling. *Comput. Methods Appl. Mech. Eng.* **254**, 181–196 (2013).

93. Lassen, N. E. *et al.* Coupling of Bone Resorption and Formation in Real Time: New Knowledge Gained From Human Haversian BMUs. *J. Bone Miner. Res.* **32**, 1395–1405 (2017).
94. Abdelgawad, M. E. *et al.* Early reversal cells in adult human bone remodeling: osteoblastic nature, catabolic functions and interactions with osteoclasts. *Histochem. Cell Biol.* **145**, 603–615 (2016).
95. Harvey, N., Dennison, E. & Cooper, C. Chapter 38. Epidemiology of Osteoporotic Fractures. in *Primer on the Metabolic Bone Diseases and Disorders of Mineral Metabolism* (ed. Rosen, C. J.) 197–203 (American Society for Bone and Mineral Research, 2008). doi:10.1002/9780470623992.ch38
96. Bliuc, D., Nguyen, T. V, Eisman, J. A. & Center, J. R. The impact of nonhip nonvertebral fractures in elderly women and men. *J. Clin. Endocrinol. Metab.* **99**, 415–23 (2014).
97. Gerdhem, P. Osteoporosis and fragility fractures: Vertebral fractures. *Best Pract. Res. Clin. Rheumatol.* **27**, 743–755 (2013).
98. Ringer, J. World Osteoporosis Day: A roadmap to reducing risks | LLUH News. (2018). Available at: https://news.llu.edu/patient-care/world-osteoporosis-day-roadmap-reducing-risks. (Accessed: 29th January 2020)
99. Johnell, O. & Kanis, J. A. An estimate of the worldwide prevalence and disability associated with osteoporotic fractures. *Osteoporos. Int.* **17**, 1726–33 (2006).
100. Kanis, J. A. & Johnell, O. Requirements for DXA for the management of osteoporosis in Europe. *Osteoporos. Int.* **16**, 229–38 (2005).
101. Sambrook, P. & Cooper, C. Osteoporosis. *Lancet (London, England)* **367**, 2010–8 (2006).
102. Raisz, L. G. Chapter 39. Overview of Pathogenesis. in *Primer on the Metabolic Bone Diseases and Disorders of Mineral Metabolism* (ed. Rosen, C. J.) 203–206 (American Society for Bone and Mineral Research, 2008). doi:10.1002/9780470623992.ch39
103. Khosla, S., Oursler, M. J. & Monroe, D. G. Estrogen and the skeleton. *Trends Endocrinol. Metab.* **23**, 576–81 (2012).
104. Perrien, D. S. *et al.* Aging alters the skeletal response to disuse in the rat. *Am. J. Physiol. Regul. Integr. Comp. Physiol.* **292**, R988–R996 (2007).
105. Rosen, C. J. & Bouxsein, M. L. Mechanisms of disease: is osteoporosis the obesity of bone? *Nat. Clin. Pract. Rheumatol.* **2**, 35–43 (2006).
106. Singh, L. *et al.* Aging alters bone-fat reciprocity by shifting in vivo mesenchymal precursor cell fate towards an adipogenic lineage. *Bone* **85**, 29–36 (2016).
107. Compston, J. E., McClung, M. R. & Leslie, W. D. Osteoporosis. *Lancet* **393**, 364–376 (2019).
108. Tu, K. N. *et al.* Osteoporosis: A Review of Treatment Options. *P T* **43**, 92–104 (2018).
109. Drake, M. T., Clarke, B. L. & Khosla, S. Bisphosphonates: mechanism of action and role in clinical practice. *Mayo Clin. Proc.* **83**, 1032–45 (2008).
110. Black, D. M., Abrahamsen, B., Bouxsein, M. L., Einhorn, T. & Napoli, N. Atypical Femur Fractures: Review of Epidemiology, Relationship to Bisphosphonates, Prevention, and Clinical Management. *Endocr. Rev.* **40**, 333–368 (2019).
111. Törring, O. Effects of denosumab on bone density, mass and strength in women with postmenopausal osteoporosis. *Ther. Adv. Musculoskelet. Dis.* **7**, 88–102 (2015).
112. Papapoulos, S. *et al.* The effect of 8 or 5 years of denosumab treatment in postmenopausal women with osteoporosis: results from the FREEDOM Extension study. *Osteoporos. Int.* **26**, 2773–2783 (2015).
113. Langdahl, B. L. & Andersen, J. D. Treatment of Osteoporosis: Unmet Needs and Emerging Solutions. *J. bone Metab.* **25**, 133–140 (2018).
114. Miller, P. D. Safety of parathyroid hormone for the treatment of osteoporosis. *Curr. Osteoporos. Rep.* **6**, 12–6 (2008).

# Chapter 2

# Connectivity Map-based discovery of parbendazole reveals targetable human osteogenic pathway

Andrea M Brum, Jeroen H van de Peppel, Cindy S van der Leije, Marijke Schreuders-Koedam, Marco Eijken, Bram CJ van der Eerden, & Johannes PTM van Leeuwen

*Proceedings of the National Academy of Sciences (PNAS) USA. (2015) 112(41):12711-6.*

Abstract

Osteoporosis is a common skeletal disorder characterized by low bone mass leading to increased bone fragility and fracture susceptibility. In this study, we have identified pathways that stimulate differentiation of bone forming osteoblasts from human mesenchymal stromal cells (hMSCs). Gene expression profiling was performed in hMSCs differentiated towards osteoblasts (at 6h). Significantly regulated genes were analyzed *in silico* and the Connectivity Map (CMap) was used to identify candidate bone stimulatory compounds. The signature of parbendazole matches the expression changes observed for osteogenic hMSCs. Parbendazole stimulates osteoblast differentiation as indicated by increased alkaline phosphatase activity, mineralization, and upregulation of bone marker genes (alkaline phosphatase/*ALPL*, osteopontin/*SPP1*, and bone sialoprotein II/*IBSP*) in a subset of the hMSC population resistant to the apoptotic effects of parbendazole. These osteogenic effects are independent of glucocorticoids because parbendazole does not upregulate glucocorticoid receptor (GR) target genes and is not inhibited by the GR antagonist mifepristone. Parbendazole causes profound cytoskeletal changes including degradation of microtubules and increased focal adhesions. Stabilization of microtubules by pretreatment with taxol inhibits osteoblast differentiation. Parbendazole upregulates bone morphogenetic protein *(BMP)*-2 gene expression and activity. Co-treatment with the BMP-2 antagonist DMH1 limits, but does not block parbendazole-induced mineralization. Using the CMap we have identified a novel, lineage specific, bone anabolic compound, parbendazole, which induces osteogenic differentiation through a combination of cytoskeletal changes and increased BMP-2 activity.

## 2.1 Introduction

Osteoporosis is a common and devastating bone disease characterized by reduced bone mass and increased fragility and fracture risk. It has been estimated that an osteoporotic fracture occurs once every 8 seconds worldwide[1] and direct healthcare costs in Europe alone are at least €31.7 billion annually[2]. Osteoporosis means porous bones and occurs when bone remodeling is disrupted. Bone remodeling is a balancing act between removal of old bone and formation of new bone, which is achieved by two distinct cells, the osteoclast and osteoblast, respectively. When uncoupling of these two processes takes place, bone resorption can overtake bone formation resulting in osteoporosis. Most osteoporosis treatments, such as bisphosphonates, reduce bone resorption and result in modest increases in bone density; however, these treatments do not result in a true bone anabolic effect so patients do not regain bone that has been lost at time of diagnosis. An ideal treatment would stimulate bone formation as well, to help repair the damage already done to the bone microarchitecture and strength. With this in mind, our goal was to search for novel molecules and/or mechanisms that stimulate human osteoblast differentiation and bone formation.

The connectivity map (CMap) is a web-based tool that allows for screening of compounds against a genome-wide disease or physiological gene signature[3,4]. This is achieved by comparing microarray data from over 1300 small molecules to a user's selected gene signature of the phenotype of interest using a pattern-matching algorithm with a high level of resolution and specificity. This results in a list of compounds with a highly correlating gene expression pattern to that of the phenotype of interest, which has the potential to aid in finding a novel treatment for a disease or to identify novel pathways or genes involved in a complex biological process. To date, the CMap has been successfully used to identify compounds and combination therapies that show promise in the treatment of osteoarthritic pain[5], adenocarcinoma[6], kidney disease[7], gliomas[8], and NK cell neoplasms[9].

Our aim was to identify novel anabolic therapeutic targets by genomic, proteomic and bioinformatic dissection of human mesenchymal stromal cell (hMSC)-derived osteoblasts. Therefore, we utilized the CMap to identify compounds with a matching gene expression profile to human mesenchymal stem cells undergoing osteogenic differentiation. By following this approach, we aimed to not only discover novel compounds that stimulate osteogenic differentiation, but also novel processes underlying this process.

## 2.2 Results

*Parbendazole has the strongest correlating gene signature to hMSCs undergoing osteoblast differentiation*

Using a pattern-matching algorithm, the CMap links compounds with disease or physiological phenotypes by measuring similarities in gene expression[3]. To identify compounds that may exert bone anabolic effects due to their ability to stimulate genes regulated during osteoblast differentiation, we performed a CMap analysis in which we searched for drugs that have a gene expression pattern positively correlating to hMSCs differentiating towards osteoblasts (Appendix C, **Table A1**). Multiple drugs were identified that have a significantly correlating gene expression pattern to that of differentiating human osteoblasts, including dexamethasone (dex) and a number of other corticosteroids (**Table 1**). These results demonstrate the validity of the CMap, because dex is the compound that we originally used to stimulate osteoblast differentiation and glucocorticoid (GC)-mediated activation of the glucocorticoid receptor (GR) is the classical stimulus for *in vitro* human osteoblast differentiation. As our aim was to identify novel compounds/pathways that stimulate osteoblast differentiation, we excluded any corticosteroid compound for further testing. We found that the strongest correlating compound ($p < 0.0001$) (**Table 1**), and only non-corticosteroid in the top 8 compounds, is the benzimidazole anthelmintic parbendazole. Based on these results we chose to scrutinize the effects parbendazole has on hMSCs in regard to its osteogenic potential.

**Table 1: CMap permuted results showing compounds with significant positive correlation to the osteogenic hMSCs gene.**

| Rank | Compound Name | Cell Line | Mean CMap Score | n | p-value |
|---|---|---|---|---|---|
| 1 | Parbendazole | PC3 | 0.855 | 2 | <0.00001 |
| 2 | Dexamethasone | PC3 | 0.913 | 2 | <0.00001 |
| 3 | Fludrocortisone | PC3 | 0.768 | 2 | 0.00002 |
| 4 | Halcinonide | PC3 | 0.788 | 2 | 0.00002 |
| 5 | Fludroxycortide | PC3 | 0.775 | 2 | 0.00002 |
| 6 | Flumetasone | PC3 | 0.854 | 2 | 0.00002 |
| 7 | Flunisolide | PC3 | 0.718 | 2 | 0.00002 |
| 8 | Fluocinonide | PC3 | 0.72 | 2 | 0.00002 |

Top matching compounds from the Connectivity Map based on the average of the replicates of a single compound for each cell line. Shading indicates a glucocorticoid. Top matching compound and only non-glucocorticoid, parbendazole, in white. Rank is based on the p-value calculated from the CMap scores all of the replicates of a single compound in a single cell line. Score is based on the relative strength of a given signature in an instance from the total set of instances calculated upon execution of a query.

*Parbendazole induces osteoblast differentiation of hMSCs in vitro*

Similar to the known stimulator of osteogenic differentiation, dex, parbendazole treatment stimulated alkaline phosphatase (ALP) activity after 1 week of culture and mineralization after 3 weeks of culture, dose-dependently up to 4 µM (Fig. **1A and B**, respectively). We confirmed the dose-dependent parbendazole-induced mineralization by alizarin red staining (Fig. **1C**). These results show that parbendazole induces biochemical changes in hMSCs leading to osteoblast differentiation and mineralization.

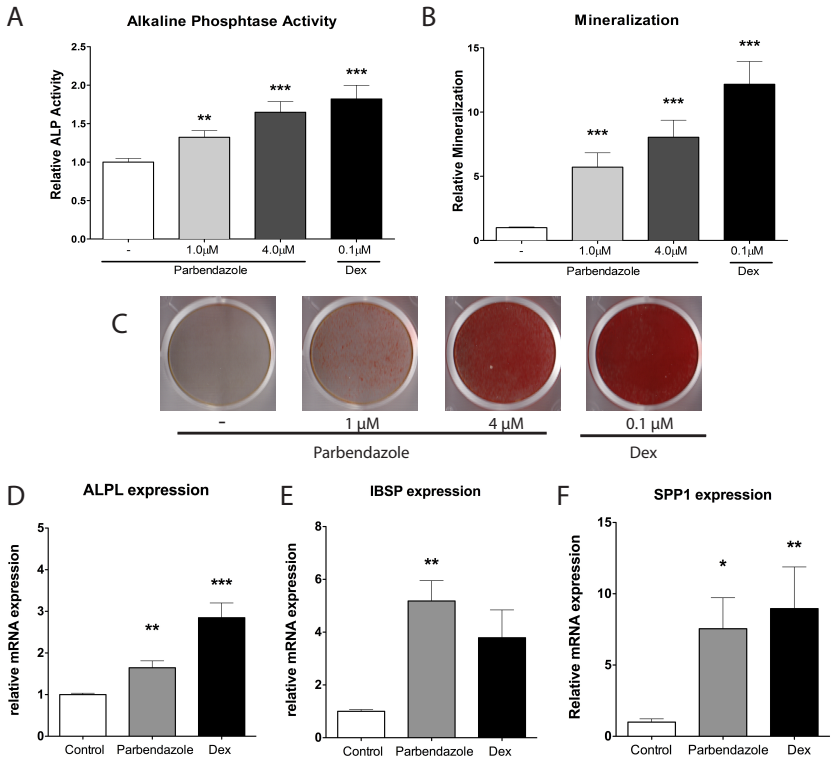


**Figure 1. Parbendazole induces osteogenic differentiation of hMSCs**. Results of ALP activity after 1 week of culture (A) and mineralization after 3 weeks of culture (B) in hMSCs treated with 1 µM parbendazole (light gray bar), 4µM parbendazole (dark gray bar) compared to negative control (control medium) (white bar) or positive control (0.1 µM dex) (black bar) treated cells. (C) Dose dependent induction of mineralization was confirmed by alizarin red staining after 3 weeks of culture. mRNA expression levels of *ALPL* (D), *IBSP* (E) and *SPP1* (F) 7 days after the start of treatment with control medium (white bar), 4 µM parbendazole (gray bar) or 0.1 µM dex (black bar) as assessed by quantitative PCR. For biochemistry n=12. For PCRs n=6. * $p < 0.05$, ** $p < 0.01$, *** $p < 0.001$. Results are presented relative to control.

We also examined if the most effective dose of parbendazole, 4µM, induces expression of well-known osteoblast marker genes by performing quantitative PCRs on hMSCs treated with parbendazole for 7 days. Parbendazole significantly increased

the expression of alkaline phosphatase (*ALPL*) (Fig. **1D**) as well as the genes encoding the matrix proteins bone sialoprotein (*IBSP*) and osteopontin (*SPP1*) (Fig. **1E-F**).

Simian virus-immortalized human fetal osteoblasts (SV-HFO), a human pre-osteoblastic cell line, treated with parbendazole did not mineralize (Fig. 2**A**) and total protein was decreased by parbendazole (Fig. **2B)** at the doses stimulating osteogenesis in the hMSCs.

Taken together, these results demonstrate that parbendazole induces osteogenic differentiation of hMSCs independent of the known osteogenic stimulus, dexamethasone.

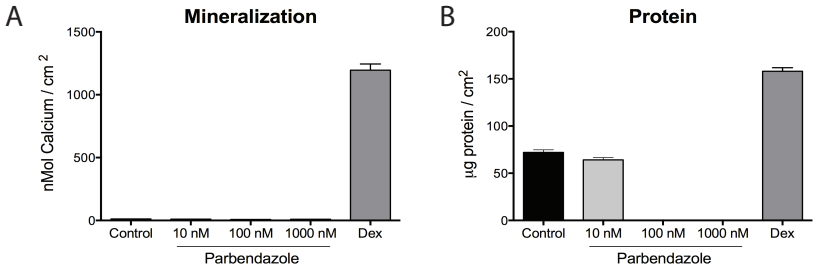


**Figure 2. Parbendazole does not induce osteogenic differentiation in human pre-osteoblast cells (SV-HFOs), but does reduce total protein.** Results of mineralization (A) and total protein content (B) after 3 weeks of culture in SV-HFOs treated with 1 µM parbendazole (light gray bar), 100 nM parbendazole (medium gray bar), and 10 nM parbendazole (dark gray bar) compared to negative control (control medium) (black bar) or positive control (100 nM dex) (darkest gray bar) treated cells. n=3. Results are of 1 representative experiment.

*Parbendazole increases both apoptosis and proliferation*

To determine how parbendazole may affect hMSC viability we used Fluorescence-Activated Cell Sorting (FACS) analysis to look at apoptosis and proliferation. Parbendazole increased apoptosis at day 5 and 8 of culture compared to control-treated hMSCs (44.8-58.5% vs. 15.8-17.9%, respectively) (Fig. **3A**). We also found that at days 5 and 8 of culture, parbendazole significantly increased proliferation compared to control-treatment (24.7-26.1% vs. 9.1-10.4% Ki67+, respectively) (Fig. **3B**). To verify the overall viability of hMSCs treated with parbendazole, we performed a PrestoBlue assay, a metabolism-based assay as a read out for cell viability. Parbendazole treatment led to a decrease in cell viability compared to both controls and dex-treated hMSCs starting at day 4 of culture (Fig. **3C**). These findings reveal that parbendazole is capable of increasing both proliferation and apoptosis in hMSCs and because apoptosis (i.e., increased cell death and decreased cell survival) exceeds proliferation conditions, the total accumulation of cells is reduced in parbendazole-treated cells.

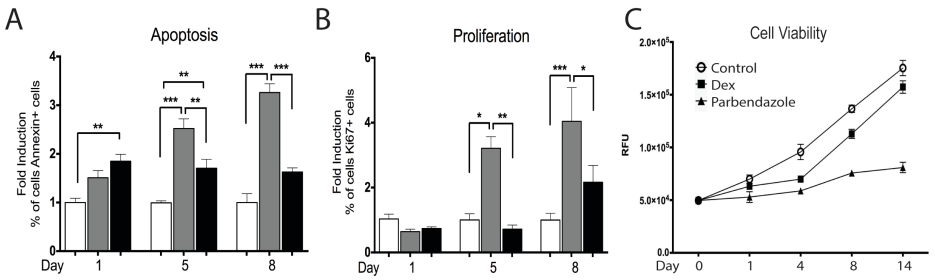


**Figure 3. Parbendazole treatment decreases cell viability by increasing apoptosis.** (*A*) FACS assessment of hMSCs treated with control medium (white bar), 4 μM parbendazole (gray bar), or 0.1 μM dex (black bar) and stained with annexin to determine combined early and late apoptosis. (*B*) FACS assessment of hMSCs treated with control medium (white bar), 4 μM parbendazole (gray bar), or 0.1 μM dex (black bar) and stained with Ki67 to determine proliferation ($n = 7$). (*C*) Relative cell viability was assessed by PrestoBlue assay as represented by the relative fluorescence units (RFU). $*P < 0.05$, $**P < 0.01$, $***P < 0.001$. Results are presented relative to control at each time point.

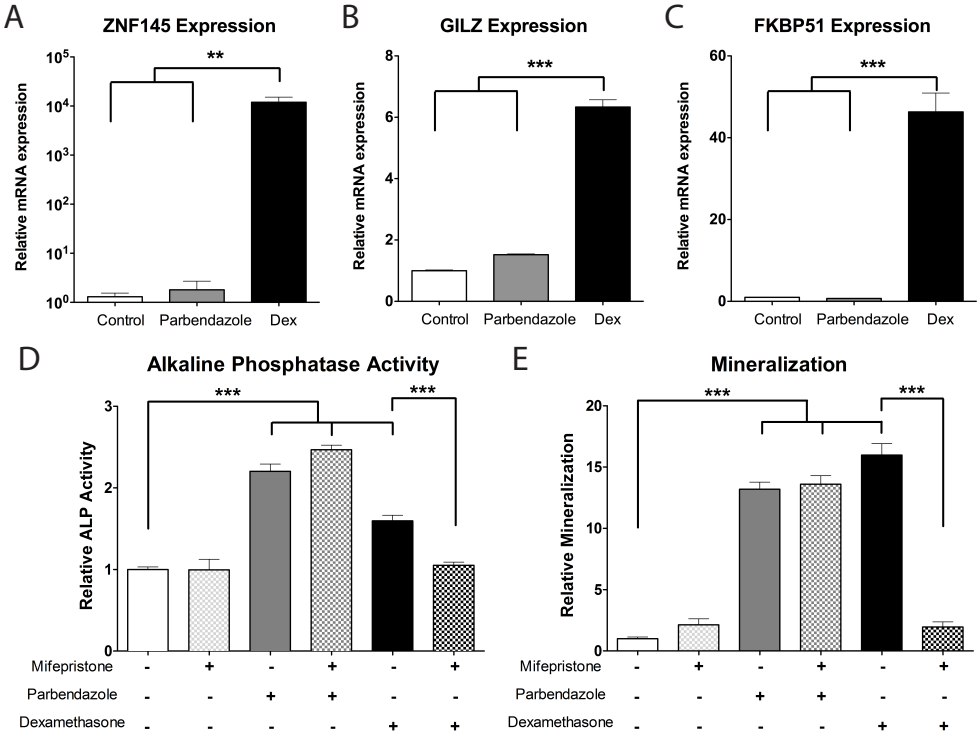


**Figure 4: Parbendazole induced osteoblast differentiation is independent of glucocorticoid receptor signaling.** (A,B,C) Quantitative PCR results from hMSCs incubated with parbendazole and from control hMSCs either undifferentiated or differentiated with dex. Relative gene expression of direct glucocorticoid receptor signaling targets, *ZNF145* (A), *GILZ* (B) and *FKBP51* (C) of hMSCs treated with control medium (white bar), 4 μM parbendazole (gray bar) or 0.1 μM dex (black bar) for 24 hours. Biochemical assays for ALP (Day 6) (D) and mineralization (week 3) (E) of hMSCs treated with control medium (white bar), 4 μM parbendazole (gray bar) or 0.1 μM dex (black bar) with (patterned bars) or without (solid bars) the GR antagonist, mifepristone, throughout the culture period. n=6. ** $p < 0.01$, *** $p < 0.001$. Results are presented relative to control at each time point.

*Parbendazole induces osteoblast differentiation independent of glucocorticoid receptor signaling*

To determine if parbendazole induces osteogenic differentiation through direct GR–mediated stimulation of osteoblast marker genes, similar to dex, we performed quantitative gene expression analyses for known GR target genes following parbendazole treatment. Dex-induced osteoblast differentiation strongly upregulated the GR target genes *ZNF145, GILZ*, and *FKBP51* (up to 10,000 fold), while parbendazole treatment did not (Fig. **4A-C**), implicating that parbendazole acts independent of GR signaling. We then cultured dex- or parbendazole-treated hMSCs in combination with the GR antagonist mifepristone (RU486), which blocks signaling through the GR, and performed biochemical assays for osteoblast differentiation. Whereas mifepristone had no effect on induction of ALP activity (Fig. **4D**) or mineralization (Fig. **4E**) by parbendazole, it completely abolished dex-induced increases in ALP activity (Fig. **4D**) and mineralization (Fig. **4E**). These results prove that parbendazole induces human osteoblast differentiation independent of GR signaling.

*Parbendazole inhibition of microtubule polymerization is required for parbendazole-induced osteogenic differentiation*

Parbendazole is known to be an inhibitor of microtubule formation[10] and we confirmed this in our hMSCs. In control (Fig. **5A,D,J**) and dex-treated (Fig. **5C,F,L**) cultures, both the actin and microtubule structures are similarly distributed throughout the cell, while in parbendazole treated hMSCs the microtubule structure is severely degraded, leaving only short strands of microtubule filaments surrounding the nucleus (Fig. **5E,K**). However, we observed numerous thick, crossing actin stress fibers present in cells treated with parbendazole (Fig. **5B**), while in control treated cells the actin filaments were primarily organized parallel to the cell axis (Fig. **5A**). To determine whether degradation of the microtubule structure is required for parbendazole-induced osteogenic differentiation we used the microtubule stabilizing agent paclitaxel (taxol). Taxol completely abolished the parbendazole-induced mineralization of hMSCs (Fig. **6**). These results clearly demonstrate that inhibition of microtubule formation is required for parbendazole to elicit osteogenic differentiation of hMSCs.

*Parbendazole increases focal adhesions*

Based on the evidence that cytoskeletal changes are induced by parbendazole during hMSC osteogenic differentiation, and previous evidence that cytoskeletal changes and integrin binding and signaling play a significant role in osteoblast

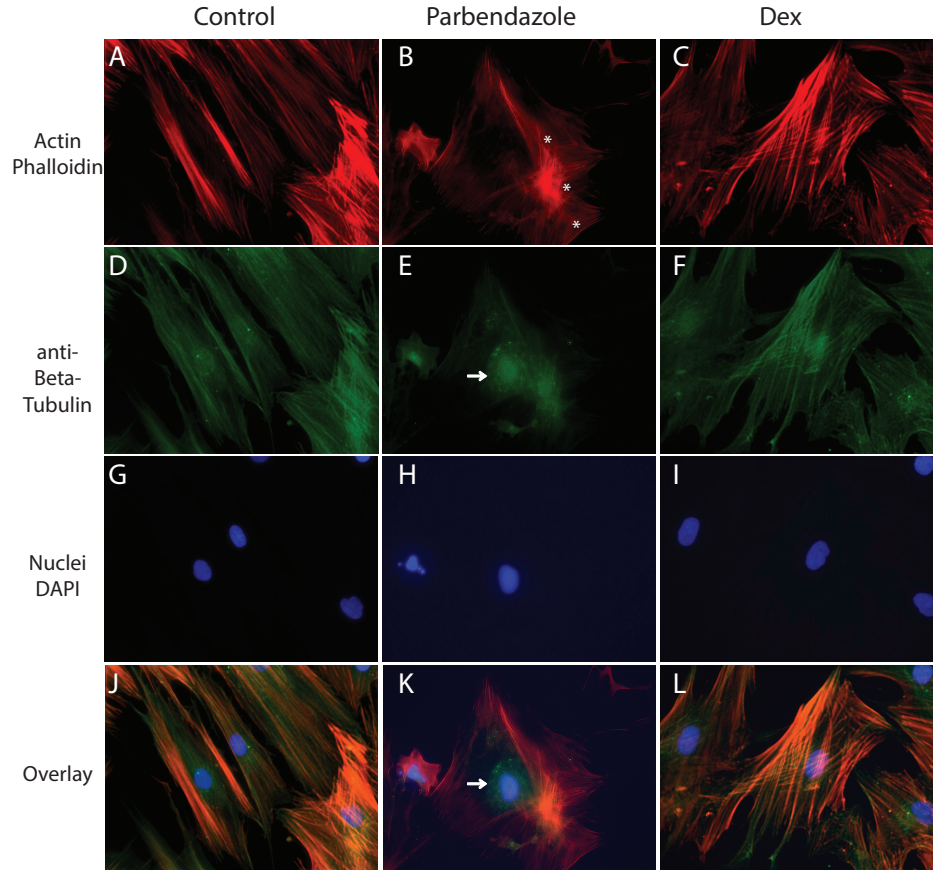


**Figure 5. Parbendazole inhibits microtubule polymerization**. hMSCs were incubated with control medium (A,D,G,J), 4 μM parbendazole (B,E,H,K), or 0.1 μM dex (C,F,I,L) for 4 days and then the actin and tubulin cytoskeleton were visualized by immunofluorescence microscopy using phalloidin and β-tubulin antibodies. Parbendazole treatment inhibits microtubule formation (E,K), with only small microtubules remaining perinuclear (white arrow). Crossing of the actin microfilaments can also be seen in parbendazole treated cells (white asterisks). 630x magnification.

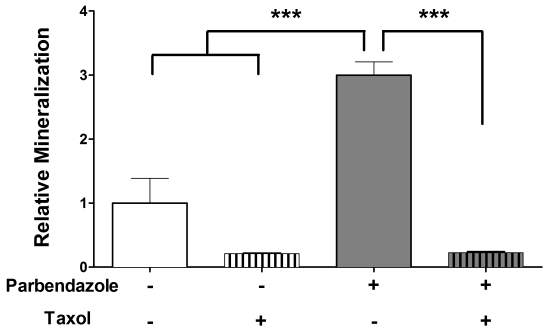


**Figure 6. Parbendazole inhibition of microtubule polymerization is required for parbendazole induced osteogenic differentiation**. Mineralization in hMSCs treated with control medium (white bar) or 4μM parbendazole (gray bar) in combination with (striped bars) or without (solid bars) the microtubule stabilizing drug taxol. n=6 *** $p < 0.001$. Results are presented relative to control.

differentiation[11-13], we investigated whether focal adhesions (FAs) are also affected by parbendazole. Analysis of immunofluorescent images show that FAs appear to be longer and more numerous following parbendazole treatment (Fig. **7E,K,N**) compared to control treatment (Fig. **7D,J,M**). Quantification of the FAs revealed that parbendazole treatment significantly increased the number of focal adhesions compared to both control and dex treatment (Fig. **8A**) and increased their length compared to control (Fig. **8B**) after 24 hours of treatment.

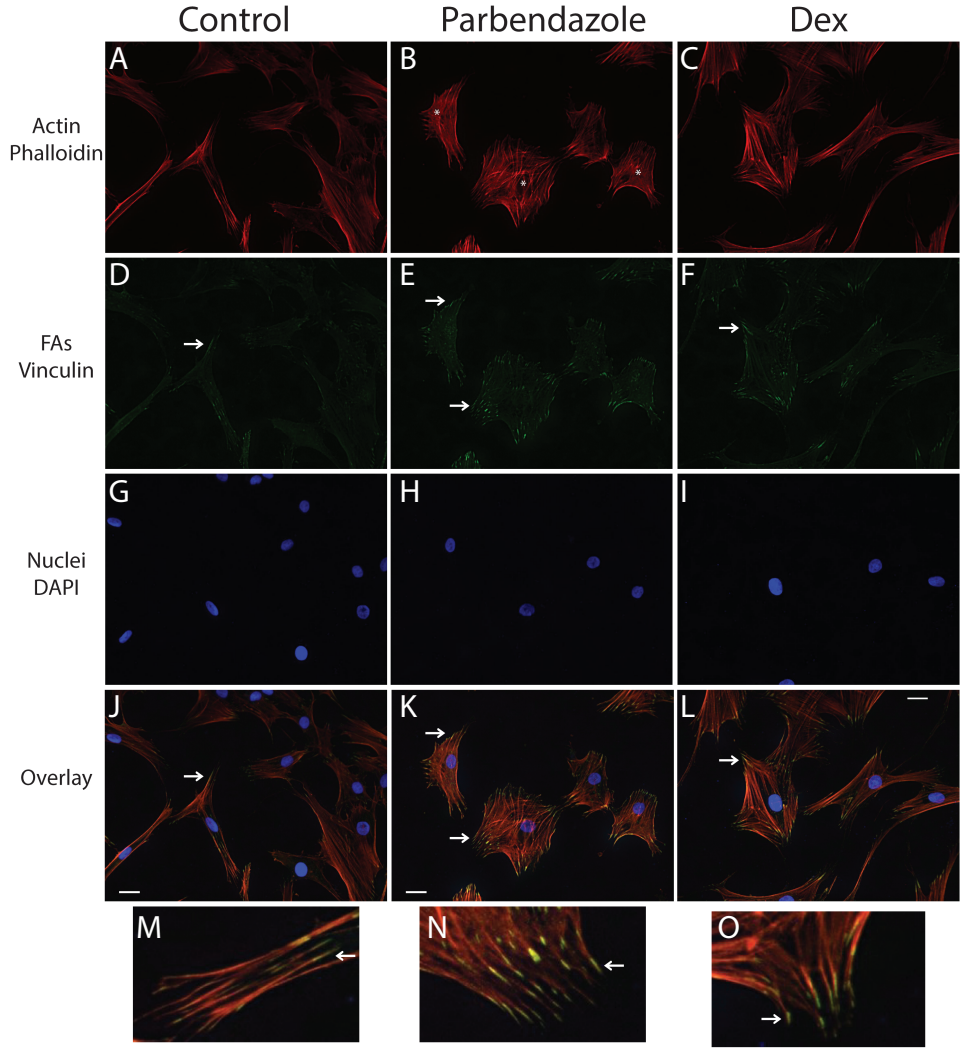


**Figure 7. Parbendazole affects focal adhesions.** hMSCs were incubated with control medium (A,D,G,J,M), 4 μM parbendazole (B,E,H,K,N), or 0.1 μM dex (C,F,I,L,O) for 24 hours and actin microfilaments and FAs were visualized by immunofluorescence microscopy using phalloidin and vinculin antibodies. FAs are identified by the filled arrow heads. Crossing of the actin microfilaments can also be seen in parbendazole treated cells (star). 20μM scale bar. 400x magnification.

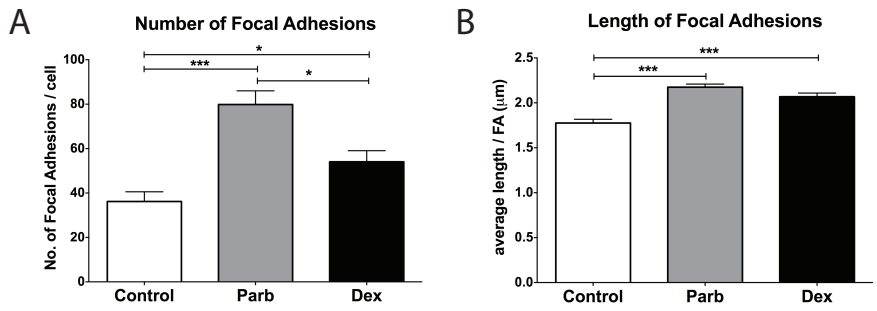


**Figure 8. Parbendazole increases number and length of focal adhesions.** Quantification of the number of (A) length (B) of focal adhesions was performed on control, parbendazole and dex treated hMSCS. n=28-30 cells. * $p < 0.05$ **, $p < 0.01$ ***, $p < 0.001$.

*Parbendazole increases BMP-2 expression and activity*

It has previously been demonstrated that microtubule inhibitors stimulate osteoblast differentiation and increase bone mass in mice through elevated levels of BMP-2[14,15]. We show that parbendazole significantly increased *BMP2* expression (Fig. **9A**), while dex significantly inhibited *BMP2* expression compared to control treated cells. To determine BMP bioactivity stimulated by parbendazole we employed a C2C12-BRE-Luc reporter cell line[16,17]. Incubation with conditioned media from hMSCs treated with parbendazole for 48 hours significantly increased luciferase activity (Fig. **9B**), while conditioned medium from control and dex treatment had no effect. These results show that parbendazole stimulates BMP-2 signaling in hMSCs.

*Inhibiting BMP-2 signaling limits parbendazole induced osteogenic hMSCs differentiation*

To determine whether BMP-2 is involved in the osteogenic effect of parbendazole, we used the BMP-specific antagonist DMH1[18]. These studies demonstrated significant interaction between parbendazole and DMH1 resulting in limitation of osteogenic differentiation following the co-treatment of parbendazole and DMH1 compared to parbendazole or DMH1 alone (Fig. **9C**). This reveals that BMP-2 signaling is involved in the effect of parbendazole on osteoblast differentiation of hMSC. In the control condition, DMH1 induced mineralization in hMSCs cultures, which is consistent with the results of Rifas[19] showing that inhibition of BMP signaling by another BMP antagonist noggin resulted in osteogenic differentiation of hMSCs.

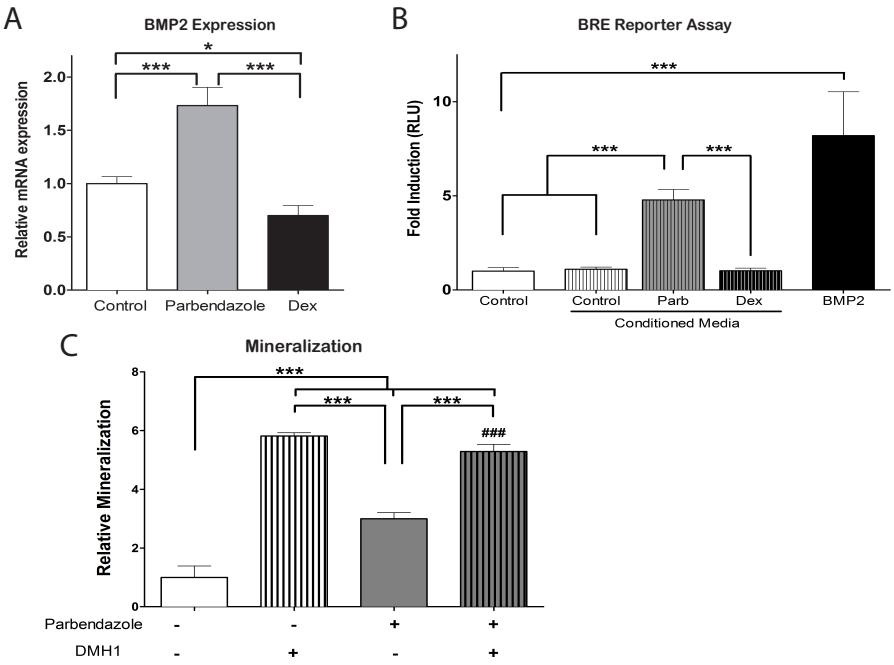


**Figure 9. Parbendazole regulates BMP-2 expression and activity**. (A) Gene expression of *BMP2* after treating hMSCS for 24 hours with control medium (white bar), 4 μM parbendazole (gray bar), or dex (black bars). (B) Luciferase reporter assay for BMP signaling reporter BRE-Luc of control medium (solid white bar), conditioned medium from hMSCs treated from control (white patterned bar), 4 μM parbendazole for 48 hours (gray patterned bar), or 0.1 μM dex (black patterned bar) for 48 hours, and the positive control, recombinant BMP-2 protein (black bar). (C) Pretreatment of hMSCs with the BMP inhibitor DMH1 (patterned bars) enhances mineralization. Relative mineralization in hMSCs cultures following control (white bar), DMH1 (white patterned bar), parbendazole (gray bar), and parbendazole + DMH1 (gray patterened bar) treatment. n=6. *** $p < 0.001$ by one-way ANOVA. ### $p < 0.001$ by two-way ANOVA. Results are presented relative to control.

## 2.3 Discussion

Using the CMap, we were able to identify a compound with a highly significant positively correlating gene expression profile to that of differentiating human osteoblasts. As expected, the top of the list of compounds was dominated by glucocorticoids, including dexamethasone; however, the top resulting compound was found to be parbendazole. We confirmed the validity and power of the CMap approach by demonstrating that parbendazole, independent of an additional osteogenic stimulus such as dexamethasone, is able to stimulate human osteoblast differentiation as evidenced by increased ALP activity, mineralization and up-regulation of genes known to be important in osteoblast differentiation and function. Mechanistically, we showed that the osteogenic effect of parbendazole occurs independent of glucocorticoid receptor signaling, but rather via affecting microtubule formation and cytoskeletal organization. Overall, our findings demonstrate that by

using the CMap, we identified a novel compound that independently stimulates human osteogenic differentiation.

The web-based resource CMap was created to identify compounds that induce a similar or opposite effect on the physiological processes or diseases of interest; as a consequence, it is a bioinformatics tool to identify novel applications for established drugs. The CMap uses several human tumor cell lines, including PC3, MCF7, and HL60, to generate gene expression profiles of more than 1300 compounds. Interestingly, all of the top eight compound profiles most strongly correlating with our human osteoblast expression profile are derived from the PC3 cell line, a cell line originating from a bone metastasis of a prostate tumor[20]. An explanation for this intriguing observation is lacking, but it is tempting to hypothesize that, based on our CMap results, there must be a resemblance in the genomic profile of both osteogenic hMSCs and the bone metastatic PC3 cells, which is potentially linked to both of their abilities to thrive in the bone environment. A prerequisite of the CMap approach for discovering bone anabolic compounds is that one has to assume similarities in how different cell types respond to the same compound regarding gene expression. However, the evidence presented here and the growing evidence from other groups[5-9], strongly supports the concept that CMap is a potent tool for identification of compounds with medicinal benefit for a wide range of diseases.

Benzimidazoles, including parbendazole, are a class of compounds that consist of the fusion of benzene and imidazole rings and are primarily used as anthelminthics[21]. The majority of these family members have a similar mechanism of action-namely, preventing tubulin polymerization through specific binding to tubulin[22,23]. Parbendazole is no exception: it binds the tubulin dimer with a mol:mol stoichiometry and microtubules withdraw from the peripheral area of the cell within 30 min of treatment with parbendazole[10]. Our immunocytological findings in osteogenic hMSC are consistent with the findings by Havercroft and coworkers. Disassembly of microtubules in other cell types has been associated with blebbing of the plasma membrane, indicative of apoptosis. Our FACS results showing that parbendazole treatment increases the number of annexin V positive cells in our cultures supports the idea that microtubule inhibition leads to increased apoptosis. However, Havercroft *et al.*[10] also showed that after 1 day of parbendazole treatment, cells flattened out without any signs of plasma membrane blebbing, despite absent microtubules. This morphology correlates to our observation that a subset of parbendazole-treated hMSCs displays a flattened, widespread morphology. Interestingly, although we do see an increase in apoptosis, we also observe an increase in the proliferation marker Ki67 at day 5 and 8 in hMSCs treated with parbendazole,

which indicates that there are at least two populations of MSC in the bone marrow with different sensitivity to parbendazole. One population, likely the true stem cells, is resistant to the apoptotic effects of parbendazole and are induced to proliferate and eventually differentiate and mineralize, and another population, the pre-committed cells, that undergoes apoptosis. Taking the hMSC FACs data together with the biochemical results in the SV-HFOs we propose that parbendazole acts at the stage of lineage allocation in hMSCs.

Microtubules are highly dynamic cytoskeletal elements that undergo continuous assembly and disassembly to maintain normal function[24,25]; they play an essential role in a variety of cellular processes including mitosis, cell motility, and intra- and intercellular trafficking[26], but are also taking part in various signaling pathways including those involving sonic hedgehog, Wnt, and MAPK[24,27]. Microtubules act as binding sites for a number of proteins and transcription factors, including RUNX2; and in the case of RUNX2, modulate transcriptional activity by acting as a shuttle between the nucleus and cytoplasm[28]. It has been shown previously that taxol treatment leads to depletion of nuclear levels of RUNX2[28], this could also be one explanation for our results demonstrating that taxol pretreatment blocks the osteogenic effect of parbendazole. Chang, *et al.*[29] observed that short-term treatment of MSCs with a related compound, nocodazole, increased cell contractility and cytoskeletal tension followed by enhanced osteoblast differentiation. Cytoskeletal tension rises, and perhaps even directly stimulates, osteoblast differentiation through changes in the actin cytoskeleton[13,30-33]. In addition, disruption of the tubulin organization also affects the kinetics of actin organization[13], indicating a regulatory role for microtubules in actin reorganization. Cytoskeletal rearrangements may also affect osteoblast differentiation through enhanced integrin signaling. FA complexes and integrins are known to directly interact with extracellular matrix proteins, including SPP1 and IBSP, which play a critical role in osteoblast survival and differentiation[11,30,34,35]. An increased number of FAs is proposed to increase adhesion to the extracellular matrix[35,36], which may also contribute to osteogenic differentiation. The fact that parbendazole treated hMSCs display a widespread, flattened morphology, prominent and rearranged actin fibers, increased focal adhesion complexes, and higher expression of *SPP1* and *IBSP*, supports the idea that cytoskeletal rearrangements contribute to osteoblast differentiation through enhanced integrin signaling and/or matrix binding. Liu et al.[14] demonstrated a role for microtubule inhibitors as a bone anabolic drug by showing that stathmin, a ubiquitously expressed protein that inhibits microtubule assembly, promotes osteoblast differentiation and inhibits osteoclast activity; and mice lacking stathmin are osteopenic as a consequence of decreased osteoblast numbers and differentiation,

and increased numbers of osteoclasts. Our results, demonstrating that changes in the balance between the tension forces of the microfilaments and the compression forces of the microtubules elicit changes in the cellular shape, function and cell fate, are in line with the cellular tensegrity model[37,38] and with previous findings that changes in cell shape and cytoskeleton can strongly influence hMSC lineage decision-making[39].

There is growing evidence that microtubule inhibitors have a positive effect on bone formation and osteoblast differentiation through increased BMP signaling. Zhao et al.,[15] showed that several types of microtubule inhibitors, including nocodazole and TN16, increased *Bmp2* expression and ALP activity in murine osteoblasts; additionally, the authors showed that short-term administration of TN16 locally over the calvaria or systemically in mice lead to increased calvarial periosteal bone formation and trabecular volume in long bones, respectively. It was shown in murine osteoblasts that the osteogenic effect of the inhibition of microtubule assembly is due to increased cytoplasmic Gli2 protein concentration through disassociation of the microtubule-Gli-Ci complex that would otherwise lead to proteasomal degradation of Gli2 (15). Gli2 enhances *Bmp2* expression through BMP promoter binding[40]. Bmp-2 is known to be a potent stimulator of osteoblast differentiation in murine cells[41,42, reviewed by 43], but the evidence for BMP-2 effects on human osteogenic differentiation *in vitro* is conflicting, ranging from strongly enhancing osteogenic differentiation[44,45] to having no positive effect[46,47]. This may be, in part, due to differences in the BMP receptor expression profiles by the various osteoblast precursors and hMSC donors[44,47]. Clinical trials looking at the efficacy of BMP-2 in fracture healing and fusions are mixed; two recent independent meta-analyses of human clinical trials comparing recombinant human BMP-2 to autologous bone grafts in spinal fusions found no significant difference in healing or pain[48,49]. In this study we found that parbendazole treatment induces both *BMP2* expression and BMP activity as evidenced by our gene expression and reporter assay data. In support of this, the BMP inhibitor DMH1[18] seems to limit the parbendazole-induced osteoblast mineralization in our hMSC cultures, but does not completely block it. Thus, our data confirms a parbendazole-induced human osteogenic pathway through inhibition of microtubule assembly and increased BMP-2 activity.

In summary, we conclude that the CMap identified compound parbendazole is a novel compound that stimulates human osteoblast differentiation *in vitro*. We have proven that parbendazole, independent of additional osteogenic stimulus, stimulates ALP activity and mineralization, and up-regulates genes important in osteoblast differentiation and extracellular matrix production in a subset of hMSCs resistant to its apoptotic effects. In line with previous reports of other microtubule inhibitors, the stimulatory effect of parbendazole is partly due to increased BMP-2 activity; however,

additional cytoskeletal driven mechanisms, such as cytoskeletal associated proteins and transcription factors, and integrin signaling, are likely to be of equal or greater importance in stimulating osteogenic differentiation of hMSCs. Though we do not propose parbendazole itself to be the ideal bone anabolic drug for treatment of osteoporosis in humans, the evidence presented here significantly strengthens the concept that cytoskeletal changes strongly influence hMSC lineage allocation and osteoblast differentiation. We envisage that cytoskeletal manipulation, or the downstream processes that results from it, hold promise as novel anti-osteoporotic treatments, but this will need to be studied further. We have also clearly demonstrated the power of the CMap as an effective tool to discover novel bone anabolic compounds.

## 2.4 Materials and Methods

*Materials*

MSCs were purchased from Lonza (MSC; PT-2501, Walkersville, MD). αMEM was purchased from Gibco BRL, Life Technologies (Paisley, UK). Dexamethasone, β-glycerophosphate, mifepristone, paclitaxel (taxol), DMH1. The calcium assay kit, alizarin Red S, ethanolamine, triton X-100, mouse monoclonal anti-β-tubulin antibody, and oligonucleotide primer pairs were purchased from Sigma–Aldrich (St. Louis, MO, USA). TRIzol, PrestoBlue cytotoxicity assay reagent, and rabbit monoclonal ABfinity anti-vinculin antibody were purchased from Invitrogen (Carlsbad, CA, USA). Illumina Human HT-12 v3 BeadChip arrays, iScan, GenomeStudio V2010.1 (Gene Expression Module 1.6.0) were obtained from Illumina Inc. (Eindhoven, The Netherlands). 2100 Bioanalyzer from Agilent Technologies (Santa Clara, CA, USA). Illumina TotalPrep RNA Amplification Kit was purchased form Ambion (Austin, TX, USA). Streptavidin-Cy3 was purchased form GE Healthcare (Piscataway, NJ, USA). BCA™ protein assay reagent A and B were purchased from Pierce (Rockford, IL). Victor2 plate reader and Steady Lite Plus Luciferase reagent was purchased from PerkinElmer Life and Analytical Science. All FACS antibodies, the Accuri C6 Personal Flow Cytometer and BD Accuri C6 software analysis program were obtained from Beckon Dickinson (Breda, The Netherlands). Alexa Fluor® 488 Goat Anti-Mouse IgG, rhodamine–conjugated phalloidin, and Alexa Fluor® 488 Goat Anti-Rabbit IgG were purchased from Molecular Probes. Vectashield mounting medium containing DAPI was from Vector Laboratories (Burlingame, CA, USA).

*Cell culture*

Human bone marrow-derived Mesenchymal Stromal Cells were cultured as described previously[50,51]. For osteogenic differentiation, MSCs were cultured in αMEM medium containing 10% heat-inactivated fetal calf serum supplemented with 100 nM dexamethasone (dex) or with various concentrations (ranging from 0.1 to 4 μM) of parbendazole, both in combination with 10 mM β-glycerophosphate. Where applicable hMSCs were treated with 10μM mifepristone, 0.1 μM paclitaxel (taxol) or 0.5μM DMH1, a highly selective dorsomorphin analogue, in β-glycerophosphate containing medium alone or 30 minutes prior to adding parbendazole or dex. Cell extracts were harvested at different time points during culture by scraping the cells in PBS/triton and storing at -80ºC for biochemical analyses or in TRIzol and stored at -20ºC for gene expression analyses. Alternatively, cells were fixed in 4% phosphate-buffered paraformaldehyde for immunocytochemical procedures or 70% ethanol for alizarin red staining.

*Illumina gene chip–based gene expression*

For analysis of whole human genome expression, we used Illumina Human HT-12 v3 BeadChip arrays. Human MSCs (in triplicate) were treated for 6 hours with dexamethasone and next RNA was isolated as previously described[51]. RNA integrity of isolated RNA was assessed by RNA 6000 Nano assay on a 2100 Bioanalyzer. The Illumina TotalPrep RNA Amplification Kit was used for RNA amplification of each sample according to manufacturer's instructions. In short, T7 oligo(dT) primer was used to generate single-stranded cDNA, followed by a second-strand synthesis to generate double-stranded cDNA. Biotin-labeled cRNA was synthesized using T7 RNA polymerase. The cRNA was column-purified and checked for quality by RNA 6000 Nano assay. A total of 750 ng of cRNA was hybridized for each array using the standard Illumina protocol, using streptavidin-Cy3 for detection. Slides were scanned on an iScan and analyzed using GenomeStudio.

*Microarray analysis*

Background was subtracted from the raw data using GenomeStudio V2010.1 (Gene Expression Module 1.6.0), and data were processed, using the Bioconductor R2.10.0 Lumi package (www.bioconductor.org)[52]. Data were transformed by variance stabilization and quantile normalization. Probes that were detected at least once in the experiments (Illumina detection p-value < 0.01) were considered to be expressed and were further analyzed. Differentially expressed probes were identified using Bioconductor Package Limma (www.bioconductor.org)[53] with p-values adjusted to reduce the false discovery rate (FDR; p <0.001).

*Connectivity map query*

To find compounds that have similar gene expression patterns compared to our human osteogenic differentiation-induced gene expression patterns, we generated gene signatures from microarray gene expression analyses of bone marrow-derived hMSCs treated with dex to stimulate osteogenic differentiation. We identified the 100 most significantly ($Z<0.001$) up- and downregulated probes based on log ratio of gene expression during osteogenic differentiation at 6 hours following the start of differentiation treatment, compared to time 0. We chose this time point to be able to temporally match it with the time of incubation of each compound within the CMap. Illumina probe IDs were converted to Affymatrix probe IDs, which are required for input into the CMap. After removal of duplicates we ended up with 77 up-regulated genes and 66 down-regulated genes (Apendix A, **Table A1**) that we submitted simultaneously for our CMap query (build02, http://www.broadinstitute.org/cmap/). Each signature was queried against the CMap using the gene set enrichment analysis algorithm described by Lamb *et al.*[3].

*Alkaline phosphatase, mineralization and protein assays*

Alkaline phosphatase (ALP) and calcium measurements were performed as described previously[54]. Briefly, ALP activity is determined by an enzymatic reaction, where the ALP-mediated conversion of PNPP to PNP during 10 min at 37°C is measured. For calcium measurements, cell lysates were incubated overnight with 0.24 M HCl at 4°C. Calcium content was determined colorimetrically with a calcium assay kit according to the manufacturer's description. ALP results were adjusted for protein content of the cell lysates. For protein measurement, 200 µl of working reagent was added to 10 µl of sonicated cell lysate. The mixture was incubated for 30 min at 37°C, cooled down to room temperature (RT) and absorbance was measured at 595 nm. All measurements were performed using a Victor2 plate reader. Staining for mineralization was performed as described previously[51]. Briefly, cells were fixed with 70% ethanol and after washing they were stained for 10-20 min with alizarin Red S solution.

*Quantification of mRNA expression*

Cultures continuously treated with control, 100 nM dex or 4 µM parbendazole were harvested during the early or middle differentiation period (6 hours, 24 hours, and 7 days). RNA isolation, cDNA synthesis and PCR reactions were performed as described previously[51]. Oligonucleotide primer pairs were designed to

be either on exon boundaries or spanning at least one intron (**Table 2**). Gene expressions were corrected for the housekeeping gene GAPDH.

**Table 2: Sequences of primer sets used for quantitative PCR in this study.**

| Gene | Forward Primer | Reverse Primer |
|---|---|---|
| GAPDH | CCGCATCTTCTTTTGCGTCG | CCCAATACGACCAAATCCGTTG |
| ALPL | TAAAGCAGGTCTTGGGGTGC | GGGTCTTTCTCTTTCTCTGGCA |
| SPP1 | AGGCATCACCTGTGCCATAC | CACAGCATTCTGCTTTTCCTCA |
| IBSP | TGCCTTGAGCCTGCTTCC | GCAAAATTAAAGCAGTCTTCATTTTG |
| Probe FAM-TAMRA: CTCCAGGACTGCCAGAGGAAGCAATCA | | |
| ZNF145 | GCGGTTCCTGGATAGTTTGC | TGATCACAGACAAAGGCTTTGG |
| Probe FAM-TAMRA: ATGCACTTACTGCGTCATTCAGCGGG | | |
| FKBP51 | CGGAAAGGAGAGGGATATTCAA | TCTGCAGTCAAACATCCTTCCA |
| GILZ | GCACAATTTCTCCATCTCCTTCTT | TCAGATGATTCTTCACCAGATCCA |
| BMP2 | ACGGACTGCGGTCTCCTAA | GGAAGCAGCAACGCTAGAAG |

Most genes were detected using SYBR green; IBSP and ZNF145 PCRs were performed with a specific probe (FAM-TAMRA).

*Flow cytometric analysis of proliferation and apoptosis*

To measure apoptosis or proliferation, hMSCs were treated with 100nM dex or 4μM parbendazole for 1, 5, or 8 days (n=7).

To measure apoptosis cells were trypsinized, collected in media and washed once in PBS before being resuspended in 50μL binding buffer and 2.5μl annexin V and 2.5μl 7-Aminoactinomycin D (7AAD). Cells were incubated in the dark for 15 minutes before an additional 75μl binding buffer was added and cell were analyzed by flow cytometry. The percentage apoptotic cells was measured by flow cytometry after staining with phyco-erythrin (PE)-conjugated annexin V and 7AAD (annexin $V^+$, $7AAD^+$). We scored viable cells as those that are negative for annexin V and 7AAD. Irrelevant isotype-matched immunoglobulin was used as a control. Fold induction of apoptosis was calculated from the increase in the percentage of apoptotic cells between the treated and untreated samples. The amount of necrotic cells (annexin $V^-$, $7AAD^+$) was always minimal.

For analysis of proliferation, hMSCs were trypsinized, collected in media and after centrifugation, 5ml of ethanol was added drop wise to the cells after which they were incubated at -20°C for 30 min. Cells were then centrifuged and resuspended in 1ml PBS plus 1% BSA before being centrifuged again. Supernatant was discarded and 55μl PBS containing 5% serum plus 2.5μl Pe-Cy7-conjugated Ki67 antibody was added. Cells were incubated 30 min in the dark at RT. After incubation, 1ml PBS containing 5% serum was added and centrifuged again. Supernatant was discarded and the pellet was dissolved in 100μl PBS containing 5% serum. Proliferating cells were identified as being Ki67 positive. Stained cells were analyzed using a BD Biosciences

Accuri C6 Personal Flow Cytometer and analyzed with BD Accuri C6 software analysis program. For each sample, a minimum of 10,000 events was collected.

*Presto blue assay for cell survival analysis*

For analysis of cell survival, hMSCs were cultured in 96 well tissue culture plates. Following incubations with control media, 100nM dex or 4μM parbendazole, cell viability was assayed at 1, 5, 8 and 14 days (n=6), using a PrestoBlue cytotoxicity assay following the manufacturers protocol. Briefly, 10μl of PrestoBlue reagent was added to each well and after a one hour incubation the plate fluorescence was measured at excitation 530nm / emission 590nm wavelength using a Victor2 plate reader. Date was corrected for background fluorescence of presto blue in media alone.

*Immunocytochemistry*

Cells were fixed with 4% paraformaldehyde in phosphate-buffered saline (PBS) for 15 minutes at RT, washed in PBS, and excess aldehyde quenched with 10 mM ethanolamine in PBS for 5 min. Cells were then permeabilized with 0.5% Triton-X-100 in PBS for 10 minutes and blocked for 30 minutes at room temperature in PBS supplemented with 1.5% bovine serum albumin (BSA) and 0.02% Triton-X-100. For visualization of microtubules cells were labeled for 1 hour with mouse monoclonal anti-β-tubulin antibody at 1:60 dilution at RT, followed by secondary Alexa Fluor® 488 Goat Anti-Mouse IgG at 1:400 dilution for a total of 1 hour, with the addition of rhodamine–conjugated phalloidin at 1:100 dilution for the last 20 minutes. For visualization and quantification of focal adhesions cells were labeled for 1 hour with rabbit monoclonal ABfinity anti-vinculin antibody at 1:200 dilution at RT, followed by secondary Alexa Fluor® 488 Goat Anti-Rabbit IgG at 1:400 dilution for a total of 1 hour, with the addition of rhodamine–conjugated phalloidin at 1:100 dilution for the last 20 minutes. Slides were mounted using Vectashield mounting medium containing DAPI and pictures were taken on a Zeiss Axiovert 200 MOT microscope. Quantitative morphometric analysis (length and number of focal adhesions per cell) was performed using image analysis soft-ware, ImageJ (NIH, Bethesda, Maryland, USA, available online at http//rsb.info.nih.gov.ij) as described previously[55].

*BMP reporter assay*

We used a previously reported C2C12 cell line stably transfected with a reporter plasmid consisting of BMP-responsive elements from the Id1 promoter fused to a luciferase reporter gene (C2C12-BRE-Luc) to detect BMP activity[16,17]

following treatment with conditioned media from hMSCs exposed to parbendazole. C2C12-BRE-Luc cells were seeded into white walled 96 well culture plates at a density of 40,000 cells/well in 50µl of media. After 30 minutes 50µl of conditioned media from hMSCs treated with parbendazole (4µM), dex (0.1µM), or control media was then added to the cells. After 24 hours, the media was removed from the cells and 100µl of the combined lysis buffer and luciferin reagent (Steady Lite Plus) was added to each well. The plates were shaken for 15 minutes in the dark and then luminescence was quantified using a Victor2 plate reader.

*Cell culture of SV-HFOs*

SV-HFO cells[56] were cultured as described previously[54].

*Statistics*

The data provided here are based on at least two independent experiments performed in at least triplicate. Values displayed are mean ± SEM. Significance was calculated using either the Student's t-test, the one-way ANOVA with Tukey's or Dunn's post-hoc test, or two-way ANOVA where appropriate, using GraphPad prism 6.0. P-values $<0.05$ were considered significant.

## References

1. Johnell O, Kanis JA. (2006) An estimate of the worldwide prevalence and disability associated with osteoporotic fractures. *Osteoporos Int.* 17(12):1726-33.
2. Kanis JA and Johnell O. (2005) Requirements for DXA for the management of osteoporosis in Europe. *Osteoporos Int.* 16:229.
3. Lamb J, Crawford ED, Peck D, Modell JW, Blat IC, Wrobel MJ, Lerner J, Brunet JP, Subramanian A, Ross KN, Reich M, Hieronymus H, Wei G, Armstrong SA, Haggarty SJ, Clemons PA, Wei R, Carr SA, Lander ES, Golub TR. (2006) The Connectivity Map: using gene expression signatures to connect small molecules, genes, and disease. *Science* 313:1929-1935.
4. Qu XA1, Rajpal DK. (2012) Applications of Connectivity Map in drug discovery and development. *Drug Discov Today* 17(23-24):1289-98.
5. Chang M, Smith S, Thorpe A, Barratt MJ, Karim F. (2010) Evaluation of phenoxybenzamine in the CFA model of pain following gene expression studies and connectivity mapping. *Mol Pain* 16;6:56.
6. Wang G, Ye Y, Yang X, Liao H, Zhao C, Liang S. (2011) Expression-based in silico screening of candidate therapeutic compounds for lung adenocarcinoma. *PLoS One* 21;6(1). e14573.
7. Zhong Y, Chen EY, Liu R, Chuang PY, Mallipattu SK, Tan CM, Clark NR, Deng Y, Klotman PE, Ma'ayan A, He JC. (2013) Renoprotective effect of combined inhibition of angiotensin-converting enzyme and histone deacetylase. *J Am Soc Nephrol* 24(5):801-11.
8. Koh LW, Koh GR, Ng FS, Toh TB, Sandanaraj E, Chong YK, Phong M, Tucker-Kellogg G, Kon OL, Ng WH, Ng IH, Clement MV, Pervaiz S, Ang BT, Tang CS. (2013) A distinct reactive oxygen species profile confers chemoresistance in glioma-propagating cells and associates with patient survival outcome. *Antioxid Redox Signal.* 20;19(18):2261-79.
9. Karube K, Tsuzuki S, Yoshida N, Arita K, Kato H, Katayama M, Ko YH, Ohshima K, Nakamura S, Kinoshita T, Seto M. (2013) Comprehensive gene expression profiles of NK cell neoplasms identify vorinostat as an effective drug candidate. *Cancer Lett* 1;333(1):47-55.10. Havercroft JC, Quinlan RA, Gull K. (1981) Binding of parbendazole to tubulin and its influence on microtubules in tissue-culture cells as revealed by immunofluorescence microscopy. *J Cell Sci* 49:195-204.
11. Marie PJ. (2013) Targeting integrins to promote bone formation and repair. *Nat Rev Endocrinol* 9(5):288-95.
12. Born AK, Rottmar M, Lischer S, Pleskova M, Bruinink A, Maniura-Weber K. (2009) Correlating cell architecture with osteogenesis: first steps towards live single cell monitoring. *Eur Cell Mater* 23;18:49-60, 61-2
13. Rodríguez JP, González M, Ríos S, Cambiazo V. (2004) Cytoskeletal organization of human mesenchymal stem cells (MSC) changes during their osteogenic differentiation. *J Cell Biochem* 1;93(4):721-31.
14. Liu H, Zhang R, Ko SY, Oyajobi BO, Papasian CJ, Deng HW, Zhang S, Zhao M. (2011) Microtubule assembly affects bone mass by regulating both osteoblast and osteoclast functions: stathmin deficiency produces an osteopenic phenotype in mice. *J Bone Miner Res* 26(9):2052-67.
15. Zhao M, Ko SY, Liu JH, Chen D, Zhang J, Wang B, Harris SE, Oyajobi BO, Mundy GR. (2009) Inhibition of microtubule assembly in osteoblasts stimulates bone morphogenetic protein 2 expression and bone formation through transcription factor Gli2. *Mol Cell Biol* 29(5):1291-305
16. Zilberberg L, ten Dijke P, Sakai LY, Rifkin DB. (2007) A rapid and sensitive bioassay to measure bone morphogenetic protein activity. *BMC Cell Biol* 19;8:41.
17. Korchynskyi O, ten Dijke P. (2002) Identification and functional characterization of distinct critically important bone morphogenetic protein-specific response elements in the Id1 promoter. *J Biol Chem* 15;277(7):4883-91.
18. Hao J, Ho JN, Lewis JA, Karim KA, Daniels RN, Gentry PR, Hopkins CR, Lindsley CW, Hong CC. (2010) In vivo structure-activity relationship study of dorsomorphin analogues identifies selective VEGF and BMP inhibitors. *ACS Chem Biol* 19;5(2):245-53.
19. Rifas L. (2007) The role of noggin in human mesenchymal stem cell differentiation. *J Cell Biochem* 1;100(4):824-34.
20. Kaighn, ME; Narayan KS, Ohnuki Y, Lechner JF, Jones LW. (1979) Establishment and characterization of a human prostatic carcinoma cell line (PC-3). *Invest Urol* 17 (1): 16–23.
21. McKellar QA, Scott EW. (1990) The benzimidazole anthelmintic agents-a review. *J Vet Pharmacol Ther* 13(3):223-47.

22. Davidse LC. (1973) Antimitotic activity of methyl benzimidazol-2-yl carbamate (MBC) in Aspergillus nidulans. Pesticide Biochemistry and Physiology. 3(3):317–325
23. Davidse LC, Flach W. (1977) Differential binding of methyl benzimidazol-2-yl carbamate to fungal tubulin as a mechanism of resistance to this antimitotic agent in mutant strains of Aspergillus nidulans. *J Cell Biol* 72(1):174-93.
24. Jordan MA, Wilson L. (2004) Microtubules as a target for anticancer drugs. *Nat Rev Cancer* 4(4):253-65.
25. Nogales E, Wang HW. (2006) Structural mechanisms underlying nucleotide-dependent self-assembly of tubulin and its relatives. *Curr Opin Struct Biol* 16(2):221-9.
26. Nogales E, Wang HW. (2006) Structural intermediates in microtubule assembly and disassembly: how and why?
27. Gundersen GG, Cook TA. (1999) Microtubules and signal transduction. *Curr Opin Cell Biol* 18(2):179-84.
28. Pockwinse SM, Rajgopal A, Young DW, Mujeeb KA, Nickerson J, Javed A, Redick S, Lian JB, van Wijnen AJ, Stein JL, Stein GS, Doxsey SJ. (2006) Microtubule-dependent nuclear-cytoplasmic shuttling of Runx2. J Cell Physiol.206(2):354-62.
29. Chang Y-C, Nalbant P, Birkenfeld J, Chang Z-F, Bokoch GM. (2008) GEF-H1 couples nocodazole-induced microtubule disassembly to cell contractility via RhoA. *Mol Biol Cell* 19:2147–2153.
30. Mathieu PS, Loboa EG. (2012) Cytoskeletal and focal adhesion influences on mesenchymal stem cell shape, mechanical properties, and differentiation down osteogenic, adipogenic, and chondrogenic pathways. *Tissue Eng Part B Rev* 18(6):436-44.
31. Drabek K1, van de Peppel J, Eijken M, van Leeuwen JP. (2011) GPM6B regulates osteoblast function and induction of mineralization by controlling cytoskeleton and matrix vesicle release. J Bone Miner Res 26(9):2045-51.
32. Kilian KA, Bugarija B, Lahn BT, Mrksich M. (2010) Geometric cues for directing the differentiation of mesenchymal stem cells. *Proc Natl Acad Sci USA* 16;107(11):4872-7.
33. Higuchi C, Nakamura N, Yoshikawa H, Itoh K. (2009) Transient dynamic actin cytoskeletal change stimulates the osteoblastic differentiation. *J Bone Miner Metab* 27(2):158-67.
34. Chen Q, Shou P, Zhang L, Xu C, Zheng C, Han Y, Li W, Huang Y, Zhang X, Shao C, Roberts AI, Rabson AB, Ren G, Zhang Y, Wang Y, Denhardt DT, Shi Y. (2014) An osteopontin-integrin interaction plays a critical role in directing adipogenesis and osteogenesis by mesenchymal stem cells. *Stem Cells* 32(2):327-37.
35. Biggs MJ, Richards RG, Dalby MJ. (2010) Nanotopographical modification: a regulator of cellular function through focal adhesions. *Nanomedicine.* 6(5):619-33.
36. Gupton SL, Waterman-Storer CM. (2006) Spatiotemporal feedback between actomyosin and focal-adhesion systems optimizes rapid cell migration. *Cell* 30;125(7):1361-74.
37. Ingber DE. (2006) Cellular mechanotransduction: putting all the pieces together again. *FASEB J* 20(7):811-27.
38. Ingber DE. (1993) Cellular tensegrity: defining new rules of biological design that govern the cytoskeleton. *J Cell Sci* 104 ( Pt 3):613-27.
39. McBeath R, Pirone DM, Nelson CM, Bhadriraju K, Chen CS. (2004) Cell shape, cytoskeletal tension, and RhoA regulate stem cell lineage commitment. *Dev Cell* 6(4):483-95.
40. Zhao M, Qiao M, Harris SE, Chen D, Oyajobi BO, Mundy GR. (2006). The zinc finger transcription factor Gli2 mediates bone morphogenetic protein 2 expression in osteoblasts in response to hedgehog signaling. *Mol Cell Biol* 26(16):6197-6208.
41. Phimphilai M, Zhao Z, Boules H, Roca H, Franceschi RT. (2006) BMP signaling is required for RUNX2-dependent induction of the osteoblast phenotype. *J Bone Miner Res* 21(4):637-46.
42. Noël D, Gazit D, Bouquet C, Apparailly F, Bony C, Plence P, Millet V, Turgeman G, Perricaudet M, Sany J, Jorgensen C. (2004) Short-term BMP-2 expression is sufficient for in vivo osteochondral differentiation of mesenchymal stem cells. *Stem Cells* 22(1):74-85.
43. Gazzerro E, Canalis E. (2006) Bone morphogenetic proteins and their antagonists. *Rev Endocr Metab Disord* 7(1-2):51-65.
44. Lavery K, Swain P, Falb D, Alaoui-Ismaili MH. (2008) BMP-2/4 and BMP-6/7 differentially utilize cell surface receptors to induce osteoblastic differentiation of human bone marrow-derived mesenchymal stem cells. *J Biol Chem* 283(30):20948-58.
45. Lecanda F, Avioli LV, Cheng SL. (1997) Regulation of bone matrix protein expression and induction of differentiation of human osteoblasts and human bone marrow stromal cells by bone morphogenetic protein-2. *J Cell Biochem* 1;67(3):386-96.

46. Cruz AC, Silva ML, Caon T, Simões CM. (2012) Addition of bone morphogenetic protein type 2 to ascorbate and β-glycerophosphate supplementation did not enhance osteogenic differentiation of human adipose-derived stem cells. *J Appl Oral Sci* 20(6):628-35.
47. Diefenderfer, DL, Osyczka AM, ReillyGC, Leboy PS. (2003) BMP responsiveness in human mesenchymal stem cells. *Connect Tissue Res* 44: 305–311.
48. Fu R, Selph S, McDonagh M, Peterson K, Tiwari A, Chou R, Helfand M. (2013) Effectiveness and harms of recombinant human bone morphogenetic protein-2 in spine fusion: a systematic review and meta-analysis. Ann Intern Med.158(12):890-902.
49. Simmonds MC, et al. (2013) Safety and effectiveness of recombinant human bone morphogenetic protein-2 for spinal fusion. A meta-analysis of individual-participant data. Ann Intern Med. 158(12):877-89.
50. Eijken M, Swagemakers S, Koedam M, Steenbergen C, Derkx P, Uitterlinden AG, van der Spek PJ, Visser JA, de Jong FH, Pols HA, van Leeuwen JP. (2007) The activin A-follistatin system: potent regulator of human extracellular matrix mineralization. *FASEB J* 21(11):2949-60.
51. Bruedigam C, Driel Mv, Koedam M, Peppel Jv, van der Eerden BC, Eijken M, van Leeuwen JP. (2011) Basic techniques in human mesenchymal stem cell cultures: differentiation into osteogenic and adipogenic lineages, genetic perturbations, and phenotypic analyses. *Curr Protoc Stem Cell Biol* Chapter 1:Unit1H.3.
52. Du P, Kibbe WA, Lin SM. (2008) lumi: a pipeline for processing Illumina microarray. *Bioinformatics* 24: 1547–1548.
53. Smyth GK. (2004) Linear models and empirical bayes methods for assessing differential expression in microarray experiments. *Stat Appl Genet Mol Biol* 3(3).
54. Eijken M, Koedam M, van Driel M, Buurman CJ, Pols HA, van Leeuwen JP. (2006) The essential role of glucocorticoids for proper human osteoblast differentiation and matrix mineralization. *Mol Cell Endocrinol* 27;248(1-2):87-93.
55. Igathinathane C, Pordesimo LO, Columbus EP, Batchelor WD, Methuku SR. (2008) Shape identification and particles size distribution from basic shape parameters using ImageJ. *Computers and Electronics in Agriculture* 63(2):168–182.
56. Chiba,H., Sawada,N., Ono,T., Ishii,S., and Mori,M. (1993) Establishment and characterization of a simian virus 40-immortalized osteoblastic cell line from normal human bone. *Jpn.J.Cancer Res.* 84, 290-297.

# Chapter 3

# Using the Connectivity Map to discover compounds influencing human osteoblast differentiation

Andrea M Brum, Jeroen H van de Peppel, Linh Nguyen, Abiden Aliev, Marijke Schreuders-Koedam, Tarini V Gajadien, Cindy S van der Leije, Anke van Kerkwijk, Marco Eijken, Johannes PTM van Leeuwen, & Bram CJ van der Eerden

*Journal of Cellular Physiology. 2018; 233: 4895– 4906.*

Abstract

Osteoporosis is a common skeletal disorder characterized by low bone mass leading to increased bone fragility and fracture susceptibility. Identification of factors influencing osteoblast differentiation and bone formation is very important. Previously, we identified parbendazole to be a novel compound that stimulates osteogenic differentiation of human mesenchymal stromal cells (hMSCs), using gene expression profiling and bioinformatic analyses, including the Connectivity Map (CMap), as an *in-silico* approach. The aim for this paper is to identify additional compounds affecting osteoblast differentiation using the CMap.

Gene expression profiling was performed on hMSCs differentiated to osteoblasts using Illumina microarrays. Our osteoblast gene signature, the top regulated genes 6-hours after induction by dexamethasone, was uploaded into CMap (www.broadinstitute.org/cmap/). Through this approach we identified compounds with gene signatures positively correlating (withaferin-A, calcium folinate, amylocaine) or negatively correlating (salbutamol, metaraminol, diprophylline) to our osteoblast gene signature. All positively correlating compounds stimulated osteogenic differentiation, as indicated by increased mineralization compared to control treated cells. One of three negatively correlating compounds, salbutamol, inhibited dexamethasone-induced osteoblastic differentiation, while the other two had no effect. Based on gene expression data of withaferin-A and salbutamol, we identified *HMOX1* and *STC1* as being strongly differentially expressed. shRNA knockdown of *HMOX1* or *STC1* in hMSCs inhibited osteoblast differentiation. These results confirm that the CMap is a powerful approach to identify positively compounds that stimulate osteogenesis of hMSCs, and through this approach we can identify genes that play an important role in osteoblast differentiation and could be targets for novel bone anabolic therapies.

### 3.1 Introduction

Osteoporosis is a common bone disease characterized by reduced bone mass and deterioration of the bone microstructure leading to increased fragility and susceptibility to fracture. It has been estimated that one osteoporotic fracture occurs every 8 seconds worldwide[1] and direct healthcare costs in Europe alone exceed €31 billion annually[2]. Bone remodeling is a balancing act between removal of old bone and formation of new bone, which is achieved by two distinct cells, the osteoclast and osteoblast as well as its terminally differentiated form the osteocyte. When uncoupling of these two processes takes place, bone resorption can overtake bone formation resulting in osteoporosis. Most currently available osteoporosis treatments, such as bisphosphonates, reduce bone resorption and result in modest increases in bone density; however, these treatments do not result in a true bone anabolic effect or improve bone microarchitecture so patients do not regain bone that has been lost at time of diagnosis. An ideal treatment would stimulate bone formation as well, to help repair the damage already done to the bone microarchitecture and strength. With this in mind, our goal is to search for novel molecules and/or mechanisms that stimulate human osteoblast differentiation and bone formation.

The connectivity map (CMap) is a web-based tool that allows for screening of compounds against a disease or physiological gene signature[3,4]. This is achieved by comparing microarray data from over 1300 small molecules to a user's selected gene signature of a phenotype of interest using a pattern-matching algorithm with a high level of resolution and specificity. This results in a list of compounds ranked from highly positively correlated (similar gene pattern to that of the phenotype of interest) to strongly negatively correlated (inverse gene expression pattern to that of the phenotype of interest). These compounds hold the potential to deliver a novel treatment for a disease or to identify novel pathways or genes involved in a complex biological process. To date, the CMap has been successfully used to identify compounds and combination therapies that show promise in the treatment of osteoarthritic pain[5], adenocarcinoma[6], skeletal muscle atrophy[7,8], emphysema-related lung disease[9], kidney disease[10], gliomas[11], NK cell neoplasms[12], Parkinson's disease related neurodegeneration[13] and medulloblastomas[14].

Recently we have successfully used the CMap to identify a novel compound, parbendazole, that independently stimulates osteoblast differentiation of human mesenchymal stem cells (hMSCs) and elucidate a targetable osteogenic pathway[15]. Our aim of the current study was to determine if we can use the CMap to detect additional molecules that modulate human osteogenesis, both positively or negatively. By doing so we may identify novel bone anabolic agents for the treatment of bone diseases such as osteoporosis, or to help us distinguish and understand the processes

underlying the process of osteoblast differentiation and bone formation and identify therapeutic candidate targets.

## 3.2 Results

*3.2.1 Identification of compounds with the most positively and negatively correlated gene signatures.*

To identify compounds that may either stimulate or inhibit bone formation, due to their ability to enhance or repress genes regulated during osteoblast differentiation, we performed a CMap analysis. For this analysis we uploaded our gene signature of hMSCs differentiating to osteoblasts (Appendix C, **Table A1**) into the CMap and focused on compounds tested in the PC3 cell line as we found in our previous work[15] that the strongest and most consistent correlating gene signatures came from this cell line.

Multiple compounds were identified that have a significant positively correlating gene expression pattern to that of differentiating hMSCs, including dexamethasone (dex) and a number of other corticosteroids, as well as the previously described novel osteogenic compound, parbendazole[15] (**Table 1**). The large number of glucocorticoid receptor (GR) binding ligands, including dex, was expected, as dex is the compound that we used to stimulate osteoblast differentiation and glucocorticoid-mediated activation of the glucocorticoid receptor is the classical stimulus for human osteoblast differentiation *in vitro*. To select novel compounds that may stimulate osteoblast differentiation we excluded any GR-ligand. We also excluded several compounds that we were unable to obtain (CP-690334-01, MG-262, F0447-0125). In addition, we considered both the mean CMap score and p-value when selecting compounds to test. Based on these criteria we selected three top positively correlating compounds, withaferin A, calcium folinate, and amylocaine for further downstream analyses (**Table 1**).

In a similar approach we identified compounds that had an opposite gene signature (negatively correlating) to that of osteoblasts differentiating from hMSCs in order to identify compounds that may inhibit osteoblast differentiation and/or gene/protein targets or (signaling) pathways that negatively affect bone formation. The top ranking negatively correlated compounds identified by the CMap are shown in **Table 2**. The top three negatively correlated compounds, salbutamol, metaraminol, and diprophylline, were selected for further testing (**Table 2**).

**Table 1: Positively correlated compounds from the CMap**

| Rank | Compound Name | Mean CMap Score | n | p-value |
|---|---|---|---|---|
| **1** | Parbendazole | 0.855 | 2 | <0.00001 |
| **2** | *Dexamethasone* | 0.913 | 2 | <0.00001 |
| **3** | *Fludrocortisone* | 0.768 | 2 | 0.00002 |
| **4** | *Halcinonide* | 0.788 | 2 | 0.00002 |
| **5** | *Fludroxycortide* | 0.775 | 2 | 0.00002 |
| **6** | *Flumetasone* | 0.854 | 2 | 0.00002 |
| **7** | *Flunisolide* | 0.718 | 2 | 0.00002 |
| **8** | *Fluocinonide* | 0.72 | 2 | 0.00002 |
| **9** | **Withaferin A** | 0.687 | 2 | 0.00002 |
| **10** | CP-690334-01 | 0.473 | 4 | 0.00002 |
| **11** | *Triamcinolone* | 0.736 | 2 | 0.00004 |
| **12** | **Calcium Folinate** | 0.627 | 2 | 0.00018 |
| **13** | MG-262 | 0.566 | 2 | 0.00028 |
| **14** | *Medrysone* | 0.514 | 2 | 0.00070 |
| **15** | Monensin | 0.492 | 2 | 0.00145 |
| **16** | Semustine | 0.479 | 2 | 0.00221 |
| **17** | Pioglitazone | 0.376 | 5 | 0.00513 |
| **18** | Tropicamide | 0.452 | 2 | 0.00626 |
| **19** | F0447-0125 | 0.491 | 2 | 0.00710 |
| **20** | **Amylocaine** | 0.548 | 2 | 0.00793 |

CMap permuted results showing compounds with significant positive correlation to the osteogenic hMSCs gene. Top matching compounds from the Connectivity Map based on the average of the replicates of a single compound in only the PC3 cell line. Compounds in bold were chosen for further testing. Compounds in italic are corticosteroids. Rank is based on the p-value calculated from the CMap scores all of the replicates of a single compound in a single cell line. Score is based on the relative strength of a given signature in an instance from the total set of instances calculated upon execution of a query.

**Table 2: Negatively correlated compounds from the CMap**

| Rank | Compound Name | Mean CMap Score | n | p-value |
|---|---|---|---|---|
| **1** | **Salbutamol** | -0.733 | 2 | 0.00048 |
| **2** | **Metaraminol** | -0.834 | 2 | 0.00074 |
| **3** | **Diprophylline** | -0.652 | 2 | 0.00519 |
| **4** | 0175029-0000 | -0.409 | 4 | 0.00627 |
| **5** | Morantel | -0.601 | 2 | 0.00861 |
| **6** | Isoxicam | -0.575 | 2 | 0.00984 |
| **7** | Acetylsalicylic Acid | -0.673 | 2 | 0.01181 |
| **8** | PHA-00816795 | -0.606 | 2 | 0.01515 |
| **9** | Chloramphenicol | -0.627 | 2 | 0.01604 |
| **10** | Isocarboxazid | -0.530 | 2 | 0.02946 |

CMap permuted results showing compounds with significant negative correlation to the osteogenic hMSCs gene. Compounds in bold were chosen for further testing. Top matching compounds from the Connectivity Map based on the average of the replicates of a single compound in only the PC3 cell line. Rank is based on the p-value calculated from the CMap scores all of the replicates of a single compound in a single cell line. Score is based on the relative strength of a given signature in an instance from the total set of instances calculated upon execution of a query.

*3.2.2 The positive correlating compounds, withaferin A, calcium folinate and amylocaine, induce osteoblast differentiation of hMSCs in vitro*

To determine if the identified correlated compounds, withaferin A, calcium folinate, and amylocaine, are able to stimulate osteoblast differentiation of hMSCs we cultured the cells with various concentrations of each compound. We then performed biochemical assays to determine if classical biological indicators of osteoblast differentiation, alkaline phosphatase (ALP) and mineralization, were induced. Withaferin A stimulated ALP activity (Fig. **1A**) after one week of culture, compared to control treated cells, and mineralization was induced (Fig. **1B**) after three weeks of culture. Calcium folinate had no effect on ALP activity (Fig. **1C**) after one week of culture, but did induce mineralization (Fig. **1D**) after three weeks of culture. Similar to calcium folinate, amylocaine also had no effect on ALP activity (Fig. **1E**), but did stimulate mineralization (Fig. **1F**) after three weeks of culture. These results show that all three positively correlated compounds induce mineralization in hMSCs, a hallmark of osteogenic differentiation.

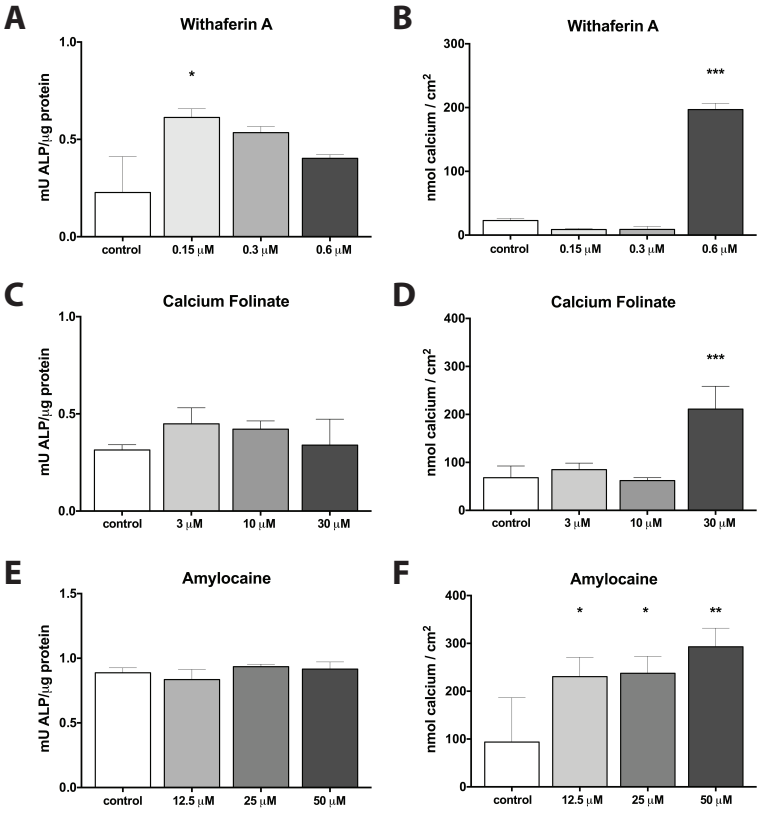


**Figure 1. Withaferin A stimulates both alkaline phosphatase activity and mineralization, while calcium folinate and amylocaine stimulate mineralization.** Results of ALP activity (A,C,E) after 1 week of culture and calcium assay after 3 weeks of culture (B,D,F) in hMSCs treated with various concentrations (shaded bars) of withaferin A (A,B), calcium folinate (C,D), or amylocaine (E,F) when compared to negative control (control medium) (white bar) treated cells. n=3-4. * $p < 0.05$, ** $p < 0.01$, *** $p < 0.001$. Graphs display 1 representative experiment.

*3.2.3 The negatively correlated compounds, salbutamol, metaraminol, and diprophylline, have varying effects on osteoblastic differentiation of hMSCs in vitro*

To determine if the negatively correlated compounds, salbutamol, metaraminol, and diprophylline, inhibit osteoblast differentiation of hMSCs we cultured hMSCs with osteogenic differentiation medium, containing 100 nM dex, along with various concentrations of each compound. We again performed the same biochemical assays to determine if ALP activity or mineralization were reduced. Salbutamol treatment resulted in decreased levels of ALP activity (Fig. **2A**) in hMSCs treated for one week. Salbutamol also inhibited mineralization (Fig. **2B**) after three weeks of culture compared to dex treatment alone. Metaraminol and diprophylline had no effect on either ALP activity (Fig. **2C,E**) or mineralization (Fig. **2D,F**) at the doses tested (1-16 μM for both). In summary, only one of the selected negatively correlated compounds, salbutamol, successfully inhibited osteoblast differentiation, while the others had no effect.

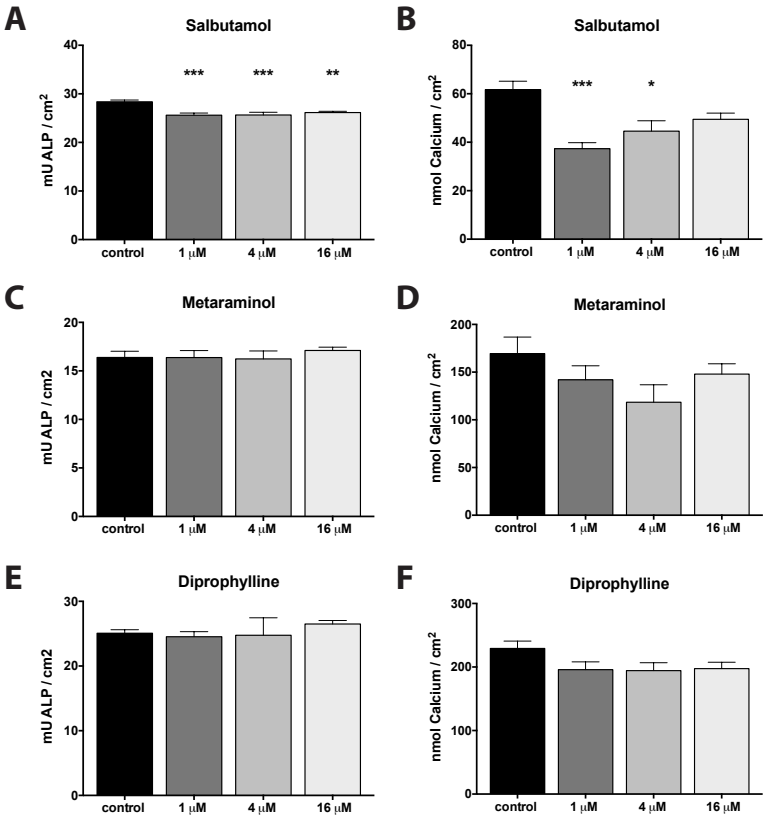


**Figure 2. Salbutamol inhibits alkaline phosphatase activity and mineralization of osteogenically differentiated hMSCs, but metaraminol or diprophylline have no effect.** Results of ALP activity (A,C,E) after 1 week of culture or calcium assay (B,D,F) after 3 weeks of culture in hMSCs treated with differentiation medium (medium+100 nM Dex) supplemented with various concentrations (shaded gray bars) of salbutamol (A,B), metaraminol (C,D), or diprophylline (E,F) when compared to control (differentiation medium alone) (black bar) treated cells. * $p < 0.05$, ** $p < 0.01$, *** $p < 0.001$. Graphs display 1 representative experiment.

**Table 3. Top Differentially Expressed Genes (DEGs).**

**Withaferin A**

| Probe ID | Gene ID | Fold Change |
|---|---|---|
| 203665_at | HMOX1 | 4.88 |
| 213418_at | HSPA6 | 3.76 |
| 117_at | HSPA6 | 3.17 |
| 200800_s_at | HSPA1A | 2.72 |
| 202581_at | HSPA1A | 2.55 |
| 201008_s_at | TXNIP | -1.57 |
| 201110_s_at | THBS1 | -1.62 |
| 201109_s_at | THBS1 | -1.68 |
| 202436_s_at | CYP1B1 | -1.75 |
| 204470_at | CXCL1 | -1.84 |

**Calcium Folinate**

| Probe ID | Gene ID | Fold Change |
|---|---|---|
| 205778_at | KLK7 | 0.62 |
| 202840_at | TAF15 | 0.62 |
| 217427_s_at | HIRA | 0.60 |
| 216745_x_at | - | 0.59 |
| 206499_s_at | RCC1 | 0.56 |
| 213513_x_at | ARPC2 | -0.67 |
| 212533_at | WEE1 | -0.72 |
| 217586_x_at | - | -0.75 |
| 205225_at | ESR1 | -0.78 |
| 214953_s_at | APP | -1.04 |

**Amylocaine**

| Probe ID | Gene ID | Fold Change |
|---|---|---|
| 210496_at | G18 | 0.73 |
| 201041_s_at | DUSP1 | 0.72 |
| 213303_x_at | ZBTB7A | 0.71 |
| 215643_at | SEMA3D | 0.67 |
| 212501_at | CEBPB | 0.67 |
| 218737_at | SBNO1 | -0.76 |
| 218411_s_at | MBIP | -0.77 |
| 212934_at | UBXN2B | -0.77 |
| 204120_s_at | ADK | -0.88 |
| 214327_x_at | TPT1 | -1.01 |

**Salbutamol**

| Probe ID | Gene ID | Fold Change |
|---|---|---|
| 204595_s_at | STC1 | 2.34 |
| 206924_at | IL11 | 1.85 |
| 201925_s_at | CD55 | 1.82 |
| 201926_s_at | CD55 | 1.78 |
| 204597_x_at | STC1 | 1.78 |
| 202627_s_at | SERPINE1 | -1.11 |
| 211160_x_at | ACTN1 | -1.13 |
| 209101_at | CTGF | -1.15 |
| 210560_at | GBX2 | -1.25 |
| 202628_s_at | SERPINE1 | -1.35 |

**Metaraminol**

| Probe ID | Gene ID | Fold Change |
|---|---|---|
| 206924_at | IL11 | 1.51 |
| 204595_s_at | STC1 | 1.47 |
| 208250_s_at | DMBT1 | 1.34 |
| 201925_s_at | CD55 | 1.19 |
| 33304_at | ISG20 | 1.13 |
| 206170_at | ADRB2 | -0.86 |
| 210560_at | GBX2 | -0.87 |
| 210538_s_at | BIRC3 | -0.88 |
| 209101_at | CTGF | -0.90 |
| 202628_s_at | SERPINE1 | -1.04 |

**Diprophylline**

| Probe ID | Gene ID | Fold Change |
|---|---|---|
| 203944_x_at | BTN2A1 | 1.31 |
| 202699_s_at | TMEM63A | 1.31 |
| 215063_x_at | LRRC40 | 1.23 |
| 215493_x_at | BTN2A1 | 1.17 |
| 203935_at | ACVR1 | 1.13 |
| 214953_s_at | APP | -0.69 |
| 215991_s_at | KIAA0090 | -0.70 |
| 221629_x_at | C8orf30A | -0.71 |
| 215055_at | B3GNTL1 | -0.73 |
| 215637_at | TSGA14 | -1.16 |

The 5 most up-regulated and 5 most down-regulated expressed probes of each compound derived from CMAP. The table contains the probe ID, its gene ID and the average fold change value of the two instances (log base 2 transformed). Top ranking DEGs are probes identified based on the average of the ratioed (instance to the control) normalized expression values for the two instances for each compound.

*3.2.4 Identification of differentially expressed genes (DEG) and biological processes affected by positively and negatively correlated CMap compounds*

In order to gain insights into how the newly identified Cmap compounds influence osteogenic differentiation, we performed *in silico* analysis of the genes regulated by these compounds from the Cmap database data. We ranked differentially expressed genes (DEGs) by their average relative expression values for each compound. **Table 3** displays the five most up-regulated and five most down-regulated genes (identified by their corresponding microarray probe) for each compound. Withaferin A treatment in PC3 cells resulted in the most differentially regulated genes, compared to control treatment, of any of the compounds. Withaferin A treatment strongly up-regulated stress-response genes, including heme oxygenase 1 (*HMOX1*), heat shock 70 kDa protein (*HSPA1A*) and heat shock protein family A member 6 (*HSPA6*), with *HMOX1* being the most strongly regulated (29.3-fold upregulation) gene of any of the Cmap compounds. Withaferin A down-regulated expression of thrombospondin 1 (*THBS1*), thioredoxin interacting protein (*TXNIP*), and a cytochrome P450 family member (*CYP1B1*). Calcium folinate and amylocaine displayed much weaker regulation (based on averaged data of the two instances) of genes. The top DEG for amylocaine was tumor protein, translationally-controlled 1 (*TPT1*) (2 fold down-regulated) and for calcium folinate we found amyloid beta precursor protein (*APP*) to be the most regulated (also 2-fold down-regulated). Of the negatively correlated compounds, salbutamol demonstrated the greatest effect on gene expression regulation, compared to control treated cells. The strongest regulated genes for salbutamol included stanniocalcin 1 (*STC1*), interleukin 11 (*IL11*), CD55 molecule (Cromer blood group) (*CD55*), and Serpin Family E Member (*SERPINE1*), with *STC1* being the next most differentially expressed (5 fold up-regulated) gene after the withaferin A regulated stress response genes. *IL11* and *STC1* were also the most strongly regulated genes by metaraminol (2.9- and 2.8-fold up-regulated, respectively). Butyrophilin subfamily 2 member A1 (*BTN2A1*) and transmembrane protein 63A (*TMEM63A*) (both 2.5-fold up-regulated) topped the list of DEGs for diprophylline.

To investigate the chosen compounds biological functions, the 100 most up-regulated and 100 most down-regulated DEGs of each compound were annotated and clustered through Gene Ontology (GO) analysis in DAVID. **Table 4** summarizes the major GO terms clusters that were identified for each compound and all identified GO terms for each individual compound are shown in Appendix C, **Table A2**. DEGs from amylocaine and salbutamol were found to be associated with the cytosolic region, which DEGs from salbutamol and metaraminol were both associated with the extracellular region. GO terms related to apoptosis, proliferation,

**Table 4. Top Gene Ontology (GO) terms based on gene expression profiles of CMap-derived compounds.**

| Compound | GO term Biological process | GO term Molecular Function | GO term Cellular component |
|---|---|---|---|
| Withaferin A | Response to unfolded protein<br>Apoptosis (+ regulation)<br>Regulation of cellular response to heat<br>Cell proliferation<br>DNA binding/transcription | Protein binding | - |
| Calcium folinate | - | Enzyme binding | - |
| Amylocaine | - | - | Cytosol |
| Salbutamol | Wound healing<br>Apoptosis (- regulation)<br>Cell proliferation<br>Cell signalling | Protein C-terminus binding | Extracellular region<br>Cytosol |
| Metaraminol | - | - | Extracellular region |
| Diprophylline | - | - | - |

Summary of top GO term clusters that have been identified by DAVID bioinformatics resources for each compound using the top 100 most upregulated and 100 most downregulated probes based on the average of the ratioed (instance to the control) normalized expression values for the two instances for each compound. The GO terms within the clusters had a significance of Benjamini corrected p-value < 0.05. The headers "biological process", "molecular function", and "cellular component" stands for the GO category to which the GO term is annotated.

and protein binding were shared by withaferin A and salbutamol. DEGs from calcium folinate annotate with the GO term enzyme binding.

Overall, little overlap in GO terms was seen between the selected compounds, with only withaferin A and salbutamol sharing multiple processes. Withaferin A and salbutamol treatment also led to the most strongly regulated genes, *HMOX1*, *HSPA1A*, *HSPA6,* and *STC1*, of all the compounds; however, there was no overlap in genes that were most strongly expressed of repressed between them.

### *3.2.5 HMOX1 and STC1 are important for human osteoblast differentiation*

To validate some of the results of our *in silico* analysis we used shRNAs to knockdown gene expression of two of the most strongly regulated genes by CMap compounds, *HMOX1* and *STC1,* and assessed ALP activity and mineralization of differentiating hMSCs. Following knockdown of *HMOX1*, hMSCs were differentiated to osteoblasts using dex and after three days of treatment *HMOX1* expression was reduced compared to scrambled control (Fig. **3A**). Knockdown of *HMOX* resulted in decreased ALP activity (Fig. **3B**) and mineralization (Fig. **3C**). Gene expression of *STC1* in differentiating osteoblasts was successfully reduced by shRNA treatment (Fig. **4A**). Reduced expression of *STC1* resulted in diminished ALP activity (Fig. **4B**)

and suppression of mineralization (Fig. **4C**) in hMSCs osteogenically stimulated with dex. These results demonstrate that two genes, *HMOX1 and STC1*, identified in our CMap analysis are essential to dex-induced human osteoblast differentiation *in vitro*.

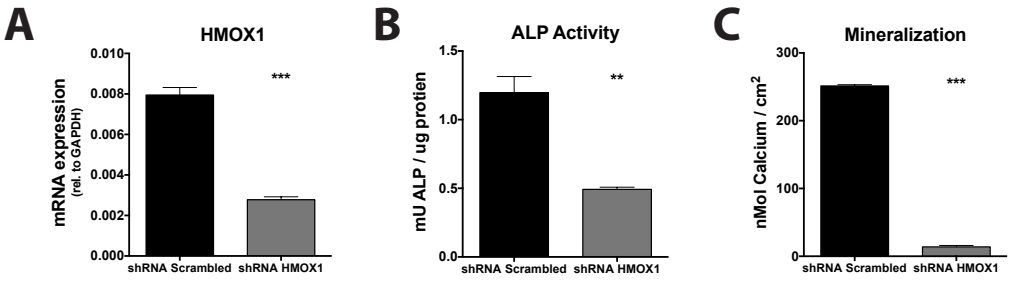


**Figure 3. *HMOX1* gene knockdown in differentiation hMSCs leads reduced gene expression, ALP activity and mineralization.** (A) mRNA expression of HMOX1 was reduced 4 days after transduction with shRNA against *HMOX1* (gray bar) compared to scrambled shRNA control (black bar). ALP activity after 1 week of culture (B) and mineralization after 3 weeks of culture (C) were inhibited by *HMOX1* shRNA treatment (gray bar) compared to scrambled (black bar) in differentiating hMSCs. * $p < 0.05$, ** $p < 0.01$, *** $p < 0.001$. Graphs display 1 representative experiment.

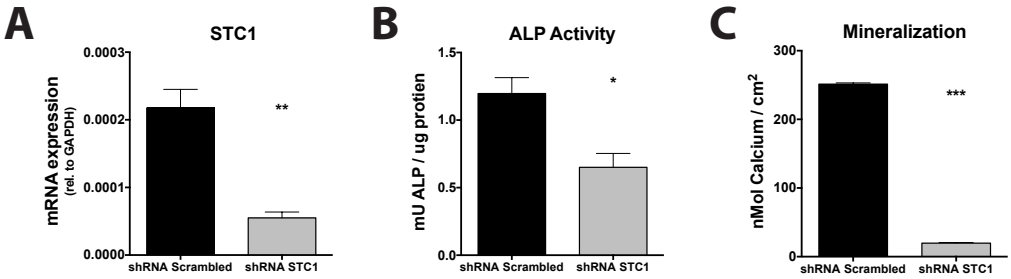


**Figure 4. *STC1* knockdown in differentiation hMSCs leads reduced gene expression, ALP activity and mineralization**. (A) mRNA expression of *STC1* was reduced 4 days after transduction with shRNA against *STC1* (gray bar) compared to scrambled shRNA control (black bar). ALP activity after 1 week of culture (B) and mineralization after 3 weeks of culture (C) were inhibited by *STC1* shRNA treatment (gray bar) compared to scrambled (black bar) in differentiating hMSCs. * $p < 0.05$, ** $p < 0.01$, *** $p < 0.001$. Graphs display 1 representative experiment.

### 3.3 Discussion

Gene expression profiling during osteoblast differentiation provides us with gene activity changes contributing to cellular process and enables targets for new treatments to be identified. In this study, we employed gene expression profiles from human MSCs differentiated towards osteoblasts to identify biologically active small molecules capable to affect this process, both positively and negatively, using a computational bioinformatics method, *i.e.* the Connectivity Map. In a proof of concept study, through this approach, we recently identified parbendazole as a novel compound that can independently induce osteogenic differentiation of hMSCs leading to our scrutinization of a targetable osteogenic pathway[15]. Using the same

approach, we have now identified 3 additional positively correlated compounds, withaferin A, calcium folinate, and amylocaine, which stimulate osteoblast differentiation and mineralization of hMSCs *in vitro*. Conversely, we also examined compounds with negatively correlated gene signatures to that of differentiating osteoblasts, the results of which we hypothesized may reveal interesting new genes and processes in the osteoblast differentiation process. We also identified three compounds, salbutamol, metaraminol, and diprophylline, which exhibit a gene signature negatively correlated to our osteogenic gene signature, but only one of these drugs, salbutamol, inhibited dex-induced osteogenic differentiation of hMSCs. Finally, we analyzed the DEGs behind the CMap identified compounds and used this approach to identify and validate two genes, *HMOX1* and *STC1*, as important factors for human osteogenesis.

The positively correlated compound withaferin A stimulated both ALP activity and mineralization in hMSCs establishing it as an osteogenic drug. These results are supported by two studies that have previously shown that withaferin A positively affects osteoblast differentiation and bone formation. Withaferin A was shown to promote *in vitro* calvarial osteoblast differentiation and proliferation by acting as a proteasomal inhibitor and binding to specific catalytic b subunit of the 20S proteasome, decreasing expression of E3 ubiquitin ligase, Smad ubiquitin regulatory factor 2 (Smurf2), and ultimately preventing degradation of Runt-related transcription factor 2 (RunX2) and relevant Smad proteins[16]. Oral administration of withaferin A to mice increased cortical bone regeneration after injury and exerted an anabolic effect on osteoporotic bone [16]and *in vivo* administration in ovariectomized mice increased new bone formation, as well as improved bone microarchitecture and biomechanical strength [17]. These bone anabolic properties were similar to 17-β-estradiol and alendronate administration, but without the estrogenic or anti-estrogenic consequences to the uterus. In this study different donors displayed different sensitivities to all of the positively correlated compounds tested, with withaferin A treatment being the most variable between donors. While withaferin A treatment induced ALP activity and mineralization in all 4 donors tests, the highest dose tolerated by various donors, as well as the dose that demonstrated the greatest response, varied between donors. These results highlight the varying sensitivity of various human donors, likely due to differing genetic and physiological makeup. This variability could also be related to the results of our DEG and GO analysis in which we saw that withaferin A induced changes in stress-response genes such as *HSPA1A* and *HMOX1*. GO analysis revealed that the DEGs were annotated to stress response biological processes such as "unfolded protein response", "apoptosis" and

"proliferation". In our study withaferin A treatment in hMSCs showed that it might have toxic effects on hMSCs after prolonged treatment at a concentration of greater than or equal to 0.6 μM, depending on the donor. These findings correlate with the known inhibitory effects of withaferin A on cell proliferation of different types of cancer cells by inducing cell cycle arrest at the G2/M phase[18–20]. The top regulated gene in our study, *HMOX1,* is an enzyme that catalyses the cleavage of heme to form biliverdin, carbon monoxide and free iron[21] and researchers have shown that *HMOX1* has a protective role during oxidative stress[22,23], which relates to our finding that DEGs of withaferin A correlate to various stress processes. Overexpression of *HMOX1* has been found to increase human osteoblast stem cell differentiation, and shift the balance of hMSCs differentiation in favor of the osteoblast lineage[24,25]. Our *HMOX* knockdown experiments strongly substantiate the role of *HMOX1* during osteogenesis.

Calcium folinate and amylocaine both stimulated mineralization in hMSCs, while, interestingly, having no consistent effect on ALP activity. As mineralization is the defining feature of a mature osteoblast we have concluded that these two compounds stimulate osteogenic differentiation of hMSCs *in vitro*. These two molecules yielded a low level of gene regulation, based on DEG analysis, which could in part be due to a low level of correlation in the regulation of the genes between the two instances for both compounds. One possibility for the lower expression levels, or reduced number of shared DEGs between instances may be batch effects (non-biological variations), for example the use of different microarray scanners, which has been reported to be commonly observed across multiple batches of microarray experiments[26,27]. As the CMap platform generated its gene profiles in multiple batches, we utilized a normalization step to adjust the probe data for the batch effect related to the use of different scanners, which should minimize the number of false positives, but may remove true positives as well. Amylocaine, also known as stovaine, was developed as a synthetic local anesthetic; however, little research has been done on the mechanisms of action of amylocaine and no data exists linking it to bone or osteoblast differentiation. Local anesthetics, including amylocaine, act by inhibiting voltage-sensitive $Na^+$ channels[28–30], and to a lesser extent voltage sensitive $Ca^{2+}$ channels[31], and it is plausible that the osteogenic effect observed with amylocaine could be related to its potential effects on ion channels, but this requires further investigation. Calcium folinate, otherwise known as folinic acid or by the brand name Leucovorin, is a derivative of tetrahydrofolic acid and is readily converted to other reduced folic acid derivatives, giving it the vitamin activity equivalent to that of folic acid. Interestingly, calcium folinate has been shown to ameliorate the negative effects of methotrexate chemotherapeutic on bone, including prevention of bone loss,

apoptosis of mesenchymal precursor cells, and bone marrow adiposity[32–34] through up-regulating Wnt/β-catenin signaling in bone[35]. Only one study, to our knowledge, has examined the effects of calcium folinate on bone, independent of methotrexate; however, only tibial and femur lengths were scrutinized and no difference was found between calcium folinate treatment and control treatment[36]. Further investigations into the effect of both amylocaine and calcium folinate treatment on osteoblast differentiation and bone growth are clearly warranted.

Using the CMap to find compounds that could inhibit osteoblast differentiation proved to be less optimal, with only of the three compounds tested working. Treatment with the top negative correlated compound, salbutamol, reduced both ALP activity and mineralization in hMSCs treated with osteogenic differentiation medium, relative to dex only treated cells, proving its ability to inhibit the dex-induced differentiation of hMSCs towards osteoblasts. Salbutamol is known to be an agonist of adrenergic β2 receptors and is used for the relief of bronchospasm in patients suffering from diseases such as asthma and chronic obstructive pulmonary disease (COPD)[37]. Salbutamol has previously been shown to have a deleterious effects on trabecular architecture, bone density, and mechanical strength of vertebrae and long bones in rats[38–40]. Our results are in line with this finding and suggest that the negative effect of salbutamol on bone may be due to reduced osteoblast differentiation. *In silico* analysis of the top DEGs following salbutamol treatment in the PC3 cell line revealed that a number of genes are shared by both instances of salbutamol, as well as metaraminol. We found *STC1* to be of particular interest as it was the most strongly regulated gene. *STC1* encodes for a glycoprotein that may play a role in the regulation of calcium and phosphate transport[41,42]. During osteogenic differentiation of fetal rat calvarial cells the knockdown of *STC1* expression using antisense oligonucleotides inhibited osteoblast differentiation, while *STC1* overexpression accelerated osteogenic development[42]. This contradicts the prediction by the connectivity map, which would suggest *STC1* to play a negative role in osteogenic differentiation, indicating that the differences in regulation may be due to use of different cell lines, species or culturing procedures and further investigation would be needed to determine the exact mechanism by which salbutamol negatively effects human osteoblast differentiation.

To conclude, this study showed that CMap is able to predict compounds that induce osteoblast differentiation but prediction of compounds that can negatively regulate osteoblast differentiation was not as accurate. For this study both positively and negatively correlated compounds were selected based on their ability to modulate genes leading to inhibition or stimulation of osteoblast differentiation. In both cases, the regulated genes are interesting to be considered as targets for therapeutic or

diagnostic purposes. Moreover, the DEGs of withaferin A, salbutamol and metaraminol contained interesting genes, HMOX1 and STC1, involved in osteoblast differentiation, giving us further insights into this process and possible therapeutic targets. Overall, this study supports the use of the CMap for the discovery of compounds and underlying genes that may stimulate human osteogenic differentiation and constitute potential new treatments for bone diseases, such as osteoporosis.

## 3.4 Materials and Methods

### *3.4.1 Materials*

MSCs were purchased from Lonza (MSC; PT-2501, Walkersville, MD, USA). αMEM was purchased from Gibco BRL, Life Technologies (Paisley, UK). Dexamethasone, β-glycerophosphate, calcium folinate, metaraminol, salbutamol, the calcium assay kit, and triton X-100 were purchased from Sigma–Aldrich (St. Louis, MO, USA). Withaferin A was purchased from LKT Laboratories Inc. (St. Paul, MN, USA). Amylocaine was purchased from Fagron Services B.V. (Uitgeest, NL). Diprophylline was purchased from Santa Cruz Biotechnology (Santa Cruz, CA, USA). Illumina Human HT-12 v3 BeadChip arrays, iScan and GenomeStudio V2010.1 (RRID:SCR_010973) (Gene Expression Module 1.6.0) were obtained from Illumina Inc. (Eindhoven, The Netherlands), the 2100 Bioanalyzer from Agilent Technologies (Santa Clara, CA, USA). Illumina TotalPrep RNA Amplification Kit was purchased from Ambion (Austin, TX, USA). BCA™ protein assay reagent A and B were purchased from Pierce (Rockford, IL, USA). Victor2 plate reader was purchased from PerkinElmer Life and Analytical Science (Waltham, MA, USA).

### *3.4.2 Cell culture*

Human bone marrow-derived Mesenchymal Stromal Cells were cultured as described previously[43,44]. hMSCs were cultured in αMEM medium containing 10% heat-inactivated fetal calf serum and 10 mM β-glycerophosphate (control medium for positively correlated compound experiments). For positively correlated compound experiments calcium folinate (ranging from 1 to 30 μM, 8mM stock prepared in $H_2O$), amylocaine (ranging from 1 to 50 μM, 15mM stock prepared in $H_2O$), or withaferin A (ranging from 0.03 to 1 μM, 1mM stock prepared in 100% ETOH) were added to the media. For experiments with the negatively correlated compounds the media was supplemented with 100 nM dexamethasone (dex) alone (control medium for negatively correlated experiments) or in combination with salbutamol (ranging from 1 to 16 μM, 20mM stock prepared in 100% ETOH), metaraminol (ranging from

1 to 16 μM, 20mM stock prepared in $H_2O$), or diprophylline (ranging from 1 to 16 μM, 20mM stock prepared in 100% ETOH). Cell extracts were harvested at different time points during culture by scraping the cells in PBS/triton (0.1%) and storing at -80ºC for biochemical analyses or in TRIzol and stored at -20ºC for gene expression analyses.

*3.4.3 Illumina gene chip–based gene expression*

For analysis of whole human genome expression, we used Illumina Human HT-12 v2 BeadChip arrays. Human MSCs (in triplicate) were treated for 6 hours with dexamethasone and next RNA was isolated as previously described[44]. RNA integrity of isolated RNA was assessed by RNA 6000 Nano assay on a 2100 Bioanalyzer. The Illumina TotalPrep RNA Amplification Kit was used for RNA amplification of each sample according to manufacturer's instructions. In short, T7 oligo(dT) primer was used to generate single-stranded cDNA, followed by a second-strand synthesis to generate double-stranded cDNA. Biotin-labeled cRNA was synthesized using T7 RNA polymerase. The cRNA was column-purified and checked for quality by RNA 6000 Nano assay. A total of 750 ng of cRNA was hybridized for each array using the standard Illumina protocol, using streptavidin-Cy3 for detection. Slides were scanned on an iScan and analyzed using GenomeStudio.

*3.4.4 Microarray analysis*

Background was subtracted from the raw data using GenomeStudio V2010.1 (Gene Expression Module 1.6.0), and data were processed, using the Bioconductor R2.10.0 Lumi package (RRID:SCR_006442, www.bioconductor.org)[45]. Data were transformed by variance stabilization and quantile normalization. Probes that were detected at least once in the experiments (Illumina detection p-value < 0.01) were considered to be expressed and were further analyzed. Differentially expressed probes were identified using Bioconductor Package Limma (www.bioconductor.org)[46] with p-values adjusted to reduce the false discovery rate (FDR; $p < 0.001$).

*3.4.5 Connectivity map query*

The CMap query was performed as previously described[15]. Briefly, to find compounds that have similar or opposite gene expression patterns compared to our human osteogenic differentiation-induced gene expression patterns, we generated gene signatures from microarray gene expression analyses of bone marrow-derived hMSCs treated with dex to stimulate osteogenic differentiation. We identified the 100 most significantly ($q<0.001$) up- and downregulated probes based on log ratio of gene

expression during osteogenic differentiation at 6 hours following the start of differentiation treatment, compared to undifferentiated cells at time point 0. Illumina probe IDs were converted to Affymetrix probe IDs, which are required as input into the CMap. After removal of duplicates we ended up with 77 up-regulated genes and 66 down-regulated genes (Appendix C, **Table A1**) that we submitted simultaneously for our CMap query (build02, http://www.broadinstitute.org/cmap/). This signature was queried against the CMap using the gene set enrichment analysis algorithm described by Lamb *et al.*[3] and a ranked list of gene profiles was generated by CMap. These steps are illustrated in figure **5**.

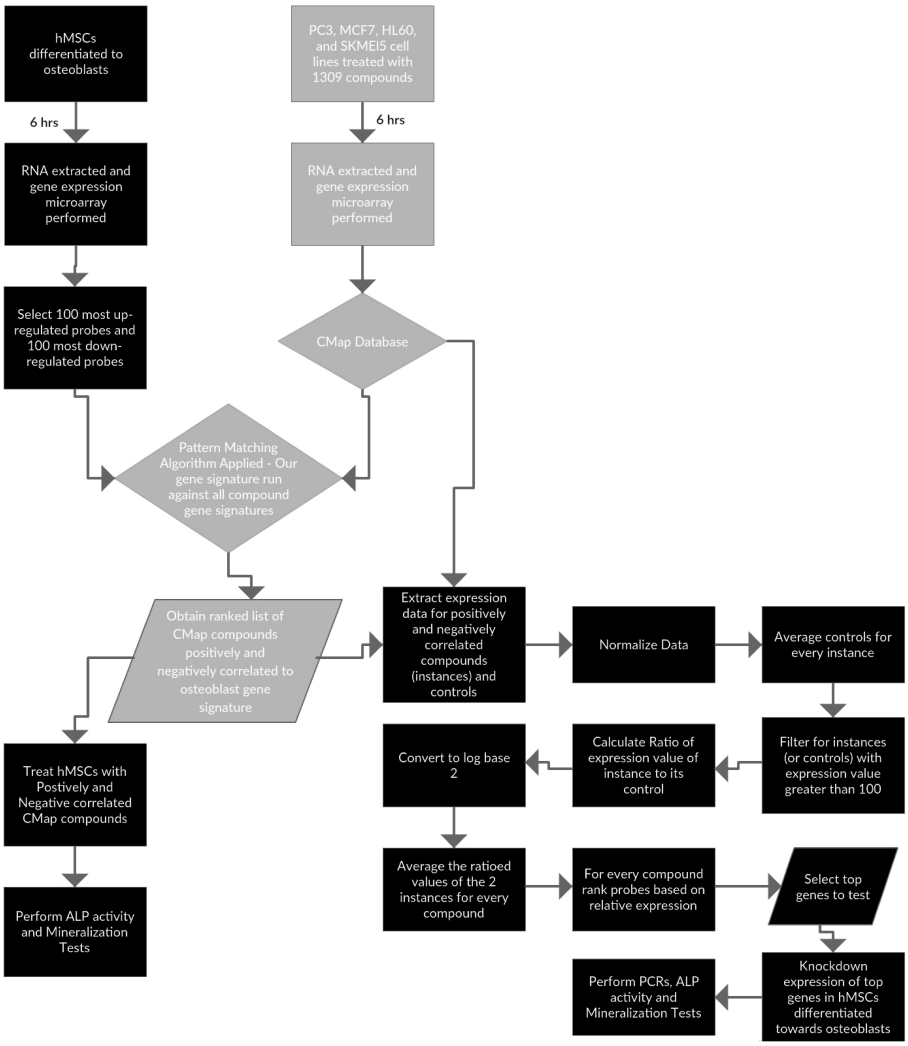

**Figure 5: Methods flow chart.** Graphical representation of the steps carried out as part of the methods for this work. Black boxes represent steps carried out by authors of this paper. Gray boxes represent steps performed by Lamb and colleagues[3] as part of the CMap and results were obtained through the web based query (www.broadinstitute.org/cmap/).

*3.4.6 Alkaline phosphatase, mineralization and protein assays*

Alkaline phosphatase (ALP) and calcium measurements were performed as described previously[47]. Briefly, ALP activity is determined by an enzymatic reaction, where the ALP-mediated conversion of PNPP to PNP during 10 min at 37°C is measured colorimetrically at 405 nm. For calcium measurements, cell lysates were incubated overnight with 0.24 M HCl at 4°C. Calcium content was determined colorimetrically using a calcium assay reagent prepared by combining 1 M ethanolamine buffer (pH 10.6) with 0.35 mM 0-cresolphthalein complexone in a ratio of 1:1. ALP results were adjusted for protein content of the cell lysates. For protein measurement, 200 µl of working reagent was added to 25 µl of sonicated cell lysate. The mixture was incubated for 30 min at 37°C, cooled down to room temperature and absorbance was measured at 595 nm. All measurements were performed using a Victor2 plate reader.

*3.4.7 In silico analysis of connectivity map data*

The gene profiles of CMap were extracted as "instances" that include the gene profiles of cells treated with the compound or vehicle. The instances were downloaded and processed by using software environment R Project for Statistical Computing (https://www.r-project.org, RRID:SCR_001905). For each instance, the raw probe data was converted into a numerical matrix diagram with the probes as row headers, conditions (treatment and controls) as column headers, and each matrix cell contained an intensity value.

Gene expression profiles in CMap were generated in multiple batches of microarrays, and thus, non-biological variation may occur between instances of a compound, such as the use of different array scanners. Therefore, a normalization step was utilised to equalize the distribution of probe intensities for every instance. The matrices of all instances were merged and the normalized intensity value in each cell was calculated by using the equation:

$$E_{normalized} = ( E_{probe} / E_{condition} ) * E_{total}$$

The intensity value in a cell ($E_{probe}$) was divided by the mean intensity value of the column ($E_{condition}$) and then multiplied by the mean intensity value of the whole matrix ($E_{total}$). After normalisation, the instances were separated into individual matrices and plotted as a box plot for visualisation (Fig **6**).

These steps are illustrated in the methods flow chart (Fig. **5**).

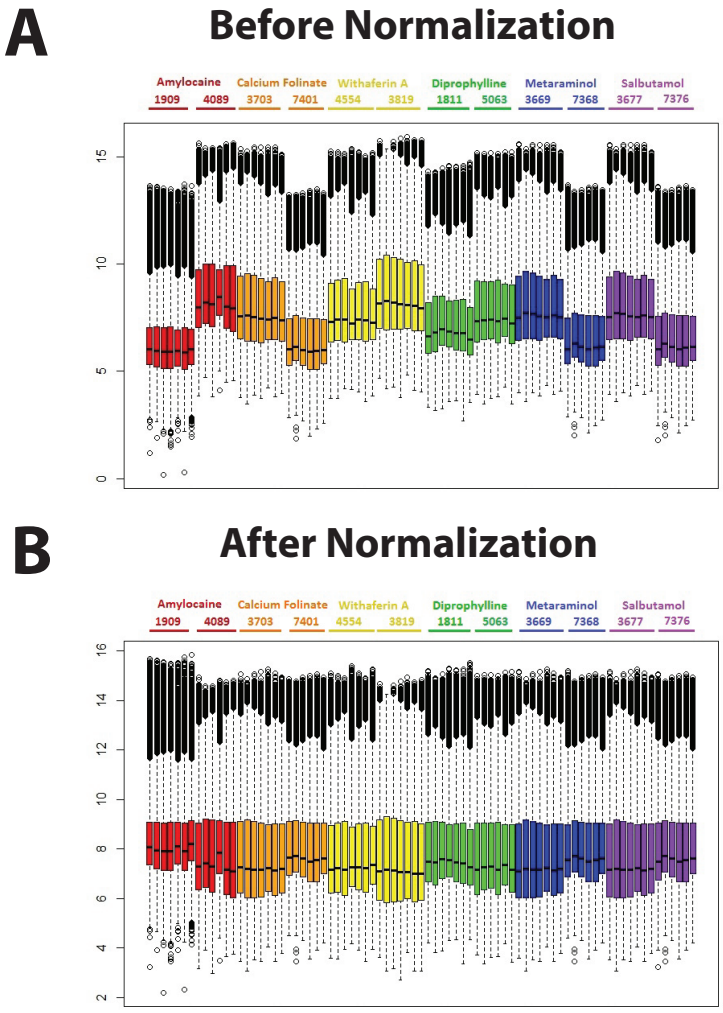


**Figure 6: Gene expression box plots pre- and post-normalization.** Box plots of all intensity values from multiple instances probe data set, before (A) and after normalization (B). The y-axis defines the probe intensity value in log base 2. The x-axis describes the instances. Each box plot represents the probes of a treatment or control.

*3.4.8 Differentially expressed gene (DEG) and gene ontology (GO) analysis*

For ease of understanding this process is illustrated in Figure **5**. DEGs analysis was performed to determine which genes are highly modulated by a treatment compared to the control. Each instance contains one treatment probe set and multiple control probe sets. First the control group of each probe was averaged. The criteria

for the threshold of the probe intensity were set as follow: For each instance if the normalized intensity of a probe for either the treatment or the averaged control samples was a value of at least 100 the probe will be included. Next, the ratio between the treatment sample and averaged control was calculated. Subsequently, the ratio value was log transformed (log base 2). For the next filtering step, only if both instances for a single compound (there were 2 instances (biological replicates) for every compound identified by the CMap) met the criteria for an intensity value of greater than 100 that probe was included for subsequent analysis. The ratio value of each probe of both instances for each compound were averaged. Probes were ranked based on their averaged, ratioed intensity value for each compound.
Functional annotation analysis was performed using the online application DAVID bioinformatics to look for functional enrichment among GO categories (biological process, cellular component and molecular function). For each CMap compound, the 100 most up-regulated and 100 most down-regulated probes (based on the above criteria) were uploaded to DAVID (RRID:SCR_001881) and the analysis was performed with default settings. The results were extracted that contained the GO term names, the Benjamini corrected p-values, the enrichment scores, and the number of genes that were annotated with the particular GO term.

*3.4.9 Quantification of mRNA expression*

RNA isolation, cDNA synthesis and PCR reactions were performed as described previously[44]. Oligonucleotide primer pairs were designed to be either on exon boundaries or spanning at least one intron (**Table 5**). Gene expressions were corrected for the housekeeping gene GAPDH. Experiments were performed in at least duplicate for at least two separate experiments.

**Table 5. Oligonucleotide primers used in the study.**

| Gene | Forward 5'-3" | Reverse 5'-3" |
|---|---|---|
| *CD55* | TACCCGTCTTCTATCTGGGCA | AGCCCATGGTTACTAGCGTC |
| *STC1* | CACTCAGGGAAAAGCATTCGT | GAAAGTGGAGCACCTCCGAA |
| *HMOX1* | ACTCCCTGGAGATGACTCCC | GCAACTCCTCAAAGAGCTGGA |
| *THBS1* | CAGGAGCAACCTCTACTCCG | CAGCAGGGATCCTGTGTGTA |
| *GAPDH* | CCGCATCTTCTTTTGCGTCG | CCCAATACGACCAAATCGTTG |

Sequences of primer sets used for qPCR in this study. All genes were detected using SYBR green.

*3.4.10 Lentiviral-mediated gene knockdown*

For gene knockdown of *HMOX1* and *STC1*, constructs from the TRC-Hs1.0 library (Thermo Scientific, Bleiswijk, Netherlands) were used (**Table 6**). Non-

targeting shRNA vector with a scrambled sequence (**Table 6**) was used as a negative control. In short, lentivirus (LV) was produced by transient transfection of each LV construct into human embryonal kidney (HEK) 293T cells (RCB Cat# RCB2202, RRID:CVCL_0063) using a standard calcium phosphate precipitation technique. The appropriate LV vector plasmid (3 μg) and the packaging vector plasmids (9 μg of ViraPower mix (ThermoFisher)) were cotransfected into subconfluent HEK-293T cells plated in 100-mm dishes. Viral supernatants were harvested 48 and 72 hours after transfection, filtered through a 0.45-μm pore size filter, and used immediately for hMSC transduction or stored at –80°C until use. One day prior to LV transduction, hMSC were seeded into 12-well plates. Transduction consisted of overnight LV incubation, after which the medium was replaced with treatment medium and the cells were cultured until further analysis.

**Table 6. shRNA Sequences.**

| **ID** | **Target Sequence** |
|---|---|
| ***HMOX1*** | CGGGCCAGCAACAAAGTGCAA |
| ***STC1*** | GCATTCGTCAAAGAGAGCTTA |
| **Non-targeting shRNA Oligo Sequence** | |
| ***Scrambled*** | CCGGCAACAAGATGAAGAGCACCAACTCGAGTTGGTGCTCTTCATCTTGTTGTTTTT |

The target sequences of shRNAs for silencing of the HMOX1 and STC1 genes and non-targeting scrambled.

### *3.4.11 Statistics*

Biochemical analysis of hMSCs treated with positively correlated compounds were performed in at least four independent experiments using cells from at least three different donors performed at least in duplicate. Negatively correlated compounds were tested in at least three independent experiments using hMSCs from at least two different donors performed at least in duplicate. Gene expression and knockdown studies were performed in at least two independent experiments at least in triplicate. Values displayed are mean +/- SEM. Significance was calculated using either the Student's t-test or the one-way ANOVA followed by Tukey's post hoc test for difference between all treatments or Bonferroni's post-hoc test for differences between a control and each other treatment, where appropriate, using GraphPad Prism 6.0 (RRID:SCR_002798). P-values $<0.05$ were considered significant.

## References


1. Johnell, O. & Kanis, J. A. An estimate of the worldwide prevalence and disability associated with osteoporotic fractures. *Osteoporos. Int.* **17**, 1726–33 (2006).
2. Kanis, J. A. & Johnell, O. Requirements for DXA for the management of osteoporosis in Europe. *Osteoporos. Int.* **16**, 229–38 (2005).
3. Lamb, J. *et al.* The Connectivity Map: using gene-expression signatures to connect small molecules, genes, and disease. *Science* **313**, 1929–35 (2006).
4. Qu, X. A. & Rajpal, D. K. Applications of Connectivity Map in drug discovery and development. *Drug Discov. Today* **17**, 1289–98 (2012).
5. Chang, M., Smith, S., Thorpe, A., Barratt, M. J. & Karim, F. Evaluation of phenoxybenzamine in the CFA model of pain following gene expression studies and connectivity mapping. *Mol. Pain* **6**, 56 (2010).
6. Wang, G. *et al.* Expression-based in silico screening of candidate therapeutic compounds for lung adenocarcinoma. *PLoS One* **6**, e14573 (2011).
7. Kunkel, S. D. *et al.* mRNA expression signatures of human skeletal muscle atrophy identify a natural compound that increases muscle mass. *Cell Metab.* **13**, 627–38 (2011).
8. Dyle, M. C. *et al.* Systems-based discovery of tomatidine as a natural small molecule inhibitor of skeletal muscle atrophy. *J. Biol. Chem.* **289**, 14913–24 (2014).
9. Campbell, J. D. *et al.* A gene expression signature of emphysema-related lung destruction and its reversal by the tripeptide GHK. *Genome Med.* **4**, 67 (2012).
10. Zhong, Y. *et al.* Renoprotective effect of combined inhibition of angiotensin-converting enzyme and histone deacetylase. *J. Am. Soc. Nephrol.* **24**, 801–11 (2013).
11. Koh, L. W.-H. *et al.* A distinct reactive oxygen species profile confers chemoresistance in glioma-propagating cells and associates with patient survival outcome. *Antioxid. Redox Signal.* **19**, 2261–79 (2013).
12. Karube, K. *et al.* Comprehensive gene expression profiles of NK cell neoplasms identify vorinostat as an effective drug candidate. *Cancer Lett.* **333**, 47–55 (2013).
13. Gao, L. *et al.* Discovery of the neuroprotective effects of alvespimycin by computational prioritization of potential anti-parkinson agents. *FEBS J.* **281**, 1110–1122 (2014).
14. Faria, C. C. *et al.* Identification of alsterpaullone as a novel small molecule inhibitor to target group 3 medulloblastoma. *Oncotarget* **6**, 21718–29 (2015).
15. Brum, A. M. A. M. *et al.* Connectivity Map-based discovery of parbendazole reveals targetable human osteogenic pathway. *Proc. Natl. Acad. Sci.* **112**, 201501597 (2015).
16. Khedgikar, V. *et al.* Withaferin A: a proteasomal inhibitor promotes healing after injury and exerts anabolic effect on osteoporotic bone. *Cell Death Dis.* **4**, e778 (2013).
17. Khedgikar, V. *et al.* Preventive effects of withaferin A isolated from the leaves of an Indian medicinal plant Withania somnifera (L.): Comparisons with 17-β-estradiol and alendronate. *Nutrition* **31**, 205–213 (2015).
18. Grogan, P. T., Sarkaria, J. N., Timmermann, B. N. & Cohen, M. S. Oxidative cytotoxic agent withaferin A resensitizes temozolomide-resistant glioblastomas via MGMT depletion and induces apoptosis through Akt/mTOR pathway inhibitory modulation. *Invest. New Drugs* **32**, 604–17 (2014).
19. Roy, R. V, Suman, S., Das, T. P., Luevano, J. E. & Damodaran, C. Withaferin A, a steroidal lactone from Withania somnifera, induces mitotic catastrophe and growth arrest in prostate cancer cells. *J. Nat. Prod.* **76**, 1909–15 (2013).
20. Park, J. W., Min, K.-J., Kim, D. E. & Kwon, T. K. Withaferin A induces apoptosis through the generation of thiol oxidation in human head and neck cancer cells. *Int. J. Mol. Med.* **35**, 247–52 (2015).
21. Choi, A. M. & Alam, J. Heme oxygenase-1: function, regulation, and implication of a novel stress-inducible protein in oxidant-induced lung injury. *Am. J. Respir. Cell Mol. Biol.* **15**, 9–19 (1996).
22. Le, W. D., Xie, W. J. & Appel, S. H. Protective role of heme oxygenase-1 in oxidative stress-induced neuronal injury. *J. Neurosci. Res.* **56**, 652–8 (1999).
23. Ghattas, M. H., Chuang, L. T., Kappas, A. & Abraham, N. G. Protective effect of HO-1 against oxidative stress in human hepatoma cell line (HepG2) is independent of telomerase enzyme activity. *Int. J. Biochem. Cell Biol.* **34**, 1619–28 (2002).
24. Vanella, L. *et al.* HO-1 expression increases mesenchymal stem cell-derived osteoblasts but decreases adipocyte lineage. *Bone* **46**, 236–43 (2010).
25. Barbagallo, I. *et al.* Overexpression of heme oxygenase-1 increases human osteoblast stem cell differentiation. *J. Bone Miner. Metab.* **28**, 276–288 (2010).
26. Larsen, M. J., Thomassen, M., Tan, Q., Sørensen, K. P. & Kruse, T. A. Microarray-based RNA profiling of breast cancer: batch effect removal improves cross-platform consistency. *Biomed Res. Int.* **2014**, 651751 (2014).
27. Harper, K. N., Peters, B. A. & Gamble, M. V. Batch effects and pathway analysis: two potential perils in cancer studies involving DNA methylation array analysis. *Cancer Epidemiol. Biomarkers Prev.* **22**, 1052–60 (2013).

28. Lee-Son, S., Wang, G. K., Concus, A., Crill, E. & Strichartz, G. Stereoselective inhibition of neuronal sodium channels by local anesthetics. Evidence for two sites of action? *Anesthesiology* **77**, 324–35 (1992).
29. Ragsdale, D. S., Scheuer, T. & Catterall, W. A. Frequency and voltage-dependent inhibition of type IIA Na+ channels, expressed in a mammalian cell line, by local anesthetic, antiarrhythmic, and anticonvulsant drugs. *Mol. Pharmacol.* **40**, 756–65 (1991).
30. Courtney, K. R. Structure-activity relations for frequency-dependent sodium channel block in nerve by local anesthetics. *J. Pharmacol. Exp. Ther.* **213**, 114–9 (1980).
31. Hirota, K., Browne, T., Appadu, B. L. & Lambert, D. G. Do local anaesthetics interact with dihydropyridine binding sites on neuronal L-type Ca2+ channels? *Br. J. Anaesth.* **78**, 185–8 (1997).
32. Fan, C.-M., Foster, B. K., Hui, S. K. & Xian, C. J. Prevention of bone growth defects, increased bone resorption and marrow adiposity with folinic acid in rats receiving long-term methotrexate. *PLoS One* **7**, e46915 (2012).
33. Fan, C. *et al.* Damaging effects of chronic low-dose methotrexate usage on primary bone formation in young rats and potential protective effects of folinic acid supplementary treatment. *Bone* **44**, 61–70 (2009).
34. Xian, C. J., Cool, J. C., Scherer, M. A., Fan, C. & Foster, B. K. Folinic acid attenuates methotrexate chemotherapy-induced damages on bone growth mechanisms and pools of bone marrow stromal cells. *J. Cell. Physiol.* **214**, 777–785 (2008).
35. Georgiou, K. R., Nadhanan, R. R., Fan, C.-M. & Xian, C. J. Methotrexate-Induced Bone Marrow Adiposity Is Mitigated by Folinic Acid Supplementation Through the Regulation of Wnt/β-Catenin Signalling. *J. Cell. Physiol.* **230**, 648–656 (2015).
36. Iqbal, M. P., Ahmed, M., Umer, M., Mehboobali, N. & Qureshi, A. A. Effect of methotrexate and folinic acid on skeletal growth in mice. *Acta Paediatr.* **92**, 1438–44 (2003).
37. Patel, M. & Thomson, N. C. (R)-salbutamol in the treatment of asthma and chronic obstructive airways disease. *Expert Opin. Pharmacother.* **12**, 1133–41 (2011).
38. Bonnet, N. *et al.* Doping dose of salbutamol and exercise: deleterious effect on cancellous and cortical bones in adult rats. *J. Appl. Physiol.* **102**, 1502–9 (2007).
39. Bonnet, N. *et al.* Alteration of trabecular bone under chronic beta2 agonists treatment. *Med. Sci. Sports Exerc.* **37**, 1493–501 (2005).
40. Bonnet, N. *et al.* Severe bone alterations under β2 agonist treatments: Bone mass, microarchitecture and strength analyses in female rats. *Bone* **37**, 622–633 (2005).
41. Chou, M.-Y. *et al.* Stanniocalcin-1 controls ion regulation functions of ion-transporting epithelium other than calcium balance. *Int. J. Biol. Sci.* **11**, 122–32 (2015).
42. Yoshiko, Y., Maeda, N. & Aubin, J. E. Stanniocalcin 1 stimulates osteoblast differentiation in rat calvaria cell cultures. *Endocrinology* **144**, 4134–43 (2003).
43. Eijken, M. *et al.* The activin A-follistatin system: potent regulator of human extracellular matrix mineralization. *FASEB J.* **21**, 2949–60 (2007).
44. Bruedigam, C. *et al.* Basic techniques in human mesenchymal stem cell cultures: differentiation into osteogenic and adipogenic lineages, genetic perturbations, and phenotypic analyses. *Curr. Protoc. Stem Cell Biol.* **Chapter 1**, Unit1H.3 (2011).
45. Du, P., Kibbe, W. A. & Lin, S. M. lumi: a pipeline for processing Illumina microarray. *Bioinformatics* **24**, 1547–8 (2008).
46. Smyth, G. K. Linear models and empirical bayes methods for assessing differential expression in microarray experiments. *Stat. Appl. Genet. Mol. Biol.* **3**, Article3 (2004).
47. Eijken, M. *et al.* The essential role of glucocorticoids for proper human osteoblast differentiation and matrix mineralization. *Mol. Cell. Endocrinol.* **248**, 87–93 (2006).

# Chapter 4

# Identification of Chloride Intracellular Channel Protein 3 as a Novel Gene Affecting Human Bone Formation

Andrea M Brum, Cindy S van der Leije, Marijke Schreuders-Koedam, Jeroen Verhoeven, Mark Janssen, Dick HW Dekkers, Jeroen AA Demmers, Marco Eijken, Jeroen van de Peppel, Johannes PTM van Leeuwen, and Bram CJ van der Eerden

*JBMR Plus. (2017) 1(1): 16–26.*

Abstract

Osteoporosis is a common skeletal disorder characterized by low bone mass leading to increased bone fragility and fracture susceptibility. The bone building cells, osteoblasts, are derived from mesenchymal stromal cells (MSCs); however, with increasing age osteogenic differentiation is diminished and more adipocytes are seen in the bone marrow, suggesting a shift in MSC lineage commitment. Identification of specific factors that stimulate osteoblast differentiation from human MSCs may deliver therapeutic targets to treat osteoporosis. The aim of this study was to identify novel genes involved in osteoblast differentiation of human bone marrow–derived MSCs (hMSCs). We identified the gene chloride intracellular channel protein 3 (*CLIC3*) to be strongly upregulated during MSC-derived osteoblast differentiation. Lentiviral overexpression of *CLIC3* in hMSCs caused a 60% increase of matrix mineralization. Conversely, knockdown of *CLIC3* in hMSCs using two short-hairpin RNAs (shRNAs) against *CLIC3* resulted in a 69% to 76% reduction in *CLIC3* mRNA expression, 53% to 37% less alkaline phosphatase (ALP) activity, and 78% to 88% less matrix mineralization compared to scrambled control. Next, we used an in vivo human bone formation model in which hMSCs lentivirally transduced with the *CLIC3* overexpression construct were loaded onto a scaffold (hydroxyapatite-tricalcium-phosphate), implanted under the skin of NOD-SCID mice, and analyzed for bone formation 8 weeks later. *CLIC3* overexpression led to a 15-fold increase in bone formation (0.33% versus 5.05% bone area relative to scaffold). Using a Clic3-His-tagged pull-down assay and liquid chromatography–mass spectrometry (LS/MS)-based proteomics analysis in lysates of osteogenically differentiated hMSCs, we showed that CLIC3 interacts with NIMA-related kinase 9 (NEK9) and phosphatidylserine synthase 1 (PTDSS1) in vitro, and this finding was supported by immunofluorescent analysis. In addition, inhibition of *NEK9* or *PTDSS1* gene expression by shRNAs inhibited osteoblast differentiation and mineralization. In conclusion, we successfully identified CLIC3 to be a lineage-specific gene regulating osteoblast differentiation and bone formation through its interaction with NEK9 and PTDSS1.

## 4.1 Introduction

Bone is a dynamic organ that throughout life undergoes constant remodeling through bone formation by osteoblasts and bone resorption by osteoclasts. Osteoporosis is a common skeletal disease characterized by reduced bone mass and increased fragility and fracture risk, occurring when bone remodeling is disrupted and bone resorption overtakes bone formation[1]. The vast majority of osteoporosis treatments, such as bisphosphonates, act through reduction of bone resorption, and result in modest increases in bone density; however, these treatments do not result in a true bone anabolic effect so patients do not regain the bone that has been lost at time of diagnosis. An ideal treatment would also stimulate osteoblast differentiation and/or bone formation to help repair the already damaged bone microarchitecture. Identification of novel genes or processes that stimulate osteoblast differentiation may therefore deliver therapeutic targets for the development of novel treatments for bone diseases such as osteoporosis.

Osteoblasts are derived from the bone marrow mesenchymal stem, or stromal, cells (MSCs) and undergo terminal differentiation to form osteocytes[2]. Besides osteoblasts, MSCs give rise to other cell types, including adipocytes and chondrocytes[3]. Osteogenic differentiation of MSCs is a tightly regulated process that progresses through several phases. MSCs are driven to the osteogenic lineage by expression of the osteoblast-specific transcription factors Runx2 and Osterix[4–6]. After initial commitment, differentiation towards mature osteoblasts is typically characterized by the expression of collagen type I, osteocalcin, osteopontin, bone sialoprotein, and alkaline phosphatase (ALP)[7]; however, the precise mechanism of how human bone marrow–derived MSCs (hMSCs) differentiate into osteoblasts is still largely unknown, including the exact mechanism by which glucocorticoids stimulate osteoblast differentiation *in vitro*[8,9].

With aging there is a decrease in bone mass and increased bone fragility, while at the same time there is an increase in total and bone marrow adiposity[10,11]. As both the osteogenic and adipogenic lineages derive from the same progenitor, it appears that there is a shift in the lineage decision-making process of MSCs with increasing age. This theory is supported by previous work showing that bone marrow derived mesenchymal progenitors from aged humans, rats, and mice preferentially differentiate toward the adipogenic, rather than osteogenic, lineage[10–14].

Our aim was to expand the knowledge of human osteoblastogenesis by identifying novel genes and processes involved in differentiation of hMSCs to the osteogenic lineage. Gene expression analysis of hMSCs undergoing osteogenic and adipogenic differentiation led us to study chloride intracellular channel protein 3 (*CLIC3*) as an osteogenic lineage specific candidate. CLIC proteins are a conserved

family of proteins first identified when a novel chloride ion channel was discovered in bovine kidney[15,16]. This family of proteins can transition between a soluble globular form and an integral membrane protein that is able to mediate ion conductance and/or ion channel formation[17,18]. However, their role as channel proteins under physiological conditions has been strongly debated. To date, six CLIC paralogues have been identified in vertebrates, all of which appear to have diversified in function[18,19]. CLIC3 is a largely unstudied 26.6-kDa member of the CLIC family. It has been implicated to be involved in cellular processes including integrin recycling[20,21], endosome trafficking[22] and cell growth via interactions with ERK7[23].

## 4.2 Results

### *4.2.1 CLIC3 is upregulated during human osteogenic differentiation and downregulated during adipogenesis*

*CLIC3* is dynamically expressed in human mesenchymal stromal cells (hMSCs) during osteogenic differentiation (Fig. **1**). Figure **1** shows that expression of *CLIC3* is increased during the osteogenic differentiation of hMSCs, peaking between 1 and 3 days of culture, compared to non-differentiating, In addition, we saw that CLIC3 expression goes down in adipogenic cells compared to non-differentiating, showing an opposite effect to that of osteoblasts. These data led us to further scrutinize *CLIC3* as a candidate gene for human osteoblastogenesis.

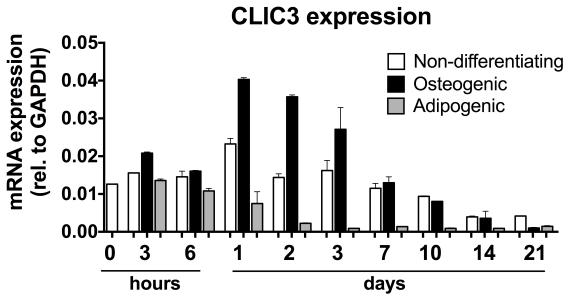


**Figure 1. *CLIC3* expression is upregulated during osteoblast differentiation and downregulated during adipocyte differentiation.** mRNA expression levels of *CLIC3* in hMSCs cultured in non-differentiating (white bars), osteogenic (black bars), and adipogenic (grey bars) conditions over 3 weeks assessed by quantitative PCR. Graph displays a representative experiment. n=2.

### *4.2.2 Overexpression of CLIC3 in hMSCs enhances in vitro osteogenic differentiation*

To determine the role CLIC3 has in human osteoblastogenesis we overexpressed *CLIC3* in hMSCs by lentiviral transduction and studied its effect on classical biochemical markers of osteoblast differentiation. Efficient overexpression of

*CLIC3* in hMSCs was determined by gene expression analysis and immunoblotting. Fig. **2A** demonstrates successfully elevated *CLIC3* mRNA expression by greater than 100-fold at both day 1 and 7 of culture in both non-differentiating and differentiating hMSCs. Concordantly, protein levels of CLIC3 were also strongly increased at day 10 of culture in non-differentiating and differentiating hMSCs (Fig. **2B**). Immunofluorescent CLIC3 detection in differentiating hMSCs reveals that *CLIC3* overexpression (Fig. **2C)** intensifies the level of CLIC3 protein in most cells, compared to empty vector (EV)-transduced cells (Fig. **2D**). CLIC3 expression is predominately localized to the perinuclear region (arrow heads, Fig. **2C,D**), In CLIC3-overexpressing cells (Fig. **2C**) there is increased expression in the cytoplasm (arrows) and nucleus (asterisk) compared to control cells (Fig. **2D**). *CLIC3* overexpression did not affect total protein levels (Fig. **2E**) or ALP activity (Fig. **2F**) in osteogenic hMSCs, but it did enhance mineralization by 60% as shown by total calcium quantification after 3 weeks of culture (Fig. **2G**). Overall, these results show that we have successfully overexpressed *CLIC3* in hMSCs and that CLIC3 enhances *in vitro* mineralization.

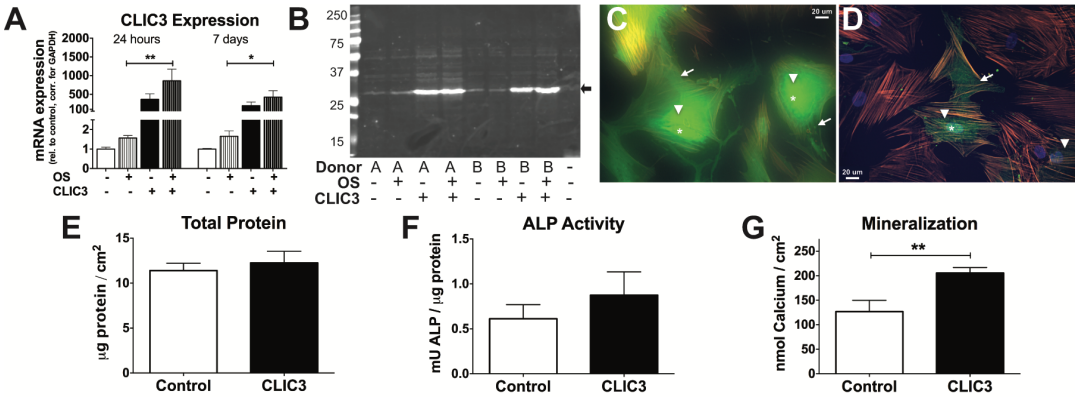


**Figure 2. *CLIC3* overexpression enhances human osteoblast differentiation**. Enhancement of *CLIC3* expression was assessed by (A) quantification of *CLIC3* mRNA expression by quantitative PCR of hMSCs transduced with empty vector (white bars) or *CLIC3* overexpression vector (black bars) under non-differentiating (solid bars) or osteogenic differentiation (patterned bars) conditions at 24 hours (left 4 bars) or 7 days (right 4 bars) after the start of differentiation, or by (B) immunoblotting in protein lysates collected 10 days post induction of differentiation in two hMSC donors (A and B) using anti-CLIC3 antibody. Arrow indicates the predicted size of CLIC3 protein at 27kDa, last lane contains loading buffer only. In additional CLIC3 expression was visualized by immunofluorescence microscopy using CLIC3 antibody in hMSCs differentiated to osteoblasts and transduced with *CLIC3* (C) or empty vector (D) at 400x total magnification after 4 days of differentiation. CLIC3, in green, is seen in the cytoplasm (arrows), the perinuclear region (arrow heads), and some nuclear staining (asterisk); actin cytoskeleton was visualized by phalloidin antibody in orange, and nuclei by DAPI in blue. Biochemical assays are shown for total protein (Day 6) (E), ALP activity (Day 6) (F), and mineralization (Week 3) (G) of hMSCs transduced with CLIC3 (black bars) or empty vector (white bars) and osteogenic culture conditions. Graphs display combined results of all experiments. (*A*) $n = 8–12$; (*E*,*F*) $n = 18$; (*G*) $n = 19$. $*p < 0.05$, $**p < 0.01$. OS = osteogenic media. CLIC3 = lentiviral transduction with *CLIC3*expression vector 1 day prior to the start of differentiation; DAPI = 4,6-diamidino-2-phenylindole.

*4.2.3 CLIC3 is critical for in vitro human osteogenic differentiation*

To determine if CLIC3 is essential for human osteoblast differentiation we used short hairpin RNAs (shRNAs) against endogenous *CLIC3* to knockdown its expression in hMSCs. Two separate shRNAs decreased *CLIC3* expression in hMSCs by 76% and 69% (Fig. **3A**), respectively, compared to cells transduced with scrambled shRNA. Total protein levels were not affected by either shRNA (Fig. **3B**). Knockdown of *CLIC3* mRNA expression reduced ALP activity by 53% and 37%, respectively, after 1 week of culture (Fig. **3C**). After 3 weeks of culture in osteogenic medium, CLIC3 silencing reduced mineralization by approximately 80% compared to the scrambled control (Fig. **3D**).

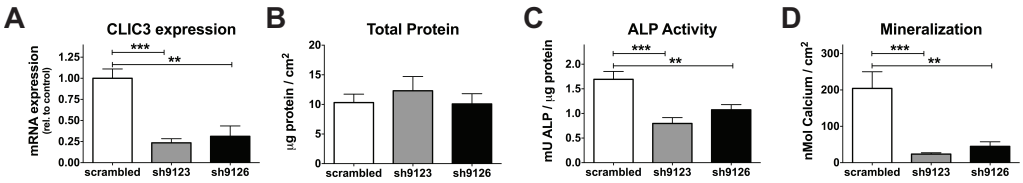


**Figure 3. Knockdown of *CLIC3* expression inhibits human osteoblast differentiation.** Transduction of hMSCs with 2 shRNAs against *CLIC3* (shaded bars) reduces (A) mRNA expression of *CLIC3* as determined by quantitative PCR (day 4), (B) Total Protein (day 6), (C) ALP activity (day 6), and (D) mineralization (week 3) compared to scrambled control (white bar). Graphs display combined results from all experiments. A: n=4-5, B: n=7, C: n=6. ** $p < 0.01$, *** $p < 0.001$.

*4.2.4 CLIC3 enhances in vivo human bone formation*

In order to test the *in vivo* effect of *CLIC3* manipulation on human bone formation we subcutaneously implanted hMSCs transduced with *CLIC3* or empty vector (control) loaded onto a hydroxyapatite/tricalcium phosphate (HA-TCP) scaffold in immune-deficient mice and quantified the amount of heterotopic bone formed. As shown in Fig. **4**, hMSCs overexpressing *CLIC3* formed a significantly greater amount of ectopic bone compared to MSCs transduced with an empty vector. This is visualized in the representative Goldner-stained sections made from implants containing *CLIC3* overexpressing hMSCs (Fig. **4A,B**) containing patches of newly formed bone and osteoblasts compared to the control-treated hMSC-implants (Fig. **4C,D**) showing low level of newly formed bone. Quantification of the amount of new bone formed revealed that implants from *CLIC3*-overexpressing hMSCs contain 15 times more bone compared to implants containing control-treated cells (Fig. **4E**). These results clearly show that *CLIC3* enhances *in vivo* bone human formation.

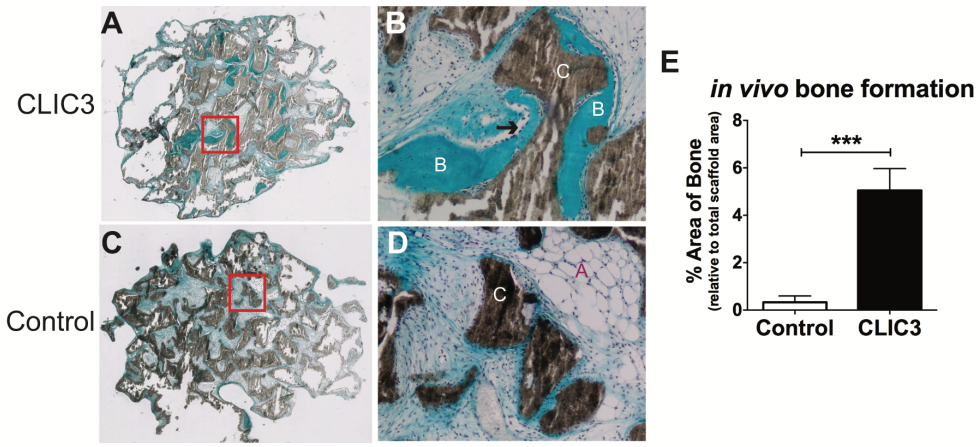


**Figure 4. *CLIC3* promotes human bone formation *in vivo*.** Histological sections of explants of *CLIC3* overexpressing hMSCs (A, low magnification; B, high magnification) implanted under the skin of immune deficient (NOD-SCID) mice show more prevalent areas of new bone formation (labeled 'B') and osteoblasts (arrow) compared to empty vector-transduced cells (C, low magnification; D, high magnification). HA-TCP ceramic scaffold is labeled 'C', adipocytes are labeled 'A'. E: *CLIC3* overexpression in hMSCs (black bar) increases the amount of newly formed bone in explants compared to control cells (white bar) based on quantification of the area of new bone formed as a percentage of total scaffold area, using ImageJ software. n=9-10. *** $p < 0.001$.

### *4.2.5 CLIC3 pull-down identifies 52 proteins as potential interacting with CLIC3 in differentiating osteoblasts*

In an attempt to gain insight into the molecular interactions by which CLIC3 acts on osteoblasts, we performed a pull-down assay followed by mass spectrometry (MS) analysis to identify which proteins, in cell extracts of hMSCs differentiated towards osteoblasts, associate with CLIC3. **Table A3** (Appendix C) lists all CLIC3-His pulled-down proteins ranked according to the average label-free quantification (LFQ) intensity ratio of CLIC3-His-baited samples versus control samples, which are based on non-specific binding. Bioinformatic analyses of these proteins were performed using Ingenuity Pathway Analysis and showed that "PRPP biosynthesis I", "gap junction signaling", "paxillin signaling", "integrin signaling" and various endocytosis and exocytosis pathways comprise the most significant canonical pathways in the list of proteins (summarized in **Table 1,** detailed in Appendix C, **Table A4**). Using DAVID Gene Ontology (GO) analysis, the most significant GO terms included processes related to RNA nuclear export and localization, transport, cell adhesion, and localization to the nuclear periphery and pores (summarized in **Table 1,** detailed in Appendix C, **Table A5**). Out of the 52 proteins identified by CLIC3-His pull-down eight proteins were uniquely present in our CLIC3 samples, as compared to control samples (**Table 2**), and we chose to analyze 2 of these proteins further: NIMA-related kinase 9 (NEK9) and phosphatidylserine synthase 1 (PTDSS1).

**Table 1: Summary of Top of Canonical Pathways and GO Terms**

| Canonical Pathway[1] | Biological Process[2] | Molecular Function[2] | Cellular Component[2] |
|---|---|---|---|
| -PRPP biosynthesis<br>-gap junction signaling<br>-paxillin signaling<br>-integrin signaling<br>-endocytosis/exocytosis | -export from nucleus<br>-RNA localization<br>-transport<br>-adhesion | -RNA binding<br>-cadherin binding<br>-cell adhesion: protein and molecule binding | -adherens cell junction<br>-cytosol<br>-nuclear periphery/pore |

Top canonical pathways determined by Ingenuity pathway analysis from the 52 proteins found to pull down with Clic3-His. GO term clusters that have been identified by DAVID bioinformatics resources for the same proteins. The GO terms within the clusters had a significance of Benjamini corrected p-value < 0.05. The headers "biological process", "molecular function", and "cellular components" stand for the GO category to which the GO term is annotated.

[1]:determined by Ingenuity pathway analysis (http://www.ingenuity.com/)

[2]:determined by DAVID Functional Annotation Analysis (http://david.ncifcrf.gov)

*4.2.6 CLIC3 interacts with NEK9 and PTDSS1 during osteogenic differentiation of MSCs*

To confirm the colocalization of CLIC3 with the proteins identified by the pull-down assay we performed immunofluorescent analysis. At day 5 of differentiation, CLIC3 (Fig. **5A**) and NEK9 (Fig. **5B**) co-localize in the perinuclear region (arrows, Fig. **5D)** in CLIC3 overexpressing hMSCs, with some CLIC3 expression seen in the nucleus as well (asterisk, Fig. **5A)**, overlapping with DAPI nuclear staining (**5C,D**).

Similar to Figure 5A, figure **5E** exhibits the cytosolic (arrowhead), perinuclear (arrows), and nuclear distribution of CLIC3 in osteogenically differentiated hMSCs, whereas PTDSS1 is localized specifically to the perinuclear (arrows) and nuclear (asterisk, overlapping with DAPI nuclear staining (**5G**)) compartments (Fig. **5F**), and colocalization is seen in the perinuclear region (Fig. **5H**).

*4.2.7 Inhibition of NEK9 and PTDSS1 affects osteogenic differentiation of hMSCs*

To determine if NEK9 or PTDSS1 play a role in human osteoblast differentiation, we studied the effects of shRNA knockdown of *NEK9* and *PTDSS1* in osteogenically differentiating hMSCs. We found five shRNAs that all reduced *NEK9* mRNA expression between 60% and 82% compared to the scrambled control 4 days post-transduction (Fig. **6A**). Four of the five shRNAs against *NEK9* inhibited mineralization by 70% or more after 3 weeks of osteogenic differentiation (Fig. **6B**). Although the majority of *NEK9* shRNAs had no effect on total protein levels, one shRNA did decrease total proteins levels after 3 weeks of treatment (Fig. **6C**). We identified five shRNAs against *PTDSS1* that all reduced mRNA expression in the range of 48% to 75% in differentiating hMSCs (Fig. **6D**). We observed that three out of the five shRNAs against *PTDSS1* strongly inhibited mineralization, by 67% to 92% (Fig. **6E**). The majority of shRNAs against *PTDSS1* had no effect on total protein

**Table 2: Top proteins identified in CLIC3-His pull down**

| Protein | Gene symbol | LFQ CLIC3_A | LFQ CLIC3_B | LFQ EV_A | LFQ EV_B | No. of Unique Peptides | Ratio LFQ CLIC3:EV |
|---|---|---|---|---|---|---|---|
| **Chloride intracellular channel protein 3** | CLIC3 | 1.27E+09 | 1.19E+09 | nd | nd | 15 | 1.23E+09 |
| **Serine/threonine-protein kinase Nek9** | NEK9 | 6.31E+06 | 5.12E+06 | nd | nd | 3 | 5.71E+06 |
| **1-phosphatidylinositol 4,5-bisphosphate phosphodiesterase beta-3** | PLCB3 | 2.84E+06 | 4.29E+06 | nd | nd | 7 | 3.56E+06 |
| **Aminoacyl tRNA synthase complex-interacting multifunctional protein 1** | AIMP1 | 2.49E+06 | 3.29E+06 | nd | nd | 3 | 2.89E+06 |
| **Casein kinase II subunit alpha 3; alpha 1** | CSNK2A1; CSNK2A3 | 1.70E+06 | 3.00E+06 | nd | nd | 3 | 2.35E+06 |
| **40S ribosomal protein S28** | RPS28 | 1.64E+06 | 1.97E+06 | nd | nd | 3 | 1.80E+06 |
| **Phosphatidylserine synthase 1** | PTDSS1 | 1.21E+06 | 1.73E+06 | nd | nd | 3 | 1.47E+06 |
| **Nuclear pore complex protein Nup160** | NUP160 | 1.15E+06 | 1.06E+06 | nd | nd | 3 | 1.11E+06 |

Proteins identified by MS from CLIC3-His pull-down assay in hMSCs undergoing osteogenic differentiation. Protein lysates from osteogenically differentiated hMSCs were isolated on day 5 in cultures either overexpressing His-tagged CLIC3 or transduced with empty vector (EV) control, and subjected to protein pull-down for the His-tagged CLIC3 and proteins binding to it. Proteins were determined by mass spectrometry measurements (n=2). The top proteins are listed here, ranked on their ratio of CLIC3 versus control average LFQ intensity (i.e. present in CLIC3 overexpressing condition and absent in the EV condition). LFQ: Label-free quantification, nd: not detected.

levels; however, sh25-treated hMSCs displayed increased levels of total protein after 3 weeks of culture (Fig. **6F**). Overall these results demonstrate that both NEK9 and PTDSS1 play a role in supporting osteoblast differentiation of hMSCs.

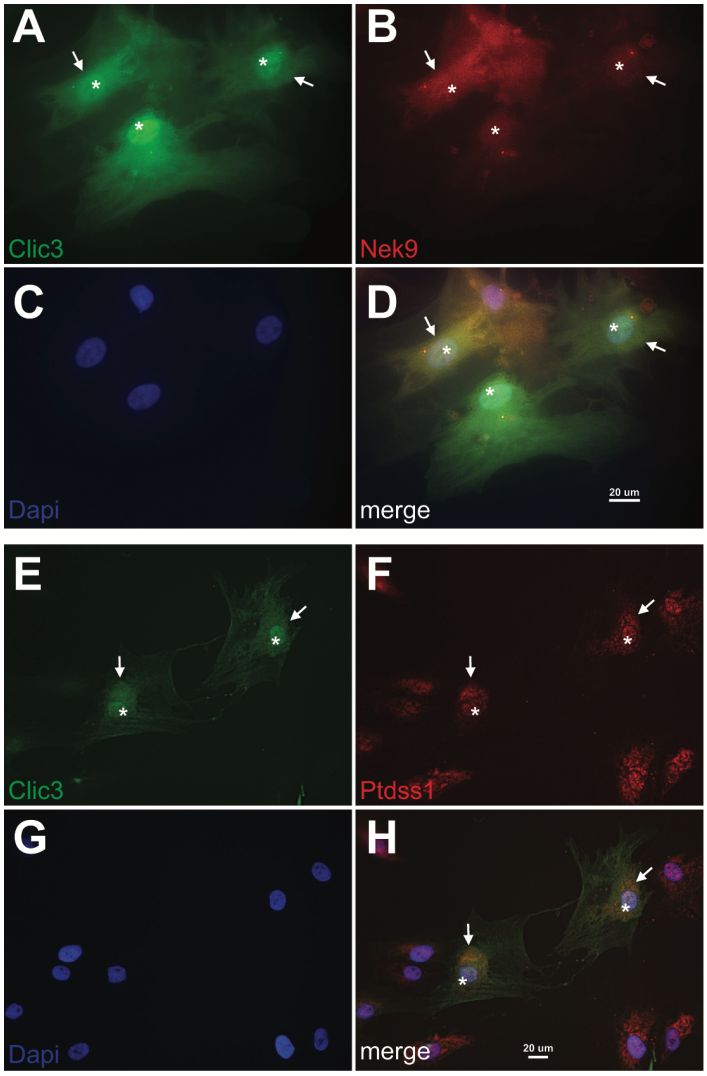


**Figure 5. CLIC3 colocalizes with PTDSS1 and NEK9 in differentiating osteoblasts.** Using immunofluorescence microscopy, CLIC3 (A,D,green) and NEK9 (B,D,red) were visualized together in hMSCs differentiated towards osteoblast and overexpressing CLIC3 at 630x magnification. Arrows indicate detection of both proteins in the perinuclear region and asterisks denote nuclear localization. Immunofluorescent detection of CLIC3 (E,H,green) and PTDSS1 (F,H,red) were visualized jointly in osteogenic hMSCs overexpressing CLIC3 at 400x magnification. PTDSS1 and CLIC3 are both seen in the perinuclear (arrows) and nuclear (asterisks) compartments. C,D,G,H show nuclear staining by dapi in blue. PTDSS1 and CLIC3 are both seen in the perinuclear (arrows) and nuclear (asterisks) compartments. DAPI = 4,6-diamidino-2-phenylindole.

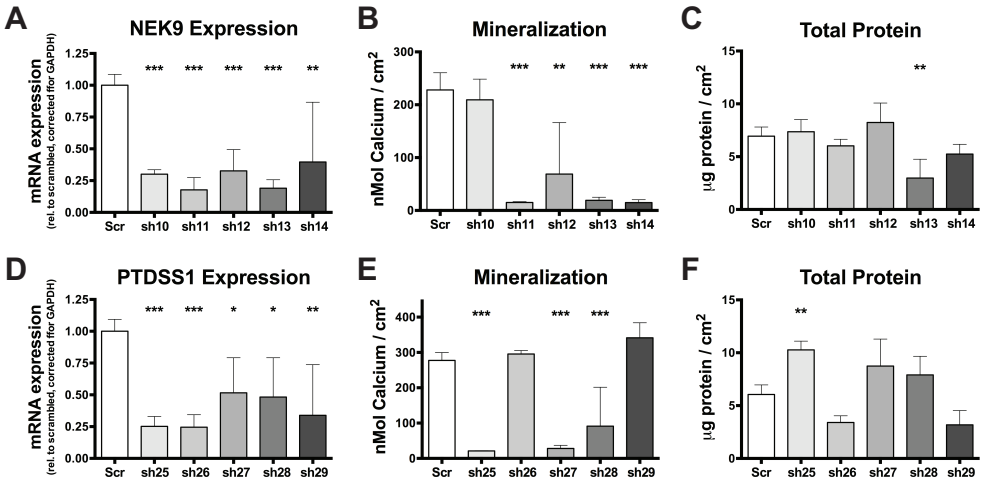


**Figure 6. Knockdown of *NEK9* and *PTDSS1* gene expression inhibits osteogenic differentiation of hMSCs.** mRNA expression of *NEK9* (*A*) as determined by quantitative PCR (day 3), mineralization (*B*) (week 3), and total protein quantification (*C*) (week 3) after transduction of hMSCs with five shRNAs against *NEK9* (shaded bars) compared to scrambled control (white bars). mRNA expression of *PTDSS1* (*D*) as determined by quantitative PCR (day 3), mineralization (*E*) (week 3), and total protein quantification (*F*) (week 3) after transduction of hMSCs with five shRNAs against *PTDSS1* (shaded bars) compared to scrambled control (white bars). Graphs display combined results from all experiments. (*A*) $n = 4–12$; (*B*) $n = 6–12$; (*C*) $n = 6–12$; (*D*) $n = 4–12$; (*E*) $n = 5–12$; (*C*) $n = 6–12$. $^{*}p < 0.05$, $^{**}p < 0.01$, $^{***}p < 0.001$.

### 4.3 Discussion

*CLIC3* was identified as a new gene specifically regulated in the osteogenic lineage of differentiating human MSCs. Lentiviral transduction-mediated overexpression and silencing of *CLIC3* during osteogenesis revealed a crucial function for CLIC3 in promoting osteoblast mineralization. Overexpression of *CLIC3* in hMSCs strongly enhanced *in vivo* bone formation in a mouse model for ectopic human bone formation, further emphasizing that CLIC3 plays an important role in human osteoblast differentiation. Bioinformatics analysis of proteins identified by CLIC3-His pull down suggests CLIC3s role during osteoblast differentiation may be related cytoskeletal associations and signaling, cell adhesion, and/or nuclear pore formation or transport of proteins or ions through nuclear pores. Finally, we identified that CLIC3 interacts with NEK9 and PTDSS1 during osteoblast differentiation, and inhibition of the *NEK9* and *PTDSS1* expression reduces osteogenic differentiation of hMSCs.

CLICs are a diverse group of proteins, having been associated with a wide variety of biological processes and cellular functions including angiogenesis[24], macrophage activation[25], DNA damage[26], maintenance of membrane structure[27], bone resorption[28] , cell growth, cell division and apoptosis[23,29,30], and acidification of intracellular organelles[24,31] All CLIC proteins contain a ~240 residue CLIC module

that adopts a GST superfamily fold[32]; within it there is conserved cysteine residue at what looks like an enzymatic active site[18,19,33]. CLIC3 was first identified based on its interaction with MAPK15, at the time known as ERK7, in a yeast two-hybrid assay and subsequently confirmed by co-immunoprecipitation in COS cells; Qian and colleagues[23] proposed that it plays a role in controlling mammalian cell growth based on its association with MAPK15. This is the first report of CLIC3 being involved in osteoblastic differentiation of hMSCs and human bone formation. Our *in vitro* results revealed the important role for CLIC3 in osteoblast differentiation and the strong induction of bone formation by hMSCs after *CLIC3* overexpression seen in our model of human ectopic bone formation in a mouse supports the strong role *CLIC3* has in ossification. It is worth noting that although this model provides an *in vivo* environment to study human bone formation, it is limited by the fact that the scaffold and cells are not within their native bone microenvironment and specific factors and vascularization may be lacking, resulting in lower bone formation overall. Our findings, which are in line with previous reports[22,23], show that CLIC3 is predominately localized to the perinuclear and nuclear regions, supporting our bioinformatics findings suggesting a role for CLIC3 in the nuclear pore complex and/or export of RNA and ribonucleoprotein complexes from the nucleus. Like our results presented here, CLIC1, which shares a high degree of homology to CLIC1, with 48–49% of the protein sequences being identical[23], was reported to be important for murine osteoblast differentiation through MSC lineage decision-making. CLIC1 was upregulated in response to Wnt treatment and downregulated following adipogenic treatment in murine MSCs; overexpression of *CLIC1* led to increased ALP activity and mineralization as well as increased expression of ALP, osterix and osteocalcin[34]. The authors showed that CLIC1 overexpression caused hyperpolarization of the mitochondrial membrane potential, suggesting that its role in osteogenic differentiation is linked to supporting energy supplementation. Based on their structural similarities, it would be possible to postulate that the two proteins may have similar functions; however, we don't have any evidence thus far that CLIC3 functions in regulating mitochondrial membrane potential or energy metabolism. Although the detailed mechanism by which CLIC3 regulates human osteoblast differentiation is still far from understood, the discovery of its interaction with NEK9 and PTDSS1 during osteoblast differentiation does give us some clues to its function.

After discovering that NEK9 associates with CLIC3 using protein pull-down and immunofluorescence, we confirmed that NEK9 is important in osteogenic differentiation by showing that *NEK9* knockdown leads to reduced mineralization. Very recently it was reported that recessive mutations in NEK9 cause a lethal skeletal dysplasia characterized by fetal akinesia, multiple contractures, shortened long bones,

thoracic dysplasia, pulmonary hypoplasia, and protruding abdomen[35]. This stop-gain mutation results in a truncated protein that misses the majority of the RCC1-like domain, all of the NEK6 interaction region, and a C-terminal coiled-coil domain[35]. In fibroblasts from these patients, the *NEK9* mutation results in a number of cell-cycle defects including reduced proliferation capability and delayed cell-cycle progression through G1/S boundary and S-phase. Analysis of *NEK9* in patient fibroblasts also showed reduced cilia number and length, and in *Caenorhabditis elegans* expression of NEKL-1, the NEK9 orthologue, was restricted exclusively to a subset of ciliated cells, suggesting that NEK9 is involved in ciliary function[35]. Previous studies have shown the importance of primary cilia in osteoblast mechanosensing and function to enhance mineralization[36,37], making this a potential mechanism through which CLIC3 interacts with NEK9; however, our CLIC3 and NEK9 immunolabelings don't appear to be specific to the primary cilia. *NEK9* is one of 11 Human NEK (NIMA-related kinases) genes that encode serine-threonine kinases with diverse biological roles including cell cycle control, cilia regulation, and DNA damage sensing and repair[38–41], and NEK9, specifically, is known to be involved in regulating spindle organization, chromosome alignment, cytokinesis, and normal cell cycle progression[42,43]. Mammalian Nek9 binds γ-tubulin and localizes to the centrosomes and spindle poles during early cell division, functioning in the microtubule organizing center during mitosis[41,44]. Our immunofluorescence results demonstrate that both CLIC3 and NEK9 are most abundant surrounding the nucleus, suggesting that CLIC3 and NEK9 are associated with the microtubule-organizing center. It has been reported that CLIC3 and other CLIC proteins associate with the cytoskeleton or scaffolding proteins for endosome trafficking[20–22]. In addition, recent work in our lab has shown that inhibition of microtubules leads to dramatic cytoskeletal modifications, and an increase in focal adhesions and BMP2 activity causing osteogenic differentiation of hMSCs[45], and osteogenic differentiation is associated with significant changes cytoskeletal protein in human osteoblasts[46]. In addition, our bioinformatics analysis of CLIC3-His pulled down proteins identified an overrepresentation of proteins involved processes related to cytoskeletal and integrin signaling. Collectively, we suggest that NEK9 and CLIC3 may regulate osteoblast differentiation via cytoskeleton-associated signaling processes, but this requires further investigation.

Our results show that CLIC3 and PSS1 associate in differentiating hMSCs and that knockdown of *PTDSS1* significantly reduces osteoblast differentiation. *PTDSS1* encodes phosphatidylserine synthase 1 (PSS1) that, along with phosphatidylserine synthase 2 (PSS2), promotes the biosynthesis of phosphatidyl serine (PS) by the exchange of L-serine with the choline moiety of phosphatidylcholine[47]. In 2014[48] it was discovered that *de novo* missense mutations in

the *PTDSS1* gene are responsible for Lenz-Majewski hyperostotic dwarfism (LMHD), an extremely rare condition characterized by sclerosing bone dysplasia, intellectual disability and distinct craniofacial, dental, cutaneous, and distal limb anomalies (OMIM #151050)[49,50], which was affirmed by Whyte and coworkers[51] reporting additional LMHD patients harboring mutations in *PTDSS1*. These *PTDSS1* mutations result in a gain of function phenotype leading to increased synthesis of PTDS[48,51]. Bone turnover markers in a female LMHD patient, who was confirmed to have a mutation in *PTDSS1*, revealed that her osteosclerosis was a result of accelerated bone formation along with unremarkable rates of bone resorption[51]. They also found elevated levels of phosphoserine in their LMHD patients' urine, which could be indicative of increased PS biosynthesis. PS has unique physical and biochemical properties that lead to its physiological importance in roles related to apoptosis, coagulation, the internalization of viruses, and Ras/Rho and protein kinase C signaling[47,52,53]. CLIC proteins have also been shown to be heavily involved in Rho signaling in a number of cell types[18,33,44] providing a potential functional link between the two proteins. In bone PS is known to bind calcium within matrix vesicles leading to hydroxyapatite crystal formation[54], and enhances osteogenic differentiation of MSCs[55] and human osteoblast progenitor cells[56] to promote bone formation. In addition, PTDS-containing liposomes were shown to inhibit osteoclast differentiation and prevent trabecular bone loss[57] making PS a potential candidate for osteoporosis treatment. Interestingly, in cultured A2780 ovarian carcinoma cells and in pancreatic and ovarian tumors that contain elevated levels of CLIC3, CLIC3 functions to mediate the return of α5β1 from late endosomes/lysosomes to the plasma membrane[20]. We hypothesize that CLIC3 may act similarly in osteoblasts to direct the transport of PS to the plasma membrane or to matrix vesicles. These previous findings, taken together with our current work, supports the idea that CLIC3 works together with PSS1 to increase biosynthesis of PS in osteoblast differentiation and bone formation.

In conclusion, we have successfully identified *CLIC3* to be a novel gene modulating osteoblast differentiation and enhancing bone formation. Although further studies are required to determine the molecular mechanisms by which CLIC3 modulates mineralization, we postulate that CLIC3 and NEK9 both play roles in the microtubule organizing center to induce cytoskeletal changes important for osteoblast differentiation, and that CLIC3 interacts with PSS1 to enhance PS synthesis and PS translocation to the plasma membrane where it plays an important role in matrix vesicle-mediated HA formation and mineralization of the bone. The specificity of *CLIC3* to promote the osteogenic lineage, while its expression decreases during adipocyte differentiation, in combination with the importance of CLIC3 during

human osteoblast differentiation could make it a potential target for future bone anabolic treatments.

## 4.4 Materials and Methods

### *4.4.1 Cell culture*

Human bone marrow-derived Mesenchymal Stem Cells (hMSCs) were cultured as described previously[58]. After 1 week of expansion, hMSCs were seeded into 12 well plates, in αMEM medium supplemented with 10% heat-inactivated fetal calf serum. One to two days later, to allow for attachment, osteogenic differentiation was initiated using 100 nM dexamethasone (dex) and 10 mM β-glycerophosphate. For adipogenic differentiation cells were treated with 0.1 μM dex, 60 μM indomethacin, and 0.5 mM 3-isobutyl-1-methylxanthine (IBMX). Media was refreshed every 3 or 4 days. Cell extracts were harvested at different time points during culture by scraping the cells either in phosphate-buffered saline containing 0.1% triton X-100 (PBS/Triton) and stored at -80°C for biochemical analyses or in TRIzol and stored at -20°C for gene expression analyses. Alternatively, cells seeded on poly-L-lysine-coated glass coverslips were fixed in 4% phosphate-buffered paraformaldehyde for immunocytochemical procedures.

### *4.4.2 Lentiviral-mediated overexpression and knockdown*

Methods for gene overexpression and silencing have been described previously[59,60]. To obtain *CLIC3* overexpression, we generated full-length human *CLIC3* cDNA (Open Biosystems, GE Dharmacon, the Netherlands) containing a His-tag stop codon into a pEntr vector and verified using proof reading PCR (**Table 3**). To generate the *CLIC3* overexpression vector E-coli were transformed with the construct and after culture plasmid DNA isolation was performed. The CLIC3 construct was ligated into a pLenti6.3 vector, using Gateway Cloning (Life Technologies, the Netherlands) and hek cells were transfected and media containing virus was collected after 48 and 72 hours.

**Table 3**. **Oligonucleotide primers used for proof-reading PCR for generation of His-tagged CLIC3 overexpression vector**

| Gene | Forward (5' - 3') | Reverse (5' - 3') |
|---|---|---|
| *CLIC3-His* | CACCATGGCGGAGACCAAGCTC CA | TCATTACTAGTGATGGTGATGGTGAT GGCGGGGTGCACGGCGGGCC |

Sequences of forward and reverse primers used for proof reading PCR in this study. Detected using SYBR green.

Lentivirus (LV) was produced by transient transfection of each LV construct into human embryonal kidney (HEK) 293T cells using a standard calcium phosphate precipitation technique. The appropriate LV vector plasmid (3 μg) and the packaging vector plasmids (9 μg of ViraPower mix (Thermo Fisher Scientific)) were cotransfected into subconfluent HEK-293T cells plated in 100-mm dishes. Viral supernatants were harvested 48 and 72 hours after transfection, filtered through a 0.45-μm pore size filter, and used immediately for hMSC transduction or stored until use at –80°C. One day prior to LV transduction, hMSC were seeded into 12-well plates. Transduction consisted of 24 hour LV incubation, after which the medium was replaced with differentiation medium and the cells were cultured until further analysis. hMSCs cells were transduced with the *CLIC3* vector or empty vector (pLenti6.3 vector without CLIC3 construct), as control. For gene knockdown of *CLIC3*, *NEK9*, and *PTDSS1*, constructs from the TRC-Hs1.0 library (Sigma-Aldrich, Zwijndrecht, the Netherlands) were used (**Table 4**). A nontargeting shRNA vector with a scrambled sequence (**Table 4**) was used as a negative control.

**Table 4. List of shRNAs used for *CLIC3*, *NEK9* and *PTDSS1***

| Target gene | ID | Target sequence |
|---|---|---|
| *CLIC3* | sh9123 | GCCTCGTTACAGGGAGTCCAA |
| | sh9126 | GCAGGAGAAAGAGTTCAAATA |
| *NEK9* | sh10 | GCCTTGATTATTGTTGCAGTT |
| | sh11 | CCGAGGAATGGAAGGTTTAAT |
| | sh12 | CCAAAGGAACTCAGACAGCAA |
| | sh13 | GTGAAGATCGTGCAAGGAATT |
| | sh14 | GTACATTTGGAGAGTGGCATT |
| *PTDSS1* | sh25 | CGAGCAGGTTAAATCTCTAAT |
| | sh26 | GCTAGATCCAAATCTTCGATA |
| | sh27 | TGGACCTATGTTCGATGGTTT |
| | sh28 | GCAACAACGAAAGCCATTCTT |
| | sh29 | GACTGAGTTGAATACCTTCTT |
| Non-targeting shRNA | | Oligo sequence |
| Scrambled | SHC002 | CCGGCAACAAGATGAAGAGCACCAACTCGAGTTGGTGCTCTTCATCTTGTTGTTTTT |

Target sequences of shRNAs for gene silencing of *CLIC3*, *NEK9* and *PTDSS1*, as well as the oligonucleotide sequence for a non-targeting scrambled control.

*CLIC3* mRNA overexpression or knockdown in osteoblast differentiating hMSCs was assessed at 24 hours and 7 days (compared to empty vector or scrambled shRNA-transduced cells, respectively) and mineralization was monitored at 3 weeks

after transduction. Western blotting of protein extracts collected 10 days after the start of differentiation was performed to confirm overexpression. Overexpression experiments were performed in at least duplicate in a minimum of two separate experiments in MSCs from three hMSCs donors. Knockdown experiments were performed in at least duplicate in a minimum of two separate experiments.

*4.4.3 Alkaline phosphatase, mineralization and protein assays*

Alkaline phosphatase (ALP) and calcium measurements were performed as described previously[8,58]. ALP activity is determined by an enzymatic reaction, in which the ALP-mediated conversion of PNPP to PNP during 10 min at 37°C was measured. For calcium measurements, cell lysates were incubated overnight with 0.24 M HCl at 4°C. Calcium content was determined colorimetrically using a calcium assay reagent prepared by combining 1 M ethanolamine buffer (pH 10.6) with 0.35 mM 0-cresolphthalein complexone in a ratio of 1:1. ALP results were adjusted for protein content of the cell lysates. For protein measurement, 200 µl of working reagent (50 volumes BCA™ reagent A and 1 volume BCA™ reagent B; Pierce, Rockford, IL) was added to 25 µl of sonicated cell lysate. The mixture was incubated for 30 min at 37°C, cooled down to room temperature (RT) and absorbance was measured at 595 nm. All measurements were performed using a Victor2 plate reader (PerkinElmer Life and Analytical Science). Staining for mineralization was performed as described previously[8]. Briefly, cells were fixed with 70% ethanol and after washing they were stained for 10-20 min with alizarin Red S solution.

*4.4.4 Western blotting*

Total protein was collected from 12-wells plate wells in RIPA lysis buffer (Santa Cruz), containing 10 µl 200mM PMSF/1 ml RIPA, 10 µl sodium 100mM orthovanadate/1 ml RIPA and 20 µl protease inhibitor cocktail (Santa Cruz)/1 ml RIPA. Equal amounts of protein per sample were loaded and separated by SDS-PAGE (12% SDS-polyacrylamide gels) and transferred onto a nitrocellulose membrane (Hybond-ECL, Amersham Biosciences, Buckinghamshire, U.K.). After blocking nonspecific signal with 5% bovine serum albumin (BSA) in Tris-buffered saline (TBS) with 0.1 % Tween-20, the membrane was incubated with a specific antibody against *CLIC3 (*ab56364, Abcam, Cambridge, UK; *1:500)*. Membranes were probed with the secondary antibody goat anti-mouse conjugated with Alexa Fluor 680 (1:5000, Invitrogen/Fisher Scientific, Landsmeer, Netherlands; Cat. A21057). Immunoreactive bands were visualized using the LI-COR Infrared Imaging System according to the manufacturer's instructions (Odyssey Lincoln, NE).

*4.4.5 Quantification of mRNA expression*

RNA isolation, cDNA synthesis and PCR reactions were performed as described previously[58]. Oligonucleotide primer pairs were designed to be either on exon boundaries or spanning at least one intron (**Table 5**). Gene expressions were corrected for expression of the housekeeping gene GAPDH. Experiments were performed in at least duplicate in a minimum of two separate experiments.

***Table 5. Oligonucleotide primers used in the study***

| *Gene* | *Forward (5' - 3')* | *Reverse (5' - 3')* |
|---|---|---|
| *GAPDH* | *CCGCATCTTCTTTTGCGTCG* | *CCCAATACGACCAAATCGTTG* |
| *CLIC3* | *CTGCCCATCCTGCTCTAT* | *CAGCGTCTCCTCCAGAAA* |
| *NEK9* | *TCAGCAATCCAGTGGAGCAG* | *CCAGTCGTCCATATTCGCCA* |
| *PTDSS1* | *TCGCCTTTACCAGGGATGAC* | *GAGTGAACGGACCATTGGGG* |

*Sequences of forward and reverse primers used for qPCR in this study. All genes were detected using SYBR green.*

*4.4.6 Immunocytochemistry*

Cells were fixed with 4% paraformaldehyde in phosphate-buffered saline (PBS) for 15 minutes at RT, washed in PBS, and excess aldehyde quenched with 10 mM ethanolamine in PBS for 5 min. Cells were then permeabilized with 0.5% Triton-X-100 in PBS for 10 minutes and blocked for 30 minutes at room temperature in PBS supplemented with 1.5% bovine serum albumin (BSA) and 0.02% Triton-X-100. Cells were incubated with primary antibody (anti-CLIC3 raised in mouse, 1:150 (ab56364, Abcam, Cambridge, UK); anti-NEK9 raised in rabbit, 1:20 (11192-1-AP, Proteintech, Manchester, UK); anti-PTDSS1 raised in rabbit, 1:50 (HPA016852, Atlas Antibodies, Bromma, Sweden)) )) either overnight at 4°C or for 1 hour at RT, followed by secondary antibody (Alexa Fluor® 488 conjugated anti-mouse; Alexa Fluor® 568 conjugated anti-rabbit 1:400) for 1 hour at RT. Slides were mounted using Vectashield mounting medium containing DAPI and pictures were taken on a Zeiss Axiovert 200 MOT microscope.

*4.4.6 In vivo implantation assay*

All animal experiments were performed in compliance with the animal ethics board of the Erasmus Medical Center. Experiments were performed based on the protocol by Abdulla and collegues[61]. Five healthy, adult (2-3 months old), female NOD.CB17-Prkdc$^{scid}$/NCrHsd (NOD-SCID) mice (Charles River Laboratories, 's-Hertogenbosch, Netherlands) were used for these studies. Animals were housed in a specific pathogen free (SPF) facility with a 12 hours day-night cycle in a controlled room with temperatures of 22±1°C and humidity of 50±5%. Mice were fed with standard rodent diet *ad libitum*. hMSCs transduced with *CLIC3* or empty vector and

treated with dex for 3 days prior to being trypsinized, were loaded ($5 \times 10^5$) onto hydroxyl-apatite/tricalcium phosphate ceramic powder (HA-TCP, 20 mg; Zimmer, Netherlands). After overnight incubation in sterile syringes the mixture was implanted subcutaneously in the dorsal surface of NOD-SCID mice. Each mouse had up to four implants surgically inserted subcutaneously under anesthesia. Implants were distributed evenly between the mice and locations within the mice (behind or in front of each leg). Implants were recovered after 8 weeks and fixed in 70% ethanol. After at least 4 hours fixation, implants were dehydrated, embedded in Methyl Methacrylate (MMA), and sectioned (6 μm thick). For identification of bone formed within the pellets we performed a Goldner stain on the sections: after sections were deacrylated and rehydrated they were stained in ordered steps of Weigert Haematoxylin, Ponceau de Xylidine/Acid Fuchsine solution, Orange G/Phosphomolybdene Acid solution, 0.2% Light Green and then dehydrated before being mounted in Entellan[62]. As a result of this Goldner stain, bone matrix and fibrous tissue appears in green (bone recognizable by morphology and the bright and dense staining), osteoid in orange/red, nuclei in blue and the HA-TCP grey/brown. All quantitative measurements were performed on 2 sections of each pellet. The first was taken from the outer quarter of the pellet and the second from the core of the pellet. From each section pictures were taken with a microscope (10x magnification) covering the entire tissue and individual pictures were stitched together to recapitulate the entire cross-section. Quantification was carried out using Image J software (NIH, Bethesda, MD, USA; https://imagej.nih.gov/ij/): ceramics areas and bone areas were determined by eye based on staining and morphology, the edges were hand drawn and the resulting pixel-measurements were calculated back to $mm^2$. The observer assessing the pellets was blinded toward their identity.

*4.4.7 Pull-down assay*

A pull-down assay was performed to isolate proteins associating with His-tagged CLIC3 using Dynabeads (10103D, Life Technologies, Bleiswijk, Netherlands). Purification of CLIC3 protein complexes was performed by a metal-based affinity between the Dynabeads and the His-tagged CLIC3. The pull down was performed according to the manufacturers' protocol. Bait protein was obtained from hMSCs differentiated with dexamethasonefor 5 days, following transduction with either His-tagged *CLIC3* or an empty vector (EV; control). Transduced cells were washed once with DPBS after which 1X Binding/Wash Buffer (Life Technologies) containing 0.1% Triton X-100 (Sigma) was added to and the flasks were placed on a shaker for 15 min at 4°C before protein extracts were collected by scraping cells on ice. Bait protein was isolated by incubating the protein lysates with His-tagged Dynabeads for

5 minutes at 4°C before washing 4 times. Proteins interacting with His-tagged CLIC3 were obtained from non-transduced extracts of hMSCs differentiated for 5 days with dex. Differentiated hMSCs were washed once with DPBS after which 1X Pull Down Buffer (Life Technologies) was added to and the flasks and protein extracts were collected as above. These samples were added to the isolated bait protein attached to the Dynabeads for 30 min at 4°C before washing 4 times. Finally, the isolated proteins were eluted in a total of 50 µl His-elution buffer. Two replicate samples from each condition were included for subsequent mass spectrometry assessment.

*4.4.8 Mass spectrometry (MS)*

The eluted His-tagged CLIC3 proteins and their interacting proteins, as well as the control samples, were run on NuPage Novex 4–12% Bis-Tris gel (Life Technologies). A total of 30 µl for each sample, containing 7.5 µl 4X sample buffer (Life technologies), 3 µl 10X reducing agent and 8 µg protein, diluted in 20 µl water of each samples was loaded onto the gel. Then the gels were run at 200V for one hour and washed three times with milliQ water (MQ). Proteins were stained with 50 ml Coomassie staining buffer (Bio-Rad) on a shaker for one hour and de-stained with MQ overnight. The next day, gels were fixed by incubating in 10% EtOH/ 1% Acetic Acid for 30 minutes at room temperature. Then the gels were washed three times with MQ. The 1D SDS-PAGE gel lanes were cut into 2 mm slices with an automatic gel slicer and subjected to in-gel reduction with dithiothreitol, alkylation with iodoacetamide (D4, 98%; Cambridge Isotope Laboratories Inc., Tewksbury, MA, USA), and digestion with trypsin (sequencing grade; Promega, Madison, WI, USA)[63]. Nanoflow liquid chromatography coupled to a tandem mass spectrometer (LC-MS/MS) was performed on a Series 1100 capillary LC system (Agilent Technologies, Santa Clara, CA, USA) coupled to an LTQ-Orbitrap XL mass spectrometer (Thermo Scientific, Waltham, MA, USA) operating in positive mode[46]. Peptide mixtures were trapped on a ReproSil C18 reverse-phase column (Dr. Maisch GmbH, Ammerbuch-Entringen, Germany; 1.5 cm × 100 µm, packed in house) at a flow rate of 8 µl/min. Peptide separation was performed on ReproSil C18 reversed-phase column (Dr. Maisch GmbH; 15 cm × 50 $\mu$m, packed in house) using a linear gradient from 0 to 80% B [A = 0.1% formic acid; B = 80% (v/v) acetonitrile, 0.1% formic acid] in 170 min and at a constant flow rate of 200 nl/min using a splitter. The column eluent was directly sprayed into the electrospray ionization source of the mass spectrometer. Mass spectra were acquired in continuum mode, and fragmentation of the peptides was performed in a data-dependent mode.

*4.4.9 Bioinformatic analysis*

The raw MS data were analyzed by MaxQuant software (version 1.3.0.5)[64]. A false discovery rate of 0.01 for proteins and peptides and a minimum peptide length of six amino acids were required. The Andromeda search engine[65] was used to search the MS/MS spectra against the Uniprot database (taxonomy: *Homo sapiens,* release HUMAN_2013_04) concatenated with the reversed versions of all sequences (maximum of 2 missed cleavages; 0.6 Da fragment mass tolerance, enzyme specificity: trypsin). The data from the replicates were combined as averages. For selection of the most relevant interacting proteins the following criteria were set: 1) a label-free quantification (LFQ) value in CLIC3 samples of greater than 1 x $10^6$, 2) number of unique peptides covering a protein equals 3 or more, and 3) ratio of CLIC3 samples versus control samples of 1.5 or greater. Proteins were then ranked based on the average LFQ ratio of the CLIC3 samples versus the control samples. Ingenuity Pathway Analysis (IPA) (www.ingenuity.com/) and Gene Ontology analysis (GO) in DAVID (https://david.ncifcrf.gov/) was performed using the 52 proteins identified by pull-down and MS.

*4.4.10 Statistics*

The data provided here are based on at least two independent experiments performed in at least in duplicate. Values displayed are mean ± SE. Significance was calculated using either the Student's t-test, Mann Whitney-test, or the one-way ANOVA with Tukey's post-hoc test where appropriate, using GraphPad prism 6.0 (GraphPad Software, Inc., La Jolla, CA, USA). Values of $p < 0.05$ were considered significant.

## References


1. Sambrook, P. & Cooper, C. Osteoporosis. *Lancet (London, England)* **367**, 2010–8 (2006).
2. Matsuo, K. & Irie, N. Osteoclast-osteoblast communication. *Arch. Biochem. Biophys.* **473**, 201–9 (2008).
3. Chamberlain, G., Fox, J., Ashton, B. & Middleton, J. Concise review: mesenchymal stem cells: their phenotype, differentiation capacity, immunological features, and potential for homing. *Stem Cells* **25**, 2739–49 (2007).
4. Ducy, P., Zhang, R., Geoffroy, V., Ridall, A. L. & Karsenty, G. Osf2/Cbfa1: a transcriptional activator of osteoblast differentiation. *Cell* **89**, 747–54 (1997).
5. Komori, T. *et al.* Targeted disruption of Cbfa1 results in a complete lack of bone formation owing to maturational arrest of osteoblasts. *Cell* **89**, 755–64 (1997).
6. Otto, F. *et al.* Cbfa1, a candidate gene for cleidocranial dysplasia syndrome, is essential for osteoblast differentiation and bone development. *Cell* **89**, 765–71 (1997).
7. Aubin, J. E. Regulation of osteoblast formation and function. *Rev. Endocr. Metab. Disord.* **2**, 81–94 (2001).
8. Eijken, M. *et al.* The essential role of glucocorticoids for proper human osteoblast differentiation and matrix mineralization. *Mol. Cell. Endocrinol.* **248**, 87–93 (2006).
9. Iba, K. *et al.* Glucocorticoids induce mineralization coupled with bone protein expression without influence on growth of a human osteoblastic cell line. *Cell Struct. Funct.* **20**, 319–30 (1995).
10. Perrien, D. S. *et al.* Aging alters the skeletal response to disuse in the rat. *Am. J. Physiol. Regul. Integr. Comp. Physiol.* **292**, R988–R996 (2007).
11. Singh, L. *et al.* Aging alters bone-fat reciprocity by shifting in vivo mesenchymal precursor cell fate towards an adipogenic lineage. *Bone* **85**, 29–36 (2016).
12. Moerman, E. J., Teng, K., Lipschitz, D. A. & Lecka-Czernik, B. Aging activates adipogenic and suppresses osteogenic programs in mesenchymal marrow stroma/stem cells: the role of PPAR-γ2 transcription factor and TGF-β/BMP signaling pathways. *Aging Cell* **3**, 379–389 (2004).
13. Kajkenova, O. *et al.* Increased adipogenesis and myelopoiesis in the bone marrow of SAMP6, a murine model of defective osteoblastogenesis and low turnover osteopenia. *J. Bone Miner. Res.* **12**, 1772–9 (1997).
14. Nuttall, M. E. & Gimble, J. M. Is there a therapeutic opportunity to either prevent or treat osteopenic disorders by inhibiting marrow adipogenesis? *Bone* **27**, 177–84 (2000).
15. Landry, D. *et al.* Molecular cloning and characterization of p64, a chloride channel protein from kidney microsomes. *J. Biol. Chem.* **268**, 14948–55 (1993).
16. Landry, D. W. *et al.* Purification and reconstitution of chloride channels from kidney and trachea. *Science* **244**, 1469–72 (1989).
17. Singh, H. Two decades with dimorphic Chloride Intracellular Channels (CLICs). *FEBS Lett.* **584**, 2112–21 (2010).
18. Jiang, L. *et al.* CLIC proteins, ezrin, radixin, moesin and the coupling of membranes to the actin cytoskeleton: a smoking gun? *Biochim. Biophys. Acta* **1838**, 643–57 (2014).
19. Littler, D. R. *et al.* The enigma of the CLIC proteins: Ion channels, redox proteins, enzymes, scaffolding proteins? *FEBS Lett.* **584**, 2093–101 (2010).
20. Dozynkiewicz, M. a *et al.* Rab25 and CLIC3 collaborate to promote integrin recycling from late endosomes/lysosomes and drive cancer progression. *Dev. Cell* **22**, 131–45 (2012).
21. Knowles, L. M. *et al.* CLT1 targets bladder cancer through integrin α5β1 and CLIC3. *Mol. Cancer Res.* **11**, 194–203 (2013).
22. Macpherson, I. R. *et al.* CLIC3 controls recycling of late endosomal MT1-MMP and dictates invasion and metastasis in breast cancer. *J. Cell Sci.* **127**, 3893–901 (2014).
23. Qian, Z., Okuhara, D., Abe, M. K. & Rosner, M. R. Molecular cloning and characterization of a mitogen-activated protein kinase-associated intracellular chloride channel. *J. Biol. Chem.* **274**, 1621–7 (1999).
24. Ulmasov, B., Bruno, J., Gordon, N., Hartnett, M. E. & Edwards, J. C. Chloride intracellular channel protein-4 functions in angiogenesis by supporting acidification of vacuoles along the intracellular tubulogenic pathway. *Am. J. Pathol.* **174**, 1084–96 (2009).
25. Malik, M. *et al.* Inducible NOS-induced chloride intracellular channel 4 (CLIC4) nuclear translocation regulates macrophage deactivation. *Proc. Natl. Acad. Sci. U. S. A.* **109**, 6130–5 (2012).
26. Fernández-Salas, E. *et al.* mtCLIC/CLIC4, an organellular chloride channel protein, is increased by DNA damage and participates in the apoptotic response to p53. *Mol. Cell. Biol.* **22**, 3610–20 (2002).
27. Berry, K. L., Bülow, H. E., Hall, D. H. & Hobert, O. A C. elegans CLIC-like protein required for intracellular tube formation and maintenance. *Science* **302**, 2134–7 (2003).
28. Edwards, J. C., Cohen, C., Xu, W. & Schlesinger, P. H. c-Src control of chloride channel support for osteoclast HCl transport and bone resorption. *J. Biol. Chem.* **281**, 28011–22 (2006).
29. Suh, K. S. *et al.* The organellular chloride channel protein CLIC4/mtCLIC translocates to the nucleus in response to cellular stress and accelerates apoptosis. *J. Biol. Chem.* **279**, 4632–41 (2004).
30. Xu, Y. *et al.* Suppression of CLIC4/mtCLIC enhances hydrogen peroxide-induced apoptosis in C6 glioma cells. *Oncol. Rep.* **29**, 1483–91 (2013).

31. Jiang, L. *et al.* Intracellular chloride channel protein CLIC1 regulates macrophage function through modulation of phagosomal acidification. *J. Cell Sci.* **125**, 5479–88 (2012).
32. Dulhunty, A., Gage, P., Curtis, S., Chelvanayagam, G. & Board, P. The glutathione transferase structural family includes a nuclear chloride channel and a ryanodine receptor calcium release channel modulator. *J. Biol. Chem.* **276**, 3319–23 (2001).
33. Ponsioen, B. *et al.* Spatiotemporal regulation of chloride intracellular channel protein CLIC4 by RhoA. *Mol. Biol. Cell* **20**, 4664–72 (2009).
34. Yang, J.-Y. *et al.* Chloride intracellular channel 1 regulates osteoblast differentiation. *Bone* **45**, 1175–85 (2009).
35. Casey, J. P. *et al.* Recessive NEK9 mutation causes a lethal skeletal dysplasia with evidence of cell cycle and ciliary defects. *Hum. Mol. Genet.* (2016). doi:10.1093/hmg/ddw054
36. Delaine-Smith, R. M., Sittichokechaiwut, A. & Reilly, G. C. Primary cilia respond to fluid shear stress and mediate flow-induced calcium deposition in osteoblasts. *FASEB J.* **28**, 430–9 (2014).
37. Chen, J. C., Hoey, D. A., Chua, M., Bellon, R. & Jacobs, C. R. Mechanical signals promote osteogenic fate through a primary cilia-mediated mechanism. *FASEB J.* (2015). doi:10.1096/fj.15-276402
38. Chen, Y., Chen, C.-F., Riley, D. J. & Chen, P.-L. Nek1 kinase functions in DNA damage response and checkpoint control through a pathway independent of ATM and ATR. *Cell Cycle* **10**, 655–63 (2011).
39. O'regan, L., Blot, J. & Fry, A. M. Mitotic regulation by NIMA-related kinases. *Cell Div.* **2**, 25 (2007).
40. Moniz, L., Dutt, P., Haider, N. & Stambolic, V. Nek family of kinases in cell cycle, checkpoint control and cancer. *Cell Div.* **6**, 18 (2011).
41. Roig, J., Groen, A., Caldwell, J. & Avruch, J. Active Nercc1 Protein Kinase Concentrates at Centrosomes Early in Mitosis and Is Necessary for Proper Spindle Assembly. *Mol. Biol. Cell* **16**, 4827–4840 (2005).
42. Fry, A. M., O'Regan, L., Sabir, S. R. & Bayliss, R. Cell cycle regulation by the NEK family of protein kinases. *J. Cell Sci.* **125**, 4423–33 (2012).
43. Wang, Y.-K. *et al.* Bone Morphogenetic Protein-2-Induced Signaling and Osteogenesis Is Regulated by Cell Shape, RhoA/ROCK, and Cytoskeletal Tension. *Stem Cells Dev.* **21**, 1176–1186 (2012).
44. Yang, S.-W. *et al.* Nek9 regulates spindle organization and cell cycle progression during mouse oocyte meiosis and its location in early embryo mitosis. *Cell Cycle* **11**, 4366–77 (2012).
45. Brum, A. M. A. M. *et al.* Connectivity Map-based discovery of parbendazole reveals targetable human osteogenic pathway. *Proc. Natl. Acad. Sci.* **112**, 201501597 (2015).
46. Alves, R. D. A. M. *et al.* Proteomic analysis of human osteoblastic cells: relevant proteins and functional categories for differentiation. *J. Proteome Res.* **9**, 4688–4700 (2010).
47. Tomohiro, S., Kawaguti, A., Kawabe, Y., Kitada, S. & Kuge, O. Purification and characterization of human phosphatidylserine synthases 1 and 2. *Biochem. J.* **418**, 421–9 (2009).
48. Sousa, S. B. *et al.* Gain-of-function mutations in the phosphatidylserine synthase 1 (PTDSS1) gene cause Lenz-Majewski syndrome. *Nat. Genet.* **46**, 70–6 (2014).
49. Lenz, W. D. & Majewski, F. A generalized disorders of the connective tissues with progeria, choanal atresia, symphalangism, hypoplasia of dentine and craniodiaphyseal hypostosis. *Birth Defects Orig. Artic. Ser.* **10**, 133–6 (1974).
50. Robinow, M., Johanson, A. J. & Smith, T. H. The Lenz-Majewski hyperostotic dwarfism. A syndrome of multiple congenital anomalies, mental retardation, and progressive skeletal sclerosis. *J. Pediatr.* **91**, 417–21 (1977).
51. Whyte, M. P. *et al.* Lenz-Majewski hyperostotic dwarfism with hyperphosphoserinuria from a novel mutation in PTDSS1 encoding phosphatidylserine synthase 1. *J. Bone Miner. Res.* **30**, 606–14 (2015).
52. Schick, P. K., Kurica, K. B. & Chacko, G. K. Location of phosphatidylethanolamine and phosphatidylserine in the human platelet plasma membrane. *J. Clin. Invest.* **57**, 1221–6 (1976).
53. Leventis, P. A. & Grinstein, S. The distribution and function of phosphatidylserine in cellular membranes. *Annu. Rev. Biophys.* **39**, 407–27 (2010).
54. Wu, L. N. Y., Genge, B. R. & Wuthier, R. E. Analysis and molecular modeling of the formation, structure, and activity of the phosphatidylserine-calcium-phosphate complex associated with biomineralization. *J. Biol. Chem.* **283**, 3827–38 (2008).
55. Xu, C. *et al.* Phosphatidylserine enhances osteogenic differentiation in human mesenchymal stem cells via ERK signal pathways. *Mater. Sci. Eng. C. Mater. Biol. Appl.* **33**, 1783–8 (2013).
56. Satsangi, A., Satsangi, N., Glover, R., Satsangi, R. K. & Ong, J. L. Osteoblast response to phospholipid modified titanium surface. *Biomaterials* **24**, 4585–9 (2003).
57. Wu, Z., Ma, H. M., Kukita, T., Nakanishi, Y. & Nakanishi, H. Phosphatidylserine-containing liposomes inhibit the differentiation of osteoclasts and trabecular bone loss. *J. Immunol.* **184**, 3191–201 (2010).
58. Bruedigam, C. *et al.* Basic techniques in human mesenchymal stem cell cultures: differentiation into osteogenic and adipogenic lineages, genetic perturbations, and phenotypic analyses. *Curr. Protoc. Stem Cell Biol.* **Chapter 1**, Unit1H.3 (2011).
59. van der Eerden, B. C. J. J. *et al.* The transient receptor potential channel TRPV6 is dynamically expressed in bone cells but is not crucial for bone mineralization in mice. *J. Cell. Physiol.* **227**, 1951–9 (2012).

60. Drabek, K., van de Peppel, J., Eijken, M. & van Leeuwen, J. P. T. M. GPM6B regulates osteoblast function and induction of mineralization by controlling cytoskeleton and matrix vesicle release. *J. Bone Miner. Res.* **26**, 2045–51 (2011).
61. Abdallah, B. M., Ditzel, N. & Kassem, M. Assessment of bone formation capacity using in vivo transplantation assays: Procedure and tissue analysis. in *Methods in Molecular Biology: Osteoporosis: Methods and Protocols* **455**, 89–100 (2008).
62. Gruber, H. E. Adaptations of Goldner's Masson trichrome stain for the study of undecalcified plastic embedded bone. *Biotech. Histochem.* **67**, 30–4 (1992).
63. Wilm, M. *et al.* Femtomole sequencing of proteins from polyacrylamide gels by nano-electrospray mass spectrometry. *Nature* **379**, 466–9 (1996).
64. Cox, J. *et al.* A practical guide to the MaxQuant computational platform for SILAC-based quantitative proteomics. *Nat. Protoc.* **4**, 698–705 (2009).
65. Cox, J. *et al.* Andromeda: a peptide search engine integrated into the MaxQuant environment. *J. Proteome Res.* **10**, 1794–805 (2011).

# Chapter 5

# Mucin 1 (Muc1) deficiency in female mice leads to temporal skeletal changes during aging

Andrea M. Brum, Cindy S. van der Leije, Marijke Schreuders-Koedam, Siham Chaibi, Johannes P.T.M. van Leeuwen, & Bram C.J. van der Eerden

*JBMR Plus. (2018) 2(6):341-350.*

Abstract

Mucin1 (MUC1) encodes a glycoprotein that has been demonstrated to have important roles in cell-cell interactions, cell-matrix interactions, cell-signaling, modulating tumor progression and metastasis, and in providing physical protection to cells against pathogens. In this study, we investigated the bone phenotype in female C57BL/6 *Muc1* null mice and the impact of the loss of *Muc1* on osteoblasts and osteoclasts. We found that deletion of *Muc1* results in reduced trabecular bone volume in 8-week-old mice compared with wild-type controls, but the trabecular bone volume fraction normalizes with increasing age. In mature female mice (16 weeks old), *Muc1* deletion results in stiffer femoral bones with fewer osteoblasts lining the trabecular surface, but increased endosteal mineralized surface and bone formation rate. The latter remains higher compared to wild-type females at 52 weeks of age. No difference was found in osteoclast numbers *in vivo*, and bone marrow osteoblast or osteoclast differentiation capacity or activity *in vitro*. Taken together, these results suggest that Muc1 depletion causes a transiently reduced trabecular bone mass phenotype in young mice, and later in life reduced numbers of osteoblasts with increased endocortical mineralization activity coincides with unaffected total bone mass and increased stiffness. In conclusion, our results show, for the first time, a role for Muc1 in bone mass and mineralization in mice in a time-dependent manner.

## 5.1 Introduction

Bone is a dynamic organ, undergoing constant remodeling that is a balancing act between removal of old bone by osteoclasts and formation of new bone controlled by osteoblasts, as well as its terminally differentiated form the osteocyte. A number of key factors and signaling pathways controlling osteoblast differentiation and activity have been identified over the last few decades. Runt-related transcription factor 2 (Runx2) and osterix (Osx) have been identified to be two essential transcription factors required for osteoblast differentiation[1–3]; and Wnt, bone morphogenetic protein (BMP), hedgehog (Hh), Notch, and transforming growth factor-beta (TGFβ) are key signaling pathways in osteoblasts[4–9]. Still, a better understanding of the signaling network, their intricate interactions, and what other genes and pathways are involved in osteoblast function is required to develop approaches to enhance bone formation and promote fracture healing for patients with disorders such as osteoporosis and nonunion fractures. Gene expression analysis of differentiating osteoblasts showed an increase in Mucin 1 (*MUC1*) expression compared to undifferentiated human mesenchymal stromal cells (hMSCs)[10], indicating a potential role for Mucin 1 in the dynamic bone formation and remodeling process.

Mucins were first identified as being a major component of many types of mucus and derive their name from the Greek word for slimy. These glycoproteins are high in O-linked glycosylation sites creating a dense, viscous, negatively charged molecule. To date 21 different mucins have been identified (MUC1-21) and can be divided into two groups: membrane-bound mucins and secretory mucins. Mucin 1 (MUC1) was the first mucin cloned and sequenced[11–14], and it encodes a high molecular weight glycoprotein well known to be expressed on the apical surface of many epithelial cells. MUC1, like all other membrane bound mucins, is a type 1 membrane protein and is composed of an N-terminal protein sequence, followed by a sequence encoding a variable number of tandem repeats (VNTR), then a transmembrane domain, and finally a cytoplasmic tail[15]. This membrane-bound protein can be released from the cell through proteolytic cleavage and, as a result of alternative splicing, a number of isoforms exist including versions that lack a transmembrane domain all together[15,16]. MUC1 falls into a family of structurally related mucin-like glycoproteins including CD34, CD43, CD162, CD164, GlyCAM1, and MAdCAM1. MUC1 has been reported to play an important role in cell-cell interactions, cell-matrix interactions, modulating tumor progression and metastasis[15–19], and also serves as an adhesion molecule for a number of pathogens, providing cells protection from bacteria[18,20,21]. The cytoplasmic tail of MUC1 functions in cell signaling, with seven evolutionary conserved tyrosine phosphorylation sites and

cytoplasmic domains that interact with other key signaling molecules including ß-catenin, p53, and NF-κß[22,23].

This study aimed to examine the skeletal phenotype of mice with global deletion of *Muc1*. To understand the dynamic effect *Muc1* deficiency may have on the skeleton over time we scrutinized bone microarchitecture, strength, mineralization, and osteoblast and osteoclast differentiation and activity at several time points during aging.

## 5.2 Results

### *5.2.1 During aging, femoral cortical bone is increased in WT and Muc1-/- female mice*

Consistent with previous studies[24], all mice developed normally, with no obvious abnormalities or illnesses. Additionally, to help rule out the possibility of bone architecture being affected by changes in overall body weight, fat deposition, or muscle mass, we also quantified body weight (Fig. **1A**, Appendix C, Fig. **A6A**), femoral and tibial muscle weight (Appendix C, Fig. **A6B,C**) and subcutaneous, scapular and gonadal adipose weights (Appendix C, Fig. **A6D,E,F**) at various time points and found no difference between WT and KO mice for any of these parameters.

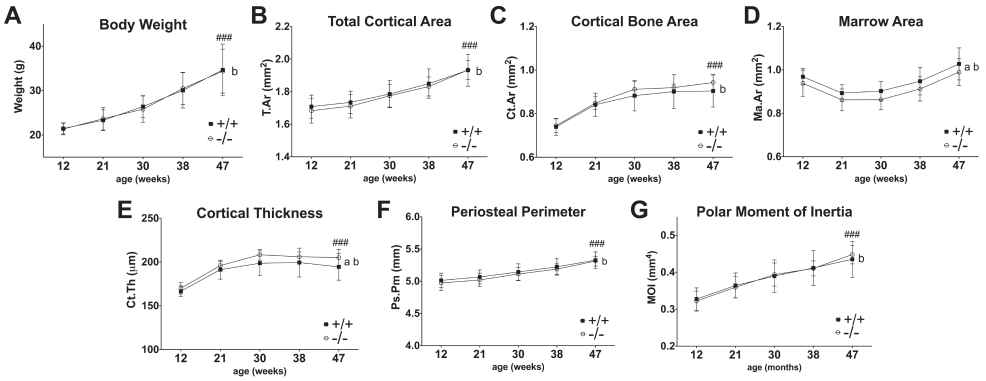


**Figure 1. Longitudinal analysis of body weight and cortical bone structure in wild type and *Muc1* deficient female mice.** Total body weight from 12 weeks to 47 weeks of age (A). *In vivo* µCT analysis of cortical bone area (C), marrow area (D), cortical thickness (E), periosteal perimeter (mid-shaft circumference) (F), and polar moment of inertia (G) were measured at diaphyseal areas. n= 9-10. Statistics: 2-way ANOVA; a-b = $p<0.01$. a= significant difference between in WT (+/+, filled squares) and *Muc1* deficient (-/-, open circles) female mice with aging, b= significant difference with aging within a genotype. Bonferroni post hoc test: ### = $p < 0.001$ significant difference between 12-weeks and 47-weeks within genotype for both WT and KO mice.

An initial study was performed into the longitudinal bone dynamics in WT and *Muc1* KO mice in order to gain a thorough view of the changes in the cortical bone over time. Female mice were analyzed every 2-months throughout adult life (12-

weeks to 47-weeks) for cortical bone architecture in the femoral diaphysis by repeated *in vivo* μCT. Aging affected all cortical bone parameters in both genotypes (Fig. **1B-G**). Both WT and *Muc1*$^{-/-}$ mice gained cortical bone (Fig. **1C**) over time, with a 22% and 27% increase in bone from 12-weeks to 47-weeks of age in WT and KO mice, respectively. A similar trend was found for cortical thickness (Fig. **1E**) in both genotypes. An overall significant difference between WT and KO mice with aging was found on marrow area ($p = 0.002$) (Fig. **1D**), and cortical thickness ($p = 0.001$) (Fig. **1E**); however, *Muc1* deletion had no significant effect on cortical bone architecture at any specific time point (Fig. **1B-G**). No significant interaction between genotype and age was observed. For all parameters, no significant difference was observed between WT and KO mice from 12-weeks of age onward.

*5.2.2 Female Muc1*$^{-/-}$ *mice have temporally reduced trabecular bone mass at young age*

To scrutinize trabecular, as well as cortical, femoral bone microarchitecture of WT and KO mice *ex vivo* μCT analysis employing higher resolution (8.82 μm compared to 20 μm) was used at 3 time points (juvenile mice at 8 weeks, mature adult mice at 16-weeks, and aged mice at 52-weeks of age). For these more in depth analyses the chosen time points included younger and older mice compared with the longitudinal study to expand the picture of the bone phenotype. The femur length (Fig **2A**) and overall morphology (Fig. **2B,C,D**) of the bones did not differ between WT and *Muc1* knockout mice at any time point.

The trabecular bone volume fraction (BV/TV) in the metaphyseal region of female 8-week-old KO mice was 22% lower ($p = 0.028$) than that of WT mice (Fig. **2E**), which can be primarily attributed to the strong trend seen in lower number of trabeculae (19% of WT at 8-weeks, $p = 0.051$) (Fig. **2F**). No difference was seen in trabecular thickness (Fig. **2G**), but trabecular separation was increased by 7% ($p = 0.040$) in KO mice compared with WT at 8-weeks of age (Fig. **2H**). The difference in the metaphyseal phenotype between *Muc1*$^{-/-}$ and WT mice disappeared by 16-weeks of age (Fig. **2E-H**) with an overall decrease of 88.8% ($p < 0.001$) and 94% ($p < 0.001$) in the trabecular bone fraction from 8 to 52 weeks in KO and WT mice, respectively. In the diaphyseal region, cortical parameters, such as total cortical bone (Fig. **2I**), marrow area (Fig. **2J**), cortical thickness (Fig. **2K**), and periosteal perimeter (Fig. **2L**) exhibited no difference between WT and KO mice at 8-, 16-, or 52-weeks of age. As was demonstrated by the *in vivo* μCT study, cortical bone increased with age, with a 39% increase ($p < 0.001$) in WT and 48% increase ($p < 0.001$) in KO mice for total cortical bone.

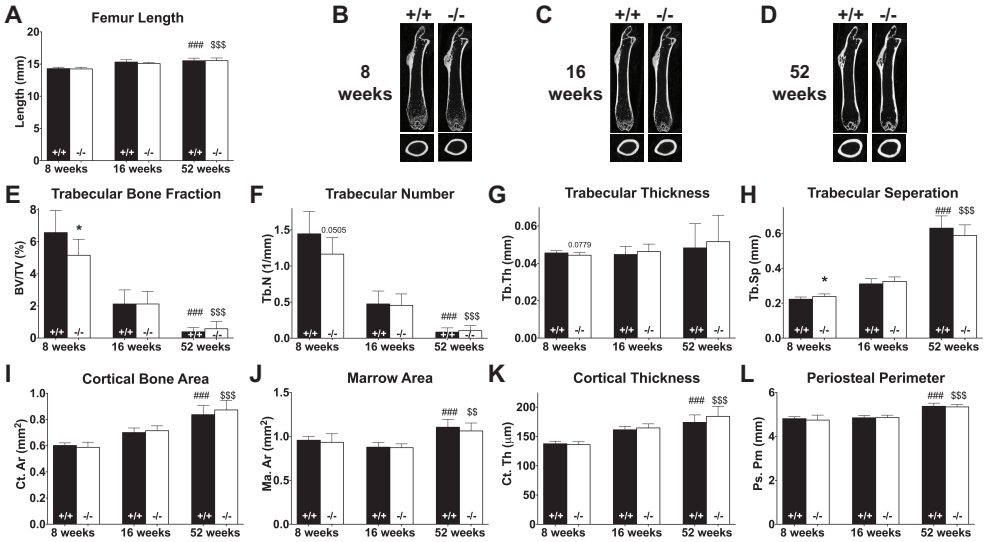


**Figure 2. *Ex vivo* evaluation of macro- and microarchitecture of femoral bones from 8-, 16-, and 52-week-old WT and *Muc1* deficient female mice.** Femur length of WT (+/+, black bar) and KO mice (-/-, white bar) (A). Representative longitudinal (top) and transverse (bottom) cross sections show bone shape and structure of WT (left) and *Muc1*$^{-/-}$(right) mice at 8 weeks (B), 16 weeks (C), and 52 weeks (D) of age. Trabecular bone fraction (E), trabecular number (F), trabecular thickness (G), and trabecular separation (H) were measured at the metaphyseal region. Cortical bone area (I), marrow area (J), cortical thickness (K), and periosteal perimeter (mid-shaft circumference) (K) were measured at diaphyseal areas. For bone length 8 weeks (n=7 WT, n=9 KO); 16 weeks (n=7); 52-weeks (n=8). For trabecular bone analysis 8 weeks (n=8 WT, n=9 KO); 16 weeks (n=9 WT, n=10 KO); 52-weeks (n=9 WT, n=10 KO). For cortical bone analysis 8 weeks (n=8 WT, n=9 KO); 16 weeks (n=9 WT, n=9 KO); 52-weeks (n=9 WT, n=10 KO). Statistics: student t-test exact p value and * = $p<0.05$ WT vs. *Muc1*$^{-/-}$ within time point. ### = $p < 0.001$ compared to 8wk WT mice. $$ = $p < 0.01$ compared to 8wk KO mice. $$$ = $p < 0.001$ compared to 8wk KO mice.

*Muc1* KO male mice show no difference, compared with WTs, in body weight (Appendix C, Fig. **A7A**) or femur length (Appendix C, Fig. **A7B**) at any time point, nor did they display a difference in any trabecular or cortical bone parameter at 8 and 16 weeks (Appendix C, Fig. **A7C-J**). At 52-weeks of age male KO mice display a mild reduction in the number of trabeculae (Appendix C, Fig. **A7D**) and increase in trabecular separation (Appendix C, Fig. **A7F**). Trends with aging for the male mice were similar to the females, with the exception that the male mice showed an increase in trabecular thickness (WT: 23%, $p = 0.0013$; KO: 24%, $p = 0.0052$) and separation (WT: 87%, $p < 0.0001$; KO: 133%, $p < 0.001$) at age 52-weeks compared with age 8-weeks. In addition, male KO mice displayed no difference in cortical thickness ($p = 0.61$) between 8- and 52-weeks of age, and WT males had a less substantial increase in cortical thickness (10%, $p = 0.0498$) between 8- and 52-weeks, which result in lower increases in total cortical bone area (WT: 19%, $p = 0.0108$; KO: 11%, $p = 0.0182$) as well.

*5.2.3 Sixteen-week-old Muc1$^{-/-}$ female mice have fewer trabecular osteoblasts, but endocortical bone formation rate is increased in 16- and 52-week-old Muc1$^{-/-}$ mice*

Histological sections of femurs from female WT and *Muc1*$^{-/-}$ mice were stained with Goldner trichrome to assess the number and distribution of cuboidal osteoblasts or with TRAP to assess the number and distribution of osteoclasts in the bone. We found that the number of osteoblasts in the femurs of 16-week-old *Muc1*$^{-/-}$ mice was 18% lower ($p = 0.034$) compared with WT mice, but the numbers did not differ in 8- or 52-week-old mice (Fig. **3A**). Although a trend was observed in percentage of osteoblast-covered surface between WT and KO mice at 16 weeks of age ($p = 0.0809$), no significant difference was observed between WT and KO mice at any time point (Fig. **3B**). Histological analysis of TRAP stained femoral sections showed no difference in the number of osteoclasts or the percent of bone covered by osteoclasts at any time point between the bones of WT and *Muc1*$^{-/-}$ mice (Fig. **3C,D**).

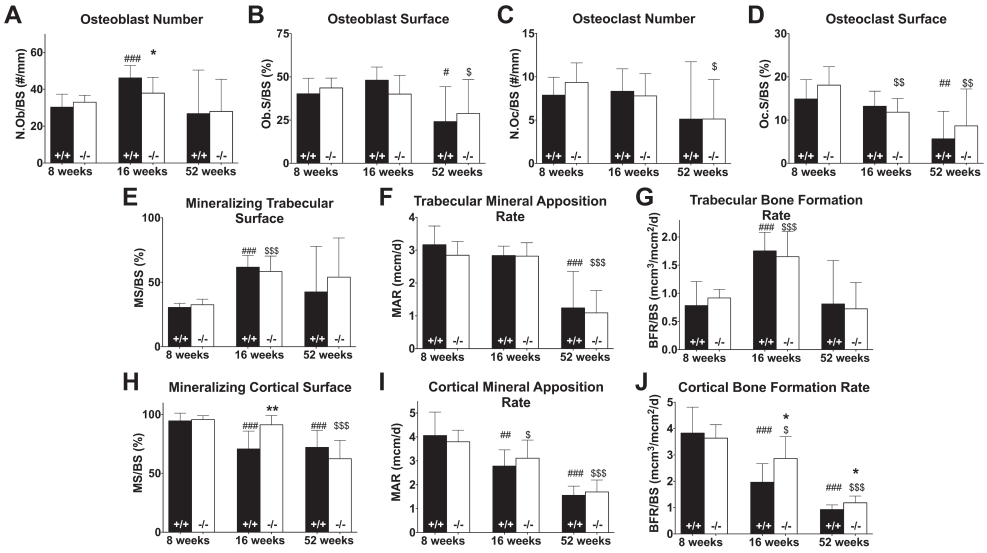


**Figure 3. Static and dynamic histomorphometry of osteoblast and osteoclast number and osteoblast activity in femoral bone sections of WT (+/+, black bar) and *Muc1* deficient (-/-, white bar) female mice at 8, 16, and 52 weeks of age.** Goldner stainings were performed on bone sections and images were taken of the metaphyses from which we quantified osteoblast number (A) and osteoblast covered surface (B). TRAP stainings were performed on femoral bone sections from WT (black bars) and *Muc1*$^{-/-}$ (white bars) mice and images were taken of the metaphyses. From these stainings, osteoclast number (C) and osteoclast surface (D) per bone surface area were quantified. Mice were injected with calcein prior sacrifice to label mineralization sites and allow for quantitative analyses trabecular bone mineralizing surface (E), mineral apposition rate (F) and bone formation rate (G), and of cortical bone endosteal mineralizing surface (H), mineral apposition rate (I), and bone formation rate (J). Statistics: student t-test * = $p<0.05$ WT vs. *Muc1*$^{-/-}$ within time point. ** = $p<0.01$ WT vs. *Muc1*$^{-/-}$ within time point. # = $p < 0.05$ compared to 8wk WT mice. ## = $p < 0.01$ compared to 8wk WT mice. ### = $p < 0.001$ compared to 8wk WT mice. $ = $p < 0.05$ compared to 8wk KO mice. $$$ = $p < 0.001$ compared to 8wk KO mice. For osteoblast bone analysis 8 weeks (n=10 WT, n=9 KO); 16 weeks (n=9 WT, n=10 KO); 52-weeks (n=9 WT, n=9 KO). For osteoclast bone analysis and trabecular bone calcein analysis 8 weeks (n=10 WT, n=9 KO); 16 weeks (n=9 WT, n=10 KO); 52-weeks (n=9 WT, n=10 KO). For cortical calcein analysis 8 weeks (n=8 WT, n=9 KO); 16 weeks (n=9 WT, n=10 KO); 52-weeks (n=9 WT, n=10 KO).

A decrease in the percent of bone surface covered by osteoblasts (Fig. **3B**) (WT p = 0.036, KO p = 0.046) and osteoclasts (Fig. **3D**) (WT p = 0.002, KO p = 0.008) between 8-week-old and 52-week-old mice was observed for both WT and KO groups. The relative number of osteoclasts on the femoral bone surface decreased only in KO mice between 8 weeks and 52 weeks of age (Fig. **3C**) (WT p = 0.225, KO p = 0.022).

To determine if *Muc1* deletion affects mineralization and bone formation rates, dynamic histomorphometric analysis was performed in sections of femurs from female WT and KO mice injected twice with calcein before they were euthanized. Trabecular mineralizing surface fractions, mineral apposition rates, and bone formation rates did not differ between WT and KO mice (Fig. **3E,F,G**). In both groups of mice, trabecular mineral apposition rates decreased over time, whereas bone formation rates were highest at age 16-weeks, nearly double that of rates at 8-(WT p < 0.001, KO p < 0.001) and 52-weeks of age. The percentage actively mineralizing endosteal cortical bone surface was 29% higher (p = 0.002) in 16-week-old *Muc1*$^{-/-}$ mice compared with WT (Fig. **3H**). Mineral apposition rate in cortical bone did not differ between WT and KO mice at any time point (Fig. **3I**), but bone formation rate in the cortex was significantly higher in KO mice at 16-(46% higher, p = 0.021) and 52-(28% higher, p = 0.022) weeks of age compared with WT controls (Fig. **3J**). For both parameters, a decline with increasing age was found, with the rate decreasing 76% (MAR p < 0.001, BFR p < 0.001) and 63% (MAR p <0.001, BFR p < 0.001) between 8- and 52-weeks in WT and KO mice, respectively.

*5.2.4 Female Muc1 knockout mice have stiffer bones at 16 weeks of age*

Structural and compositional changes in the bone can lead to changes in bone strength. To determine if the strength of the femurs was affected in mice lacking *Muc1*, we performed 3-point bending tests and measured three parameters: energy to failure, ultimate load and stiffness[25]. In female mice, no difference was found for ultimate load (Fig. **4A**), but bone stiffness was increased by 15% (p = 0.028) in 16-week-old KO compared with WT mice (Fig. 4**B**). Energy to failure (Fig. **4C**) did not differ between WT and KO mice at any time point.

As with female mice, male KO and WT mice did not differ in ultimate load (Appendix C, Fig. **A8A**) or energy to failure (Appendix C, Fig. **A8C**), but male KO mice did display stiffer femoral bones at 8 weeks of age, compared with WT males (21%, p = 0.0303); however, this difference disappeared by 16 weeks of age (Appendix C, Fig. **A8B**).

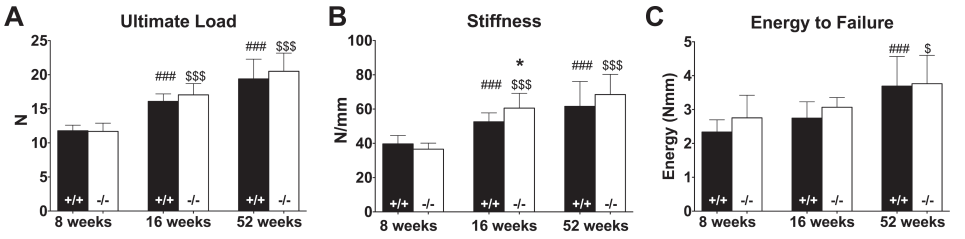


**Figure 4. Mechanical testing of femurs of 8-, 16-, and 52-week old WT (+/+, black bar) and *Muc1* deficient (-/-, white bar) female mice.** Three-point bending tests performed on the femurs of WT and KO mice allowed for quantification of the energy to failure (A), ultimate load (B), and bone stiffness (C) of the bones. Statistics: student t-test * = p<0.05 WT vs. *Muc1*$^{-/-}$ within time point. ### = p < 0.001 compared to 8wk WT mice. $ = p < 0.05 compared to 8wk KO mice. $$$ = p < 0.001 compared to 8wk KO mice. 8 weeks (n=9 WT, n=9 KO); 16 weeks (n=9 WT, n=10 KO); 52-weeks (n=9 WT, n=10 KO).

*5.2.5 Bone marrow-derived osteoblast differentiation does not differ between WT and KO mice*

To study the differentiation capacity of mesenchymal stromal cells (MSCs) toward osteoblasts, we isolated bone marrow containing MSCs and osteogenic progenitors from 8-, 16-, and 52-week-old female WT and *Muc1*$^{-/-}$ mice and analyzed their differentiation into osteoblasts in *ex vivo* cultures. After one week of culture, we counted the number of alkaline phosphatase (ALP)-positive colonies. No difference was observed in the number of colonies between marrow cultures from WT and KO mice, but a trend was found for an increased number of osteoblast colonies in bone marrow cells from 16-week-old KO mice (p = 0.062) (Fig. **5A,B**). After 3 weeks of culture in osteogenic differentiation medium cells were stained with alizarin red to determine the level of mineralization in the bone marrow culture. No difference in mineralization from cells from WT and KO mice was observed (Fig. **5C,D**).

*5.2.6 Bone marrow-derived osteoclast differentiation capacity and activity are not affected by depletion of Muc1*

Although our hypothesis is that *Muc1* plays a role in murine bone because of changes in osteoblast function, Leong and colleagues[26] have found that human monocyte/macrophage cells express moderate levels of Muc1 protein and we find that differentiating murine osteoclasts express low, but detectable levels of *Muc1* (Appendix C, Fig. **A9**). To study if *Muc1* deletion affects the differentiation capacity of PBMCs toward osteoclasts and/or osteoclast activity, we isolated bone marrow from 8-, 16-, and 52-week-old female WT and *Muc1*$^{-/-}$ mice and analyzed their differentiation into osteoclasts and their resorption capacity in *ex vivo* cultures. From the bone marrow samples we saw no difference in the relative number of small or large TRAP positive osteoclasts, or the total number of multinucleated osteoclasts (Fig. **6A,B,C**), nor did the resorption capacity of osteoclasts differ between cells from WT or KO mice (Fig. **6D,E**).

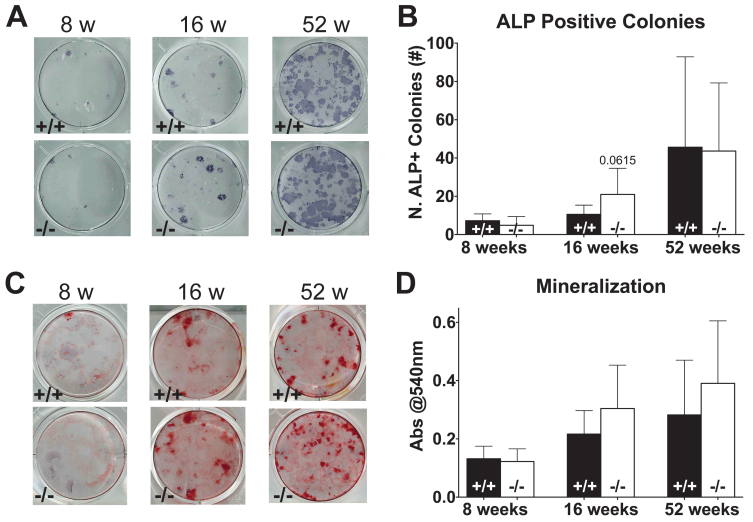


**Figure 5. Osteoblast cultures of bone marrow from 8-, 16-, and 52-week-old WT (+/+, black bars) and Muc1 deficient (-/-, white bars) female mice.** Analyses were performed of osteoblast differentiation capacity and activity in bone marrow cell cultures. Representative stainings of alkaline phosphatase (ALP) positive osteoblast colonies (C) in WT (top) and Muc1$^{-/-}$ (bottom) mice and quantification of the number of ALP positive colonies (D). Representative alizarin red stainings of osteoblast produced mineralization (E) in WT (top) and Muc1$^{-/-}$ (bottom) mice and quantification of alizarin red staining indicative of mineralization activity of bone marrow derived osteoblasts (F). Statistics: student t-test * = $p<0.05$ WT vs. Muc1$^{-/-}$. For ALP analysis 8 weeks (n=8 WT, n=7 KO); 16 weeks (n=8); 52-weeks (n=7 WT, n=8 KO). For alizarin red analysis 8 weeks (n=8 WT, n=7 KO); 16 weeks (n=8); 52-weeks (n=8). Results represent the combined results of 2 independent experiments.

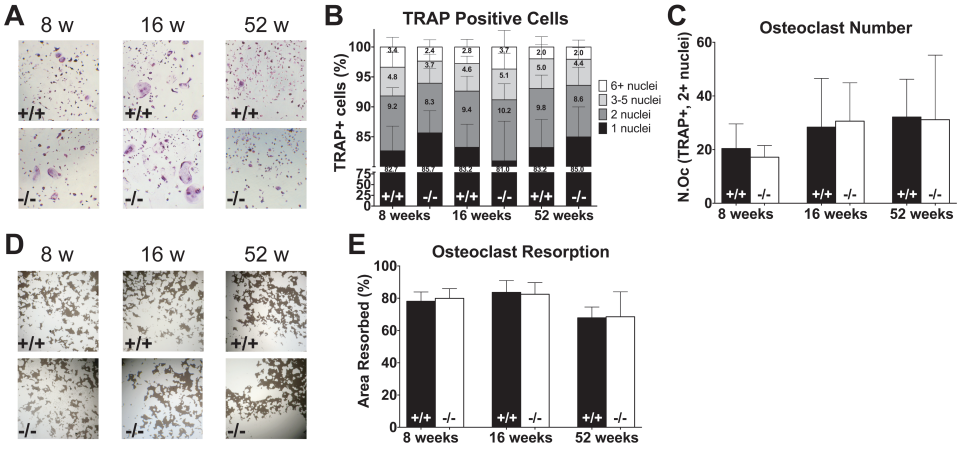


**Figure 6. Osteoclast cultures of bone marrow cells from 8-, 16-, and 52-week-old WT (+/+) and Muc1 deficient (-/-) female mice.** Assessment of osteoclast differentiation capacity and activity in bone marrow cell cultures in WT and Muc1$^{-/-}$ mice was performed. Representative stainings of tartrate-resistant acid phosphatase (TRAP) positive osteoclasts (A) in WT (top) and Muc1$^{-/-}$ (bottom) mice and quantification of the distribution in number of nuclei contained within TRAP-positive osteoclasts (B) and the total number of multinucleated TRAP positive osteoclasts (C). Representative images of von kossa staining showing resorption activity of osteoclasts (D) from bone marrow of WT (top) and Muc1$^{-/-}$ (bottom) mice and quantification of surface resorption by osteoclasts of WT and Muc1$^{-/-}$ mice (E). Statistics: student t-test * = $p<0.05$ WT vs. Muc1$^{-/-}$. 8 weeks (n=8 WT, n=7 KO); 16 weeks (n=8); 52-weeks (n=8). Results represent the combined results of 2 independent experiments.

## 5.3 Discussion

The results of this extensive and detailed skeletal phenotype analysis demonstrate that deletion of *Muc1* in mice leads to mild and temporally shifting changes in long bones and bone metabolism.

Eight-week-old female *Muc1*$^{-/-}$ mice display decreased trabecular bone compared with WT females; however, this difference disappears by 16-weeks. At the same time, endocortical bone formation rate and femoral stiffness are increased at 16-weeks of age in *Muc1* deficient female mice, with a higher rate of endocortical bone formation persisting to 52-weeks of age in KO mice. Histomorphometric analysis demonstrated that femurs of 16-week-old *Muc1*$^{-/-}$ female mice displayed lower numbers of osteoblasts lining the bone surface, whereas femurs from 8- and 52-week old KO and WT mice did not differ in their number of osteoblasts, again demonstrating a temporal effect of *Muc1* deletion.

### *5.3.1 Changes in murine femoral bone with aging*

In both WT and *Muc1*$^{-/-}$ we observed a number of changes in the femoral bone over time. We found that the trabecular bone fraction dramatically declined between 8- to 52-weeks of age (88.8% in KO and 94% in WT mice). These rates of loss are similar to a previously published study looking at age related changes in the femoral bones of female wild-type C57Bl/6 mice[27]. We also saw that both WT and *Muc1*$^{-/-}$ mice gained cortical bone with aging (39% increase in WT and 48% increase in KO) between 8- and 52-weeks, and a similar trend was seen for cortical thickness. While Glatt and colleagues found that femoral cortical bone area remained steady between 2 and 12 months and cortical thickness in female C57Bl/6 mice increased markedly between 1 to 3 months of age and was then maintained through 12-months[27], our results showed an increase between each time point although the gain is less between 16- and 52-weeks. The difference is likely to be explained by the method of analysis: while Glatt used the distal femur region to assess both trabecular and cortical bone properties, we used the mid-shaft of the femur for our cortical measurements. Consistent with the increase in cortical bone with aging, all mechanical strength properties increased with time as well. The larger, thicker cortex of the older bones directly contributes to a stronger femur, requiring more force to fracture, assuming the material properties are the same. In this study, trabecular bone formation rate peaked at 16-weeks, while cortical bone formation rate declined over time. In concordance Glatt found that adult (5-month-old) female mice had a higher level of trabecular bone formation rate relative to younger (1- and 3-month old) mice; however, they did not see a decrease later in life (12-months)[27]. As the time points

between the two studies are not identical it is possible that this could be the reason for the observed difference. Cortical bone formation rate was not investigated in their study[27]. The peak in trabecular bone formation rate at 16-weeks goes along with the peak in osteoblast number that we also saw at 16-weeks of age.

*5.3.2 Muc1 deficient mice display a temporally shifting bone phenotype*

In 8-week-old *Muc1* deficient mice trabecular bone volume fraction was reduced primarily because of lower trabecular number. Interestingly, although we observe a 22% decrease in the fraction of trabecular bone/ no other bone parameter is altered in young mice including trabecular mineralization rates, total number of osteoblasts, and bone strength parameters. This may indicate that osteoblast differentiation capacity and activity are not affected at 8-weeks of age and the reason for the lower amount of trabecular bone may lie in a preceding developmental defect or a hindrance in the growth plate in mice younger than the ages we studied. Another possibility is that lack of *Muc1* expression in osteoblasts could cause increased degradation of estrogen receptor alpha (ERα) which can lead to decreased bone mass. Previous studies have shown that the MUC1 C-terminal subunit binds directly to the ERα DNA binding domain and stabilizes ERα by blocking its ubiquitination and degradation[28]. Indeed, mice lacking ERα expression in osteoblasts display decreased trabecular and cortical bone mass in tibial, femoral, and vertebral bones[29]. Unfortunately, they only studied mice at 12 and 18 weeks of age precluding observing temporal effects at ages we studied. Because we only see decreased trabecular bone in young *Muc1*$^{-/-}$ mice, it is possible that the temporal trabecular phenotype is overcome by redundancy in the system, for example by other MUC proteins. Future studies demonstrating how estrogen deprivation may affect the phenotype in *Muc1* KO mice would greatly add to our understanding the role of *Muc1* in bone.

The bone phenotype of *Muc1*$^{-/-}$ mice changes over time. By 16-weeks of age trabecular bone volume in *Muc1*$^{-/-}$ mice has normalized to the level of wild types, but cortical bone formation rate and stiffness are increased. As the mice age, even though the total number of osteoblasts in the bone is lower in KOs, they have an increased capacity to produce cortical bone, as illustrated by higher endocortical mineralized surface and mineral apposition rate at 16- and 52-weeks of age compared with WT mice. It has been previously established that stiffer bones result from increased cortical bone and/or changes in the material properties of the bone[25]. The increase in stiffness in the KO mice is paralleled by increased cortical mineralizing surface and bone formation rate, which could lead to changes in the material properties of the bone and explain the increased stiffness. Future studies involving proteomic analysis

of the bone matrix proteins in mice lacking *Muc1* would be useful in delineating the mechanism behind these changes in osteoblast activity and increased femoral stiffness. Two-way ANOVA analysis showed an overall significant difference in marrow area and cortical thickness between WT and *Muc1*$^{-/-}$ with aging, but no significant effect was found at any one time point by post hoc or Student-t-test. The mild bone architectural phenotype we observed may be partially due to the mouse strain; C57Bl/6 mice are known to have a lower bone mass than other strains of mice and this may limit observations on genetic changes in bone microarchitecture.

*Muc1* deletion also caused mild temporally shifting effects in the long bones of male mice; however, these effects differed somewhat from the females. *Muc1*$^{-/-}$ male mice show no difference, compared with WTs, in any trabecular or cortical bone parameter at 8- and 16-weeks. At 52-weeks of age male *Muc1*$^{-/-}$ mice display a mild reduction in the number of trabeculae and increase in trabecular separation. These data are in contrast to the female *Muc1*$^{-/-}$ data in which we found that the trabecular bone fraction was strongly reduced at 8 weeks of age, but no difference in trabecular bone parameter between *Muc1*$^{-/-}$ and WT mice later in life. Femoral stiffness was also temporarily increased in *Muc1*$^{-/-}$ male mice, but at 8-weeks of age, earlier than in females. Differences between males and females could partially be related to differences in estrogen regulation in males and females, and regulation of ERα as discussed above. Further experiments are required to determine the mechanism of action of *Muc1* in the bones of both female and male mice; however, the male data supports the overall conclusion that *Muc1* deletion has a temporal effect on bone biology.

### *5.3.3 The importance of utilizing multiple time points when evaluating murine models for skeletal abnormalities*

Our results demonstrating a temporal bone phenotype in *Muc1*$^{-/-}$ mice underpin the importance of looking at multiple time points when investigating *in vivo* bone phenotypes. Analyzing only a single time point in our study, as is common routine in many mouse genetic studies, would have led to either over-interpretation or missing aspects of *Muc1* deficiency on bone metabolism. We are not alone in identifying a transient or changing bone phenotype in genetically altered mice as many other studies report age-dependent effects following gene perturbations. Mice genetically engineered to overexpress epidermal growth factor receptor ligand amphiregulin (AREG) demonstrate greater femoral BMD and total bone in the metaphyseal region at 4- and 8-weeks of age compared to WT controls but after 10-weeks of age there is no difference between the genotypes anymore[30]. In addition, Shi and colleagues identified that deletion of BMP receptor BMPR1B resulted in

trabecular bone loss at 8 weeks of age, which was not seen either just after birth or at 11 weeks of age[31]. Our lab also previously reported a temporal difference in skeletal changes with age between trabecular and cortical bone in DNA repair deficient female Trichothiodystrophy (TTD) mice where these mice show accelerated bone aging after 39-weeks of age[32]. Taken together our results suggest that the bone, and in particular the metaphysis of the long bones due to its relatively high bone turnover, may be most sensitive to gene/protein deficiency in an age-related fashion, i.e. coinciding with the time of most intense longitudinal growth and shows great temporal dynamics.

### *5.3.4 Conclusion*

In conclusion, this study demonstrates, for the first time, a role for *Muc1* in bone biology. Further studies are required to understand the mechanism of action by which *Muc1* affects osteoblast differentiation and bone formation in these mice and the reason for the temporal dynamics of the effects on bone. Given its explicit expression patterns in early human osteoblast differentiation[10], it will also be pivotal to investigate the expression patterns of *MUC1* in human MSCs and osteoblasts and its potential role in human bone homeostasis.

## 5.4 Materials and Methods

### *5.4.1 Mice*

*Muc1*$^{-/-}$ mice were constructed as described by Spicer et al.[24]. The mice were backcrossed onto C56BL/6 and then wild-type (WT) and *Muc1*$^{-/-}$ mice were bred from heterozygous parents in the same facility. Mice were genotyped by PCR using specific primer sets as follows: wild-type allele was detected using 5'-ACC TCA CAC ACG GAG CGC CAG -3' and 5'- TCC CCC CTG GCA CAT ACT GGG -3', and the mutant allele was detected by 5'- ACC TCA CAC ACG GAG CGC CAG -3' and 5'- CAA CTG TTG GGA AGG GCG AT -3'. An amplified fragment of 260 bp corresponds to the WT allele and of 240 bp to the mutant allele.

Mice were housed standard microisolator or individually ventilated cages in groups of 1-5 animals in specific pathogen-free (SPF) rooms at a 12-hour light-dark cycle and had *ad libitum* access to food and water. Female mice (n=9-10 per genotype) were sacrificed at 8-, 16- and 52-weeks of age and bones were collected for microcomputed tomography and histomorphometry (left femurs), 3-point bending tests (right femurs), and bone marrow cultures (tibiae). Male mice (n=9-10 per genotype) were sacrificed at 8-, 16- and 52-weeks of age and bones were collected for

microcomputed tomography (left femurs) and 3-point bending tests (right femurs). Mice were healthy for the duration of the study, with the exception of one WT female mouse in the longitudinal study/52-week group that was found to have a wound at 36 weeks of age and it was deemed too severe to survive and was humanely euthanized and one KO male mouse in the longitudinal study/52-week group that was found dead at 44-weeks of age without any apparent cause. To determine the number of mice used in each treatment group power calculations were performed utilizing data from a pilot experiment assessing bone microarchitecture and strength parameters of bones from *Muc1*$^{-/-}$ and WT litter mates provided by the Gendler Lab group. Researchers were blinded to the genotype of the mice during all experimental procedures and at sacrifice. All animal experiments were performed in compliance with the animal ethics board of the Erasmus Medical Center.

*5.4.2 Microcomputed tomography (μCT)*

*In vivo* μCT of the left femur was carried out on WT and *Muc1*$^{-/-}$ mice (n = 10) every 2 months from 3 months until 11 months of age. The scans were performed at 20 μm resolution using a Quantum FX system (PerkinElmer, Groningen, The Netherlands). Mice were anesthetized in an induction chamber by inhalation of 4% isoflurane. Under 4% isoflurane anesthesia the animal was placed on a specially constructed holder that allows for fixation of the left femur. The holder with the animal was fixed on the animal bed of the scanner with a nose cone supplying 1.5-2.0% isoflurane in an air/oxygen mixture. The following scan settings were used: X-ray power and tube current were 90 kV and 0.16 mA, respectively. Beam hardening and ring-artifacts were reduced, and the total scan time was 3 min. For export of image files, the Quantum FX generated VOX files were loaded into Analyze 12 software (AnalyzeDirect, Overland Park, KS, USA) where a cutoff intensity of 900-2600 (or max if less than 2600) was applied and the complete set of multiple 2D images were saved in BMP format for downstream analysis. Analysis only includes data for 9 WT females at 38- and 47-week time points due to the sacrifice of one mouse for a wound as described in previous methods section. During the analysis of the *in vivo* scans one scan from a KO female at the 47-week time point was found to have motion blurring and was excluded from the analysis.

For *ex vivo* μCT analysis the left femurs from female *WT* and *Muc1*$^{-/-}$ mice sacrificed at 8, 16 and 52 weeks (n = 8-10) were scanned at a resolution of 8.82 μm, using a SkyScan 1076 system (Bruker MicroCT, Kontich, Belgium). According to guidelines recently published[33], the following settings were used: X-ray power and tube current were 40 kV and 0.25 mA, respectively. Beam hardening (20%) was reduced using a 1 mm aluminum filter, ring-artifacts were reduced (set at 5), exposure

time was 5.9 s and an average of three pictures was taken at each angle (0.8°) to generate final images. 3D images were reconstructed using NRecon from Bruker MicroCT (Skyscan, Kontich, Belgium, http://www.skyscan.be/products/downloads.htm).

For both *in vivo* and *ex vivo* μCT data analysis we used software packages from Bruker MicroCT, (CtAn and Dataviewer, Skyscan, Kontich, Belgium, http://www.skyscan.be/products/downloads.htm). Bone microarchitectural parameters were assessed in cortical bone for the *in vivo* data and in both trabecular and cortical bone for the *ex vivo* data of all mice (n = 8-10 per genotype). For *ex vivo* scans (100 sections) the metaphyseal area was selected for analysis starting 135 (8-week-old mice), 110 (16-week-old mice), and 95 (52 week-old-mice) sections below our offset landmark within the epiphyseal growth plate. The diaphyseal (50 sections for 8.82 μm *ex vivo* scans, 25 sections for 20 μm *in vivo* scans) area was selected for at the mid-shaft of the femur. The trabecular bone parameters trabecular tissue volume, bone volume, trabecular volume fraction (BV/TV), trabecular thickness, trabecular number and trabecular patterning factor (connectivity of trabeculae) were determined in the distal metaphysis of the femur. In the mid-diaphysis, cortical volume, endocortical volume, cortical thickness, and perimeter were analyzed. For image processing, trabecular bone was manually selected and cortical bone was automatically selected. Global thresholding was applied for segmentation using threshold levels of 85 (lower) and 255 (higher) for trabecular and levels of 140 and 255 for cortical bone measurements.

*5.4.3 Bone mechanical testing*

Right femurs (n = 9-10) were stored in phosphate-buffered saline at −20 °C until further use. The procedure was carried out as previously described in detail [34]. Briefly, femurs were placed in a custom made 3-point bending device, with the loading posts 10 mm apart. Mechanical testing was performed, using a Single Column Lloyd LRX System (Lloyd Instruments, Fareham, UK). Displacement (mm) and force (N) were registered. From the resulting displacement to force graphs, ultimate force (N), stiffness (N/mm) and work to failure (mJ) were determined as described before[35].

*5.4.4 Bone histomorphometry*

To determine the dynamic histomorphometric indices, WT and *Muc1*$^{-/-}$ mice (n = 8-10) were injected with calcein (15 mg/kg, Sigma, St. Louis, MO, USA) intraperitoneally prior to sacrifice on the following schedule: 5 and 2 days prior for 8-week-old mice, 6 and 2 days prior for 16-week-old mice, and 8 and 2 days prior for

52-week-old mice. After excision, femurs were routinely embedded in methylmetacrylate as described previously[36].

For bone histomorphometry analysis the blocks were sectioned at 6 μm. For osteoblast measurements, sections were stained with a Goldner staining as described before[37,38]. For detection of osteoclasts Tartrate-resistant acid phosphatase (TRAP) staining was performed. Sections were rinsed in 0.2 M sodium acetate/100 mM tartaric acid for 20 min, after which Naphtol AS-MX (0.5 mg/ml) and Fast red TR salt (1.1 mg/ml) (both from Sigma, St. Louis, MO, USA) were added and incubated for 20 min at 37 °C. Sections were counterstained with haematoxylin for 15 sec, rinsed, air-dried and embedded in glycergel (Agilent, Amstelveen, The Netherlands). Dynamic trabecular and cortical analysis was performed separately. Cortical measurements were performed in the metaphysis between 0.5 mm and 2.5 mm below the growth plate. The trabecular measurements were performed in the entire bone marrow region between 0.5mm to 1.5 mm below the growth plate. Labeled surfaces were hand-drawn within Bioquant (Version 7.20; Bioquant image analysis corporation, Nashville, Tennessee, USA) resulting in the following measurements: mineral surface (MS), bone surface (BS), tissue volume (TV), mineral apposition rate (MAR) and bone formation rate (BFR).

For TRAP and Goldner stainings at least 5 images in the trabecular area were taken with a Zeiss Axiovert 200 MOT system (Carl Zeiss BV, Jena, Germany) at 20x magnification (0.5 mm to 2.5 mm below the growth plate). All quantitative measurements were performed on longitudinal sections that were taken from the anterior-posterior middle of the bone. All measurements were performed in ImageJ (NIH, Bethesda, Maryland, USA, available online at https://imagej.nih.gov/ij/): osteoblasts, osteoclasts, osteoblast surface (contact area with the bone), osteoclast surface (contact surface with the bone) and bone perimeters were determined by eye based on staining and morphology (cuboidal cells on the bone surface). The number of osteoblasts and osteoclasts, as well as the surfaces were hand drawn and the resulting pixel-measurements were calculated back to $mm^2$. Histomorphometric indices were defined and calculated according to the American Society of Bone and Mineral Research (ASBMR) nomenclature[39] and analysis was performed blinded towards the genotypes.

*5.4.5 Bone marrow cultures*

Bone marrow cells derived from WT and *Muc1*$^{-/-}$ mice (n=7-8) were isolated and cultured towards osteoclasts and osteoblasts as described in detail[36,40]. After 7 days of culture, TRAP staining was used to stain for osteoclasts[36]. Osteoclast-generated resorption pits on calcium phosphate coating of Osteo Assay plates

(Corning Life Sciences BV, Amsterdam, The Netherlands) were stained by von Kossa after 10 days of culture. Alkaline phosphatase (ALP) and alizarin red staining were performed on osteoblast cultures at days 10 and 21 of culture, respectively, as described earlier[36]. Osteoclast number and the number of nuclei per cell were measured using the freely available ImageJ software (version 1.41; http://rsbweb.nih.gov/ij/). ALP positive colonies and resorption surface were measured using the software package Bioquant (Version 7.20; Bioquant image analysis corporation, Nashville, Tennessee, USA). To evaluate the mineralized nodule formation i*n vitro*, cell/matrix layers were washed with PBS, fixed with 10% formaldehyde, and stained with alizarin red S (Sigma, St. Louis, MO, USA) solution. To quantify alizarin red S bound to mineralized nodules in the cultures, cultures were stained with alizarin red S, extensively rinsed with water, and extracted with 10% (w/v) acetic acid for 30 minutes at room temperature, after which the wells were scraped and contents added to Eppendorf tubes and vortexed for 30 sec. Mineral oil was added to the mixture and incubated at 85 °C for 10 min and then the tubes were placed on ice for 5 min. The tubes were centrifuged at 20,000 g for 15 min and 250 µl supernatant was pipetted into a clean tube and 100 µl 10% NaOH was added to neutralize the solution. The dye concentrations in the extracts were determined by absorbance at 540 nm using a Victor2 plate reader (PerkinElmer Life and Analytical Science). For each test 2-3 technical replicates (bone marrow culture wells) from each mouse were averaged. Results are combined from 2 independent experiments (n=3-4 mice/experiment).

*5.4.6 Collection of Muscle and Adipose Tissues*

After sacrifice the musculus gastrocnemius of the tibia and the quadriceps muscle of the femur were dissected out from the left hindlimb and weighed immediately. Scapular adipose deposits (representative brown fat), subcutaneous adipose deposits (white adipose tissue), and gonadal adipose deposits (white adipose tissue) from the right side of each mouse were identified and excised as described by Mann et. al.[41]. Immediately after dissection the tissues were weighed. Weights are expressed as a percent of total body weight for each mouse.

*5.4.7 Quantification of mRNA expression*

RNA isolation, cDNA synthesis and PCR reactions were performed as described previously[42]. Oligonucleotide primer pairs were designed to be either on exon boundaries or spanning at least one intron (**Table 1**). Gene expressions were corrected for the housekeeping gene *Hprt*. Experiment was performed in triplicate.

**Table 1. Oligonucleotide primers used in the study**

| Gene | **Forward 5'-3''** | **Reverse 5'-3''** |
|---|---|---|
| *Muc1* | CCCTATGAGGAGGTTTCGGC | GTGGGGTGACTTGCTCCTAC |
| *Hprt* | TTATCAGACTGAAGAGCTACTGTAATGATC | TTACCAGTGTCAATTATATCTTCAACAATC |

Sequences of primer sets used for qPCR in this study. All genes were detected using SYBR green.

*5.4.8 Statistical analysis*

Values displayed are mean ± SD. The *ex vivo* μCT parameters, histomorphometric data, femur length, mechanical loading tests, and parameters of cell culture analyses were compared between genotypes for all age groups separately using two-tailed unpaired student t-tests. For the *in vivo* μCT data significances were calculated using the two-way ANOVA with Bonferroni's multiple comparison post-hoc test. All statistical analyses were performed using GraphPad prism 6.0. p-values $<0.05$ were considered significant.

## References


1. Ducy, P., Zhang, R., Geoffroy, V., Ridall, A. L. & Karsenty, G. Osf2/Cbfa1: a transcriptional activator of osteoblast differentiation. *Cell* **89**, 747–54 (1997).
2. Komori, T. *et al.* Targeted disruption of Cbfa1 results in a complete lack of bone formation owing to maturational arrest of osteoblasts. *Cell* **89**, 755–64 (1997).
3. Otto, F. *et al.* Cbfa1, a candidate gene for cleidocranial dysplasia syndrome, is essential for osteoblast differentiation and bone development. *Cell* **89**, 765–71 (1997).
4. Gazzerro, E. & Canalis, E. Bone morphogenetic proteins and their antagonists. *Rev. Endocr. Metab. Disord.* **7**, 51–65 (2007).
5. Rosen, V. BMP and BMP Inhibitors in Bone. *Ann. N. Y. Acad. Sci.* **1068**, 19–25 (2006).
6. Chen, G., Deng, C. & Li, Y.-P. TGF-β and BMP Signaling in Osteoblast Differentiation and Bone Formation. *Int. J. Biol. Sci.* **8**, 272–288 (2012).
7. Hojo, H., Ohba, S. & Chung, U. Signaling pathways regulating the specification and differentiation of the osteoblast lineage. *Regen. Ther.* **1**, 57–62 (2015).
8. Komori, T. Signaling networks in RUNX2-dependent bone development. *J. Cell. Biochem.* **112**, 750–755 (2011).
9. Abdallah, B. M., Jafari, A., Zaher, W., Qiu, W. & Kassem, M. Skeletal (stromal) stem cells: An update on intracellular signaling pathways controlling osteoblast differentiation. *Bone* **70**, 28–36 (2015).
10. Van De Peppel, J. *et al.* Stem Cell Reports Identification of Three Early Phases of Cell-Fate Determination during Osteogenic and Adipogenic Differentiation by Transcription Factor Dynamics. (2017). doi:10.1016/j.stemcr.2017.02.018
11. Gendler, S. J. *et al.* Molecular cloning and expression of human tumor-associated polymorphic epithelial mucin. *J. Biol. Chem.* **265**, 15286–93 (1990).
12. Lan, M. S., Batra, S. K., Qi, W. N., Metzgar, R. S. & Hollingsworth, M. A. Cloning and sequencing of a human pancreatic tumor mucin cDNA. *J. Biol. Chem.* **265**, 15294–9 (1990).
13. Ligtenberg, M. J., Vos, H. L., Gennissen, A. M. & Hilkens, J. Episialin, a carcinoma-associated mucin, is generated by a polymorphic gene encoding splice variants with alternative amino termini. *J. Biol. Chem.* **265**, 5573–8 (1990).
14. Wreschner, D. H. *et al.* Human epithelial tumor antigen cDNA sequences. Differential splicing may generate multiple protein forms. *Eur. J. Biochem.* **189**, 463–73 (1990).
15. Apostolopoulos, V., Stojanovska, L. & Gargosky, S. E. MUC1 (CD227): a multi-tasked molecule. *Cell. Mol. Life Sci.* **72**, 4475–500 (2015).
16. Singh, P. K. & Hollingsworth, M. A. Cell surface-associated mucins in signal transduction. *Trends Cell Biol.* **16**, 467–476 (2006).
17. Kufe, D. W. Mucins in cancer: function, prognosis and therapy. *Nat. Rev. Cancer* **9**, 874–885 (2009).
18. Carson, D. D. The Cytoplasmic Tail of MUC1: A Very Busy Place. *Sci. Signal.* **1**, pe35–pe35 (2008).
19. Nath, S. & Mukherjee, P. MUC1: a multifaceted oncoprotein with a key role in cancer progression. *Trends Mol. Med.* **20**, 332–342 (2014).
20. Lillehoj, E. P., Kim, B. T. & Kim, K. C. Identification of *Pseudomonas aeruginosa* flagellin as an adhesin for Muc1 mucin. *Am. J. Physiol. - Lung Cell. Mol. Physiol.* **282**, L751–L756 (2002).
21. Lu, W. *et al.* Cutting edge: enhanced pulmonary clearance of Pseudomonas aeruginosa by Muc1 knockout mice. *J. Immunol.* **176**, 3890–4 (2006).
22. Kufe, D. W. MUC1-C oncoprotein as a target in breast cancer: activation of signaling pathways and therapeutic approaches. *Oncogene* **32**, 1073–1081 (2013).
23. Brayman, M., Thathiah, A. & Carson, D. D. MUC1: a multifunctional cell surface component of reproductive tissue epithelia. *Reprod. Biol. Endocrinol.* **2**, 4 (2004).
24. Spicer, A. P., Rowse, G. J., Lidner, T. K. & Gendler, S. J. Delayed mammary tumor progression in Muc-1 null mice. *J. Biol. Chem.* **270**, 30093–101 (1995).
25. Jepsen, K. J., Silva, M. J., Vashishth, D., Guo, X. E. & Ch Van Der Meulen, M. Establishing Biomechanical Mechanisms in Mouse Models: Practical Guidelines for Systematically Evaluating Phenotypic Changes in the Diaphyses of Long Bones HHS Public Access. *J Bone Min. Res. J Bone Min. Res* **30**, 951–966 (2015).
26. Leong, C.-F., Raudhawati, O., Cheong, S.-K., Sivagengei, K. & Noor Hamidah, H. Epithelial membrane antigen (EMA) or MUC1 expression in monocytes and monoblasts. *Pathology* **35**, 422–7 (2003).
27. Glatt, V., Canalis, E., Stadmeyer, L. & Bouxsein, M. L. Age-Related Changes in Trabecular Architecture Differ in Female and Male C57BL/6J Mice*. *J Bone Min. Res* **22**, 1197–1207 (2007).
28. Wei, X., Xu, H. & Kufe, D. MUC1 Oncoprotein Stabilizes and Activates Estrogen Receptor α. *Mol. Cell* **21**, 295–305 (2006).
29. Melville, K. M. *et al.* Female Mice Lacking Estrogen Receptor-Alpha in Osteoblasts Have Compromised Bone Mass and Strength. *J. Bone Miner. Res.* **29**, 370–379 (2014).
30. Vaidya, M. *et al.* Osteoblast-specific overexpression of amphiregulin leads to transient increase in femoral cancellous bone mass in mice. *Bone* **81**, 36–46 (2015).

31. Shi, C. *et al.* Deletion of BMP receptor type IB decreased bone mass in association with compromised osteoblastic differentiation of bone marrow mesenchymal progenitors. *Sci. Rep.* **6**, 24256 (2016).
32. Diderich, K. E. M. *et al.* Bone fragility and decline in stem cells in prematurely aging DNA repair deficient trichothiodystrophy mice. *Age (Dordr).* **34**, 845–61 (2012).
33. Bouxsein, M. L. *et al.* Guidelines for assessment of bone microstructure in rodents using micro-computed tomography. *J. Bone Miner. Res.* **25**, 1468–1486 (2010).
34. Westbroek, I. *et al.* Long-term fluoxetine administration does not result in major changes in bone architecture and strength in growing rats. *J. Cell. Biochem.* **101**, 360–368 (2007).
35. Turner, C. H. & Burr, D. B. Basic biomechanical measurements of bone: a tutorial. *Bone* **14**, 595–608
36. van der Eerden, B. C. J. *et al.* The epithelial Ca2+ channel TRPV5 is essential for proper osteoclastic bone resorption. *Proc. Natl. Acad. Sci. U. S. A.* **102**, 17507–12 (2005).
37. Gruber, H. E. Adaptations of Goldner's Masson trichrome stain for the study of undecalcified plastic embedded bone. *Biotech. Histochem.* **67**, 30–4 (1992).
38. Brum, A. M. *et al.* Identification of Chloride Intracellular Channel Protein 3 as a Novel Gene Affecting Human Bone Formation. *JBMR Plus* (2017). doi:10.1002/jbm4.10003
39. Dempster, D. W. *et al.* Standardized nomenclature, symbols, and units for bone histomorphometry: a 2012 update of the report of the ASBMR Histomorphometry Nomenclature Committee. *J. Bone Miner. Res.* **28**, 2–17 (2013).
40. de Vries, T. J., Schoenmaker, T., Beertsen, W., van der Neut, R. & Everts, V. Effect of CD44 deficiency on in vitro and in vivo osteoclast formation. *J. Cell. Biochem.* **94**, 954–66 (2005).
41. Mann, A., Thompson, A., Robbins, N. & Blomkalns, A. L. Localization, identification, and excision of murine adipose depots. *J. Vis. Exp.* (2014). doi:10.3791/52174
42. Bruedigam, C. *et al.* Basic techniques in human mesenchymal stem cell cultures: differentiation into osteogenic and adipogenic lineages, genetic perturbations, and phenotypic analyses. *Curr. Protoc. Stem Cell Biol.* **Chapter 1**, Unit1H.3 (2011).

# Chapter 6

# General Discussion

Andrea M. Brum

## 6.1. Overview

Modern technologies allow us to quickly and easily probe the expression status of every gene in every tissue at any point in time under various conditions through the use of microarrays. In this thesis we utilized the results of gene expression microarrays performed on human mesenchymal stromal cells (hMSCs) differentiated towards osteoblasts to identify genes, processes and compounds affecting osteoblast differentiation with the ultimate goal that the knowledge gained could be used toward the development of a novel bone anabolic treatment for conditions such as osteoporosis.

In Chapters 2 and 3 we employ the Connectivity Map (CMap) to identify compounds that affect osteoblast differentiation. Parbendazole was discovered as the compound with the most positively correlated genetic profile to osteogenically differentiated hMSCs and, in Chapter 2, we delved into its mechanism of action and determined its effects are due to profound cytoskeletal changes that up-regulate osteoblast specific genes, enhance BMP2 activity, and increase focal adhesion numbers and length. In Chapter 3 we found that the CMap can successfully identify other compounds that influence human osteoblast differentiation; three additional positively correlated compounds, withaferin A, amylocaine, and calcium folinate, stimulated osteogenic differentiation and one negatively correlated compound, salbutamol, inhibited osteoblast differentiation. We used *in silico* analysis to better understand how these compounds affect hMSCs *in vitro* and ascertained genes and processes vital to the differentiation process. In Chapter 4 we revealed a role for *CLIC3* in human *in vitro* osteoblast differentiation and mineralization and *in vivo* bone formation, and discovered that NEK9 and PSS1 interact with CLIC3 to enhance differentiation. In Chapter 5 we showed that deletion of *Muc1* in mice leads to mild and temporally shifting changes in long bones and bone metabolism, as well as highlighted changes in the murine skeleton with normal aging. Figure **1** shows some of the main findings and hypothesis presented in this thesis related to the cellular signaling involved in osteoblast differentiation. In this chapter the main findings in this thesis will be discussed and their importance in the field of bone biology. Furthermore, the prospects for the future will be considered.

## 6.2. Using the Connectivity Map to identify new targets in bone biology

The CMap database (build 02) contains profiles of 1309 FDA-approved small molecules. These small molecules are tested in up to five human cell lines, generating over 6000 expression profiles in the CMap catalog based on gene expression profiling

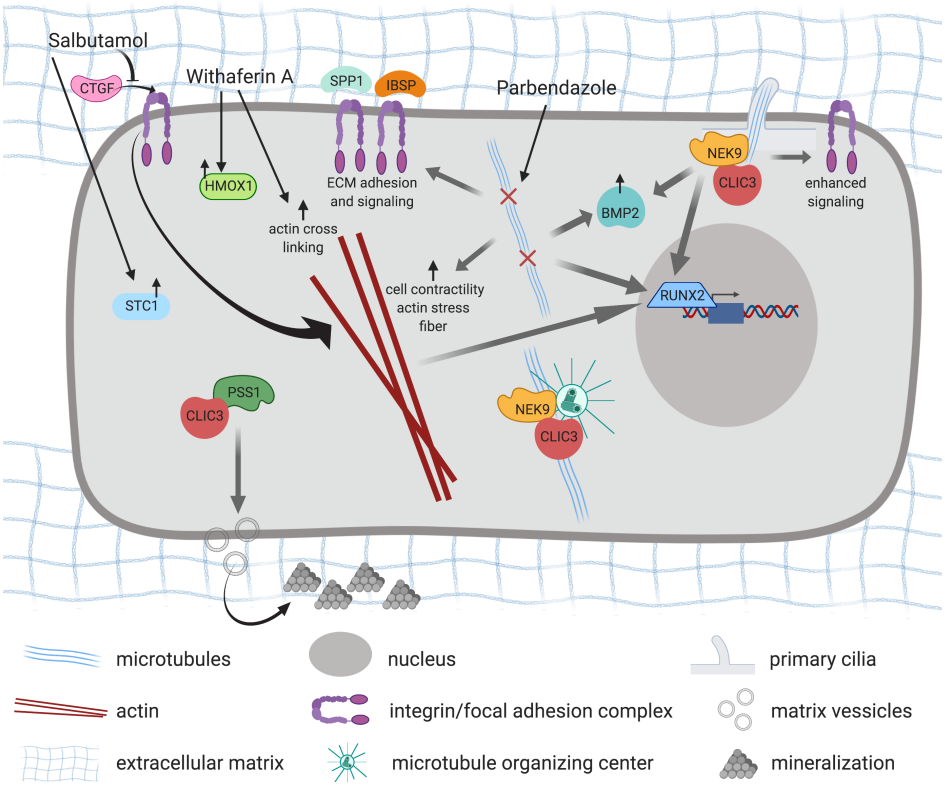


**Figure 1. Proposed cell signaling processes involved in osteoblast differentiation of hMSCs.**

experiments carried out using Affymetrix microarrays. The instance is the basic unit of data in CMap and consists of each individual treatment-control pair. The fold change of treatment to control values was calculated for each probe set, sorted into decreasing order and converted to a rank vector. Thus, the probe set that is most up-regulated will receive Rank 1 and the most down-regulated will receive Rank 22,283 (based on the total number of probes in the microarray). Using the online tool (http://www.broadinstitute.org/cmap) users can query their gene signature of interest (i.e. genes regulated by a disease state or biological phenotype) against the chemical reference catalogues. The gene signature of the user is simply two lists of affymetrix ids, one containing up-regulated genes, up genes, and the other containing down-regulated genes, down genes, without any expression data attached to them.

Successful identification of true biological connections between the CMap reference profiles and the user's gene signature are likely highly dependent on the quality of the chosen gene signature. There is no guideline for creating an optimal gene signature, but the conventional approach is to identify and use the differentially expressed genes associated with the phenotype that are statistically significant. The

results of Zhang[1] suggest that gene signatures with between 10 to 100 genes are optimal. For our analysis, we used 77 up-regulated genes and 66 down-regulated genes, based on identification of the 100 most significantly ($Z<0.001$) up- and down-regulated Illumina probes 6 hours (matching CMap treatment times) after the start of osteogenic differentiation of hMSCs (Illumina IDs were converted to Affymetrix IDs and duplicates were removed).

The CMap uses a simple, but efficient pattern matching algorithm based on the non-parametric rank-ordered Kolmogorov–Smirnov statistics to compare the users lists of up and down regulated genes with the ranked probe sets of the instance gene expression profiles. A 'connectivity score' is generated for each instance, ranging from +1 to -1 to reflect the similarity, or connection, between the expression profile of the user's interest and each of the drugs (instances). Positive connectivity scores (closest to +1) denote a high degree of similarity in gene regulation and negative connectivity scores (closest to -1) signify an inverse relationship.

An important consideration when using the CMap is how to interpret the results. Results can be viewed for each individual test (detailed results) or as permuted results. The results we used for our analysis in Chapters 2 and 3 come from the permuted results. These results use the arithmetic means of the CMap connectivity scores of each compound and are ranked based on the permutation p-value. The permutation p-value is an estimate of the likelihood that the enrichment of a set of instances in the list of all instances for a given result would be observed by chance. This test is based on a basic resampling procedure determined empirically by computing the enrichment of one hundred thousand sets of instances selected at random from the set of all instances in the result. Using the permuted results for selection of drug candidates decreases the likelihood of selecting false positives. Zhang and colleagues found that at the individual treatment instance level, the CMap does not provide effective safeguards against possible false connections; however, when they compared the CMap permuted results using the permutation p-value to their results obtained using a more rigorous null hypothesis $H^{set}_0$ equation applied to original CMap data, both results controlled for false connections equally well[1].

The permuted results can be further divided, with the choice to view the individual compounds (all cell lines combined, yielding a greater replicate number), each compound separated by cell line, or by ATC code (Anatomical Therapeutic Chemical Classification System). When we examined the individual and the permuted results separated by cell line we found that individual compounds ranked quite differently based on the cell line tested in and the majority of our top hits were in the human prostate cancer cell line (PC3). Examples of individual instance CMap scores and rankings of the top positively correlated compound, parbendazole, and most

**Table 1: Examples of Individual Instances in Detailed Results**

| Instance ID | Compound | Cell Line | Rank (1 to 6100) | Score (+1 to -1) |
|---|---|---|---|---|
| 4535 | parbendazole | PC3 | 5 | 0.87 |
| 3799 | parbendazole | PC3 | 7 | 0.841 |
| 4357 | parbendazole | MCF7 | 5247 | -0.468 |
| 3881 | parbendazole | MCF7 | 5357 | -0.487 |
| | | | | |
| 2344 | salbutamol | HL60 | 891 | 0.308 |
| 2306 | salbutamol | MCF7 | 2995 | 0 |
| 7376 | salbutamol | PC3 | 6008 | -0.682 |
| 4700 | salbutamol | MCF7 | 6047 | -0.728 |
| 3677 | salbutamol | PC3 | 6073 | -0.784 |

negatively correlated compound, salbutamol, based on the permuted results can be seen in **Table 1**. While the individual instances of both parbendazole and salbutamol in the PC3 cell line have strong and similar scores to their respective replicates, instances in the other cell lines can differ greatly from these. We have hypothesized that there is a resemblance in the genomic profiles of both osteogenic hMSCs and the bone metastatic PC3 cells, which potentially link both of their abilities to thrive in the bone environment. This finding highlights one of the limitations of the CMap, which requires an assumption that the genetic response of the cell lines utilized will be similar to those studied by individual CMap users. It also does not account for the dynamics associated with a disease or phenotype or *in vivo* multi-organ effects. While using the cell line based permuted results excludes any compound that was not tested multiple times in any cell line (their permuted p-value is quantified as 0 when only 1 replicate exists), we felt this extra level of security was necessary.

The methodology behind the CMap is fairly simple, notably the original Kolmogorov–Smirnov (KS) statistics used as the 'similarity metric' and the lack of true null hypothesis testing, and has been criticized for a high level of noise and failure to apply a comprehensive measure to validate the significance of a gene signature when queried against reference profiles. Several studies have increased the specificity and reliability of the CMap by creating new methods of data normalization and scoring algorithms which can be applied to the original KS statistics, or by incorporating additional models and data sources into the CMap[2,3]. That being said, the utility of the CMap is undeniable. The CMap has been successfully used to identify compounds and combination therapies that show promise in the treatment of osteoarthritic pain[4], adenocarcinoma[5], skeletal muscle atrophy[6,7], emphysema-related lung disease[8], kidney disease[9], gliomas[10], natural killer (NK) cell neoplasms[11], Parkinson's disease related neurodegeneration[12] and medulloblastomas[13]. Our results

add proof to the value of the CMap approach and methodology. All four selected positively correlated compounds instigated osteoblast differentiation of hMSCs. The rest of the top-ranking compounds were predominately made up of glucocorticoid receptor (GR) binding ligands, including dexamethasone (dex), which was expected, as dex is the compound that we used to stimulate osteoblast differentiation and glucocorticoid-mediated activation of the glucocorticoid receptor is the classical stimulus for human osteoblast differentiation *in vitro*. The connectivity map proved to be less successful when selecting compounds that we hoped would inhibit osteoblast differentiation of hMSCs. Only one, salbutamol, out of three negatively correlated compounds proved to successfully inhibit differentiation as determined by biochemical assays for alkaline phosphatase (ALP) activity and mineralization. The fact that metaraminol shares six out of 10 top differentially expressed genes with salbutamol makes this finding even more intriguing. These results could indicate that inhibiting the dex-induced osteoblast differentiation is a complicated process that requires a more sensitive experimental setup that facilitates the effectiveness of the compound, for example pre-treatment with the prospective inhibitors or treatment with a stronger dose.

Our results highlight the valuable role bioinformatics approaches, such as the CMap, have as tools in expanding our knowledge of bone biology and providing potential novel treatments for disorders such as osteoporosis, but validation of these results through experimental approaches is critical.

### 6.3. The cytoskeleton is a major influence in regulating osteoblast differentiation

One of the key highlights that can be gained from this research is the importance of the cytoskeleton in osteoblast differentiation. This became clear in Chapter 2, where we showed that the osteogenic effect of CMap identified compound, parbendazole, is a result of changes to the cytoskeleton owing to parbendazole's ability to depolymerize the microtubules. Further use of the CMap identified Withaferin A as another osteogenic stimulator in Chapter 3, and previous studies have demonstrated that Withaferin A also exerts its influence, at least in part, by causing changes to the actin cytoskeleton. In Chapter 4 we demonstrated a novel role for CLIC3 in osteoblast differentiation and bone formation which, based on our bioinformatic analysis of proteins identified by CLIC3-His pull down and literature, also potentially coupled to microtubule associations and signaling. Remarkably, 15 of the top differentially expressed genes from the successful CMap-identified compounds are known to affect cytoskeletal organization or signaling (DUSP1[14],

SEMA3D[15], UBXN2B[16], TPT1[17], HMOX1[18], HSPA1A[19], TXNIP[20], THBS1[21], CXCL1[22], RCC1[23], ARPC2[24], APP[25], CD55[26], ACTN1[27,28], CTGF[29]), providing additional support for the role of the cytoskeletal in osteoblast differentiation. In addition, three out of seven of the top proteins identified by CLIC3-pull down (NEK9[30], PLCB3[31], NUP160[32]) have been proven to alter cytoskeletal elements.

Microtubules are highly dynamic cytoskeletal elements that undergo continuous assembly and disassembly to maintain normal function[33,34]. They play a role in a variety of cellular processes including mitosis, cell motility, and intra- and inter-cellular trafficking[35], but are also playing a functional role in signal transduction, through interaction with members of sonic hedgehog, Wnt, Indian hedgehog/parathyroid hormone-related protein and MAPK signaling pathways[33,36,37]. In hMSCs, parbendazole's inhibitory effect on the microtubules leads to enhancement of actin stress fibers, increases focal adhesions, and up-regulates bone morphogenetic protein (BMP2) gene expression and activity (Fig. **1**). Our elucidation of parbendazole's cytoskeletal driven osteoblast differentiation is supported by previous works that together demonstrate that inhibition of microtubules leads to increased cell contractility, cytoskeletal tension and f-actin stress fiber formation through RhoA/ROCK signaling, which ultimately leads to enhanced osteoblast differentiation[38–43].

The actin cytoskeleton supports a great variety of cellular processes, such as endocytosis, oriented growth, adhesion and migration, and is an important factor in osteogenic, adipogenic and chondrogenic differentiation of MSCs[40]. As we saw with parbendazole, disruption of microtubules leads quickly to changes in the actin microfilaments[40]. In our study, microtubule depolymerization lead to a large, widespread appearance and increased actin stress fibers. Experiments using cultured hMSCs and murine pre-ostoblast calls have also demonstrated that osteoblast differentiation alters the actin cytoskeleton, transforming from numerous, thin actin filaments running parallel along the long axis of the cell, to fewer, thicker fibers criss-crossing strands; furthermore, disruption of the actin cytoskeleton inhibits osteogenic differentiation[39,44–46]. In addition, Mishra *et. al.* recently demonstrated through real-time labeling and tracking of F-actin turnover dynamics that there is quickly (within minutes) divergence in the dynamics of the actin cytoskeleton between hMSCs stimulated with osteogenic, adipogenic or chondrogenic media, and these changes precedes the lineage specific morphological changes (seen after 24 hours)[47]. They propose that these early changes in the actin network could serve as a marker of lineage divergence. Actin stress fibers are one of the stiffest structures within hMSCs[48] and osteogenic differentiation appears to require a stiff, spread actin cytoskeleton[40], which seems logical because, *in vivo*, osteoblasts are generally found as flat cells, sitting

on the surface of the bone. This idea is further strengthened by the finding that stiffer biomaterials promote osteogenic differentiation of MSCs, while softer materials stimulate chondrogenic and adipogenic differentiation[49,50].

Evidence of withaferin A's effect on the cytoskeleton comes from Falsey *et al.* who demonstrated that withaferin A covalently binds annexin II and stimulates basal F-actin cross-linking activity[51] (Fig. **1**). In addition, withaferin A disrupts the vimentin cytoskeleton[52]. Vimentin, is an intermediate filament protein of the cytoskeleton. Interestingly, vimentin is proven to suppress ATF4-dependent osteocalcin transcription and osteoblast differentiation[53], but in the case of withaferin A treatment ATF4 expression is enhanced, in turn stimulating osteoblast differentiation.

It has been reported that CLIC3 and other CLIC proteins associate with the cytoskeleton or scaffolding proteins for endosome trafficking[54–56]. In addition, our bioinformatics analysis of CLIC3-His pulled down proteins identified an overrepresentation of proteins involved in processes related to cytoskeletal and integrin signaling. CLIC3 protein pull-down identified NEK9 as a binding partner and *in vitro* shRNA knockdown experiments proved that NEK9 is required for hMSC osteoblast differentiation and mineralization. NEK9 is known to be involved in regulating spindle organization, chromosome alignment, cytokinesis, and normal cell cycle progression[57,58]. Mammalian Nek9 binds gamma-tubulin and localizes to the centrosomes and spindle poles during early cell division and functions in the microtubule organizing center during mitosis[30,59]. Recessive mutations in *NEK9* cause a lethal skeletal dysplasia and analysis of *NEK9* mutations in patient fibroblasts that also showed reduced cilia number and length, suggesting that NEK9 is involved in ciliary function[60]. Another role for primary cilia in bone was demonstrated by Oliazadeh *et al.* who investigated the role of the cilia in patients with idiopathic scoliosis, which causes abnormal curvature of the spine and of which nearly half (38% to 65% in different cohorts) suffer from osteopenia and/or osteoporosis. They found that the bone cells of idiopathic scoliosis patients had significant elongation of the primary cilia and after mechanical stimulation the bone-derived cells had reduced responses of *BMP2*, *RUNX2*, and *PTGS2*[61]. The primary cilium is a microtubule-based organelle that has emerged as a novel extracellular sensor in bone. It is able to sense mechanical stimulus and transduce them into biochemical responses, which regulate bone adaptation, increasing osteogenic gene expression and bone formation[62]. Taken together, these findings suggest that NEK9 and CLIC3 may regulate osteoblast differentiation via cytoskeleton-associated signaling processes (Fig. **1**).

The research presented in this thesis, along with others, confirms that dynamic cytoskeletal changes appear to be one of intracellular signals that control

osteoblast differentiation. The changes that we see in the balance between the tension forces of the actin microfilaments and the compression forces of the microtubules that further elicit changes in cell shape, function, gene expression, and fate, are in line with the cellular tensegrity model[63,64] and with previous findings that changes in cell shape and cytoskeleton can strongly influence hMSC fate[65]. A fundamental aspect within the cellular tensegrity model is that every structural element within the system is poised to sense and immediately respond to physical stimuli from both inside and outside the cell[64]. Meaning that, for example, when mechanical forces are applied to the bone, bone cells respond by coordinated changes in the extracellular matrix, cell, cytoskeleton and without producing any structural breakage or disconnection between these parts. The dynamic nature of the cytoskeleton makes it difficult to study changes in the cytoskeleton and determine the roles of the many accessory molecules that modulate organization of it, but this work is vital to fully understand the differentiation process and develop new bone anabolic treatments. The evidence presented in this thesis significantly strengthens the concept that cytoskeletal changes strongly influence hMSC lineage allocation and osteoblast differentiation.

### 6.4. Focal Adhesion Complexes and Integrin Signaling influence osteoblast differentiation

Focal adhesions complexes are clusters of transmembrane integrin molecules associated with a complex network of plaque proteins that connect to actin filaments. Focal adhesions are used by cells to respond to the external environment through a variety of signaling cascades. The complexes can regulate cell adhesion, migration, proliferation, and differentiation[66].

We discovered that parbendazole treatment in hMSCs leads to an increase in focal adhesion number and length (Fig. **1**). Other groups have also shown that disruption of microtubules by microtubule-depolymerizing agents, similar to parbendazole, leads to a substantial increase in the size and the number of mature focal adhesions[67,68], and reestablishment of microtubule polymerization causes a transient decrease in size or even the disappearance of focal adhesions[69]. Osteogenic differentiation is promoted in MSCs with a stiff, spread actin cytoskeleton and greater numbers of focal adhesions[40]. Focal adhesions are also important in differentiation and MSC lineage decision making. Osteogenesis requires larger numbers of focal adhesions, while differentiation towards adipocytes or chondrocytes are encouraged by preventing focal adhesion attachment[40].

CLIC3 has been previously shown to associate with integrins in cultured A2780 ovarian carcinoma cells and in pancreatic and ovarian tumors that contain

elevated levels of CLIC3, where it functions to mediate the transport and recycling of α5β1 integrins from late endosomes/lysosomes to the plasma membrane[54]. Our bioinformatics pathway analysis of CLIC3-His pulled down proteins in Chapter 4 identified an overrepresentation of proteins involved in paxillin and integrin signaling and gene ontology (GO) analysis showed "protein binding involved in cell adhesion" and "cell adhesion molecule binding" to be significant GO terms associated with molecular function. As discussed above, the CLIC3-associated protein NEK9 localizes to the primary cilium. Integrins are also localized to the primary cilium[70] and it has been demonstrated previously that mechanical stimuli modulates integrin-mediated signals, which are transferred through focal adhesion complexes and actin microfilaments[71] (Fig. **1**).

In Chapter 3, we demonstrated that the CMap-identified compound salbutamol inhibited osteoblast differentiation and that the gene *CTGF/CCN2* was consistently down-regulated by salbutamol treatment in PC3 cells. The work of Hendesi and colleagues revealed that osteoblast differentiation and matrix mineralization is enhanced in osteoblasts cultured on CTGF containing matrix. It was shown that adhesion to CTGF was mediated through integrin binding, which promoted cytoskeletal reorganization, cell spreading and Rac activation in the osteoblasts, ultimately leading to increased Runx2 binding of the osteocalcin gene promoter, and increased expression of osteogenic genes that are regulated by Runx2[29]. Based on these results we can hypothesize down-regulation of *CTGF* by salbutamol contributes to its inhibitory effects on osteoblast differentiation through integrin binding and signaling (Fig. **1**).

Taken together these results support the importance of focal adhesion complexes and integrin signaling in osteoblast differentiation. Increases in focal adhesion number and length can influence osteoblast differentiation through enhanced extracellular matrix binding and/or integrin mediated signaling. Cytoskeletal rearrangements may also affect osteoblast differentiation though enhanced integrin signaling. Focal adhesion complexes and integrins are known to directly interact with extracellular matrix proteins, including SPP1 and IBSP who play a critical role in osteoblast survival and differentiation[40,72–74]. This increase in the number of focal adhesion complexes and interaction with matrix proteins allows for enhanced adhesion to the extracellular matrix[74,75], which may also contribute to osteogenic differentiation (Fig. **1**). Due to the direct signaling and binding of integrins with the extracellular matrix and actin cytoskeleton, integrins may play a direct role in regulating osteoblast differentiation and mineralization. Targeting of integrin signaling could make an attractive candidate for development of future bone anabolic treatments.

### 6.5. Consideration of timing for *in vitro* and *in vivo* bone models

A remarkable theme among these works is the significance of temporal properties in bone formation and osteoblast differentiation and importance of considering the cell type, stage of differentiation, and age of an organism when planning experiments and examining data.

In Chapter 5 we demonstrated that deletion of *Muc1* results in a mild, but also transient phenotype in the femoral bones of female mice. We found that the trabecular bone volume was reduced in 8-week-old mice compared to wild type (WT) controls, but this normalizes with increasing age. As the mice age, *Muc1* deletion results in stiffer femoral bones with fewer osteoblasts lining the trabecular surface, but increased endosteal mineralized surface and bone formation rate (16 weeks of age). While the cortical bone formation rate remains higher in knockout mice compared to wild type females at 52 weeks of age, all other parameters normalize. These results demonstrate the importance of examining multiple time points when investigating *in vivo* bone phenotypes. Analyzing only a single time point or a single parameter of bone morphology/strength in our study, as is common routine in many mouse genetic studies, would have led to either over-interpretation or missing aspects of *Muc1* deficiency on bone metabolism.

Data from the study of *Muc1* deficiency in mice also emphasizes the dramatic effect aging has on the femoral bone over time. Trabecular bone fraction dramatically declined (over 90% in WT mice), while cortical bone area (roughly 40% in WT mice), thickness, and periosteal perimeter increased during aging between 8 and 52 weeks of age. All mechanical strength properties increased with time, which is expected given that the larger, thicker cortex of the older bones directly contributes to a stronger femur, requiring more force to fracture, assuming the material properties do not change. With regards to histomorphometry measurements, trabecular bone formation rate and osteoblast numbers peaked at 16 weeks, while cortical bone formation rate declined over time. Our results suggest that different components of the bone may be more sensitive to perturbagens and/or may react differently depending on the age of the organism. For example, the metaphysis of the long bones has a relatively high rate of bone turnover compared to diaphyseal cortical bone and developmental phases involving intense longitudinal growth may show greater temporal dynamics. While our *Muc1* studies are limited due to the use of the mouse model and potential differences in bone biology between mice and humans, evidence from human studies also supports the idea of age-related changes in bone. In humans after the attainment of peak bone mass in early adulthood, bone remodeling is balanced and bone mass is

stable for a decade or two until age-related bone loss begins. In healthy adults, increased resorptive activity is linked to complementary increased bone formation; however, in postmenopausal women and elderly men the balance between resorption and subsequent formation at each bone remodeling unit is negative with increased resorptive activity leading to irreversible bone loss that is irreversible[76]. Understanding this dynamic process of bone metabolism over time is greatly important to planning *in vivo* experiments related to bone biology and interpreting the results. Our results in studying the *in vivo* function of Muc1 in mice highlights the issue of bone loss during aging and could be an interesting model to delve into this topic more fully.

In Chapter 2 we found that different populations of human cell types react differently to parbendazole treatment *in vitro*. When hMSCs were cultured with parbendazole we found an increase in both proliferation and in apoptosis. This indicates that there are at least two populations of cells within our bone marrow derived MSCs with different sensitivity to parbendazole. One population, likely the true stem cells, is resistant to the apoptotic effects of parbendazole and are induced to proliferate and eventually differentiate and mineralize, and another population, the pre-committed cells, that undergoes apoptosis. This hypothesis is supported by the observation that human pre-osteoblast cells, SV-HFOs, treated with parbendazole did not display an increase in ALP activity or mineralization. Based on these data we proposed that parbendazole acts at the stage of lineage allocation in hMSCs. These findings are important in strengthening the role for cytoskeletal changes influences hMSC lineage decision making and furthering the need for understanding how to target these processes for therapeutic development.

In Chapter 3 we used the CMap to identify calcium folinate, otherwise known as folinic acid or by the brand name Leucovorin, as a potential stimulator of osteoblast differentiation and confirmed its ability to induce osteogenic differentiation of hMSCs through *in vitro* experiments. Calcium folinate, a derivative of tetrahydrofolic acid, is already used clinically to help ameliorate some of the negative side effects of the chemotherapeutic agent methotrexate, which functions as a dihydrofolate reductase inhibitor in soft tissues through its capacity to readily be converted to folic acid derivatives without the action of dihydrofolate reductase. Interestingly, research in rodent models has demonstrated that calcium folinate reduces bone loss and damage to the growth plate and bone marrow compartments normally seen with methotrexate treatment[77–80]. Furthermore, it has been observed that there is an increase in bone marrow adiposity following methotrexate treatment alone, and when calcium folinate is administered concurrently these effects are amended and an increase in bone marrow MSC proliferation is also observed[78,81]. These effects are proposed to be due to up-regulation of Wnt/ß-catenin signaling in

the bone through normalizing the level of the Wnt antagonist sFRP-1 that was elevated by methotrexate alone[81]. However, whether these effects are a direct effect of calcium folinate on Wnt/ß-catenin signaling or an indirect outcome of changes to cellular folate metabolism requires further investigation, as in-depth studies on the *in vivo* bone effect of calcium folinate alone are still lacking. Combining our observations that calcium folinate can independently stimulate differentiation of hMSCs *in vitro* with the available *in vivo* results demonstrating that calcium folinate can prevent methotrexate induced bone marrow adiposity while preserving bone, strongly indicating that calcium folinate alone acts at the stage of lineage allocation in osteoblast differentiation.

Another observation related to the study of differences in cell type response and its relationship to stages of differentiation include the likely role of HMOX1 in withaferin A-induced osteoblast differentiation. As we described in Chapter 3, withaferin A induces osteoblast differentiation of hMSCs and the gene we found to be most up-regulated by withaferin A treatment, *HMOX1*, was also required for osteoblast differentiation. Previous work has shown that overexpression of *HMOX1* increases human osteoblast stem cell differentiation, and shifts the balance of hMSCs differentiation in favor of the osteoblast lineage[82,83]. It has been observed that certain cell types are more sensitive to the same doses of withaferin A treatment, with some cell lines demonstrating higher levels of apoptosis and cell death[52]. We used bone marrow hMSCs as our cell of choice to test the CMap compound and we speculate, based on these previous results, that the true MSCs are responsible for the effect we see and that if we had used a committed cell line we might not see the same effect.

Our choice of cell comes from our interest in understanding lineage commitment of hMSC as an important part of understanding osteoblast differentiation and our original selection of genes for further studies considered differential regulation of them in the osteoblast versus adipocyte lineages during differentiation of hMSCs. Since it has been observed that the there is an increase in the adiposity of the bone marrow in osteoporosis patients[84–86] and that bone marrow-derived mesenchymal progenitors from aged humans and mice preferentially differentiate toward the adipogenic, rather than osteogenic, lineage[87–90], I believe that one avenue for the development of novel therapeutics for osteoporosis should target the lineage commitment of hMSCs.

### 6.6. Therapeutic potential

All four compounds we identified using the CMap as having positively correlating gene expression profiles to that of osteogenically differentiated hMSCs,

parbendazole, withaferin A, amylocaine, and calcium folinate, successfully stimulated *in vitro* osteoblast differentiation. This alone gives us reason to consider each of them as possible candidates for bone anabolic treatments. Parbendazole and withaferin A produced the strongest response in our cultures, both stimulating alkaline phosphatase activity and mineralization, and there is mounting *in vitro* and *in vivo* data demonstrating the osteo-anabolic effect of microtubule inhibitors[91,92] and on withaferin A[93,94] treatment. However, *in vitro* testing of compounds in a cell culture environment is very different from testing in an *in vivo* environment and we must consider the fact that these compounds may have varying and/or negative effects on other cell types and organ systems. Both parbendazole and withaferin A have been shown to have cytotoxic effects in certain cell types making them poor candidates as bone anabolic therapies, but development of a drug that harnesses the mechanisms that drive the osteogenic effect of these compounds at the level of MSC lineage decision making, such as integrin signaling, enhancing cytoskeletal tension and up-regulation of expression of *HMOX1* and *HSPA1A*, could provide us with the most beneficial new treatments for osteoporosis or other disorders requiring bone (re)generation.

Calcium folinate and amylocaine both stimulated mineralization in hMSCs, while, interestingly, having no consistent effect on ALP activity. As mineralization is the defining feature of a mature osteoblast we have concluded that these two compounds stimulate osteogenic differentiation of hMSCs *in vitro*. There is little research and date annotated to amylocaine, also known as stovaine, and it was developed as a synthetic local anesthetic; however, no data exists linking it to bone or osteoblast differentiation. Its anesthetic properties are attributed to the ability to inhibit voltage-sensitive $Na^+$ channels[95–97], and to a lesser extent voltage sensitive $Ca^{2+}$ channels[98], and it is plausible that the osteogenic effect observed with amylocaine could be related to its potential effects on ion channels, but this requires further investigation. Calcium folinate, as we discussed previously, is currently used in the clinic to ameliorate the negative effects of methotrexate chemotherapeutic on a variety of tissues including bone[77–79]. Unfortunately, data is lacking with regard to calcium folinate's effect on osteoblast differentiation and bone formation independent of methotrexate treatment. Only one study has examined the effects of calcium folinate on bone, independent of methotrexate; however, only tibial and femur lengths were scrutinized and no difference was found between calcium folinate treatment and control treatment[80]. In addition there is evidence for a potential role in a preference for osteoblast lineage allocation through up-regulating Wnt/β-catenin signaling in bone[81]. Further investigation into the effects of calcium folinate and amylocaine on *in vivo* bone formation and regulation of osteoblast differentiation as

potential bone anabolic treatments, particular in models of osteoporosis such as ovariectomy mouse models, are highly warranted. Both of these compounds have been used in humans for other proposes, which further strengthens the cause of studying them more in depth for use in osteoporosis treatments

Our discovery of *CLIC3* and *MUC1* as novel genes involved in bone formation makes them potential candidates as targets for development of bone anabolic therapeutics as well. While more research is required to understand the role *MUC1* may play in human bone formation in order to seriously consider it for drug development, *CLIC3* is a particularly interesting candidate. The specificity of *CLIC3* to promote the osteogenic lineage, while its expression decreases during adipocyte differentiation, in combination with the importance of *CLIC3* during human osteoblast differentiation could make it a potential target for future bone anabolic treatments. Our discovery that CLIC3 interacts with two proteins, PTDSS1 and NEK9, that are both known to cause severe human skeletal defects when they are mutated[60,99,100] further strengthens its importance in bone. Development of a drug that could target CLIC3 and in turn regulate PTDSS1 and NEK9 to enhance osteoblast differentiation and bone production would be ideal.

### 6.7. Final conclusion and future outlook

This thesis has presented a number of novel findings in the bone biology field and highlights the complexity of the biology and study of osteoblast differentiation. Through the use of gene expression analysis of hMSCs undergoing osteogenic differentiation we have identified important genes and processes controlling osteoblast differentiation. These studies, and studies like it, are vital gaining greater knowledge about MSC lineage decision making and osteoblasts differentiation which is required to develop much needed bone anabolic therapeutics. Although the overall aim of this project was to identify novel factors enhancing osteoblast differentiation and bone production that could ultimately lead to new treatments for osteoporosis patients, this research is also useful in the field of bone (re)generation in general. Bone has the ability to regenerate and repair itself, but large bone defects or disease states can impair this process. By enhancing these innate properties of bone, we can improve treatments and recovery times for patients suffering from serious bone defects and bone loss.

The work presented here has demonstrated the power of the CMap as an effective tool to discover novel bone anabolic compounds. All of the top positively correlating compounds we tested in our human osteoblast differentiation model using hMSCs induced mineralization independent of any additional stimulus. Amylocaine

and calcium folinate hold promise as novel bone anabolic treatments and additional studies into their mechanism of action and *in vivo* effects are required.

The evidence presented here supports the concept that cytoskeletal changes strongly influence hMSC lineage allocation and osteoblast differentiation. I envisage that cytoskeletal manipulation, or the down-stream processes that results from it, hold promise as novel anti-osteoporotic treatments, but this will need to be studied further.

We identified two novel lineage specific genes that influence osteoblast differentiation, *CLIC3* and *MUC1*. Very little evidence exists pertaining to CLIC3s function or role in other tissues and more research is required to understand if our hypothesis that CLIC3 regulates osteoblast differentiation through interactions with NEK9 in the microtubule organizing center to induce cytoskeletal changes or in the function of the primary cilia and/or working together with PTDSS1 to increase biosynthesis of phosphatidylserine enhancing osteoblast differentiation and matrix vesicle-mediated hydroxyapatite formation and mineralization of the bone (Fig. **1**).

Although deletion of *Muc1* resulted in only subtle changes in the bone, we were intrigued that the phenotype changed over time. I believe that it is worthwhile to investigate the role of *MUC1* in bone further, particularly in regards to what role it might have in younger mice (less than 8 weeks of age), situations where estrogen is depleted, given the known links it has to estrogen receptor beta signaling, and in bone fracture models. Based on our discovery of *MUC1* as explicitly expressed in the osteogenic lineage in early human osteoblast differentiation[104], it will also be pivotal to further investigate the function of *MUC1* in human MSCs and osteoblasts and its potential role in human bone homeostasis. Another remarkable finding of MUC1s function comes from Kitamoto and collegues[101], who reported that MUC1 enhances hypoxia driven angiogenesis through studies showing that increased *MUC1* expression in pancreatic cancer cells derived from metastatic tumors cultured in hypoxic conditions promoted angiogenesis of endothelial cells. Within bone MSCs reside in stem cell niches of low-oxygen atmospheres and local levels of oxygen are reduced at the site of fractures[102,103]. Based on this I wonder whether *MUC1* may play an additional role in the bone to stimulate angiogenesis via secretion from MSCs and/or osteoblasts during times in hypoxic conditions, which could be investigated in bone fracture models.

Bone biology is a complicated and fascinating field of study. All models have limitations and advantages. When studying osteoblast differentiation in the context of looking for bone anabolic treatments for conditions such as osteoporosis, considering the cell type and stage of differentiation affected by a candidate is important as well as the reality of not studying these cells in their natural environment. In my opinion, the knowledge that a switch in lineage decision making of MSCs could be a major

contributor to the development of osteoporosis is of the utmost importance. With this information in mind we should consider that different pathways, drugs and genes affect varying stages of the differentiation process and candidates should target the very early stages of differentiation, i.e. at the level of the MSC. Our discovery of novel genes, compounds and processes that play a role in osteoblast differentiation, in particular in the lineage decision making of MSCs, constitute potential therapeutic targets for the development of novel treatments for bone diseases, such as osteoporosis, and should be investigated further.

## References


1. Zhang, S.-D. & Gant, T. W. A simple and robust method for connecting small-molecule drugs using gene-expression signatures. *BMC Bioinformatics* **9**, 258 (2008).
2. Musa, A. *et al.* A review of connectivity map and computational approaches in pharmacogenomics. *Brief. Bioinform.* **19**, 506–523 (2018).
3. Qu, X. A. & Rajpal, D. K. Applications of Connectivity Map in drug discovery and development. *Drug Discov. Today* **17**, 1289–98 (2012).
4. Chang, M., Smith, S., Thorpe, A., Barratt, M. J. & Karim, F. Evaluation of phenoxybenzamine in the CFA model of pain following gene expression studies and connectivity mapping. *Mol. Pain* **6**, 56 (2010).
5. Wang, G. *et al.* Expression-based in silico screening of candidate therapeutic compounds for lung adenocarcinoma. *PLoS One* **6**, e14573 (2011).
6. Kunkel, S. D. *et al.* mRNA expression signatures of human skeletal muscle atrophy identify a natural compound that increases muscle mass. *Cell Metab.* **13**, 627–38 (2011).
7. Dyle, M. C. *et al.* Systems-based discovery of tomatidine as a natural small molecule inhibitor of skeletal muscle atrophy. *J. Biol. Chem.* **289**, 14913–24 (2014).
8. Campbell, J. D. *et al.* A gene expression signature of emphysema-related lung destruction and its reversal by the tripeptide GHK. *Genome Med.* **4**, 67 (2012).
9. Zhong, Y. *et al.* Renoprotective effect of combined inhibition of angiotensin-converting enzyme and histone deacetylase. *J. Am. Soc. Nephrol.* **24**, 801–11 (2013).
10. Koh, L. W.-H. *et al.* A distinct reactive oxygen species profile confers chemoresistance in glioma-propagating cells and associates with patient survival outcome. *Antioxid. Redox Signal.* **19**, 2261–79 (2013).
11. Karube, K. *et al.* Comprehensive gene expression profiles of NK cell neoplasms identify vorinostat as an effective drug candidate. *Cancer Lett.* **333**, 47–55 (2013).
12. Gao, L. *et al.* Discovery of the neuroprotective effects of alvespimycin by computational prioritization of potential anti-parkinson agents. *FEBS J.* **281**, 1110–1122 (2014).
13. Faria, C. C. *et al.* Identification of alsterpaullone as a novel small molecule inhibitor to target group 3 medulloblastoma. *Oncotarget* **6**, 21718–29 (2015).
14. Farwell, S. L. N. *et al.* Heparin Decreases in Tumor Necrosis Factor α (TNFα)-induced Endothelial Stress Responses Require Transmembrane Protein 184A and Induction of Dual Specificity Phosphatase 1. *J. Biol. Chem.* **291**, 5342–54 (2016).
15. Aghajanian, H. *et al.* Semaphorin 3d and Semaphorin 3e Direct Endothelial Motility through Distinct Molecular Signaling Pathways. *J. Biol. Chem.* **289**, 17971–17979 (2014).
16. Lee, B. H., Schwager, F., Meraldi, P. & Gotta, M. p37/UBXN2B regulates spindle orientation by limiting cortical NuMA recruitment via PP1/Repo-Man. *J. Cell Biol.* **217**, 483–493 (2018).
17. Huang, H.-Y. *et al.* Involvement of cytoskeleton-associated proteins in the commitment of C3H10T1/2 pluripotent stem cells to adipocyte lineage induced by BMP2/4. *Mol. Cell. Proteomics* **10**, M110.002691 (2011).
18. Campbell, J. H. & Heikkila, J. J. Effect of hemin, baicalein and heme oxygenase-1 (HO-1) enzyme activity inhibitors on Cd-induced accumulation of HO-1, HSPs and aggresome-like structures in Xenopus kidney epithelial cells. *Comp. Biochem. Physiol. Part C Toxicol. Pharmacol.* **210**, 1–17 (2018).
19. Fang, C.-T., Kuo, H.-H., Pan, T. S., Yu, F.-C. & Yih, L.-H. HSP70 regulates the function of mitotic centrosomes. *Cell. Mol. Life Sci.* **73**, 3949–3960 (2016).
20. Lee, S.-Y. *et al.* Thioredoxin-Interacting Protein Regulates Glucose Metabolism and Affects Cytoplasmic Streaming in Mouse Oocytes. *PLoS One* **8**, e70708 (2013).
21. Huang, W.-T. *et al.* Pigment epithelium-derived factor inhibits lung cancer migration and invasion by upregulating exosomal thrombospondin 1. *Cancer Lett.* **442**, 287–298 (2019).
22. Deftu, A. F., Filippi, A., Gheorghe, R. O. & Ristoiu, V. CXCL1 activates TRPV1 via Gi/o protein and actin filaments. *Life Sci.* **193**, 282–291 (2018).
23. Hoffmann, C. *et al.* Spatiotemporal control of microtubule nucleation and assembly using magnetic nanoparticles. *Nat. Nanotechnol.* **8**, 199–205 (2013).
24. Rotty, J. D. *et al.* Arp2/3 Complex Is Required for Macrophage Integrin Functions but Is Dispensable for FcR Phagocytosis and In Vivo Motility. *Dev. Cell* **42**, 498-513.e6 (2017).
25. Rush, T. *et al.* Synaptotoxicity in Alzheimer's Disease Involved a Dysregulation of Actin Cytoskeleton Dynamics through Cofilin 1 Phosphorylation. *J. Neurosci.* **38**, 10349–10361 (2018).
26. Peiffer, I., Servin, A. L. & Bernet-Camard, M. F. Piracy of decay-accelerating factor (CD55) signal transduction by the diffusely adhering strain Escherichia coli C1845 promotes cytoskeletal F-actin rearrangements in cultured human intestinal INT407 cells. *Infect. Immun.* **66**, 4036–42 (1998).
27. Hamill, K. J. *et al.* Alpha actinin-1 regulates cell-matrix adhesion organization in keratinocytes: consequences for skin cell motility. *J. Invest. Dermatol.* **135**, 1043–1052 (2015).
28. Kunishima, S. *et al.* ACTN1 mutations cause congenital macrothrombocytopenia. *Am. J. Hum. Genet.* **92**, 431–8 (2013).
29. Hendesi, H., Barbe, M. F., Safadi, F. F., Monroy, M. A. & Popoff, S. N. Integrin Mediated Adhesion of

Osteoblasts to Connective Tissue Growth Factor (CTGF/CCN2) Induces Cytoskeleton Reorganization and Cell Differentiation. *PLoS One* **10**, e0115325 (2015).
30. Yang, S.-W. *et al.* Nek9 regulates spindle organization and cell cycle progression during mouse oocyte meiosis and its location in early embryo mitosis. *Cell Cycle* **11**, 4366–77 (2012).
31. Janjanam, J., Chandaka, G. K., Kotla, S. & Rao, G. N. PLCβ3 mediates cortactin interaction with WAVE2 in MCP1-induced actin polymerization and cell migration. *Mol. Biol. Cell* **26**, 4589–606 (2015).
32. Mishra, R. K., Chakraborty, P., Arnaoutov, A., Fontoura, B. M. A. & Dasso, M. The Nup107-160 complex and gamma-TuRC regulate microtubule polymerization at kinetochores. *Nat. Cell Biol.* **12**, 164–9 (2010).
33. Jordan, M. A. & Wilson, L. Microtubules as a target for anticancer drugs. *Nat. Rev. Cancer* **4**, 253–265 (2004).
34. Nogales, E. & Wang, H.-W. Structural mechanisms underlying nucleotide-dependent self-assembly of tubulin and its relatives. *Curr. Opin. Struct. Biol.* **16**, 221–9 (2006).
35. Nogales, E. & Wang, H.-W. Structural intermediates in microtubule assembly and disassembly: how and why? *Curr. Opin. Cell Biol.* **18**, 179–84 (2006).
36. Lam, M. H. C. *et al.* Nuclear Transport of Parathyroid Hormone (PTH)-Related Protein Is Dependent on Microtubules. *Mol. Endocrinol.* **16**, 390–401 (2002).
37. Gundersen, G. G. & Cook, T. A. Microtubules and signal transduction. *Curr. Opin. Cell Biol.* **11**, 81–94 (1999).
38. Chang, Y.-C., Nalbant, P., Birkenfeld, J., Chang, Z.-F. & Bokoch, G. M. GEF-H1 couples nocodazole-induced microtubule disassembly to cell contractility via RhoA. *Mol. Biol. Cell* **19**, 2147–53 (2008).
39. Pablo Rodriguez, J., Gonzalez, M., Rios, S. & Cambiazo, V. Cytoskeletal organization of human mesenchymal stem cells (MSC) changes during their osteogenic differentiation. *J. Cell. Biochem.* **93**, 721–731 (2004).
40. Mathieu, P. S. & Loboa, E. G. Cytoskeletal and focal adhesion influences on mesenchymal stem cell shape, mechanical properties, and differentiation down osteogenic, adipogenic, and chondrogenic pathways. *Tissue Eng. Part B. Rev.* **18**, 436–444 (2012).
41. Drabek, K., van de Peppel, J., Eijken, M. & van Leeuwen, J. P. T. M. GPM6B regulates osteoblast function and induction of mineralization by controlling cytoskeleton and matrix vesicle release. *J. Bone Miner. Res.* **26**, 2045–51 (2011).
42. Kilian, K. A., Bugarija, B., Lahn, B. T. & Mrksich, M. Geometric cues for directing the differentiation of mesenchymal stem cells. *Proc. Natl. Acad. Sci. U. S. A.* **107**, 4872–7 (2010).
43. Higuchi, C., Nakamura, N., Yoshikawa, H. & Itoh, K. Transient dynamic actin cytoskeletal change stimulates the osteoblastic differentiation. *J. Bone Miner. Metab.* **27**, 158–167 (2009).
44. Yourek, G., Hussain, M. A. & Mao, J. J. Cytoskeletal changes of mesenchymal stem cells during differentiation. *ASAIO J.* **53**, 219–228 (2007).
45. Sonowal, H., Kumar, A., Bhattacharyya, J., Gogoi, P. K. & Jaganathan, B. G. Inhibition of actin polymerization decreases osteogeneic differentiation of mesenchymal stem cells through p38 MAPK pathway. *J. Biomed. Sci.* **20**, 71 (2013).
46. Zouani, O. F., Rami, L., Lei, Y. & Durrieu, M.-C. Insights into the osteoblast precursor differentiation towards mature osteoblasts induced by continuous BMP-2 signaling. *Biol. Open* **2**, 872–81 (2013).
47. Mishra, P., Martin, D. C., Androulakis, I. P. & Moghe, P. V. Fluorescence Imaging of Actin Turnover Parses Early Stem Cell Lineage Divergence and Senescence. *Sci. Rep.* **9**, 10377 (2019).
48. Lu, L., Oswald, S. J., Ngu, H. & Yin, F. C.-P. Mechanical Properties of Actin Stress Fibers in Living Cells. *Biophys. J.* **95**, 6060–6071 (2008).
49. Park, J. S. *et al.* The effect of matrix stiffness on the differentiation of mesenchymal stem cells in response to TGF-β. *Biomaterials* **32**, 3921–3930 (2011).
50. Wang, Y.-K. & Chen, C. S. Cell adhesion and mechanical stimulation in the regulation of mesenchymal stem cell differentiation. *J. Cell. Mol. Med.* **17**, 823–32 (2013).
51. Falsey, R. R. *et al.* Actin microfilament aggregation induced by withaferin A is mediated by annexin II. *Nat. Chem. Biol.* **2**, 33–8 (2006).
52. Nishikawa, Y. *et al.* Withaferin A Induces Cell Death Selectively in Androgen-Independent Prostate Cancer Cells but Not in Normal Fibroblast Cells. *PLoS One* **10**, e0134137 (2015).
53. Lian, N. *et al.* Transforming growth factor β suppresses osteoblast differentiation via the vimentin activating transcription factor 4 (ATF4) axis. *J. Biol. Chem.* **287**, 35975–84 (2012).
54. Dozynkiewicz, M. a *et al.* Rab25 and CLIC3 collaborate to promote integrin recycling from late endosomes/lysosomes and drive cancer progression. *Dev. Cell* **22**, 131–45 (2012).
55. Knowles, L. M. *et al.* CLT1 targets bladder cancer through integrin α5β1 and CLIC3. *Mol. Cancer Res.* **11**, 194–203 (2013).
56. Macpherson, I. R. *et al.* CLIC3 controls recycling of late endosomal MT1-MMP and dictates invasion and metastasis in breast cancer. *J. Cell Sci.* **127**, 3893–901 (2014).
57. Fry, A. M., O'Regan, L., Sabir, S. R. & Bayliss, R. Cell cycle regulation by the NEK family of protein kinases. *J. Cell Sci.* **125**, 4423–33 (2012).
58. Wang, Y.-K. *et al.* Bone Morphogenetic Protein-2-Induced Signaling and Osteogenesis Is Regulated by Cell

Shape, RhoA/ROCK, and Cytoskeletal Tension. *Stem Cells Dev.* **21**, 1176–1186 (2012).
59. Roig, J., Groen, A., Caldwell, J. & Avruch, J. Active Nercc1 Protein Kinase Concentrates at Centrosomes Early in Mitosis and Is Necessary for Proper Spindle Assembly. *Mol. Biol. Cell* **16**, 4827–4840 (2005).
60. Casey, J. P. *et al.* Recessive NEK9 mutation causes a lethal skeletal dysplasia with evidence of cell cycle and ciliary defects. *Hum. Mol. Genet.* (2016). doi:10.1093/hmg/ddw054
61. Oliazadeh, N., Gorman, K. F., Eveleigh, R., Bourque, G. & Moreau, A. Identification of Elongated Primary Cilia with Impaired Mechanotransduction in Idiopathic Scoliosis Patients. *Sci. Rep.* **7**, 44260 (2017).
62. Hoey, D. A., Chen, J. C. & Jacobs, C. R. The primary cilium as a novel extracellular sensor in bone. *Front. Endocrinol. (Lausanne).* **3**, 75 (2012).
63. Ingber, D. E. Cellular mechanotransduction: putting all the pieces together again. *FASEB J.* **20**, 811–27 (2006).
64. Ingber, D. E. Cellular tensegrity: defining new rules of biological design that govern the cytoskeleton. *J. Cell Sci.* **104 ( Pt 3**, 613–27 (1993).
65. McBeath, R., Pirone, D. M., Nelson, C. M., Bhadriraju, K. & Chen, C. S. Cell shape, cytoskeletal tension, and RhoA regulate stem cell lineage commitment. *Dev. Cell* **6**, 483–95 (2004).
66. Wozniak, M. A., Modzelewska, K., Kwong, L. & Keely, P. J. Focal adhesion regulation of cell behavior. *Biochim. Biophys. Acta - Mol. Cell Res.* **1692**, 103–119 (2004).
67. Enomoto, T. Microtubule disruption induces the formation of actin stress fibers and focal adhesions in cultured cells: possible involvement of the rho signal cascade. *Cell Struct. Funct.* **21**, 317–26 (1996).
68. Bershadsky, A., Chausovsky, A., Becker, E., Lyubimova, A. & Geiger, B. Involvement of microtubules in the control of adhesion-dependent signal transduction. *Curr. Biol.* **6**, 1279–89 (1996).
69. Rafiq, N. B. M. *et al.* A mechano-signalling network linking microtubules, myosin IIA filaments and integrin-based adhesions. *Nat. Mater.* **18**, 638–649 (2019).
70. McGlashan, S. R., Jensen, C. G. & Poole, C. A. Localization of Extracellular Matrix Receptors on the Chondrocyte Primary Cilium. *J. Histochem. Cytochem.* **54**, 1005–1014 (2006).
71. Kuo, J.-C. Mechanotransduction at focal adhesions: integrating cytoskeletal mechanics in migrating cells. *J. Cell. Mol. Med.* **17**, 704–12 (2013).
72. Marie, P. J. Targeting integrins to promote bone formation and repair. *Nat. Rev. Endocrinol.* **9**, 288–295 (2013).
73. Chen, Q. *et al.* An osteopontin-integrin interaction plays a critical role in directing adipogenesis and osteogenesis by mesenchymal stem cells. *Stem Cells* **32**, 327–37 (2014).
74. Biggs, M. J. P., Richards, R. G. & Dalby, M. J. Nanotopographical modification: a regulator of cellular function through focal adhesions. *Nanomedicine* **6**, 619–33 (2010).
75. Gupton, S. L. & Waterman-Storer, C. M. Spatiotemporal feedback between actomyosin and focal-adhesion systems optimizes rapid cell migration. *Cell* **125**, 1361–74 (2006).
76. Langdahl, B., Ferrari, S. & Dempster, D. W. Bone modeling and remodeling: potential as therapeutic targets for the treatment of osteoporosis. *Ther. Adv. Musculoskelet. Dis.* **8**, 225–235 (2016).
77. Xian, C. J., Cool, J. C., Scherer, M. A., Fan, C. & Foster, B. K. Folinic acid attenuates methotrexate chemotherapy-induced damages on bone growth mechanisms and pools of bone marrow stromal cells. *J. Cell. Physiol.* **214**, 777–785 (2008).
78. Fan, C.-M., Foster, B. K., Hui, S. K. & Xian, C. J. Prevention of bone growth defects, increased bone resorption and marrow adiposity with folinic acid in rats receiving long-term methotrexate. *PLoS One* **7**, e46915 (2012).
79. Fan, C. *et al.* Damaging effects of chronic low-dose methotrexate usage on primary bone formation in young rats and potential protective effects of folinic acid supplementary treatment. *Bone* **44**, 61–70 (2009).
80. Iqbal, M. P., Ahmed, M., Umer, M., Mehboobali, N. & Qureshi, A. A. Effect of methotrexate and folinic acid on skeletal growth in mice. *Acta Paediatr.* **92**, 1438–44 (2003).
81. Georgiou, K. R., Nadhanan, R. R., Fan, C.-M. & Xian, C. J. Methotrexate-Induced Bone Marrow Adiposity Is Mitigated by Folinic Acid Supplementation Through the Regulation of Wnt/β-Catenin Signalling. *J. Cell. Physiol.* **230**, 648–656 (2015).
82. Vanella, L. *et al.* HO-1 expression increases mesenchymal stem cell-derived osteoblasts but decreases adipocyte lineage. *Bone* **46**, 236–43 (2010).
83. Barbagallo, I. *et al.* Overexpression of heme oxygenase-1 increases human osteoblast stem cell differentiation. *J. Bone Miner. Metab.* **28**, 276–288 (2010).
84. Perrien, D. S. *et al.* Aging alters the skeletal response to disuse in the rat. *Am. J. Physiol. Regul. Integr. Comp. Physiol.* **292**, R988–R996 (2007).
85. Rosen, C. J. & Bouxsein, M. L. Mechanisms of disease: is osteoporosis the obesity of bone? *Nat. Clin. Pract. Rheumatol.* **2**, 35–43 (2006).
86. Singh, L. *et al.* Aging alters bone-fat reciprocity by shifting in vivo mesenchymal precursor cell fate towards an adipogenic lineage. *Bone* **85**, 29–36 (2016).
87. Taylor-Jones, J. M. *et al.* Activation of an adipogenic program in adult myoblasts with age. *Mech. Ageing Dev.* **123**, 649–61 (2002).

88. Nuttall, M. E. & Gimble, J. M. Is there a therapeutic opportunity to either prevent or treat osteopenic disorders by inhibiting marrow adipogenesis? *Bone* **27**, 177–84 (2000).
89. Moerman, E. J., Teng, K., Lipschitz, D. A. & Lecka-Czernik, B. Aging activates adipogenic and suppresses osteogenic programs in mesenchymal marrow stroma/stem cells: the role of PPAR-γ2 transcription factor and TGF-β/BMP signaling pathways. *Aging Cell* **3**, 379–389 (2004).
90. Kajkenova, O. *et al.* Increased adipogenesis and myelopoiesis in the bone marrow of SAMP6, a murine model of defective osteoblastogenesis and low turnover osteopenia. *J. Bone Miner. Res.* **12**, 1772–9 (1997).
91. Liu, H. *et al.* Microtubule assembly affects bone mass by regulating both osteoblast and osteoclast functions: stathmin deficiency produces an osteopenic phenotype in mice. *J. Bone Miner. Res.* **26**, 2052–67 (2011).
92. Zhao, M. *et al.* Inhibition of microtubule assembly in osteoblasts stimulates bone morphogenetic protein 2 expression and bone formation through transcription factor Gli2. *Mol. Cell. Biol.* **29**, 1291–305 (2009).
93. Khedgikar, V. *et al.* Withaferin A: a proteasomal inhibitor promotes healing after injury and exerts anabolic effect on osteoporotic bone. *Cell Death Dis.* **4**, e778 (2013).
94. Khedgikar, V. *et al.* Preventive effects of withaferin A isolated from the leaves of an Indian medicinal plant Withania somnifera (L.): Comparisons with 17-β-estradiol and alendronate. *Nutrition* **31**, 205–213 (2015).
95. Lee-Son, S., Wang, G. K., Concus, A., Crill, E. & Strichartz, G. Stereoselective inhibition of neuronal sodium channels by local anesthetics. Evidence for two sites of action? *Anesthesiology* **77**, 324–35 (1992).
96. Ragsdale, D. S., Scheuer, T. & Catterall, W. A. Frequency and voltage-dependent inhibition of type IIA Na+ channels, expressed in a mammalian cell line, by local anesthetic, antiarrhythmic, and anticonvulsant drugs. *Mol. Pharmacol.* **40**, 756–65 (1991).
97. Courtney, K. R. Structure-activity relations for frequency-dependent sodium channel block in nerve by local anesthetics. *J. Pharmacol. Exp. Ther.* **213**, 114–9 (1980).
98. Hirota, K., Browne, T., Appadu, B. L. & Lambert, D. G. Do local anaesthetics interact with dihydropyridine binding sites on neuronal L-type Ca2+ channels? *Br. J. Anaesth.* **78**, 185–8 (1997).
99. Sousa, S. B. *et al.* Gain-of-function mutations in the phosphatidylserine synthase 1 (PTDSS1) gene cause Lenz-Majewski syndrome. *Nat. Genet.* **46**, 70–6 (2014).
100. Whyte, M. P. *et al.* Lenz-Majewski hyperostotic dwarfism with hyperphosphoserinuria from a novel mutation in PTDSS1 encoding phosphatidylserine synthase 1. *J. Bone Miner. Res.* **30**, 606–14 (2015).
101. Kitamoto, S. *et al.* MUC1 enhances hypoxia-driven angiogenesis through the regulation of multiple proangiogenic factors. *Oncogene* **32**, 4614–4621 (2013).
102. Lu, C. *et al.* Tibial fracture decreases oxygen levels at the site of injury. *Iowa Orthop. J.* **28**, 14–21 (2008).
103. Volkmer, E. *et al.* Hypoxic preconditioning of human mesenchymal stem cells overcomes hypoxia-induced inhibition of osteogenic differentiation. *Tissue Eng. Part A* **16**, 153–64 (2010).
104. Van De Peppel, J. *et al.* Stem Cell Reports Identification of Three Early Phases of Cell-Fate Determination during Osteogenic and Adipogenic Differentiation by Transcription Factor Dynamics. (2017). doi:10.1016/j.stemcr.2017.02.018

# Appendices

**Appendix A**
*Summary*

**Appendix B**
*Samenvatting*

**Appendix C**
*Supplementary Tables and Figures*

**Appendix D**
*Abbreviation Index*

**Appendix E**
*Curriculum Vitae*

**Appendix F**
*Publications*

**Appendix G**
*Ph.D. Portfolio*

**Appendix H**
*Acknowledgements*

# A. Summary

Bone is a dynamic organ that throughout life undergoes constant remodeling controlled in a balancing act between removal of old bone by osteoclasts and formation of new bone controlled by osteoblasts, as well as its terminally differentiated form the osteocyte. The process of building bone starts with the mesenchymal stromal cell (MSC), a multipotent cell that has the ability to differentiate into a number of cell types including osteoblasts, chondrocytes, and adipocytes. A number of key factors and signaling pathways controlling osteoblast differentiation and activity have been identified over the last few decades; however, a better understanding of the signaling network, their intricate interactions, and what other genes and pathways are involved in osteoblast function is required to develop approaches to enhance bone formation and promote fracture healing for patients with disorders such as osteoporosis. The overall aim of this thesis, through a combined use of bioinformatic, genomic, molecular, and proteomic approaches, was to identify novel factors (compounds, genes, and processes) involved osteoblast differentiation and bone formation to expand the basic knowledge of osteoblast differentiation which can ultimately be used the development of a novel bone anabolic treatment for conditions such as osteoporosis.

In **chapters 2 and 3** we demonstrated the use of the web-based Connectivity Map (CMap) tool to find compounds with correlating gene expression profiles to that of human MSCs (hMSCs) undergoing osteoblast differentiation that can affect osteoblast differentiation. The CMap identified parbendazole as the top positively correlating compound and in **chapter 2** we showed that parbendazole, independent of an additional osteogenic stimulus, was able to stimulate *in vitro* human osteoblast differentiation as evidenced by increased ALP activity, mineralization and upregulation of genes important in osteoblast differentiation and extracellular matrix production. Mechanistically, it was found that the osteogenic effect of parbendazole occurs independent of glucocorticoid receptor signaling, but rather via affecting microtubule formation, cytoskeletal organization, focal adhesion distribution, and BMP2 activity. In **chapter 3,** three additional positively correlated compounds, withaferin A, calcium folinate, and amylocaine, which stimulate osteoblast differentiation and mineralization of hMSCs *in vitro* were identified. Conversely, compounds with negatively correlated gene signatures to that of differentiating osteoblasts, the results of which we hypothesized may reveal interesting new genes and processes in the osteoblast differentiation process, were examined. Three compounds, salbutamol, metaraminol, and diprophylline, which exhibit a gene signature negatively correlated to our osteogenic gene signature were identified, but

only one of these drugs, salbutamol, inhibited dexamethasone-induced osteogenic differentiation of hMSCs were identified Finally, the differentially expressed genes behind the CMap identified compounds and used this approach to find and validate two genes, *HMOX1* and *STC1*, as important factors for human osteogenesis were analyzed.

In **chapter 4**, *CLIC3* was identified as a new gene specifically regulated in the osteogenic lineage of differentiating hMSCs. Lentiviral transduction-mediated overexpression and silencing of *CLIC3* during osteogenesis revealed a crucial function for *CLIC3* in promoting osteoblast mineralization. Overexpression of *CLIC3* in hMSCs strongly enhanced in vivo bone formation in a mouse model for ectopic human bone formation further emphasizing that *CLIC3* plays an important role in human osteoblast differentiation. Bioinformatics analysis of proteins identified by CLIC3-His pull down suggests CLIC3s role during osteoblast differentiation may be related cytoskeletal associations and signaling, cell adhesion, and/or nuclear pore formation or transport through. Finally, it was identified that CLIC3 interacts with NEK9 and PTDSS1 during osteoblast differentiation, and inhibition of the *NEK9* and *PTDSS1* expression reduces osteogenic differentiation of hMSCs.

**Chapter 5** describes a novel and temporally shifting role for *Muc1* in bone biology. It was showed that deletion of *Muc1* in female mice leads to decreased trabecular bone volume in 8-week-old compared to wild type (WT) females; however, this difference disappears by 16 weeks. At the same time, endocortical bone formation rate and femoral stiffness are increased at 16 weeks of age in *Muc1* deficient female mice, with a higher rate of endocortical bone formation persisting to 52 weeks of age in *Muc1*$^{-/-}$ mice. Histomorphometric analysis demonstrated that femurs of 16-week-old *Muc1*$^{-/-}$ female mice displayed lower numbers of osteoblasts lining the bone surface, while femurs from 8- and 52-week old KO and WT mice did not differ in their number of osteoblasts.

In conclusion, this thesis has presented a number of novel findings in the bone biology field and highlights the complexity of the biology and study of osteoblast differentiation. These studies, and studies like it, are vital in gaining greater knowledge about MSC lineage decision making and osteoblasts differentiation, which is required to develop much needed bone anabolic therapeutics. The findings presented in this thesis highlight the importance of the cytoskeleton in regulating and influencing osteoblast differentiation, and may hold promise as novel anti-osteoporotic treatments, with further research. The discovery of a number of novel factors affecting osteoblast differentiation, including the CMap identified compounds and *CLIC3* and *MUC1*, opens up new avenues in the bone biology field for development of bone anabolic therapeutics.

# B. Samenvatting

Bot is een dynamisch orgaan dat gedurende het hele leven een constante remodellering ondergaat, gecontroleerd in een evenwichtsoefening tussen verwijdering van oud bot door osteoclasten en vorming van nieuw bot gecontroleerd door osteoblasten, evenals zijn terminaal gedifferentieerde vorm de osteocyt. Het proces van het bouwen van bot begint met de mesenchymale stromale cel (MSC), een multipotente cel die het vermogen heeft om te differentiëren in een aantal celtypen, waaronder osteoblasten, chondrocyten en adipocyten. De afgelopen decennia zijn een aantal sleutelfactoren en signaalroutes vastgesteld die de differentiatie en activiteit van osteoblast beheersen; een beter begrip van het signaalnetwerk, hun ingewikkelde interacties en welke andere genen en routes betrokken zijn bij de osteoblastfunctie is echter vereist om benaderingen te ontwikkelen om de botvorming te verbeteren en fractuurgenezing te bevorderen voor patiënten met aandoeningen zoals osteoporose. Het algemene doel van dit proefschrift was, door een gecombineerd gebruik van bioinformatische, genomische, moleculaire en proteomische benaderingen, om nieuwe factoren (verbindingen, genen en processen) te identificeren die te maken hadden met osteoblastdifferentiatie en botvorming om de basiskennis van osteoblastdifferentiatie uit te breiden welke uiteindelijk kan worden gebruikt voor de ontwikkeling van een nieuwe botanabole behandeling voor aandoeningen zoals osteoporose.

In de **hoofdstukken 2 en 3** is het gebruik van het webgebaseerde Connectivity Map-hulpmiddel (CMap) aangetoond om verbindingen te vinden met correlerende genexpressieprofielen met die van menselijke MSC's (hMSC's) die osteoblastdifferentiatie ondergaan welke de osteoblastdifferentiatie kunnen beïnvloeden. De CMap identificeerde parbendazol als de bovenste positief correlerende verbinding en in **hoofdstuk 2** is aangetoond dat parbendazol, onafhankelijk van een extra osteogene stimulus*, in vitro* humane osteoblastdifferentiatie kon stimuleren zoals bewezen door verhoogde ALP-activiteit, mineralisatie en opregulatie van genen die belangrijk zijn in osteoblast differentiatie en extracellulaire matrixproductie. Mechanistisch is gevonden dat het osteogene effect van parbendazol onafhankelijk van de glucocorticoïdereceptorsignalering optreedt, maar eerder via het beïnvloeden van de vorming van microtubuli, cytoskeletorganisatie, focale adhesieverdeling en BMP2-activiteit. In **hoofdstuk 3** zijn drie extra positief gecorreleerde verbindingen geïdentificeerd; metaferine A, calciumfolinaat en amylocaïne, die osteoblast differentiatie en mineralisatie van hMSC's in vitro stimuleren. Omgekeerd zijn ook verbindingen met negatief gecorreleerde gensignaturen met die van differentiërende osteoblasten, waarvan de

resultaten waarvan verondersteld is dat ze interessante nieuwe genen en processen in het osteoblastdifferentiatieproces kunnen onthullen onderzocht. Ook zijn drie verbindingen geïdentificeerd, salbutamol, metaraminol en diprophylline, die een gensignatuur vertonen die negatief gecorreleerd is met onze osteogene gensignatuur, maar slechts één van deze geneesmiddelen, salbutamol, remde door dexamethason geïnduceerde osteogene differentiatie van hMSC's. Ten slotte, zijn de de differentieel tot expressie gebrachte genen achter de CMap-geïdentificeerde verbindingen geanalyseerd, en deze benadering gebruikt om twee genen, *HMOX1* en *STC1*, te vinden en te valideren, als belangrijke factoren voor menselijke osteogenese.

In **hoofdstuk 4** is *CLIC3* geïdentificeerd als een nieuw gen dat specifiek wordt gereguleerd in de osteogene lijn van differentiërende hMSC's. Lentivirale transductie-gemedieerde overexpressie en "silencing" van *CLIC3* tijdens osteogenese onthulde een cruciale functie voor *CLIC3* bij het bevorderen van osteoblastmineralisatie. Overexpressie van *CLIC3* in hMSC's verhoogde de in vivo botvorming sterk in een muismodel voor ectopische menselijke botvorming en benadrukte verder dat *CLIC3* een belangrijke rol speelt bij de differentiatie van menselijke osteoblasten. Bioinformatica-analyse van eiwitten, geïdentificeerd door CLIC3-His pull-down suggereert dat CLIC3s rol tijdens osteoblastdifferentiatie gerelateerd kan zijn aan cytoskeletale associaties en signalering, celadhesie en / of nucleaire porievorming of transport doorheen. Ten slotte hebben is vastgesteld dat CLIC3 een interactie aangaat met NEK9 en PTDSS1 tijdens osteoblastdifferentiatie, en remming van de expressie van *NEK9* en *PTDSS1* vermindert de osteogene differentiatie van hMSC's.

**Hoofdstuk 5** beschrijft een nieuwe en in tijd veranderende rol voor *Muc1* in botbiologie. Er is aangetoond dat verwijdering van *Muc1* bij vrouwelijke muizen leidt tot een verminderd trabeculair botvolume bij 8 weken oude dieren in vergelijking met wildtype (WT) vrouwtjes; dit verschil verdwijnt echter na 16 weken. Tegelijkertijd neemt de snelheid van de endocorticale botvorming en de stijfheid van het dijbeen toe op de leeftijd van 16 weken bij *Muc1*$^{-/-}$ vrouwelijke muizen, met een hogere snelheid van de endocorticale botvorming tot 52 weken bij de *Muc1*$^{-/-}$ muizen. Histomorfometrische analyse toonde aan dat femora van 16-weken oude *Muc1*$^{-/-}$ vrouwelijke muizen lagere aantallen osteoblasten vertoonden langs het botoppervlak, terwijl femora van 8- en 52-weken oude KO- en WT-muizen niet verschilden in hun aantal osteoblasten.

Concluderend heeft dit proefschrift een aantal nieuwe bevindingen op het gebied van botbiologie gepresenteerd en de nadruk gelegd op de complexiteit van de biologie en studie van osteoblastdifferentiatie. Deze onderzoeken, en dergelijke studies, zijn van vitaal belang om meer kennis te vergaren over MSC-besluitvorming

en osteoblasten differentiatie, die nodig is om de hoognodige anabole therapeutica te ontwikkelen. De bevindingen in dit proefschrift benadrukken het belang van het cytoskelet bij het reguleren en beïnvloeden van osteoblastdifferentiatie, en kunnen veelbelovend zijn als nieuwe anti-osteoporotische behandelingen, met verder onderzoek. De ontdekking van een aantal nieuwe factoren die de osteoblastdifferentiatie beïnvloeden, waaronder de CMap-geïdentificeerde verbindingen en *CLIC3* en *MUC1*, opent nieuwe wegen op het gebied van botbiologie voor de ontwikkeling van botanabole therapeutica.

# C. Supplementary Tables and Figures

**Table A1: Probes used for CMap query**

**Up-regulated Probes**

| | Affymetrix Probe ID HG-U133A | Gene symbol |
|---|---|---|
| 1 | 205730_s_at | ABLIM3 |
| 2 | 201963_at | ACSL1 |
| 3 | 207589_at | ADRA1B |
| 4 | 204174_at | ALOX5AP |
| 5 | 221009_s_at | ANGPTL4 |
| 6 | 206029_at | ANKRD1 |
| 7 | 206176_at | BMP6 |
| 8 | 218723_s_at | C13orf15 |
| 9 | 218309_at | CAMK2N1 |
| 10 | 219398_at | CIDEC |
| 11 | 221541_at | CRISPLD2 |
| 12 | 209283_at | CRYAB |
| 13 | 214724_at | DIXDC1 |
| 14 | 204602_at | DKK1 |
| 15 | 203810_at | DNAJB4 |
| 16 | 201041_s_at | DUSP1 |
| 17 | 209457_at | DUSP5 |
| 18 | 214445_at | ELL2 |
| 19 | 201324_at | EMP1 |
| 20 | 205521_at | ENDOGL1 |
| 21 | 208962_s_at | FADS1 |
| 22 | 204560_at | FKBP5 |
| 23 | 206860_s_at | FLJ20323 |
| 24 | 205021_s_at | FOXN3 |
| 25 | 202723_s_at | FOXO1 |
| 26 | 203592_s_at | FSTL3 |
| 27 | 209892_at | FUT4 |
| 28 | 203725_at | GADD45A |
| 29 | 207574_s_at | GADD45B |
| 30 | 201841_s_at | HSPB1 |
| 31 | 206375_s_at | HSPB3 |

**Down-regulated Probes**

| | Affymetrix Probe ID HG-U133A | Gene symbol |
|---|---|---|
| 1 | 222162_s_at | ADAMTS1 |
| 2 | 201034_at | ADD3 |
| 3 | 218631_at | AVPI1 |
| 4 | 204907_s_at | BCL3 |
| 5 | 207510_at | BDKRB1 |
| 6 | 201169_s_at | BHLHB2 |
| 7 | 211518_s_at | BMP4 |
| 8 | 216598_s_at | CCL2 |
| 9 | 203666_at | CXCL12 |
| 10 | 212977_at | CXCR7 |
| 11 | 202434_s_at | CYP1B1 |
| 12 | 204977_at | DDX10 |
| 13 | 218858_at | DEPDC6 |
| 14 | 201340_s_at | ENC1 |
| 15 | 215704_at | FLG |
| 16 | 204948_s_at | FST |
| 17 | 203925_at | GCLM |
| 18 | 221576_at | GDF15 |
| 19 | 206614_at | GDF5 |
| 20 | 210640_s_at | GPER |
| 21 | 218468_s_at | GREM1 |
| 22 | 206432_at | HAS2 |
| 23 | 202934_at | HK2 |
| 24 | 203665_at | HMOX1 |
| 25 | 209905_at | HOXA9 |
| 26 | 201565_s_at | ID2 |
| 27 | 201631_s_at | IER3 |
| 28 | 206332_s_at | IFI16 |
| 29 | 214059_at | IFI44 |
| 30 | 205207_at | IL6 |
| 31 | 201625_s_at | INSIG1 |

| | | |
|---|---|---|
| 32 | 218934_s_at | HSPB7 |
| 33 | 209184_s_at | IRS2 |
| 34 | 201389_at | ITGA5 |
| 35 | 204301_at | KBTBD11 |
| 36 | 208960_s_at | KLF6 |
| 37 | 212442_s_at | LASS6 |
| 38 | 218574_s_at | LMCD1 |
| 39 | 215322_at | LONRF1 |
| 40 | 212859_x_at | MT1E |
| 41 | 204745_x_at | MT1G |
| 42 | 217546_at | MT1M |
| 43 | 204326_x_at | MT1X |
| 44 | 203036_s_at | MTSS1 |
| 45 | 218330_s_at | NAV2 |
| 46 | 213012_at | NEDD4 |
| 47 | 201502_s_at | NFKBIA |
| 48 | 218786_at | NT5DC3 |
| 49 | 205960_at | PDK4 |
| 50 | 212239_at | PIK3R1 |
| 51 | 207290_at | PLXNA2 |
| 52 | 204285_s_at | PMAIP1 |
| 53 | 206631_at | PTGER2 |
| 54 | 204748_at | PTGS2 |
| 55 | 206157_at | PTX3 |
| 56 | 204916_at | RAMP1 |
| 57 | 202388_at | RGS2 |
| 58 | 212099_at | RHOB |
| 59 | 202082_s_at | SEC14L1 |
| 60 | 204541_at | SEC14L2 |
| 61 | 202627_s_at | SERPINE1 |
| 62 | 201739_at | SGK1 |
| 63 | 214719_at | SLC46A3 |
| 64 | 209453_at | SLC9A1 |
| 65 | 212797_at | SORT1 |
| 66 | 219257_s_at | SPHK1 |
| 67 | 220983_s_at | SPRY4 |

| | | |
|---|---|---|
| 32 | 201464_x_at | JUN |
| 33 | 210261_at | KCNK2 |
| 34 | 201650_at | KRT19 |
| 35 | 206969_at | KRT34 |
| 36 | 206481_s_at | LDB2 |
| 37 | 206953_s_at | LPHN2 |
| 38 | 218559_s_at | MAFB |
| 39 | 212530_at | NEK7 |
| 40 | 206814_at | NGF |
| 41 | 220132_s_at | NPM1 |
| 42 | 203708_at | PDE4B |
| 43 | 220343_at | PDE7B |
| 44 | 203131_at | PDGFRA |
| 45 | 217996_at | PHLDA1 |
| 46 | 203354_s_at | PSD3 |
| 47 | 207017_at | RAB27B |
| 48 | 202677_at | RASA1 |
| 49 | 209568_s_at | RGL1 |
| 50 | 204337_at | RGS4 |
| 51 | 212724_at | RND3 |
| 52 | 213236_at | SASH1 |
| 53 | 202656_s_at | SERTAD2 |
| 54 | 205856_at | SLC14A1 |
| 55 | 205396_at | SMAD3 |
| 56 | 208127_s_at | SOCS5 |
| 57 | 202935_s_at | SOX9 |
| 58 | 203217_s_at | ST3GAL5 |
| 59 | 210612_s_at | SYNJ2 |
| 60 | 203083_at | THBS2 |
| 61 | 209386_at | TM4SF1 |
| 62 | 206025_s_at | TNFAIP6 |
| 63 | 204932_at | TNFRSF11B |
| 64 | 215111_s_at | TSC22D1 |
| 65 | 204881_s_at | UGCG |
| 66 | 220976_s_at | KRTAP1-1 |

| | | |
|---|---|---|
| 68 | 219315_s_at | TMEM204 |
| 69 | 207001_x_at | TSC22D3 |
| 70 | 205480_s_at | UGP2 |
| 71 | 206796_at | WISP1 |
| 72 | 221029_s_at | WNT5B |
| 73 | 205883_at | ZBTB16 |
| 74 | 212704_at | ZCCHC11 |
| 75 | 211962_s_at | ZFP36L1 |
| 76 | 204131_s_at | ZNF286C |
| 77 | 212742_at | ZNF364 |

List of up-regulated and down-regulated genes at 6 hours after start of osteogenic differentiation in hMSCs and their associated affymetrix probe IDs used for initial CMap query.

**Table A2. Gene Ontology (GO) terms associated with CMap compound genes**

**Withaferin A**

| Category | Term | Fold Enrichment | Count | Benjamini corrected p-value |
|---|---|---|---|---|
| BP | GO:0006986~response to unfolded protein | 34.88 | 13 | 1.90E-12 |
| BP | GO:0043065~positive regulation of apoptotic process | 5.63 | 15 | 3.33E-04 |
| BP | GO:1900034~regulation of cellular response to heat | 12.02 | 8 | 2.23E-03 |
| MF | GO:0005515~protein binding | 1.35 | 105 | 2.53E-03 |
| MF | GO:0051082~unfolded protein binding | 8.18 | 8 | 4.77E-03 |
| BP | GO:0008284~positive regulation of cell proliferation | 3.87 | 16 | 4.95E-03 |
| MF | GO:0051087~chaperone binding | 9.73 | 7 | 5.68E-03 |
| MF | GO:0031625~ubiquitin protein ligase binding | 4.71 | 12 | 5.77E-03 |
| MF | GO:0031072~heat shock protein binding | 16.08 | 6 | 5.78E-03 |
| BP | GO:0045944~positive regulation of transcription from RNA polymerase II promoter | 2.76 | 24 | 6.15E-03 |
| BP | GO:0042127~regulation of cell proliferation | 6.09 | 10 | 1.00E-02 |
| BP | GO:0045766~positive regulation of angiogenesis | 7.84 | 8 | 1.56E-02 |
| BP | GO:0048008~platelet-derived growth factor receptor signaling pathway | 19.43 | 5 | 1.98E-02 |
| BP | GO:0071372~cellular response to follicle-stimulating hormone stimulus | 40.98 | 4 | 2.02E-02 |
| MF | GO:0008083~growth factor activity | 5.56 | 8 | 3.41E-02 |
| BP | GO:0042026~protein refolding | 30.05 | 4 | 4.29E-02 |
| BP | GO:0043122~regulation of I-kappaB kinase/NF-kappaB signaling | 30.05 | 4 | 4.29E-02 |

**Calcium Folinate**

| Category | Term | Fold Enrichment | Count | Benjamini corrected p-value |
|---|---|---|---|---|
| MF | GO:0019899~enzyme binding | 3.99 | 13 | 3.84E-02 |

**Amylocaine**

| Category | Term | Fold Enrichment | Count | Benjamini corrected p-value |
|---|---|---|---|---|
| CC | GO:0005829~cytosol | 1.67 | 52 | 2.75E-04 |

**Salbutamol**

| Category | Term | Fold Enrichment | Count | Benjamini corrected p-value |
|---|---|---|---|---|
| CC | GO:0005615~extracellular space | 2.59 | 31 | 4.09E-04 |
| BP | GO:0042060~wound healing | 10.83 | 8 | 1.06E-02 |

| | | | | |
|---|---|---|---|---|
| BP | GO:0043066~negative regulation of apoptotic process | 3.81 | 16 | 1.20E-02 |
| MF | GO:0008022~protein C-terminus binding | 5.87 | 10 | 1.73E-02 |
| BP | GO:0042127~regulation of cell proliferation | 5.86 | 10 | 2.17E-02 |
| BP | GO:0008283~cell proliferation | 3.85 | 13 | 3.49E-02 |
| BP | GO:0007267~cell-cell signaling | 4.69 | 11 | 3.64E-02 |
| BP | GO:0001525~angiogenesis | 4.86 | 10 | 3.80E-02 |
| BP | GO:0001666~response to hypoxia | 5.67 | 9 | 3.83E-02 |
| BP | GO:0030335~positive regulation of cell migration | 5.30 | 9 | 4.51E-02 |
| CC | GO:0005737~cytoplasm | 1.44 | 67 | 4.59E-02 |

**Metaraminol**

| Category | Term | Fold Enrichment | Count | Benjamini corrected p-value |
|---|---|---|---|---|
| CC | GO:0005615~extracellular space | 2.46 | 30 | 1.82E-03 |

All GO terms that were identified by DAVID bioinformatics in the DEGs derived from the CMAP-gene profiles. For the search the 100 most upregulated and 100 most downregulated probes were selected based on the average of the ratioed (instance to the control) normalized expression values for the two instances for each compound. The GO terms within the clusters had a significance of Benjamini corrected p-value < 0.05. The headers "biological process", "molecular function", and "cellular component" stands for the GO category to which the GO term is annotated.

**Table A3: All proteins found by CLIC3-His pull down**

| Protein name | Gene ID | Ratio LFQ CLIC3 / EV |
|---|---|---|
| Chloride intracellular channel protein 3 | CLIC3 | 1227400000 |
| Serine/threonine-protein kinase Nek9 | NEK9 | 5714650 |
| 1-phosphatidylinositol 4,5-bisphosphate phosphodiesterase beta-3 | PLCB3 | 3564350 |
| Aminoacyl tRNA synthase complex-interacting multifunctional protein 1 | AIMP1 | 2891250 |
| Casein kinase II subunit alpha 3; Casein kinase II subunit alpha | CSNK2A1; CSNK2A3 | 2350900 |
| 40S ribosomal protein S28 | RPS28 | 1803250 |
| Phosphatidylserine synthase 1 | PTDSS1 | 1471350 |
| Nuclear pore complex protein Nup160 | NUP160 | 1106150 |
| Rho guanine nucleotide exchange factor 7 | ARHGEF7 | 2.72 |
| Lipoamide acyltransferase component of branched-chain alpha-keto acid dehydrogenase complex | DBT | 2.39 |
| Centrosomal protein of 170 kDa | CEP170 | 2.24 |
| Cytosolic acyl coenzyme A thioester hydrolase | ACOT7 | 2.20 |
| LIM domain only protein 7 | LMO7 | 2.08 |
| Splicing factor, proline- and glutamine-rich | SFPQ | 2.03 |
| cAMP-dependent protein kinase type I-alpha regulatory subunit | PRKAR1A | 2.03 |
| BTB/POZ domain-containing protein KCTD12 | KCTD12 | 2.00 |
| Serine/arginine repetitive matrix protein 1 | SRRM1 | 1.96 |
| Phostensin | PPP1R18 | 1.95 |
| Heterogeneous nuclear ribonucleoprotein D0 | HNRNPD | 1.89 |
| Actin, aortic smooth muscle; Actin, gamma-enteric smooth muscle | ACTA2; ACTG2 | 1.85 |
| Kinectin | KTN1 | 1.80 |
| Mesoderm-specific transcript homolog protein | MEST | 1.79 |
| Sorting nexin-33 | SNX33 | 1.78 |
| Transitional endoplasmic reticulum ATPase | VCP | 1.76 |
| Nucleoporin NUP188 | NUP188 | 1.76 |
| 5-nucleotidase | NT5E | 1.74 |
| 26S proteasome non-ATPase regulatory subunit 4 | PSMD4 | 1.72 |
| Heterogeneous nuclear ribonucleoprotein U-like protein 2 | HNRNPUL2-BSCL2 | 1.72 |
| Pinin | PNN | 1.69 |
| Heterogeneous nuclear ribonucleoprotein M | HNRNPM | 1.68 |
| Formin-binding protein 1-like | FNBP1L | 1.68 |
| RuvB-like 1 | RUVBL1 | 1.66 |
| Nexilin | NEXN | 1.66 |
| E3 SUMO-protein ligase RanBP2 | RANBP2 | 1.65 |
| LIM and SH3 domain protein 1 | LASP1 | 1.65 |
| Sorbin and SH3 domain-containing protein 2 | SORBS2 | 1.65 |
| Lamin-B2 | LMNB2 | 1.65 |
| Caveolin-1; Caveolin | CAV1 | 1.62 |
| H/ACA ribonucleoprotein complex subunit 4 | DKC1 | 1.61 |
| Importin subunit beta-1 | KPNB1 | 1.61 |
| Caldesmon | CALD1 | 1.58 |
| Ribose-phosphate pyrophosphokinase 1; Ribose-phosphate pyrophosphokinase 2; Ribose-phosphate pyrophosphokinase 3 | PRPS1; PRPS2; PRPS1L1 | 1.58 |
| Protein FAM98B | FAM98B | 1.58 |
| Plasminogen activator inhibitor 1 | SERPINE1 | 1.57 |
| THO complex subunit 2 | THOC2 | 1.55 |

| | | |
|---|---|---|
| Heterogeneous nuclear ribonucleoproteins C1/C2; Heterogeneous nuclear ribonucleoprotein C-like 1; Heterogeneous nuclear ribonucleoprotein C-like 2 | HNRNPC; HNRNPCL1; HNRNPCL2 | 1.53 |
| Pentraxin-related protein PTX3 | PTX3 | 1.52 |
| Nuclear RNA export factor 1 | NXF1 | 1.52 |
| Alpha-parvin | PARVA | 1.52 |
| Casein kinase I isoform delta; Casein kinase I isoform epsilon | CSNK1E; CSNK1D | 1.51 |
| Oxysterol-binding protein 1 | OSBP | 1.51 |
| Glia-derived nexin | SERPINE2 | 1.50 |

All proteins found by His-tagged CLIC3 pull down that met our selection criteria: 1) LFQ value in CLIC3 samples of greater than 1 x $10^6$, 2) number of unique peptides covering a protein equals 3 or more, and 3) ratio of CLIC3 samples versus control samples of 1.5 or greater. Protein lysates from osteogenically differentiating hMSCs were isolated on day 5 in cultures either overexpressing His-tagged CLIC3 or transduced with empty vector (EV) control, and subjected to protein pull-down for the His-tagged CLIC3 and proteins binding to it. Proteins were determined by mass spectrometry measurements (n=2). The top proteins are listed here, ranked on their ratio of CLIC3 versus control average LFQ intensity (i.e. present in CLIC3 overexpressing condition and absent in the EV condition). LFQ: Label-free quantification.

**Table A4: Canonical Pathways associated with CLIC3-His pull-down proteins**

| Rank | Ingenuity Canonical Pathways | p-value |
|---|---|---|
| **1** | PRPP Biosynthesis I | 0.00000002 |
| **2** | Gap Junction Signaling | 0.00005623 |
| **3** | Paxillin Signaling | 0.00015136 |
| **4** | Mechanisms of Viral Exit from Host Cells | 0.00017783 |
| **5** | Integrin Signaling | 0.00019055 |
| **6** | Cellular Effects of Sildenafil (Viagra) | 0.00038019 |
| **7** | Agrin Interactions at Neuromuscular Junction | 0.00081283 |
| **8** | Caveolar-mediated Endocytosis Signaling | 0.00089125 |
| **9** | RAN Signaling | 0.00091201 |
| **10** | FAK Signaling | 0.00162181 |
| **11** | Virus Entry via Endocytic Pathways | 0.00169824 |
| **12** | Stearate Biosynthesis I (Animals) | 0.00389045 |
| **13** | RhoA Signaling | 0.00416869 |
| **14** | MSP-RON Signaling Pathway | 0.00660693 |
| **15** | Epithelial Adherens Junction Signaling | 0.00691831 |
| **16** | Amyloid Processing | 0.00812831 |

All canonical pathways determined by Ingenuity pathway analysis of the 52 proteins obtained from CLIC3-His pull down. Cutoff for selection set at $p < 0.01$

**Table A5: Gene Ontology (GO) terms associated with CLIC3-His pull-down proteins**

| GO term: Biological Process | Benjamini corrected p-value | Fold Enrichment |
|---|---|---|
| RNA localization | 0.000351 | 14.16 |
| transport of virus | 0.000698 | 29.13 |
| multi-organism localization | 0.000767 | 27.55 |
| multi-organism transport | 0.000767 | 27.55 |
| ribonucleoprotein complex localization | 0.000776 | 19.03 |
| RNA export from nucleus | 0.000942 | 19.34 |
| ribonucleoprotein complex export from nucleus | 0.001107 | 20.16 |
| nuclear export | 0.002483 | 12.86 |
| establishment of RNA localization | 0.002626 | 12.93 |
| biological adhesion | 0.002811 | 3.37 |
| cell adhesion | 0.002987 | 3.38 |
| nucleic acid transport | 0.003287 | 13.14 |
| RNA transport | 0.003287 | 13.14 |
| mRNA-containing ribonucleoprotein complex export from nucleus | 0.003353 | 19.80 |
| mRNA export from nucleus | 0.003353 | 19.80 |
| endomembrane system organization | 0.003963 | 6.12 |
| viral life cycle | 0.005063 | 6.68 |
| nucleobase-containing compound transport | 0.005094 | 11.01 |
| interspecies interaction between organisms | 0.005137 | 4.03 |
| symbiosis, encompassing mutualism through parasitism | 0.005137 | 4.03 |
| multi-organism cellular localization | 0.005237 | 24.99 |
| multi-organism intracellular transport | 0.005237 | 24.99 |
| RNA processing | 0.005512 | 4.48 |
| intracellular transport of virus | 0.005597 | 25.36 |
| mRNA transport | 0.007155 | 13.59 |
| regulation of protein catabolic process | 0.008455 | 7.33 |
| positive regulation of protein catabolic process | 0.008496 | 9.26 |
| RNA splicing | 0.011931 | 6.83 |
| multi-organism cellular process | 0.014118 | 3.80 |
| mitotic cell cycle process | 0.014203 | 4.21 |
| viral process | 0.014511 | 3.83 |
| regulation of cellular component organization | 0.014704 | 2.61 |
| mitotic nuclear envelope disassembly | 0.020010 | 30.89 |
| positive regulation of catabolic process | 0.023241 | 7.12 |
| nucleocytoplasmic transport | 0.023247 | 5.80 |
| nuclear transport | 0.023529 | 5.70 |
| cell cycle process | 0.023977 | 3.25 |
| cell-cell adhesion | 0.024154 | 3.48 |
| mitotic cell cycle | 0.024168 | 3.87 |
| membrane disassembly | 0.024965 | 28.32 |
| nuclear envelope disassembly | 0.024965 | 28.32 |
| regulation of catabolic process | 0.033027 | 5.33 |
| mRNA metabolic process | 0.033389 | 4.57 |
| regulation of proteolysis | 0.047213 | 4.30 |
| **GO term: Molecular Function** | **Benjamini corrected p-value** | **Fold Enrichment** |
| poly(A) RNA binding | 0.000003 | 4.92 |
| RNA binding | 0.000007 | 3.90 |
| cadherin binding | 0.002150 | 8.04 |
| protein binding involved in cell adhesion | 0.002475 | 8.09 |
| protein binding involved in cell-cell adhesion | 0.002786 | 8.23 |
| cadherin binding involved in cell-cell adhesion | 0.002993 | 8.51 |

| | | |
|---|---|---|
| cell adhesion molecule binding | 0.022222 | 5.35 |
| organic cyclic compound binding | 0.048282 | 1.58 |
| **GO term: Cellular Component** | **Benjamini corrected p-value** | **Fold Enrichment** |
| anchoring junction | 0.000198 | 5.47 |
| adherens junction | 0.000513 | 5.20 |
| cytosol | 0.002340 | 2.16 |
| cell junction | 0.003319 | 3.24 |
| nuclear periphery | 0.003662 | 13.61 |
| cell-cell adherens junction | 0.006602 | 6.72 |
| nuclear pore | 0.006943 | 17.22 |
| nucleoplasm | 0.022067 | 2.05 |
| nuclear body | 0.043307 | 5.47 |
| cell-cell junction | 0.044715 | 3.89 |

GO terms that were identified by DAVID bioinformatics analysis of the 52 proteins obtained from CLIC3-His pull down. Cutoff for selection set at benjamini corrected $p < 0.05$

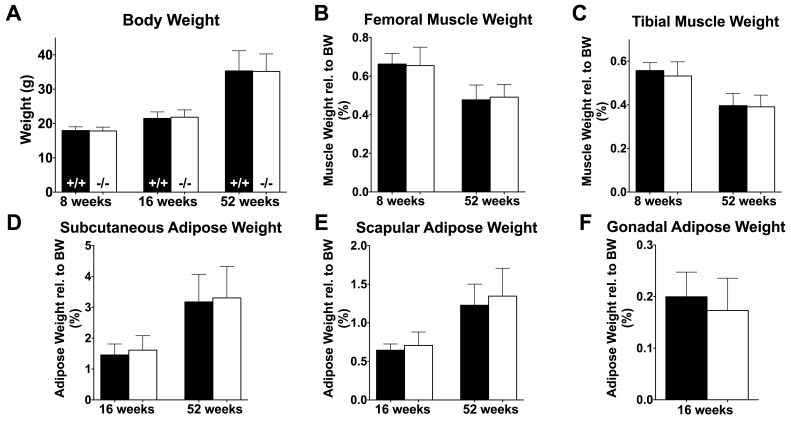


**Figure A6. Cross sectional study of body, muscle and adipose depot weights from WT (+/+, black bar) and *Muc1* deficient (-/-, white bar) mice at 8, 16, and 52 weeks of age.** Total body weight (A). Femoral (B) and tibial (C) muscle weight relative to total body weight. Relative weights of subcutaneous (D), scapular (E), and gonadal (F) adipose deposits. Statistics: student t-test * = p<0.05 WT vs. Muc1$^{-/-}$ comparing WT versus KO at each time point. For body weight 8 weeks (n=10 WT, n=9 KO); 16 weeks (n=9 WT, n=10 KO); 52 weeks (n=9 WT, n=10 KO). For muscle weights 8 weeks (n=10 WT, n=9 KO); 52 weeks (n=8 WT, n=9 KO). For subcutaneous and scapular adipose weights 16 weeks (n=7 WT, n=8 KO); 52 weeks (n=8 WT, n=10 KO). For gonadal adipose weights 16 weeks (n=7 WT, n=8 KO).

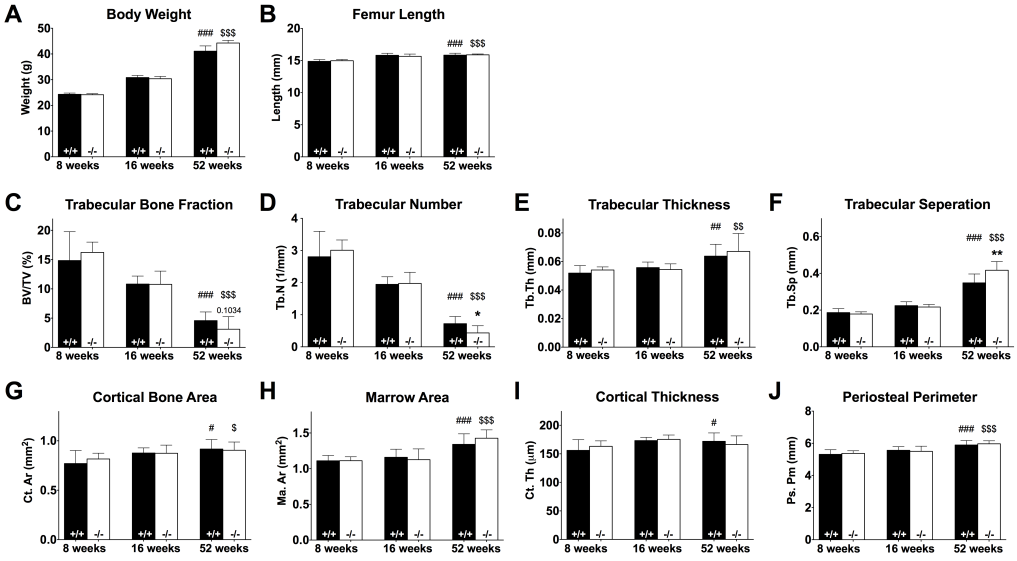


**Figure A7. Body weight, femur length, and *ex vivo* evaluation of microarchitecture of femoral bones from 8-, 16-, and 52-week-old WT and *Muc1* deficient male mice.** Total body weight of WT (+/+, black bar) and KO (-/-, white bar) male mice (A). Femur length of WT and KO male mice (B). Trabecular bone fraction (C), trabecular number (D), trabecular thickness (E), and trabecular separation (F) were measured at the metaphyseal region. Cortical bone area (G), marrow area (H), cortical thickness (I), and periosteal perimeter (mid-shaft circumference) (J) were measured at diaphyseal areas. For body weight 8 weeks (n=10); 16 weeks (n=9); 52-weeks (n=10 WT, n=9 KO). For bone length 8 weeks (n=9 WT, n=10 KO); 16 weeks (n=9 WT, n=8 KO); 52-weeks (n=8 WT, n=7 KO). For trabecular and cortical bone analysis 8 weeks (n=10); 16 weeks (n=9); 52-weeks (n=10 WT, n=8 KO). Statistics: student t-test exact p value, * = p<0.05 WT vs. *Muc1*$^{-/-}$ within time point, and ** = p<0.01 WT vs. *Muc1*$^{-/-}$ within time point. # = p < 0.05 compared to 8wk WT mice, ## = p < 0.01 compared to 8wk WT mice, ### = p < 0.001 compared to 8wk WT mice. $ = p < 0.05 compared to 8wk KO mice, $$ = p < 0.01 compared to 8wk KO mice, $$$ = p < 0.001 compared to 8wk KO mice.

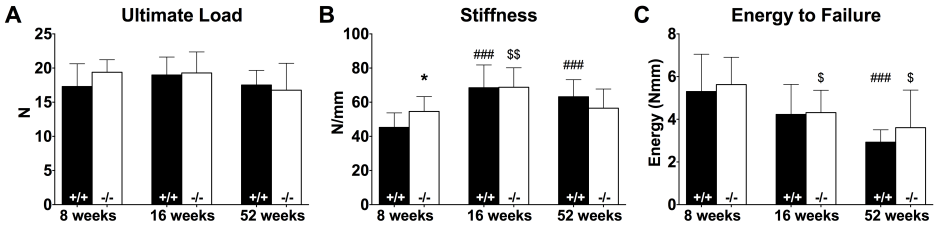


**Figure A8: Mechanical testing of femurs of 8-, 16-, and 52-week old WT (+/+, black bar) and *Muc1* deficient (-/-, white bar) male mice.** Three-point bending tests performed on the femurs of WT and KO mice allowed for quantification of the energy to failure (A), ultimate load (B), and bone stiffness (C) of the bones. Statistics: student t-test * = p<0.05 WT vs. *Muc1*$^{-/-}$ within time point. ### = p < 0.001 compared to 8wk WT mice. $ = p < 0.05 compared to 8wk KO mice. $$ = p < 0.01 compared to 8wk KO mice. 8 weeks (n=10 WT, n=9 KO); 16 weeks (n=9 WT, n=10 KO); 52-weeks (n=10 WT, n=9 KO).

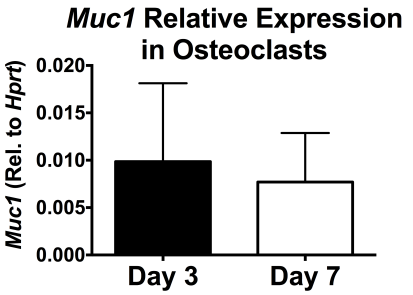


**Figure A9: *Muc1* expression in osteoclasts.** mRNA expression levels of *Muc1* in differentiation murine osteoclasts at day 3 (black bar) and 7 (white bar) as assessed by quantitative PCR. Results are presented as relative to the housekeeping gene *Hrpt*. n = 3 donor mice.

# D. Abbreviation Index

| | |
|---|---|
| αMEM | alpha minimum essential medium |
| μCT | micro–computed tomography |
| ALP | alkaline phosphatase (enzyme/activity) |
| ALPL | alkaline phosphatase liver/bone/kidney (gene) |
| ATF4 | Activating Transcription Factor 4 |
| BFR | bone formation rate |
| BGLAP | osteocalcin (gene) |
| BMD | bone mineral density |
| BMP | Bone Morphogenetic Protein |
| BRU | bone remodeling unit |
| BSA | bovine serum albumen |
| BV | bone volume |
| BV/TV | bone volume fraction |
| CBFA1 | core-binding factor subunit alpha-1 |
| CLIC3 | Chloride Intracellular Channel Protein 3 |
| CMap | Connectivity Map |
| COL1A1 | collagen type I alpha 1 chain |
| cRNA | complementary RNA |
| DAPI | 4',6-diamidino-2-phenylindole |
| DEG | Differentially Expressed Gene |
| dex | dexamethasone |
| DNA | deoxyribonucleic acid |
| DXA | Dual energy X-ray absorptiometry |
| ECM | extracellular matrix |
| ERα | estrogen receptor alpha |
| EV | empty vector |
| FA | focal adhesion |
| FACS | Fluorescence-Activated Cell Sorting |
| FGF | Fibroblast Growth Factor |
| FITC | fluorescein isothiocyanate |
| GAPDH | glyceraldehyde 3-phosphate dehydrogenase |
| GO | Gene Ontology |
| GR | glucocorticoid receptor |
| HMOX1 | heme oxygenase 1 |
| Hprt | hypoxanthine Phosphoribosyltransferase 1 |
| IBSP | bone sialoprotein |
| IGF-I | Insulin-like Growth Factor I |
| kDa | kilodalton |
| KO | knockout |
| LFQ | label-free quantification |
| LMHD | Lenz-Majewski hyperostotic dwarfism |
| LS/MS | liquid chromatography–mass spectrometry |

| | |
|---|---|
| MAR | mineral apposition rate |
| M-CSF | macrophage-Colony Stimulating Factor |
| mRNA | messenger RNA |
| MSC | Mesenchymal stromal cell |
| MUC1 | Mucin 1 |
| NEK9 | NIMA-related kinase 9 |
| OPG | osteoprotegerin |
| OSX | Osterix |
| PBMC | peripheral blood mononuclear cell |
| PBS | phosphate-buffered saline |
| PCR | polymerase chain reaction |
| PNP | p-nitrophenol |
| PNPP | p-nitrophenyl phosphate |
| PPAR-γ2 | peroxisome proliferator-activated receptor-gamma 2 |
| PS | phosphatidyl serine |
| PSS | phosphatidylserine synthase |
| PTDSS1 | phosphatidylserine synthase 1 |
| PTH | Parathyroid hormone |
| RANKL | Receptor Activator of Nuclear kappa B Ligand |
| RFU | relative fluorescence units |
| RLU | Relative Light Unit |
| RNA | Ribonucleic acid |
| RUNX2 | Runt-related transcription factor 2 |
| SATB2 | Special AT-rich Binding 2 |
| SEM (or SE) | standard error of the mean |
| SD | standard deviation |
| shRNA | short hairpin RNA |
| SOX9 | Sex determining region Y-box 9 |
| SP7 | Osterix (gene) |
| SPP1 | osteopontin |
| STC1 | Stanniocalcin-1 |
| SV-HFO | Simian virus-immortalized human fetal osteoblasts |
| TGFß | transforming growth factor-ß |
| TRAcP (TRAP) | Tartrate-resistant acid phosphatase |
| WT | wild type |

# E. Curriculum Vitae

**Andrea M. Brum**

| | |
|---|---|
| 20 Nov. 1981 | Born in Castro Valley, California, USA |
| 1999 - 2004 | B.Sc. *Animal Science, emphasis in molecular biology*<br>University of California, Davis. Davis, California, USA |
| 2004 – 2005, 2007 | Junior Specialist Research Assistant<br>Equine Reproduction Group, Prof. Barry Ball<br>Department of Population Health and Reproduction<br>University of California, Davis. Davis, California, USA |
| 2005 - 2007 | M.Sc. *Animal Biology, emphasis in reproductive biology*<br>Equine Reproduction Group, Prof. Barry Ball<br>Department of Population Health and Reproduction<br>University of California, Davis. Davis, California, USA |
| 2008 – 2010 | Research Technician<br>Gene Therapy Department<br>Imperial College, London, UK |
| 2010 – 2014 | Ph.D. Research<br>Calcium and Bone Metabolism Group<br>Department of Internal Medicine<br>Erasmus University Medical Center, Rotterdam, the Netherlands |
| Oct. - Dec. 2012 | Marie Curie Fellow – Exchange at Columbia University<br>INTERBONE project, Laboratory of Dr. Stavroula Kousteni<br>Columbia University, New York, New York, USA |
| 2015-2017 | Volunteer<br>Gabon Biodiversity Program<br>Center for Conservation and Sustainability<br>Smithsonian Conservation Biology Institute, Gamba, Gabon |

# F. Publications

### Related to this thesis:

**Brum AM**, van der Leije CS, Schreuders-Koedam M, Chaibi S, van Leeuwen JP, van der Eerden BC. Mucin 1 (Muc1) Deficiency in Female Mice Leads to Temporal Skeletal Changes During Aging. JBMR Plus. 2018 Jul 14;2(6):341-350.

**Brum AM**, van de Peppel J, Nguyen L, Aliev A, Schreuders-Koedam M, Gajadien T, van der Leije CS, van Kerkwijk A, Eijken M, van Leeuwen JPTM, van der Eerden BCJ. Using the Connectivity Map to discover compounds influencing human osteoblast differentiation. J Cell Physiol. 2018 Jun;233(6):4895-4906.

**Brum AM**, van der Leije CS, Schreuders-Koedam M, Verhoeven J, Janssen M, Dekkers DHW, Demmers JAA, Eijken M, van de Peppel J, van Leeuwen JPTM, van der Eerden BC. Identification of Chloride Intracellular Channel Protein 3 as a Novel Gene Affecting Human Bone Formation. JBMR Plus. 2017 Apr 28;1(1):16-26.

**Brum AM**, van de Peppel J, van der Leije CS, Schreuders-Koedam M, Eijken M, van der Eerden BC, van Leeuwen JP. Connectivity Map-based discovery of parbendazole reveals targetable human osteogenic pathway. Proc Natl Acad Sci U S A. 2015 Oct 13;112(41):12711-6.

### Other Publications:

Pauwels OSG, Braun JJ, **Brum A**, Carlino P, Chirio L, Glaizot O, Meirte D, Morelle S, Royauté L. Miscellanea Herpetologica Gabonica XI. Bulletin of the Chicago Herpetological Society. 2017 52(12):205-211.

Kode A, Manavalan JS, Mosialou I, Bhagat G, Rathinam C, Luo N, Khiabanian H, Lee A, Vundavalli M, Friedman R, **Brum A**, Park D, Galili N, Mukherjee S, Teruya-Feldstein J, Raza A, Rabadan R, Berman E, Kousteni S. Leukemogenesis induced by an activating beta-catenin mutation in osteoblasts. Nature. 2014. 506:240-244.

Griesenbach U, Inoue M, Meng C, Farley R, Chan M, Newman NK, **Brum A**, You J, Kerton A, Shoemark A, Boyd AC, Davies JC, Higgins TE, Gill DR, Hyde SC, Innes JA, Porteous DJ, Hasegawa M, Alton EW. Assessment of F/HN-pseudotyped lentivirus as a clinically relevant vector for lung gene therapy. Am J Respir Crit Care Med. 2012 Nov 1;186(9):846-56.

Mitomo K, Griesenbach U, Inoue M, Somerton L, Meng C, Akiba E, Tabata T, Ueda Y, Frankel GM, Farley R, Singh C, Chan M, Munkonge F, **Brum A**, Xenariou S, Escudero-Garcia S, Hasegawa M, Alton EW. Toward Gene Therapy for Cystic Fibrosis Using a Lentivirus Pseudotyped With Sendai Virus Envelopes. Mol Ther. 2010. Jun;18(6):1173-82.

**Brum AM**, Sabeur K, Ball BA. Apoptotic-like changes in equine spermatozoa separated by density-gradient centrifugation or after cryopreservation. Theriogenology. 2008. June:69(9):1041-1055.

**Brum AM**. Apoptotic-like changes in equine spermatozoa. Thesis (M.S.). University of California Press. University of California, Davis. 2007.

**Brum AM**, Thomas AD, Sabeur K, Ball BA. Evaluation of Coomassie blue staining of the acrosome of equine and canine spermatozoa. Am J Vet Res. 2006 Feb;67(2):358-62.

# G. Ph.D. Portfolio

| | |
|---|---|
| **Name:** | Andrea M. Brum |
| **Institute:** | Erasmus University Medical Center, Rotterdam, the Netherlands |
| **Department:** | Internal Medicine |
| **Group:** | Calcium and Bone Metabolism |
| **Ph.D. Period:** | October 2010 – December 2014 |
| **Research School:** | Postgraduate School Molecular Medicine |
| **Supervisor:** | Prof. dr. J.P.T.M. van Leeuwen |
| **Co-Supervisor:** | Dr. B.C.J. van der Eerden |

## PhD. Training Activities

### Courses and Workshops

2010 'From Molecule to Organism' In Vivo Imaging course
Proefdierkunde (Laboratory Animal Science) course for procurement of Article 9 status by KNAW

2011 'From Mouse to Man' Translational Imaging Workshop by AMIE
Molecular Medicine Course
Regenerative Medicine – From Bench to Bedside (Module 5)
Biomedical Research Techniques X course
Basic Data Analysis on Gene Expression Arrays workshop
Regenerative Medicine – Molecular and Cellular Basis of Regenerative Medicine (Module 2)

2012 European Calcified Tissue Society Ph.D. training course

### (Inter)National Conferences

2010 Dutch Society for Calcium and Bone Annual Meeting, Zeist

2011 Internal Medicine Science Days, Antwerp, Belgium
Molecular Medicine Day, Rotterdam
Dutch Society for Calcium and Bone Annual Meeting, Zeist

2012 Molecular Medicine Day, Rotterdam (*Poster presentation*)
European Calcified Tissue Society Annual Meeting, Stockholm, Sweden

Internal Medicine Science Days, Antwerp, Belgium (*Oral presentation*)

2013 Molecular Medicine Day, Rotterdam (*Poster presentation*)

European Calcified Tissue Society Annual Meeting, Lisbon, Portugal (*Poster presentation)*

International Conference on Children's Bone Health, Rotterdam (*Oral presentation*)

The Netherlands Institute for Regenerative Medicine Annual Meeting, Utrecht (*Poster presentation*)

Dutch Society for Calcium and Bone Annual Meeting, Zeist (*Oral presentation*)

Library of Integrated Network-based Cellular Signatures (LINCS) Symposium Workshop, Boston, USA (*Poster presentation*)

2014 Internal Medicine Science Days, Antwerp, Belgium (*Oral presentation*)

Molecular Medicine Day, Rotterdam (*Plenary oral presentation*)

Dutch Society for Stem Cell Research Annual Meeting, Groningen (*Oral presentation*)

Dutch Society for Calcium and Bone Annual Meeting, Zeist (*Oral presentation*)

2015 Joint Meeting European Calcified Tissue Society – International Bone & Mineral Society, Rotterdam (*Oral presentation*)

## Teaching Activities

| | |
|---|---|
| 2011 | HBO Internship: Rodrigo Drop |
| 2012 – 2013 | B.Sc. Internship: Abiden Aliev |
| 2013 – 2014 | HBO Internship: Siham Chaibi |

## Awards

*Best Poster Award*: Annual Molecular Medicine Day, Rotterdam, 2013

*Travel Award*: Meeting European Calcified Tissue Society, Lisbon, Portugal, 2013

*New Investigator Award*: International Conference on Children's Bone Health, Netherlands, 2013

*New Investigator Award*: Joint Meeting European Calcified Tissue Society – International Bone & Mineral Society, Rotterdam, Netherlands, 2015

## Other activities

Weekly endocrinology lectures (2010 – 2014)

Organization of Internal Medicine Lab Day (2013)

Organization of the International Conference on Children's Bone Health Meeting (2013)

# H. Acknowledgements

It has been a long and winding road, but I am so happy and grateful to be near the end of this path that is a PhD. I would like to try to put into words my extreme gratitude to all the people that helped make this possible.

To my promoter, Hans, thank you. Thank you for your enthusiasm, for your ideas, for your critiques, for your friendly character, and most importantly thank you for your guidance and support. You were always incredibly encouraging and inspiring, and I will forever be grateful for opportunities and guidance you have imparted on me.

Bram, my co-promoter, office-mate, and mentor, I greatly appreciate you and everything you've done for me. You are one of the hardest working people I know and I thank you for all of your time, wisdom and patience you have given me. Finally, I hope that I have been able to impart somethings on you too (maybe "ish"?) and that we can continue to collaborate in the future, in whatever form that may be.

I would like to give me deepest thanks to everyone who worked in the "bone lab": Adriana, Anke, Bianca, Bram, Cindy, Hans, Iris, Jeroen, Jyoti, Katja, Linh, Marco, Mark, Marijke, Marjolein, Marta, Rodrigo, Ruben, Tanja, and Tarini. You all have helped make my time in the bone lab incredibly special and I have so many wonderful memories of all of you. Thanks to all of each of you for your help along the way. Special thanks go to the students I supervised: Ricardo, Abiden and Siham. You were all amazing students that worked very hard and were enthusiastic for the work we did together.

The results presented in this thesis, as well as good deal that didn't make it in, were truly a group effort and I could not have done it without the very hard work and support of several key people.

Cindy, you are an incredible co-worker, cheerleader, and friend. You put your heart and soul into the work we did together, even when it was difficult for you. You thought along-side me every step of the way, coming up with new ideas and always voiced your opinion if you thought we could do something better. You were always there for me when I had challenges. I have fond memories of the countless hours we spent with the Muc1s in the microCT room. And I greatly appreciate your continued work on my projects after my time in the lab came to an end. No one can ask for anything more from a colleague and friend.

Marijke, I believe you really are the glue that holds the bone lab together. You can and do jump into any ongoing project, producing beautiful results always. You keep the lab running when complications arise. You make everyone feel at ease

around you, but don't let anyone bowl you over. Thank you for being a wonderful teacher and colleague, and for all of your hard work on my projects.

Thank you to Arcarios, without whom this project may not have existed. I am extremely grateful for the funding and support. Marco, I really value your guidance and support of my projects. Anke, Bianca and Mark, your outstanding work on the connectivity map and candidate genes experiments are hugely appreciated.

Significant contributions to this project were also made by a number of student interns: Abiden, Linh, Siham, and Tarini. Thank you very much for your assistance and enthusiasm.

I was incredibly lucky to start my PhD on the same day as my friend and colleague, Jess. I can't think of a better person to have gone on this ride together with. Not only are you a brilliant scientist, you are hard-working, creative and caring person. You have inspired me, supported me, and listened to me. I'm so glad this lab brought us together and that I have you as a friend.

Thank you so much to my family and friends for your support and encouragement. To my mother and father, Diane and Steve, I am so grateful for your love, constant belief in me, and interest in my work. I definitely could not have done this without you. Aan mijn schoonouders, Ad en Adje, dank voor jullie liefde, vriendelijkheid en steun, ik ben blij om deel te mogen uitmaken van jullie familie. Ariana, my best friend, I am so appreciative to have an amazing of friend as you in my life. Thank you for your encouragement and nagging to just get it done already.

To my daughter, Celine, thank you for inspiring me and challenging me. I appreciate you "helping" me type the last bits of my thesis and being patient (well as patient as a toddler can be) when I just needed to finish "one last little bit."

Finally, and most importantly, thank you to my husband, Teun. I simply cannot put into words how much your mean to me, how much I appreciate you and how inspiring you are to me. You've always loved and supported me no matter how difficult or moody I've been while working on my PhD. I'm so grateful for how you've listening to me talk about osteoblast "gobbledy gook", that you're always willing to help me work through problems I have, and are happy to bounce ideas around with me. Thank you for your shared passion to travel, for without you I'm sure I would have not have lived in all the different places that we have, which provided me such unique opportunities, like this PhD project. I love you and am forever grateful to you.